ABSTRACT

Humphreys, Abigail Elaine. Influence of Residual Stress on the Initiation of Fatigue Cracks at Welded Piping Joints. (Under the direction of Dr. Tasnim Hassan)

Fatigue failures of small bore piping systems have historically occurred in nuclear power plants, resulting in unanticipated plant downtime and substantial financial loss. These failures have been reported with increasing frequency over the past 20 years and have motivated the research described in this thesis. Recent research at North Carolina State University (NCSU) pointed to the strain ratcheting response of the welded joint as a probable reason for fatigue failure and indicated that welding residual stresses might be responsible for inducing this strain ratcheting response. It was the primary objective in this investigation to determine what happens to residual stresses at the welded piping joint under the application of low-cycle fatigue loading and to understand how residual stresses induce strain ratcheting and thus affect the fatigue life of the welded joint.

In order to achieve stated objectives, a systematic set of residual stress measurements and low-cycle fatigue tests was conducted. Initial residual stresses near the weld toe of six welded piping specimens were measured using the technique of x-ray diffraction. The specimens were then loaded in low-cycle fatigue to intermediate points in their fatigue lives and residual stresses were measured again. Strain response data near the weld toe was gathered throughout specimen fatigue life. Residual stress data and recorded strain responses in fatigue prompted conclusions concerning the role of residual stresses in inducing strain ratcheting which were verified by additional material level experiments.

Initial residual stress measurements obtained from the welded specimens revealed that residual stresses near the weld toe—the location of fatigue crack initiation and final failure—

were compressive in the overwhelming majority of measurement cases. It is widely accepted that compressive residual stresses are beneficial in fatigue. However, in this set of experiments, it was observed that compressive residual stresses induced tensile strain ratcheting and were thereby detrimental to fatigue life. Residual stress measurements obtained at intermediate points in specimen fatigue lives showed that residual stresses relaxed with fatigue cycles. The extent of relaxation at a point on the welded specimen in fatigue was dependent upon the amplitude of strain cycle experienced. At the location of maximum strain cycling in fatigue, complete relaxation of residual stresses was observed in all specimens. Strain response data gathered in the fatigue tests reiterated earlier findings at NCSU—positive axial strain ratcheting occurred at the top and bottom weld toes of all specimens subjected to displacement-controlled fatigue cycles. In light of residual stress relaxation and strain response data gathered in the welded specimen tests, it was anticipated that during residual stress relaxation, the prescribed fatigue interactions between multiaxial stresses exerted a *reverse mean stress effect* , which induced ratcheting response. In other words, the relaxation of the compressive residual stress in the axial direction induced a positive mean stress effect in the prescribed fatigue loading cycle. Consequently, tensile strain ratcheting in the presence of compressive residual stresses resulted. In order to gain insight into this newly observed phenomenon of reverse mean stress effect, the mechanism of multiaxial stress interaction was further investigated through additional laboratory experimentation and cyclic plasticity analysis at the material level. Results from this step more directly explain the new observation. This study reveals the mechanism of recently observed ratcheting fatigue failures of welded joints. Additional research is required to understand the failure mechanism in full and for incorporation of this mechanism in design methodology.

Influence of Residual Stress on the Initiation of Fatigue Cracks at Welded Piping Joints

by
Abigail Elaine Humphreys

A thesis submitted in partial fulfillment of the requirements for the degree of

Master of Science

Department of Civil Engineering
North Carolina State University

Under the guidance of
Dr. Tasnim Hassan

Raleigh, North Carolina
May 2004

Approved by:

_____
Chair of Advisory Committee

_____

_____

BIOGRAPHY

Abigail Elaine Humphreys was born to Tom and Linda Zechman on February 29, 1980, in Piqua, Ohio. She attended Ohio University and obtained her Bachelor of Science in Civil Engineering in June of 2002. She married Brett Humphreys in July of 2002 and moved to Raleigh, North Carolina, to pursue her Master of Science in Civil Engineering at North Carolina State University.

ACKNOWLEDGEMENTS

I would like to extend my sincerest thanks and appreciation to Dr. Tasnim Hassan for his guidance and support throughout this research project. I am truly grateful for his willingness to share his time, wisdom, and enthusiasm with me over the last two years.

I would also like the thank the staff members of the High Temperature Materials Laboratory at Oak Ridge National Laboratory, specifically Dr. Camden Hubbard and Dr. Thomas Watkins, for their time and effort invested in this research.

I would like to gratefully acknowledge financial support provided by the National Science Foundation, the Center for Nuclear Power Plant Structures, Equipment, and Piping, and the Department of Civil Engineering without which this research could not have been conducted.

Special thanks go to Kevin Wilkins for his time and effort spent training me in the NCSU laboratory. I would also like to thank Syed Mizanur Rahman for his assistance in conducting plasticity analysis.

I would like to thank my sister, Emily Zechman, for her listening ear and encouraging words.

I want to thank my husband, Brett Humphreys, for his unfailing love and support.

TABLE OF CONTENTS

LIST OF TABLES

LIST OF FIGURES

CHAPTER 1
INTRODUCTION

1.1 Background

1.1.1 Motivation

Fatigue failures of small bore piping systems have historically occurred in nuclear power plants in the United States (Riccardella et al. [1998]). These failures take place, almost without exception, at welded connections and are one of the major sources of complication in nuclear power plants (Yamashita et al. [1997]). The Electric Power Research Institute (EPRI) accumulated data from 642 fatigue failures that occurred over a period of 20 years. The EPRI reported that of these 642 failures, more than 80 percent were caused by mechanical vibratory fatigue (Gosselin [1994], Higuchi et al. [1998]). Upon compiling data gathered from 40 years of fatigue failure investigations, the ASME Section XI Task Group on Fatigue in Operating Plants reported that the overwhelming majority of these vibratory fatigue failures at welded connections occurred at socket-welded joints (Vecchio [1996]).

Fatigue failures in small bore piping systems have had a major detrimental impact on nuclear power plant maintenance costs and productivity (Smith [1996]). Failures at welded connections are detected as small cracks or leaks. Repairs are required, and they are costly on several different levels. Primarily, crack repairs often lead to forced outages. In many cases, the location of a leak makes isolating it from the reactor pressure vessel impossible (Riccardella [1998]). As repairs must be made immediately to control radiological contamination, forced outages result (Vecchio [1996]). In such cases, plant owners must absorb the cost of providing replacement power as well as the upfront cost of repairs and the incurred cost of unplanned outages (Smith [1996]).

In addition to the adverse effects that fatigue failures have on plant economics and productivity, several characteristics of these failures at welded connections raise significant concern. Vibratory fatigue failures are being reported with increasing frequency at nuclear power plants in the United States (Higuchi et al. [1998]). The Center for Nuclear Power Plant Structures, Equipment, and Piping (C-NPP-SEP) compiled a data set of 74 case studies of welded joint fatigue failures. Of the 74, 32 failures occurred between 1975 and 1989 while the remaining 42 occurred between 1990 and 1994 (Liu [1998]). Clearly, the frequency of these fatigue failures has increased. In addition to this alarming fact, the piping system components being considered are failing prematurely. Small bore piping connections are designed for a

service life of 40 years in accordance with what are considered to be conservative design procedures. However, many of the fatigue failures examined in the EPRI study previously cited failed in fatigue in less than 10 years (Gosselin [1994]). The combined impact of the nature, frequency, and detrimental effects on the nuclear power industry of fatigue failures at welded piping connections has motivated the research described within this thesis.

1.1.2 Effect of Welding Residual Stresses on Fatigue Life

Fatigue failures at welded connections in small bore piping systems are influenced by many factors. These factors include stress concentrations, environment, loading, and residual stresses. While all four factors listed are worthy of researchers' attention, only the effect of residual stresses on the fatigue life of welded piping components is explored here.

Residual stresses arise in welded piping components as an unavoidable byproduct of the welding process. In this process, both the base metal and the weld material are exposed to heating and cooling cycles. Due to the nonuniform geometry of the joint, nonuniform cooling and hence residual stresses result. It is commonly known that tensile residual stresses in the surface layers of piping components reduce fatigue life by encouraging early crack initiation. However, in the course of this research, it was discovered that welding residual stresses were compressive near the weld toe in the six piping specimens considered. Therefore, the effect of compressive residual stresses on fatigue life of welded piping joints is explored in the literature review.

Researchers' positions on the topic of the effect of compressive residual stresses on the fatigue life of welded piping components range from one extreme to the other. It is held by many that compressive residual stresses induced at the surface of welded piping components are beneficial in fatigue (Nguyen and Wahab [1998], Torres and Voorwald [2002], Zhuang and Halford [2001]). According to Zhuang and Halford, surface compressive residual stresses achieve improvement in fatigue life by mitigating fatigue cracks that normally initiate at the surface. The extent of the crack mitigation experienced is directly related to the magnitude of compressive residual stresses induced (Zhuang and Halford [2001]). In an attempt to solidify this correlation, Torres and Voorwald [2002] conducted experiments exploring whether or not increased magnitude of compressive residual stresses resulted in proportionally longer specimen fatigue lives. This correlation was not supported by the experimental data obtained. The two researchers could therefore not endorse the idea that increasing compressive residual stresses

increases the fatigue life of steel specimens (Torres and Voorwald [2002]). At the midpoint of the gamut, some researchers maintain that welding residual stresses exert no influence—positive or negative—on fatigue life of welded piping components (Iida et al. [1997]). Finally, certain investigators have proposed that welding residual stresses negatively impact length of fatigue life by combining with service stresses to significantly shorten component life (Withers and Bhadeshia [2001]). Clearly, no consensus has been reached among researchers as to what effect compressive residual stresses have on the fatigue life of welded piping components.

1.1.3 Preceding Research on Role of Residual Stresses in Fatigue Failure

The research preceding that described in this thesis, which was carried out by Lu [2003] at North Carolina State University, serves as the foundation of and the springboard to this investigation of the influence of residual stress on fatigue failure of welded joints. Lu [2003] tested four welded piping specimens in displacement-controlled low-cycle fatigue. In Lu's tests, strain response at the weld toe during fatigue was monitored. The phenomenon of strain ratcheting was observed for the first time in the four tests.

Strain ratcheting is defined as the phenomenon by which maximum strain progressively increases with fatigue cycles. This accumulation of strain leads to fatigue crack initiation, which in turn eventually leads to failure. Generally, strain ratcheting occurs in the presence of a mean or steady stress. In Fig. 1.1 of nominal axial stress and strain, the phenomenon of uniaxial ratcheting is graphically depicted. The prescribed stress cycle to which the tubular stainless steel specimen was subjected in this test appears in the inset figure and is symmetric about a positive mean stress. Consequently, positive strain ratcheting results as evidenced in Fig. 1.1 by the gradual migration of the hysteresis loop in the positive strain direction. The mean strain—that is, the midpoint of the peak-to-peak strain range of each cycle—is plotted versus cycles in Fig. 1.2 and conveys strain ratcheting; the mean strain increases with cycles.

The strain response of a tubular stainless steel specimen subjected to a biaxial state of stress is shown in Fig. 1.3. The strain cycle to which the specimen was subjected appears in the inset figure. After a positive circumferential steady stress was achieved, the specimen was symmetrically strain cycled in the axial direction. Due to the steady circumferential stress, positive ratcheting of circumferential strain occurred and is observed in Fig. 1.3; the strain response loops move in the positive circumferential direction as cycles increase. This ratcheting

response is reiterated in Fig. 1.4, in which it is apparent that the mean circumferential strain increases with cycles.

Lu [2003] tested four welded piping specimens—one butt-welded and three socket-welded specimens—in the cantilever setup shown in Fig. 1.5. An example of each type of specimen can be seen in Fig. 1.6. Each specimen was subjected to displacement-controlled fatigue cycles; the applied displacement cycle appears in Fig. 1.7. Biaxial strain gages were installed at the top and bottom weld toes prior to testing to monitor the strain responses at the weld toe in fatigue. In Fig. 1.8, axial and circumferential strain response at the top weld toe from one of Lu's tests is depicted. Ratcheting in both the axial and circumferential directions is observed in this figure. In Fig. 1.9, the strain cycle amplitude—one half of the peak-to-peak strain range—and the mean strain—the midpoint of the peak-to-peak strain range—in each cycle of strain response at both top and bottom weld toes are shown. Lu's fatigue tests were conducted in a displacement-controlled setup and consequently, relatively constant amplitude of strain was recorded at both weld toes. However, the mean strain responses at both weld toes reveal ratcheting with cycles. The occurrence of strain ratcheting in these particular tests was surprising as no mean stress was externally applied. In spite of this fact, strain ratcheting was observed without exception at the top and bottom weld toes of the four welded piping specimens fatigue tested by Lu [2003]. This finding prompted the following hypothesis: "residual stresses at the welded joints may not relax to zero after a few inelastic cycles as assumed in the fatigue design methods" (Lu [2003]). In such case, the residual stresses act as a mean stress to the prescribed fatigue cycle, thus inducing ratcheting and playing a notable role in fatigue failure. This hypothesis, however, contradicts the commonly accepted assumption that welding residual stresses relax in low-cycle fatigue. This thesis makes effort to resolve this contradiction.

1.1.4 Residual Stress Relaxation in Fatigue

An extensive literature review was conducted to ascertain what exactly happens to welding residual stresses in fatigue. The results of this search follow.

The classical, widely accepted assumption concerning residual stresses referred to above is reiterated here: welding residual stresses relax immediately and completely in low-cycle fatigue. This assumption stems from the elastic-perfectly plastic idealization; residual stresses are thought to relax when the superposition of the applied stress and residual stress exceeds the material's yield stress (Smith et al. [2001]). While this assumption is a simplification, there are

researchers who lend wholehearted support to it. Berge and Eide [1982], in their experimental work, found that residual stresses in welded structural carbon-manganese steel specimens subjected to constant-amplitude fatigue tests were completely eliminated when the peak stress applied was equal in magnitude to the yield stress. At the other end of the spectrum, researchers assert that residual stresses in stainless steel and carbon steel specimens do not relax in fatigue. Instead, they exert a mean stress in the prescribed fatigue cycle and thereby affect the fatigue strength of the joint (Withers and Bhadeshia [2001], Yamashita et al. [1997]). Several papers were found proposing partial relaxation of residual stresses in carbon-manganese, stainless, and structural steel specimens, the authors of which occupy the middle ground (Blom [1995], Chiarelli et al. [1999], Iida et al. [1997], Lachmann et al. [2002], Smith et al. [2001], Torres and Voorwald [2002], Zhuang and Halford [2001]).

The proponents of the theory of partial relaxation of residual stresses in fatigue attribute this relaxation and the manner in which it occurs to a myriad of factors. Many identify amplitude of loading as the key factor. As the amplitude of applied stress increases, so follows the extent of relaxation (Iida et al. [1997], Lachmann et al. [2002], Smith et al. [2001]). Others credit both the amplitude of loading and the number of fatigue cycles to which the component is subjected (Torres and Voorwald [2002]). It is not asserted by these researchers that complete relaxation is ever attained. Fairly extensive early relaxation of residual stress has been documented (Blom [1995], Iida et al. [1997]). However, the residual stresses, after sustaining significant relaxation, stabilize at a nonzero value (Blom [1995], Torres and Voorwald [2002]). Relaxation is ultimately incomplete.

Two mathematical models for predicting relaxation of residual stresses were discovered in the course of the literature review and are discussed herein. The first, proposed by Chiarelli et al. [1999], suggests that residual stress at an intermediate point in the fatigue life of a welded specimen can be predicted by subtracting from the yield stress of the material the maximum stress experienced by the specimen during fatigue. The authors reported favorable results from the fatigue test of a single welded specimen made of structural steel. Using their proposed approach, they predicted the residual stress at an intermediate point in the fatigue life within 10 MPa of the measured residual stress (Chiarelli et al. [1999]). However, no further experimental validation of this approach was found.

The second mathematical model for prediction of residual stress relaxation was proposed by Kodama [1971]. Based on his experimental data, he identified a linear-logarithmic relationship between residual stress relaxation and number of fatigue cycles. The rate of residual stress relaxation was found to be proportional to the amplitude of applied stress (Smith et al. [2001]). A limitation to this model must be noted. The linear-logarithmic relationship did not accurately predict residual stress relaxation occurring in the first fatigue cycle (Zhuang and Halford [2001]). Again, no substantial body of supporting experimental data was found to verify this model.

As was the case when the topic of the effect of residual stresses on fatigue life of welded specimens was probed, no consensus among researchers was found concerning relaxation of residual stresses in fatigue. The lack of substantial experimental data concerning this topic was a major motivation for the research conducted and prompted the primary objective defined in the following section.

1.2 Overview of Research

In the present research, it was the primary goal of the investigators to determine what happens to residual stresses at welded piping joints under the application of low-cycle fatigue loading and to understand how residual stresses induce strain ratcheting at the welded joints. In order to gain this insight, the initial residual stresses near the weld toe of six welded piping specimens were measured using x-ray diffraction. The specimens were then cyclically loaded to intermediate points in their respective fatigue lives before residual stresses were measured again. Finally, the specimens were fatigued to failure. Residual stress measurements obtained at intermediate points in fatigue provided conclusive evidence by which the first part of the primary objective was met.

Strain response data near the weld toe was also gathered in the welded specimen tests and was critically examined in light of the relaxation data to determine how residual stresses induce the strain ratcheting recorded. Four of the six specimens were subjected to displacement-controlled fatigue cycles while the remaining two specimens were subjected to force-controlled fatigue cycles. This differentiation was introduced in an attempt to explore the fatigue failure mechanisms of displacement- and force-controlled fatigue loading. Due to different equilibrium conditions, residual stress relaxation in the two types of fatigue tests may not be identical. Thus, relaxation may play a different role in fatigue failure depending upon the type of loading. It was

the aim of the investigators to explore both types of fatigue loading and document observed differences in residual stress relaxation, strain response, and failure mechanisms.

In both the displacement- and force-controlled experiments, welded specimens were tested in low-cycle fatigue conditions. In low-cycle fatigue, components are subjected to stresses large enough to cause appreciable plastic deformation prior to failure. Components fail after a relatively low number of cycles. In high-cycle fatigue, specimens are subjected to smaller stresses. In general, the material deforms primarily elastically and the component remains functional through a larger number of cycles (Suresh [1998]). However, at points of stress concentration, localized plastic deformation occurs. In both types of fatigue, repeated cyclic straining at the location of stress concentration induces slip within the crystals of the material in the direction of greatest shear (Day [1964]). Irreversible shear deformation, or plastic deformation, results leading to fatigue crack nucleation (Bannantine et al. [1990], Kravchenko [1964], Suresh [1998], Wood [1958]). Thus, crack initiation in both low-cycle and high-cycle fatigue is caused by plastic deformation. Low-cycle fatigue conditions were chosen in the present investigation because the effects of plastic deformation are more pronounced. Understanding of low-cycle fatigue failure can be applied to and serve as the foundation for future research probing high-cycle fatigue failure due to the commonality of the fatigue crack nucleation mechanism in both fatigue ranges.

Additional fatigue experiments were conducted on material specimens and plasticity analysis was carried out in an attempt to discern what role welding residual stresses play in stimulating the recorded strain response. This tier of research was conducted in the hopes that understanding of the fatigue failure mechanism and the effect of residual stresses on fatigue life might be deepened and strengthened, eventually leading to improved fatigue design procedures.

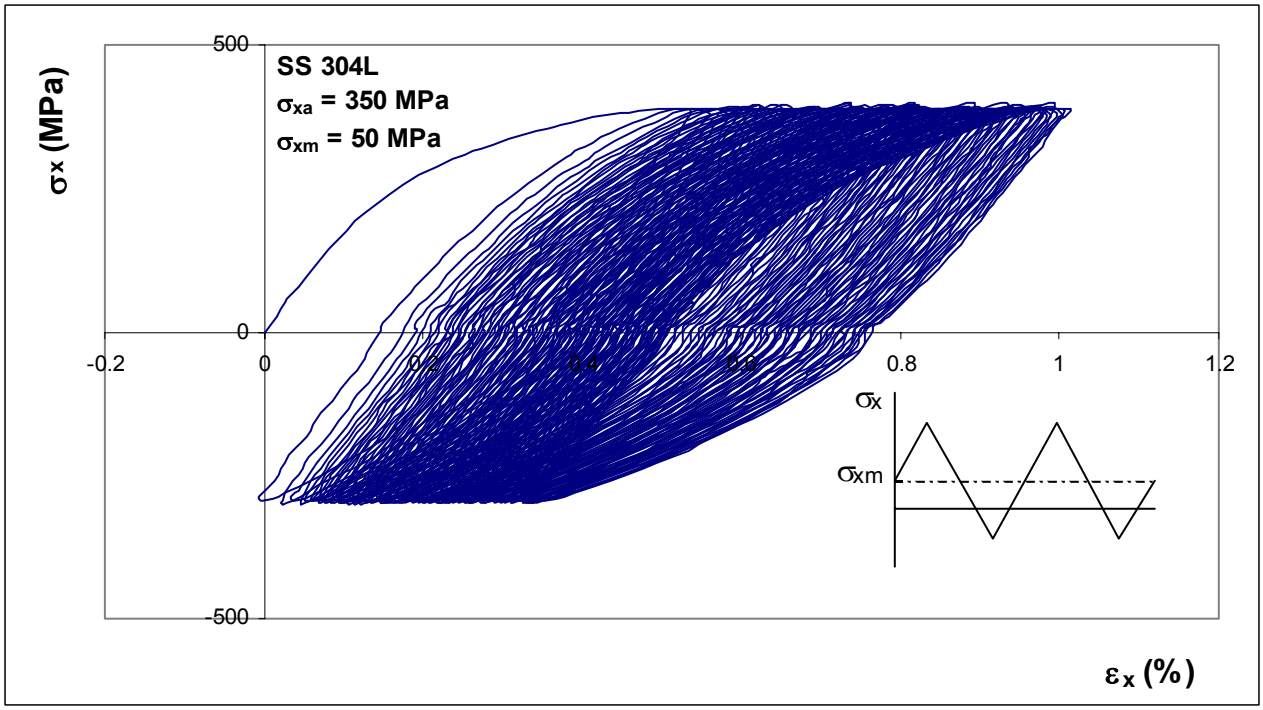

Figure 1.1 Axial strain ratcheting in uniaxial test

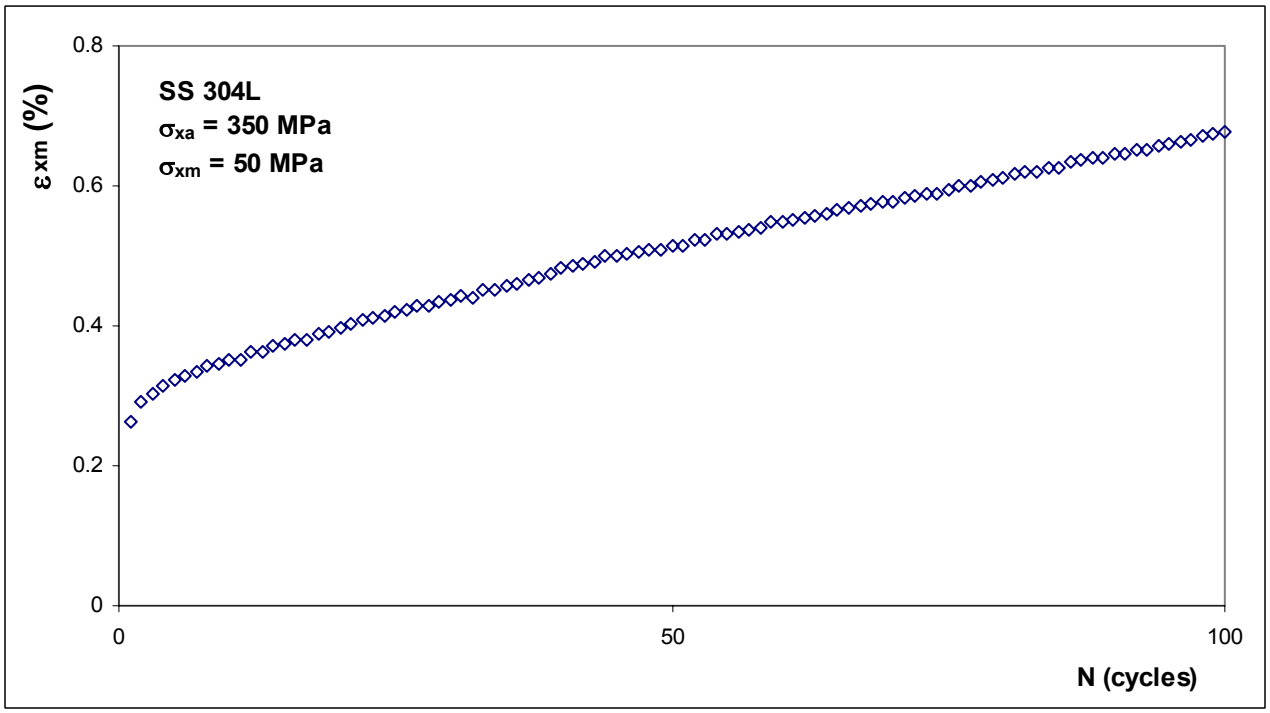

Figure 1.2 Mean axial strain versus cycles in uniaxial ratcheting test

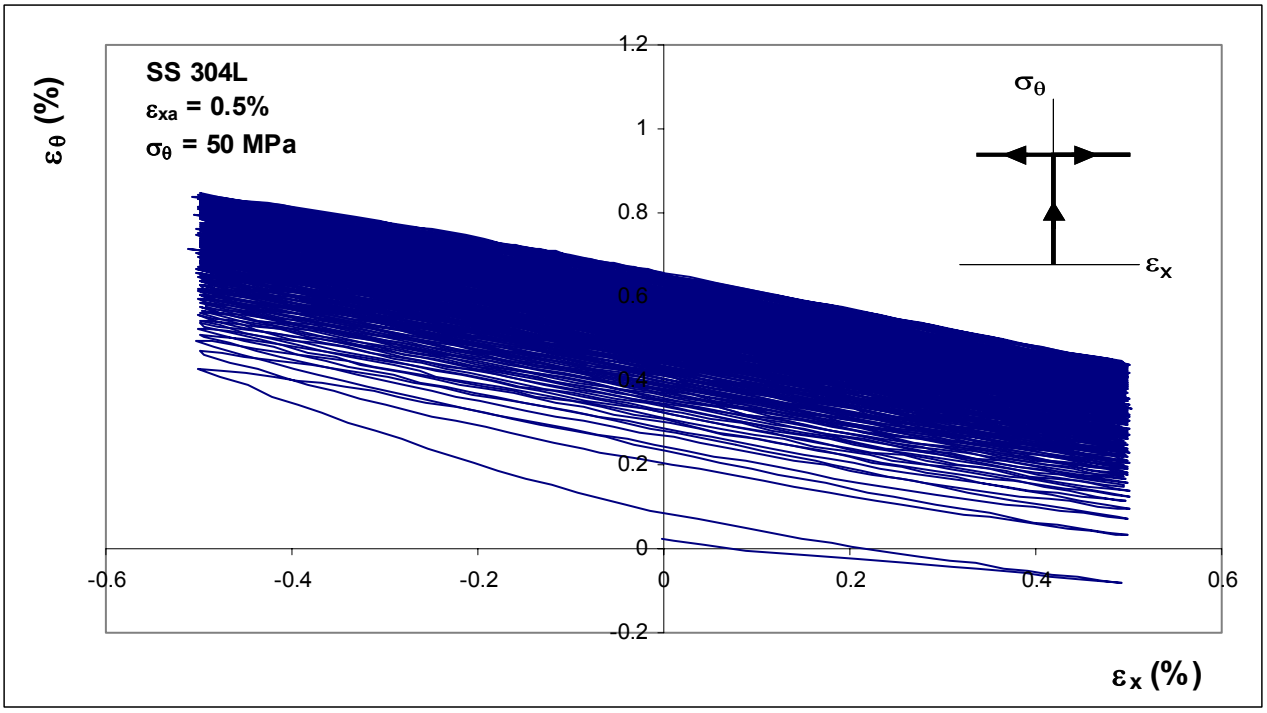

Figure 1.3 Circumferential strain ratcheting in biaxial test

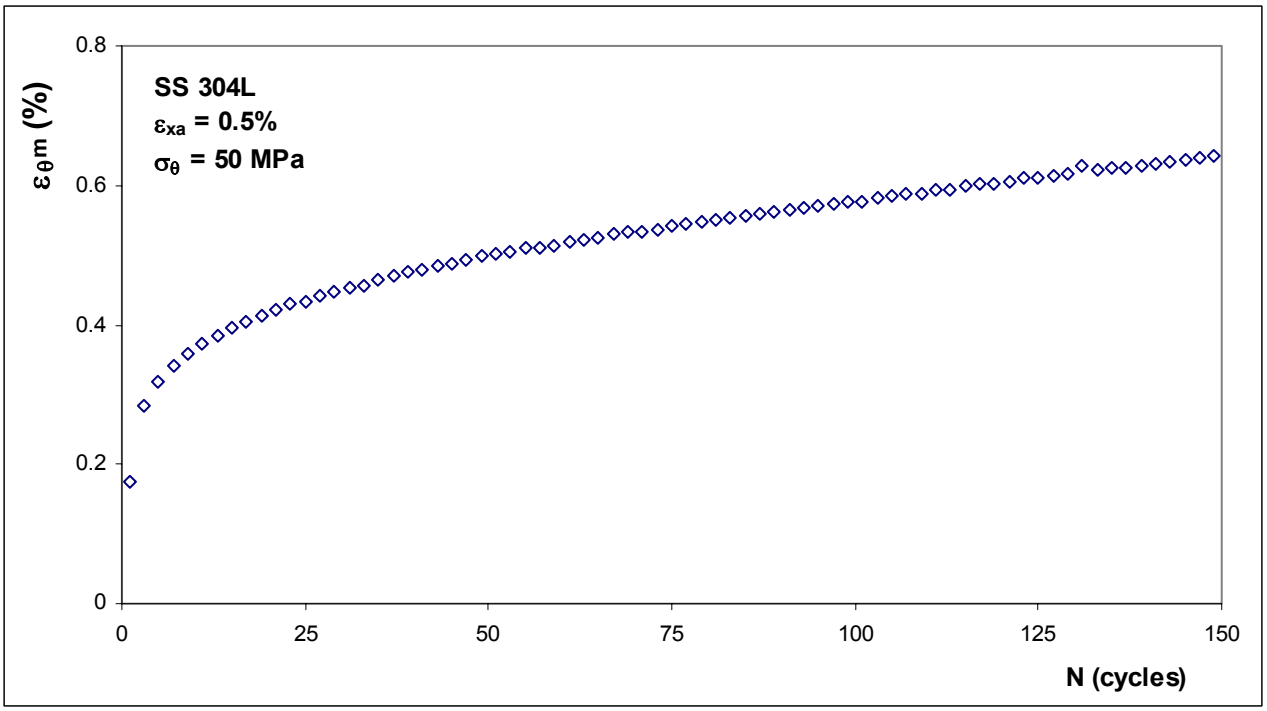

Figure 1.4 Mean circumferential strain versus cycles in biaxial ratcheting test, every 2nd cycle

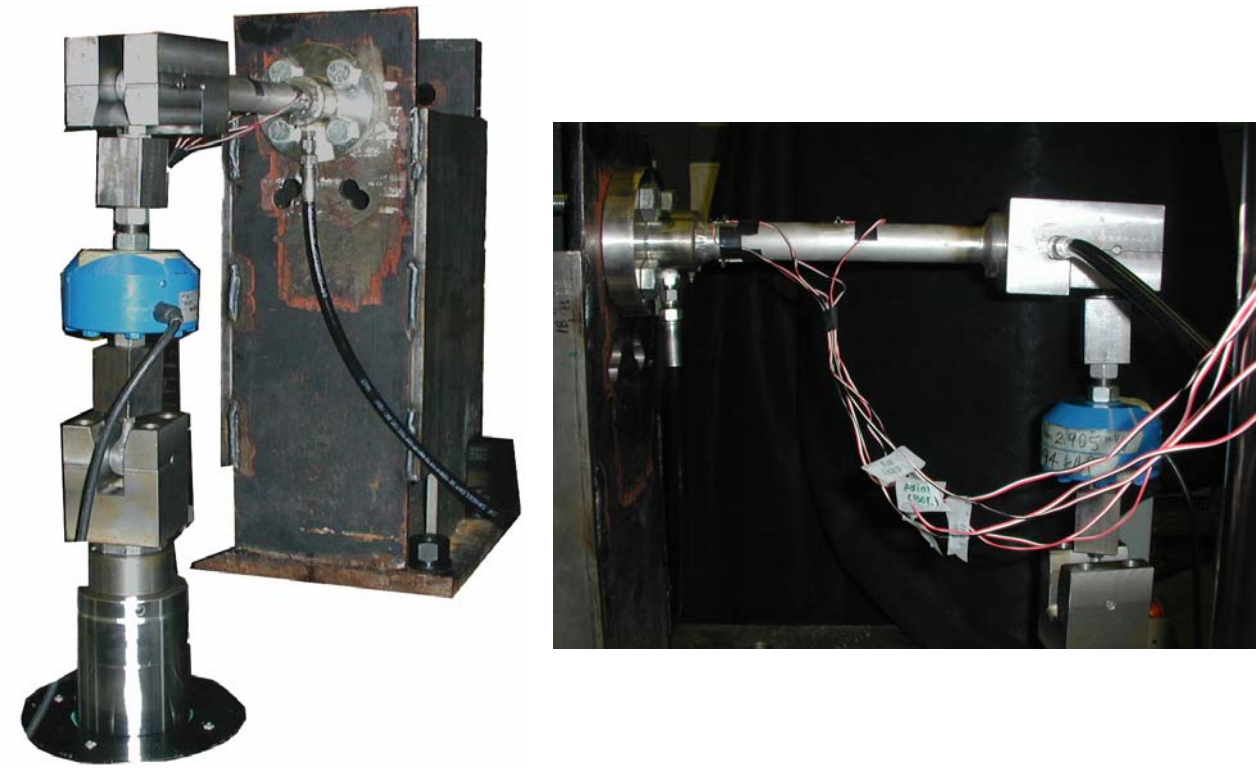

Figure 1.5 Cantilever setup (two views) for welded specimen fatigue testing (Lu [2003])

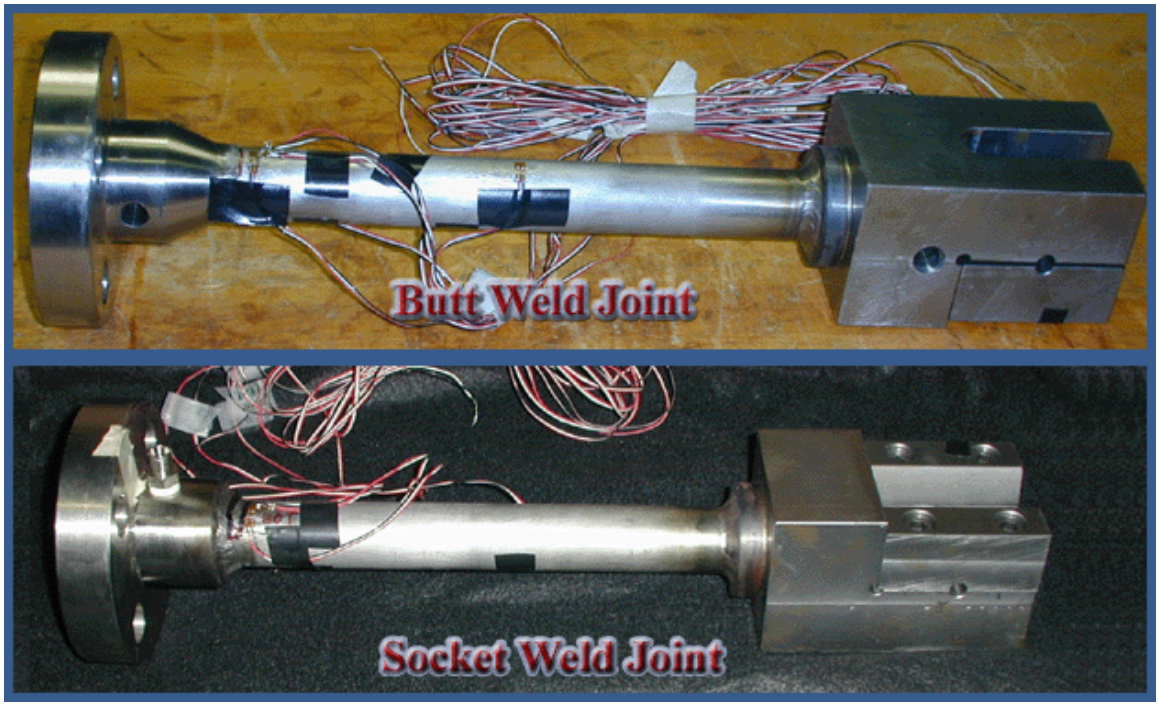

Figure 1.6 Butt- and socket-welded specimens (Lu [2003])

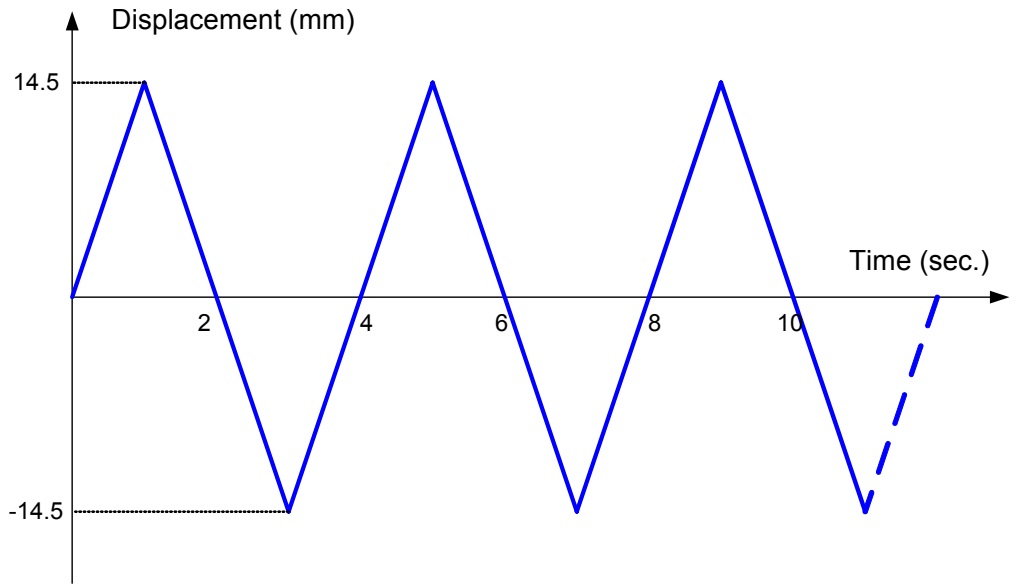

Figure 1.7 Displacement-controlled fatigue cycle (Lu [2003])

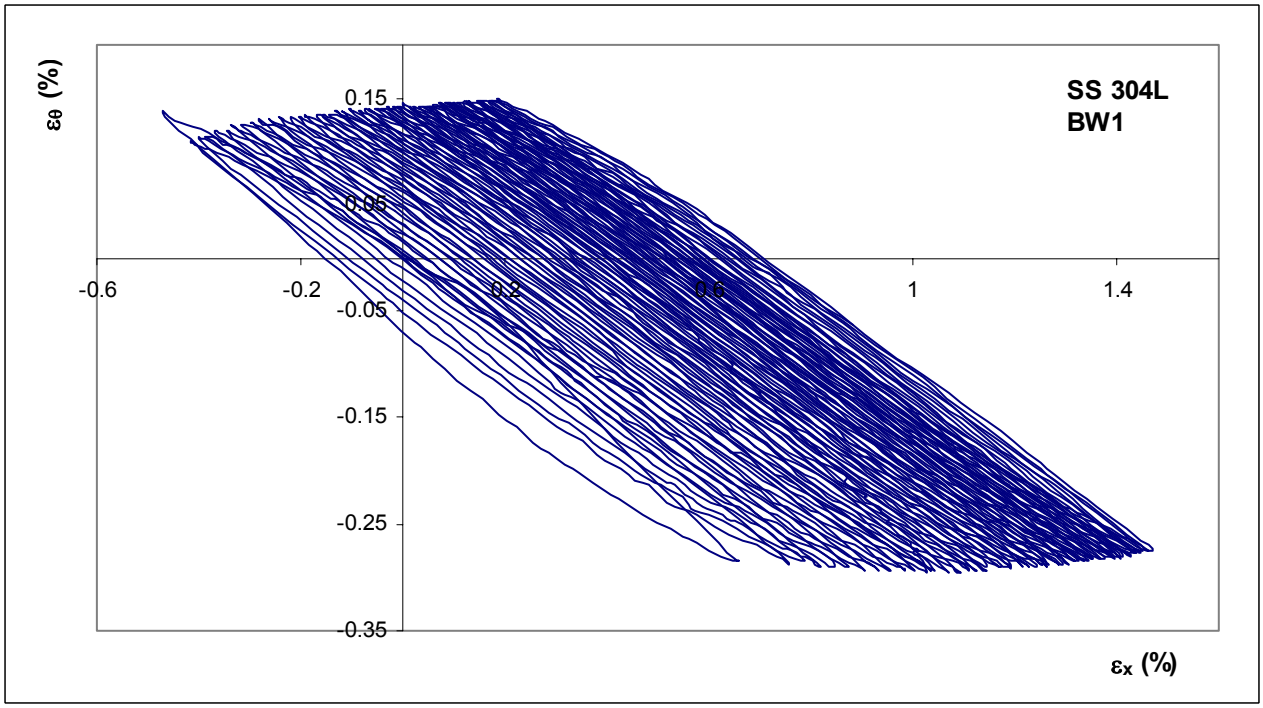

Figure 1.8 Axial and circumferential strain response at top weld toe, every 10th cycle (Lu [2003])

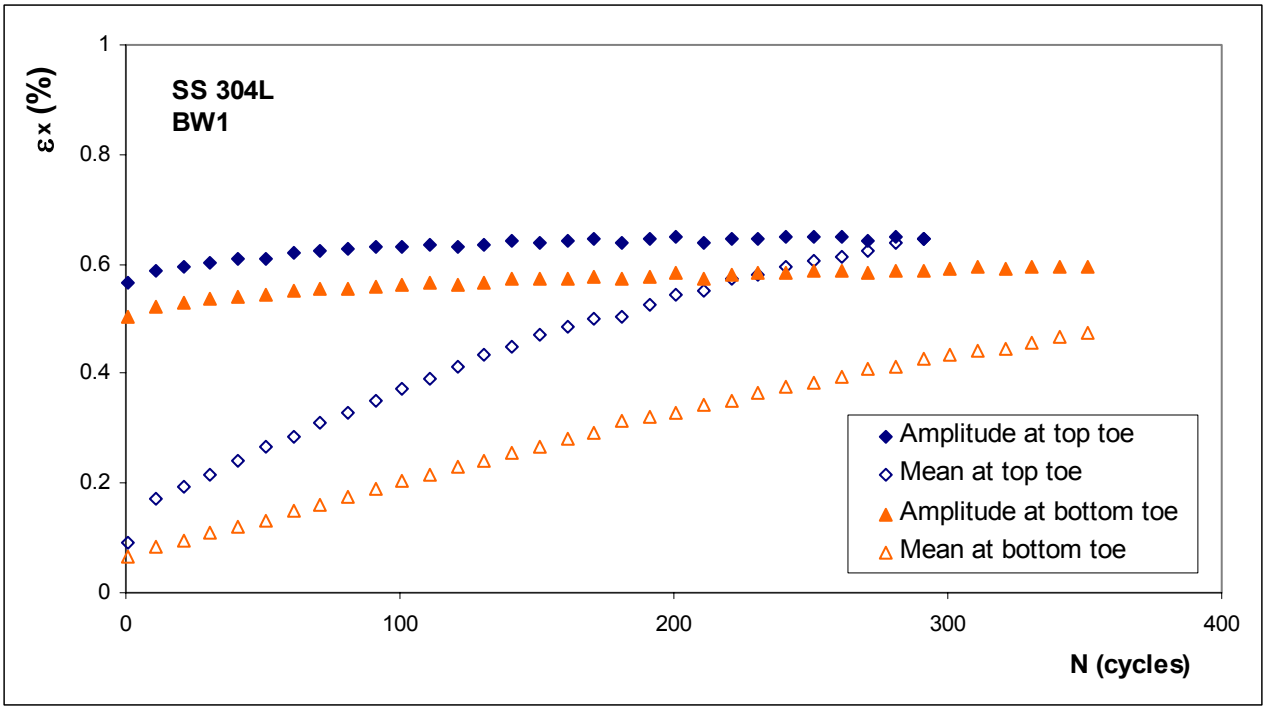

Figure 1.9 Strain amplitude and mean in welded specimen test, every 10^{th} cycle (Lu [2003])

CHAPTER 2
EXPERIMENTAL SETUP

2.1 Specimen Description

Six piping joints were tested in this research project and can be divided into the following categories: butt- and socket-welded joints. The naming scheme used for the specimens was a continuation of that employed by Lu [2003]. Table 2.1 lists all specimens tested in this thesis and in Lu's research, including the data from a specimen tested by Lu that is yet unpublished. Along with each specimen name, the type of weld joint, number and sequence of weld passes, fatigue loading type, and the points in the fatigue life of each specimen at which residual stresses were measured are included in the table.

2.1.1 Socket-Welded Specimens

Five of the six specimens tested in the present investigation were socket-welded specimens (Fig. 2.1). The material of each piping specimen was stainless steel (SS) 304L. The weld filler used was SS 308. Both the end flanges and all end fixtures were machined from SS 304L blocks. Material tests were performed on tubular samples from the SS 304L pipe. From the monotonic curve of a multi-step uniaxial strain-controlled test, the modulus of elasticity (190 GPa) and yield stress (365 MPa) of the stainless steel were obtained (Fig. 2.2). In this same test, the stainless steel pipe exhibited neither cyclic hardening nor cyclic softening behavior, as evidenced in Fig. 2.3 by the stable appearance of the hysteresis loops. In the first two stages of the test, noise interfered significantly. However, the hysteresis loops from the final two stages convey stable stress-strain behavior. Nominal dimensions for the socket-welded specimens can be seen in Fig. 2.4. They are as follows: each pipe section had a nominal diameter of 1.25 inches (31.75 mm) and wall thickness of 0.1875 inches (4.76 mm). Due to the geometry of the socket weld, the required end-to-end length of each pipe section was 11 inches (279.4 mm), which allowed for the distance from the toe of the weld to the end of the pipe to be 10.125 inches (257.18 mm). Within the category of socket-welded joints, two types were tested. One of the five socket-welded specimens was welded according to ASME design code, while the other four socket-welded specimens were fabricated using a modified design.

A certified welder for nuclear power plant welding performed the welding for all specimens. Welding was carried out on the specimens in the upright position. Tack welds were first placed at quarter points around the circumference in the order A, C, B, and D. Following

the tack welds, weld passes were carried out for each quarter of the circumference in the sequence AB, CD, BC, DA. This sequence of weld passes is illustrated in Fig. 2.5. All five socket welds consisted of three sets of quarter circumferential passes. This method of welding has been shown in the past to yield minimal distortion as compared to full circumferential welding (Lu [2003]). Additional information pertaining to the welding process, such as start and stop temperatures, duration, time out, current, voltage, and weld bead dimensions for all five socket specimens, can be seen in Tables 2.2-2.6. Such detailed information was recorded for future use in the analysis of the failure and residual stress response of the welded specimens presented in this study.

2.1.2 Butt-Welded Specimen

The single butt-welded specimen, which can be seen in Fig. 2.6, was identical to the socket-welded specimens in terms of material make-up. The pipe section was SS 304L, the weld filler was SS 308, and the end flange and end fixtures were machined from blocks of SS 304L. The geometry of the butt-welded joint and specimen dimensions can be seen in Fig. 2.7. In order for all six specimens to experience the same bending moment at the weld toe, the length from weld toe to pipe end had to be consistent from one specimen to the next. Consequently, the end-to-end length of the pipe section used in the butt weld joint was 10.125 inches (257.18 mm). The welding process for the butt-welded specimen was identical to the process used on the socket-welded specimens. Tack welds were placed at the quarter points around the pipe's circumference, and quarter circumferential welding was carried out. The butt weld consisted of three passes. Detailed information pertaining to the welding process is included in Table 2.7.

2.2 Residual Stress Measurement

2.2.1 Literature Review of Residual Stress Measurement Techniques

The field of residual stress measurement is populated with many different techniques. These techniques can be classified into two categories—destructive and nondestructive. In this literature review, three of the most popular residual stress measurement techniques are considered, one destructive and two nondestructive.

2.2.1.1 Hole Drilling

Hole drilling is a destructive residual stress measurement technique with certain limitations but wide applicability. In carrying out hole drilling, a hole is drilled in the specimen in the center of a rosette of strain gages. The location of the hole is coincident with the spot

where residual stresses are being measured. As the hole is drilled, metal is removed as well as a portion of the residual stress field. Deformation results and a new state of equilibrium is established. The deformation is measured by the strain gages and used to back-calculate the average residual stress at the location of the hole (Lu et al. [1994]). Using the hole drilling method, residual stresses down to a depth equal to the diameter of the hole can be found; however, accuracy of results tends to drop off at depths greater than one half of the hole diameter (Ruud [2002]).

Step-by-step hole drilling is a slightly modified version of the above procedure by which the residual stress gradient through a thickness can be obtained. In step-by-step hole drilling, the strain gages are read at incremental drilling depths. The difference between successive measurement depths ranges from ten to twenty percent of the hole diameter (Ruud [2002]). Residual stresses corresponding to the incremental depths are calculated and the stress gradient over the thickness is thereby determined.

Certain limitations associated with hole drilling must be given proper attention when the applicability of this method is under consideration. Areas of high stress gradient over a distance on the surface of a specimen are not prime sites for hole drilling due to the following: in hole drilling, it is assumed that the stress gradient is constant across the diameter of the hole. In addition, the hole drilling method should not be employed when residual stresses are expected to exceed one third of the yield stress. When residual stresses are of this magnitude, erroneous measurements can result due to local plastic yielding that occurs during drilling. Finally, it should be noted that preparation of the specimen's surface for strain gage application often involves sanding. Sanding induces compressive residual stresses at the surface and can introduce significant error in the measurement process (Ruud [2002]).

When compared to methods of measurement such as x-ray and neutron diffraction, hole drilling usually yields results of lower accuracy and larger scatter (Dupas et al. [1998]). In spite of this disadvantage, the hole drilling technique offers several advantages that improve its appeal. Because step-by-step hole drilling allows for the determination of residual stress at different depths, this method outshines strictly surface probes. In addition, the equipment, instrumentation, and procedure required to obtain residual stress measurements are relatively simple. The added advantage of relatively low cost makes hole drilling a popular residual stress measurement technique.

2.2.1.2 X-ray Diffraction

X-ray diffraction is a nondestructive residual stress measurement technique whose merit has been acknowledged by much of the scientific community since the 1960s (Ruud [2002]). In x-ray diffraction, a dimension in the crystal lattice of the metal—the distance between atomic planes—is measured. The atomic planes act as strain gages. The distance that exists when the metal is subjected to stress is transformed to strain via comparison to the interplanar atomic spacing characteristic of the unstressed metal. Operating under the assumption that stress is proportional to strain, stress values can be obtained by applying the elastic constant to the strains calculated from the measured interplanar atomic distances (Lu et al. [1994]).

X-ray diffraction offers key advantages over other residual stress measurement techniques. The fact that x-ray diffraction is a nondestructive technique is of great importance as the component's ability to function as designed need not be compromised in the process of determining residual stresses. In addition to this advantage, x-ray diffraction generally yields significantly lower scatter and increased accuracy of results when compared to destructive methods (Dupas et al. [1998]). However, this technique also has certain limitations and disadvantages that must be taken into account. X-ray diffraction is strictly a surface probe. The stresses obtained represent the state of stress in the specimen at depths less than 0.001 inches (0.025 mm). Further, while some destructive methods can be used to find residual stresses in components in the field, x-ray diffraction is a non-portable measurement technique that has been largely restricted to the laboratory. The equipment used, procedure followed, and interpretation of results in x-ray diffraction are complex. Trained technologists must carry out testing if accurate, dependable results are to be obtained. In addition to these limitations, it should be noted that x-ray diffraction is more time-consuming and less economical than other residual stress measurement techniques (Ruud [2002]).

2.2.1.3 Neutron Diffraction

Like x-ray diffraction, neutron diffraction is a nondestructive residual stress measurement technique in which the spacing between crystallographic planes is measured and used to determine the residual stress that exists in the metal. When carried out carefully, neutron diffraction can yield highly accurate measurements with less than half as much scatter as x-ray diffraction results. In addition, neutron diffraction is not strictly a surface probe. Measurements of residual stresses at depths up to a few centimeters can be obtained (Webster [2000]).

However, there are also a few drawbacks associated with this technique. Again, like x-ray diffraction, neutron diffraction is a non-portable method. Components to be tested must be transported to the laboratory. The equipment, procedure, and interpretation of results are complex and require trained technologists. Finally, measurements by neutron diffraction are very costly and time-consuming, even more so than x-ray diffraction measurements (Ruud [2002]).

2.2.2 Justification of X-ray Diffraction as Residual Stress Measurement Technique

For the series of experiments upon which this thesis is based, the residual stress measurement technique chosen for implementation was x-ray diffraction. The reasons for this choice are numerous, but two reasons were of particular significance in the selection process. One main objective of this research project was to study what happens to residual welding stresses when the welded component is subjected to cyclic loading. In order to satisfy this objective, measurements of residual stresses before each component was loaded and at intermediate points in the specimen fatigue lives were needed. This sequence of steps within each experiment mandated that the method of measurement be nondestructive in nature, as each component's ability to function as designed could not be compromised in the process of obtaining residual stress measurements.

Accessibility was the weightiest factor in determining which nondestructive residual stress measurement technique would be chosen for this research. The High Temperature Materials Laboratory (HTML) within Oak Ridge National Laboratory (ORNL) sponsors a user program through which researchers from industry, academia, and government institutions can gain access to characterization instrumentation, such as x-ray and neutron diffraction equipment, for exploring and solving materials problems. It was through this user program that our research team gained access to x-ray diffraction equipment at HTML. While neutron diffraction was a very attractive measurement technique for this project, the neutron diffraction facility at ORNL was not yet operational at the time of proposal submittal nor did it becoming operational during our participation in the user program.

2.2.3 Theoretical Background on X-ray Diffraction

A brief description of the theoretical background of x-ray diffraction is included herein. For a more thorough treatment, the reader is referred to Noyan and Cohen [1987]. The basic measurements obtained using x-ray diffraction are the angles at which the maximum diffracted

beam intensity occurs when a crystalline sample is irradiated with x-rays. In the measurement process, an x-ray beam containing photons of wavelength λ impinges upon the surface of the specimen. Photons collide with the electrons and nuclei of the atoms in the crystal lattice. Most of the collisions are between photons and electrons since the electrons effectively shield the nuclei of the atoms. Two types of collisions can occur—elastic and inelastic.

An elastic collision takes place when an x-ray photon collides with an electron that resides in one of the inner orbitals and is tightly bound to the nucleus. In such a collision, no momentum is transferred from the photon to the electron. The photon bounces off with all of its original energy and thus its original wavelength. This occurrence is referred to as coherent scattering. There is a definite phase relationship between the incident and the scattered x-ray. In inelastic collisions, a photon collides with an electron inhabiting one of the outer orbitals. Electrons in these orbitals are not as tightly bound to their respective nuclei, and a transfer of momentum from the photon to the electron takes place upon impact. The photon is deflected and, having given up energy to the electron, travels with a larger wavelength. This type of scattering is called Compton modified or incoherent scattering. There is no definite phase relationship between the incident and scattered x-ray. In both types of collisions, photons are scattered in all directions. The intensity of the scattered beam is dependent upon the scattering angle.

In the process described above, an x-ray beam impinges upon the parallel planes of a crystal as depicted in Fig. 2.8. In this figure, waves ABC and DEF are in phase in the incident beam. After impact with the electrons closely bound to the nuclei, the x-ray waves bounce off of the atoms in the crystal and coherently scatter—that is, the wavelength with which the photons struck the electrons is maintained after impact. Waves ABC and DEF will constructively interfere with each other after scattering if the path difference between the two (GEH) is an integer multiple of the radiation wavelength λ. Thus, at correct angles of θ, the coherently scattered x-rays constructively interference with each other; that is, the phenomenon of diffraction occurs. The values of θ at which diffraction takes place can then be used to find the spacing between atomic planes (d) using Bragg's law, which follows.

$$n\lambda = 2d \sin \theta$$

The value of the lattice spacing obtained in the above measurement and calculation process is different from the unstressed plane spacing if the specimen is under load; the

difference between the two is proportional to the stress to which the specimen is subjected. Elastic theory can be applied at this point to determine the actual value of residual stress that the specimen is experiencing (Noyan and Cohen [1987]).

2.2.4 Measurement of Residual Stresses by X-ray Diffraction at Oak Ridge National Laboratory

At Oak Ridge National Laboratory, residual stress measurements were obtained using the TEC large specimen stress analyzer. The steps of the measurement process are outlined in the following subsections.

2.2.4.1 Specimen Preparation

The first step in the residual stress measurement process was specimen preparation. In preparing specimens that had not yet been fatigued, masking was the only required step. As seen in Fig. 2.9, electrical tape was used to mask off five spots that were 4 mm by 4 mm. The first spot was 2 mm from the toe of the weld, and each successive spot was 9.5 mm from the previous spot, center-to-center. This grid of five spots was created at the location of maximum strain cycling during fatigue loading—that is, either the top or bottom surface of the pipe—and was replicated 90 degrees away, circumferentially, at the location of minimum strain cycling during fatigue loading. On each specimen, a total of 20 residual stress measurements were obtained—at each of the ten spots, residual stress in the axial and circumferential directions was measured.

In preparing specimens that had already been fatigued for residual stress measurement, an additional step became necessary. As with the unfatigued specimens, the measurement spots at the locations of maximum and minimum strain cycling were masked off using an electrical tape grid. Once the masks were securely in place, the spots that had corresponded to strain gage locations during the first stage of fatigue testing had to be electropolished before residual stresses could be measured. The application of strain gages involves sanding the surface of the specimen, which is known to induce compressive residual stresses (Ruud [2002]). Electropolishing is a popular technique by which layers of the specimen in which compressive residual stresses have been induced can be removed. In order to justify electropolishing, we performed a small study on one of the specimens at two locations far removed from the weld toe; this study was carried out before the specimen had been subjected to any loading. To begin the study, the residual stresses at the two spots were measured. The spots were then prepared for strain gage installation. However, no gages were applied. After the necessary sanding was

completed, the residual stresses at these same two spots were measured again. The spots were then electropolished and the residual stress measurements were obtained a third time. After being sanded a second time, the residual stresses at Spots 1 and 2 were measured again. Lastly, the spots were electropolished, and the residual stresses were measured a final time. The results of this study can be seen in Fig. 2.10. Results of the electropolishing study are interpreted in light of the ±50 MPa error bars associated with the technique of x-ray diffraction in the literature (Dupas et al. [1998]). As is made apparent by the graph, sanding did indeed induce significant compressive stresses, ranging in magnitude from 30 to 60 percent of the yield stress, in the surface layers of the stainless steel pipe. The first round of electropolishing relieved the induced compressive stress at Spot 1 remarkably well. However, at Spot 2, the relief of induced stress was slightly overzealous. The settings of the electropolishing process were tweaked, and more consistent results were obtained in the second round of electropolishing. Figure 2.10 illustrates these findings and bears witness to the fact that electropolishing is an efficient means by which residual stresses induced by sanding can be relieved. Electropolishing allowed our research team to obtain residual stress measurements that reflected the effects of fatigue alone—not the effects of strain gage application—on the welding residual stresses.

2.2.4.2 Specimen Mounting

After appropriate preparation, the specimen was mounted on the motorized sample holder as depicted in Fig. 2.11. The specimen was positioned with the spots to be measured at the top surface of the pipe and was secured. The specimen was then properly aligned using a contact probe accurate to ±0.25 mm. Adjustments in the x and y directions were made by moving the sample. The height of the x-ray diffraction equipment itself was adjusted in order to obtain proper alignment in the z direction. The location of all five spots in terms of x and y coordinates was determined and recorded; these points were input into the LabVIEW program used to control the TEC machine remotely so that the process of obtaining axial and circumferential residual stresses at all five spots might be automated. A mounted specimen ready for measurement can be seen in Fig. 2.12.

2.2.4.3 Scanning

A single axis goniometer was employed for stress measurements. In the course of obtaining a single spot measurement, the goniometer performed scans at nine different tilt angles (ψ). During scanning, the goniometer oscillated ±2 degrees about each tilt angle for a specified

amount of time before moving to the next tilt. The duration of scan time for each tilt was either 90 or 180 seconds. In the interest of time, during the day, each scan was limited to 90 seconds. When measurements were set up to run overnight, the scan time was increased to 180 seconds. Specific experimental conditions in addition to those already enumerated are given in Table 2.8.

2.2.4.4 Processing

The data gathered in the measurement process was analyzed with the SaraTEC™ Windows™ software. Stresses were calculated using the "$\sin^2\psi$" technique assuming a biaxial state of stress. An explanation of this technique is not included here but can be found in *Residual Stress Measurement by Diffraction and Interpretation* (Noyan and Cohen [1987]).

2.3 Fatigue Experiment Setup

Welded piping specimens were fatigue tested in a cantilever setup as depicted in Fig. 2.13. In each test, the end flange of the specimen was bolted to the heavy, stiff support column, which was securely fastened to the T-slot table of the testing machine. As the figure portrays, the weld joint was located near the support column. Fatigue loading cycles were applied at the end of the pipe specimen opposite the support column. Prescribed loading was transmitted to the pipe end via the actuator of a servo-hydraulic testing machine through a pin-end fixture assembly. This assembly can also be seen in Fig. 2.13. One SS 304L end fixture was screwed onto the actuator rod of the testing machine while the other end fixture was welded to the pipe specimen. A pin at the bottom of the pin-end assembly snuggly fitted to a self-aligning ball bearing was tightly attached to the end fixture atop the actuator. A similar pin-ball-bearing system attached the pin-end assembly to the end fixture that had been welded to the pipe specimen. Small access holes were machined into the end flange and welded end fixture of each specimen. During the final stage of fatigue testing, each piping specimen was filled with oil using the access holes, and a small internal pressure was applied using a pneumatic pump. The pressurized oil allowed for immediate detection of through-wall cracks in the course of the fatigue test. The test setup described herein was developed by Kevin Wilkins, Vernon Matzen, and Tasnim Hassan.

Four of the six fatigue tests were carried out by prescribing a displacement-controlled saw tooth loading cycle with predetermined amplitude. Three specimens, BW2, SW5, and SW7, were subjected to displacement amplitude of 14 mm while the fourth specimen, SW8, endured displacement amplitude of 10 mm. In the remaining two tests, a force-controlled saw tooth

loading cycle with amplitude of 3.5 kN was prescribed. The prescribed loading cycle for all specimens can be seen in Fig. 2.14 through 2.16. As was previously mentioned, a small internal hydraulic pressure—approximately 100 psi (0.69 MPa)—was applied to each specimen. This allowed for immediate detection of through-wall fatigue cracks. This applied internal pressure did induce a small axial stress of 0.89 MPa and circumferential stress of 1.77 MPa. As these stresses were approximately 0.25 and 0.50 percent of the yield stress, respectively, no significant influence on recorded ratcheting behavior is attributed to the internal pressure. The cycle number at which through-wall cracks occurred was recorded in each test. In addition, the weld toe area of each specimen was closely visually monitored for fatigue crack initiation throughout the fatigue test. The number of cycles at which fatigue crack initiation was observed was also recorded.

In all of the fatigue tests carried out, the displacement, force, and strain at various locations on the pipe specimen were measured. These measurements were digitized and stored every 0.032 second using a LabVIEW data acquisition program developed by Glen Wheeler and Shafiqul Bari. Three different types of strain gages were used in the fatigue tests. Tables 2.9 through 2.14 contain information regarding the types and locations of all strain gages used in the fatigue experiments.

Table 2.1 Overview of welded specimen experiments

	Specimen Name	Joint Type	Number of Weld Passes	Sequence of Welding	Fatigue Loading Type	σ_R at N
LU	BW1	Butt	2	Quarter	δ	-----
	SW1	Socket	3	Quarter	δ	-----
	SW2	Socket	4	Quarter	δ	-----
	SW3	Socket	4	Full	δ	-----
	SW4	Socket	5	Quarter	δ	-----
HUMPHREYS	BW2	Butt	3	Quarter	δ	N = 0 N = 400
	SW5	Socket	3	Quarter	δ	N = 0 N = 400
	SW6	Socket	3	Quarter	P	N = 0 N = 200
	SW7	Socket	3	Quarter	δ	N = 0 N = 160 N = 480
	SW8	Socket	3	Quarter	δ	N = 0
	SW9	Socket	3	Quarter	P	N = 0 N = 100

Table 2.2 Welding parameters measured during welding of socket weld specimen SW5
Welding Batch #3

	Weld Sequence	Current (Amps)	Voltage (Volts)	Start Temp. (°C)	Stop Temp. (°C)	Duration (sec.)	Time Out (sec.)	Weld Bead Length (inch)	Weld Bead Width (inch)	Weld Bead Depth (inch)
Tack Weld	A	100	10	24.3	231.0	27	421	0.341	0.303	0.124
	C	100	10	40.2	294.0	44	303	0.384	0.314	0.152
	B	100	10	69.3	309.0	30	360	0.406	0.340	0.124
	D	100	10	64.6	260.0	25	500	0.411	0.331	0.124
1st Pass	AB	100	10	53.8	306.7	64	401	1.227	0.312	0.125
	CD	100	10	76.0	321.5	85	412	1.205	0.333	0.126
	BC	100	10	111.6	401.0	43	285	1.262	0.367	0.150
	DA	100	10	117.4	385.0	72	1698	1.191	0.370	0.146
2nd Pass	AB	100	10	46.5	276.8	65	475	1.269	0.335	0.075
	CD	100	10	71.8	322.1	53	412	1.217	0.341	0.040
	BC	100	10	79.4	359.0	80	895	1.556	0.359	0.049
	DA	100	10	78.0	320.5	56	634	1.475	0.381	0.050
3rd Pass	AB	100	10	71.0	299.7	62	448	1.137	0.320	0.080
	CD	100	10	83.5	280.5	57	1263	1.120	0.307	0.070
	BC	100	10	54.2	269.9	80	340	1.395	0.360	0.081
	DA	100	10	106.0	263.6	60	DONE	1.300	0.301	0.075

Note: Temperature is measured at the midpoint of the welded length.

Table 2.3 Welding parameters measured during welding of socket weld specimen SW6
Welding Batch #1

	Weld Sequence	Current (Amps)	Voltage (Volts)	Start Temp. (°C)	Stop Temp. (°C)	Duration (sec.)	Time Out (sec.)	Weld Bead Length (inch)	Weld Bead Width (inch)	Weld Bead Depth (inch)
Tack Weld	A	100	10	30.1	280.0	40	260	0.350	0.281	0.127
	C	100	10	58.0	295.0	36	204	0.378	0.330	0.092
	B	100	10	79.2	184.0	34	206	0.442	0.330	0.126
	D	100	10	91.3	296.0	33	627	0.352	0.340	0.145
1st Pass	AB	100	10	55.0	409.0	95	375	1.164	0.341	0.120
	CD	100	10	98.0	362.6	70	420	1.062	0.352	0.139
	BC	100	10	90.5	452.0	92	388	1.208	0.357	0.130
	DA	100	10	100.8	308.8	84	1326	1.208	0.363	0.110
2nd Pass	AB	100	10	58.0	330.9	71	454	1.430	0.384	0.054
	CD	100	10	85.8	316.4	50	340	1.324	0.348	0.065
	BC	100	10	100.1	447.0	75	300	1.496	0.394	0.052
	DA	100	10	124.0	367.6	60	2325	1.400	0.378	0.053
3rd Pass	AB	100	10	49.8	275.0	68	637	1.233	0.317	0.060
	CD	100	10	66.9	296.9	60	390	1.090	0.345	0.083
	BC	100	10	85.7	308.3	60	330	1.300	0.320	0.061
	DA	100	10	116.8	311.0	55	DONE	1.239	0.344	0.071

Note: Temperature is measured at the midpoint of the welded length.

Table 2.4 Welding parameters measured during welding of socket weld specimen SW7
Welding Batch #4

	Weld Sequence	Current (Amps)	Voltage (Volts)	Start Temp. (°C)	Stop Temp. (°C)	Duration (sec.)	Time Out (sec.)	Weld Bead Length (inch)	Weld Bead Width (inch)	Weld Bead Depth (inch)
Tack Weld	A	100	10	35.0	194.0	20	265	0.325	0.323	0.142
	C	100	10	51.5	243.7	29	241	0.318	0.302	0.122
	B	100	10	68.5	282.0	26	289	0.356	0.299	0.133
	D	100	10	70.0	257.4	23	562	0.390	0.356	0.133
1st Pass	AB	100	10	55.7	307.2	52	323	1.172	0.315	0.125
	CD	100	10	91.6	365.0	72	333	1.145	0.290	0.133
	BC	100	10	109.9	319.0	54	321	1.139	0.342	0.124
	DA	100	10	103.6	351.2	64	1121	1.238	0.343	0.132
2nd Pass	AB	100	10	55.0	325.0	58	377	1.273	0.370	0.055
	CD	100	10	90.0	373.7	65	340	1.303	0.362	0.057
	BC	100	10	112.6	355.3	62	313	1.390	0.386	0.068
	DA	100	10	123.5	331.6	69	1491	1.503	0.369	0.042
3rd Pass	AB	100	10	55.4	291.2	62	823	1.200	0.355	0.070
	CD	100	10	60.6	315.2	65	550	1.132	0.340	0.050
	BC	100	10	77.2	338.0	59	1576	1.215	0.332	0.055
	DA	100	10	50.4	274.3	72	DONE	1.540	0.338	0.065

Note: Temperature is measured at the midpoint of the welded length.

Table 2.5 Welding parameters measured during welding of socket weld specimen SW8
Welding Batch #4

	Weld Sequence	Current (Amps)	Voltage (Volts)	Start Temp. (°C)	Stop Temp. (°C)	Duration (sec.)	Time Out (sec.)	Weld Bead Length (inch)	Weld Bead Width (inch)	Weld Bead Depth (inch)
Tack Weld	A	100	10	22.7	182.8	23	427	0.339	0.318	0.122
	C	100	10	38.2	271.2	31	409	0.249	0.285	0.119
	B	100	10	46.8	277.2	38	272	0.376	0.299	0.128
	D	100	10	69.2	300.0	29	661	0.359	0.340	0.114
1st Pass	AB	100	10	46.7	267.5	50	340	0.916	0.313	0.104
	CD	100	10	7.1	353.0	76	464	1.205	0.324	0.117
	BC	100	10	79.8	370.0	75	315	1.300	0.348	0.113
	DA	100	10	108.3	352.0	57	663	1.173	0.329	0.120
2nd Pass	AB	100	10	71.2	333.5	62	478	1.460	0.369	0.048
	CD	100	10	96.2	320.0	60	570	1.438	0.343	0.057
	BC	100	10	79.2	344.4	53	337	1.188	0.326	0.060
	DA	100	10	101.3	357.7	63	1227	1.205	0.382	0.057
3rd Pass	AB	100	10	59.5	295.2	60	510	1.284	0.340	0.060
	CD	100	10	78.4	305.2	77	493	1.215	0.331	0.052
	BC	100	10	92.3	301.2	60	300	1.254	0.360	0.063
	DA	100	10	119.3	281.0	42	DONE	1.279	0.324	0.064

Note: Temperature is measured at the midpoint of the welded length.

Table 2.6 Welding parameters measured during welding of socket weld specimen SW9
Welding Batch #2

	Weld Sequence	Current (Amps)	Voltage (Volts)	Start Temp. (°C)	Stop Temp. (°C)	Duration (sec.)	Time Out (sec.)	Weld Bead Length (inch)	Weld Bead Width (inch)	Weld Bead Depth (inch)
Tack Weld	A	100	10	23.7	201.2	33	282	0.422	0.311	0.126
	C	100	10	52.1	314.0	30	255	0.368	0.295	0.135
	B	100	10	70.5	340.4	38	397	0.437	0.328	0.137
	D	100	10	68.7	306.7	36	624	0.460	0.294	0.102
1st Pass	AB	100	10	53.2	362.0	67	353	1.062	0.305	0.137
	CD	100	10	89.5	368.0	75	465	1.122	0.326	0.133
	BC	100	10	84.2	354.7	75	375	1.332	0.301	0.138
	DA	100	10	101.5	334.9	62	1588	1.342	0.309	0.127
2nd Pass	AB	100	10	51.5	338.0	72	498	1.348	0.345	0.061
	CD	100	10	76.1	344.0	65	460	1.391	0.348	0.049
	BC	100	10	93.9	360.0	11	349	1.561	0.369	0.062
	DA	100	10	112.5	370.1	69	636	1.431	0.403	0.060
3rd Pass	AB	100	10	78.5	330.1	71	364	1.242	0.333	0.072
	CD	100	10	102.3	352.2	65	415	1.130	0.378	0.059
	BC	100	10	106.2	360.4	68	747	1.314	0.321	0.062
	DA	100	10	76.3	330.0	67	DONE	1.388	0.295	0.082

Note: Temperature is measured at the midpoint of the welded length.

Table 2.7 Welding parameters measured during welding of butt weld specimen BW2
Welding Batch #1

	Weld Sequence	Current (Amps)	Voltage (Volts)	Start Temp. (°C)	Stop Temp. (°C)	Duration (sec.)	Time Out (sec.)	Weld Bead Length (inch)	Weld Bead Width (inch)	Weld Bead Depth (inch)
Tack Weld	A	100	10	32.8	100.0	15	285	0.272	0.201	0.117
	C	100	10	35.9	78.7	9	141	0.284	0.242	0.115
	B	100	10	46.9	98.4	12	123	0.254	0.226	0.095
	D	100	10	49.0	99.6	7	616	0.299	0.214	0.110
1st Pass	AB	100	10	38.0	212.6	82	300	0.808	0.263	0.100
	CD	100	10	65.7	239.0	30	270	0.891	0.225	0.119
	BC	100	10	68.8	203.7	39	336	0.975	0.236	0.112
	DA	100	10	79.8	276.9	35	730	0.940	0.272	0.129
2nd Pass	AB	85	9	51.5	275.0	66	444	0.995	0.278	0.044
	CD	85	9	73.0	243.9	45	465	0.904	0.277	0.050
	BC	85	9	68.0	270.6	30	360	1.023	0.288	0.075
	DA	85	9	70.5	293.9	60	645	1.114	0.302	0.058
3rd Pass	AB	85	9	69.5	316.0	75	540	1.082	0.322	0.063
	CD	85	9	78.5	333.6	60	840	1.172	0.309	0.050
	BC	85	9	66.3	308.0	68	472	1.068	0.330	0.040
	DA	85	9	82.6	303.7	61	DONE	1.129	0.335	0.460

Note: Temperature is measured at the midpoint of the welded length.

Table 2.8 Experimental conditions of the x-ray measurements made on the TEC large specimen stress anlayzer

Parameter	**Condition**
Equipment	TEC Model 1600 x-ray stress analyzer
	Position sensitive detector (PSD), 14° 2θ range
Power	52.5 W; 35 kV; 1.5 mA
Radiation	CrKb
Source to specimen distance	220 mm
Specimen to detector distance	220 mm
Axial tilt angles	0, ±16.40, ±23.50, ±29.20, -34.30, -38.50 (equal steps of $\sin^2\psi$)
Circumferential tilt angles	0, ±16.40, -12.00, 23.50, 29.20, 34.30, 38.00, 42.00 (equal steps of $\sin^2\psi$)

Table 2.9 BW2 strain gage locations and descriptions

BW2	Gage	Description	Location	Distance from Weld Toe (mm)	Type
First Stage of Loading N = 0 to 400	1	Uniaxial	Top	2.09	CEA-06-032UW-120
	2	Biaxial	Bottom	2.40	CEA-06-032WT-120
	3	Uniaxial	Bottom	21.56	CEA-06-032UW-120
	4	Uniaxial	Bottom	39.56	CEA-06-032UW-120
	5	Uniaxial	Bottom	127.00	CEA-06-032UW-120
Second Stage N = 400 to failure	1	Uniaxial	Top	2.37	CEA-06-032UW-120
	2	Uniaxial	Bottom	2.25	CEA-06-032UW-120

Table 2.10 SW5 strain gage locations and descriptions

SW5	Gage	Description	Location	Distance from Weld Toe (mm)	Type
First Stage of Loading N = 0 to 400	1	Biaxial	Top	3.10	CEA-06-032WT-120
	2	Uniaxial	Top	20.04	CEA-06-032UW-120
	3	Uniaxial	Top	39.64	CEA-06-032UW-120
		Uniaxial	Top	127.66	CEA-06-032UW-120
	4	Uniaxial	Bottom	2.88	CEA-06-032UW-120
	5	Uniaxial	Bottom	20.06	CEA-06-032UW-120
		Uniaxial	Bottom	39.65	CEA-06-032UW-120
		Uniaxial	Side 1	2.20	CEA-06-032UW-120
	6	Uniaxial	Side 2	2.83	CEA-06-032UW-120
Second Stage N = 400 to failure	1	Uniaxial	Top	2.54	CEA-06-032UW-120
	2	Uniaxial	Bottom	2.12	CEA-06-032UW-120

Table 2.11 SW6 strain gage locations and descriptions

SW6	Gage	Description	Location	Distance from Weld Toe (mm)	Type
First Stage of Loading N = 0 to 200	1	Uniaxial	Top	2.22	CEA-06-032UW-120
	2	Uniaxial	Bottom	2.36	CEA-06-032UW-120
	3	Uniaxial	Bottom	19.82	CEA-06-032UW-120
	4	Uniaxial	Bottom	39.92	CEA-06-125UN-120
	5	Uniaxial	Bottom	125.40	CEA-06-125UN-120
Second Stage N = 200 to failure	1	Uniaxial	Top	2.15	CEA-06-032UW-120
	2	Uniaxial	Bottom	2.54	CEA-06-032UW-120

Table 2.12 SW7 strain gage locations and descriptions

SW7	Gage	Description	Location	Distance from Weld Toe (mm)	Type
First Stage of Loading N = 0 to 160	1	Uniaxial	Top	3.02	CEA-06-125UN-120
	2	Biaxial	Bottom	4.18	CEA-06-032WT-120
	3	Uniaxial	Bottom	21.00	CEA-06-032UW-120
	4	Uniaxial	Bottom	40.00	CEA-06-125UN-120
	5	Uniaxial	Bottom	128.67	CEA-06-125UN-120
Second Stage N = 160 to 480	1	Uniaxial	Top	2.99	CEA-06-032UW-120
	2	Uniaxial	Bottom	2.85	CEA-06-032UW-120
Third Stage N = 480 to failure	1	Uniaxial	Top	2.65	CEA-06-032UW-120
	2	Uniaxial	Bottom	2.24	CEA-06-032UW-120

Table 2.13 SW8 strain gage locations and descriptions

SW8	Gage	Description	Location	Distance from Weld Toe (mm)	Type
First Stage of Loading N = 0 to failure	1	Biaxial	Top	3.14	CEA-06-032WT-120
	2	Uniaxial	Top	20.40	CEA-06-032UW-120
	3	Uniaxial	Top	39.68	CEA-06-125UN-120
	4	Uniaxial	Top	126.45	CEA-06-125UN-120
	5	Uniaxial	Bottom	2.33	CEA-06-125UN-120

Table 2.14 SW9 strain gage locations and descriptions

SW9	Gage	Description	Location	Distance from Weld Toe (mm)	Type
First Stage of Loading N = 0 to 100	1	Uniaxial	Top	3.04	CEA-06-032UW-120
	2	Biaxial	Bottom	21.18	CEA-06-032WT-120
	3	Uniaxial	Bottom	39.86	CEA-06-032UW-120
	4	Uniaxial	Bottom	126.80	CEA-06-125UN-120
	5	Uniaxial	Bottom	2.72	CEA-06-125UN-120
Second Stage N = 100 to failure	1	Uniaxial	Top	2.34	CEA-06-032UW-120
	2	Uniaxial	Bottom	2.93	CEA-06-032UW-120

Figure 2.1 Socket-welded piping specimen

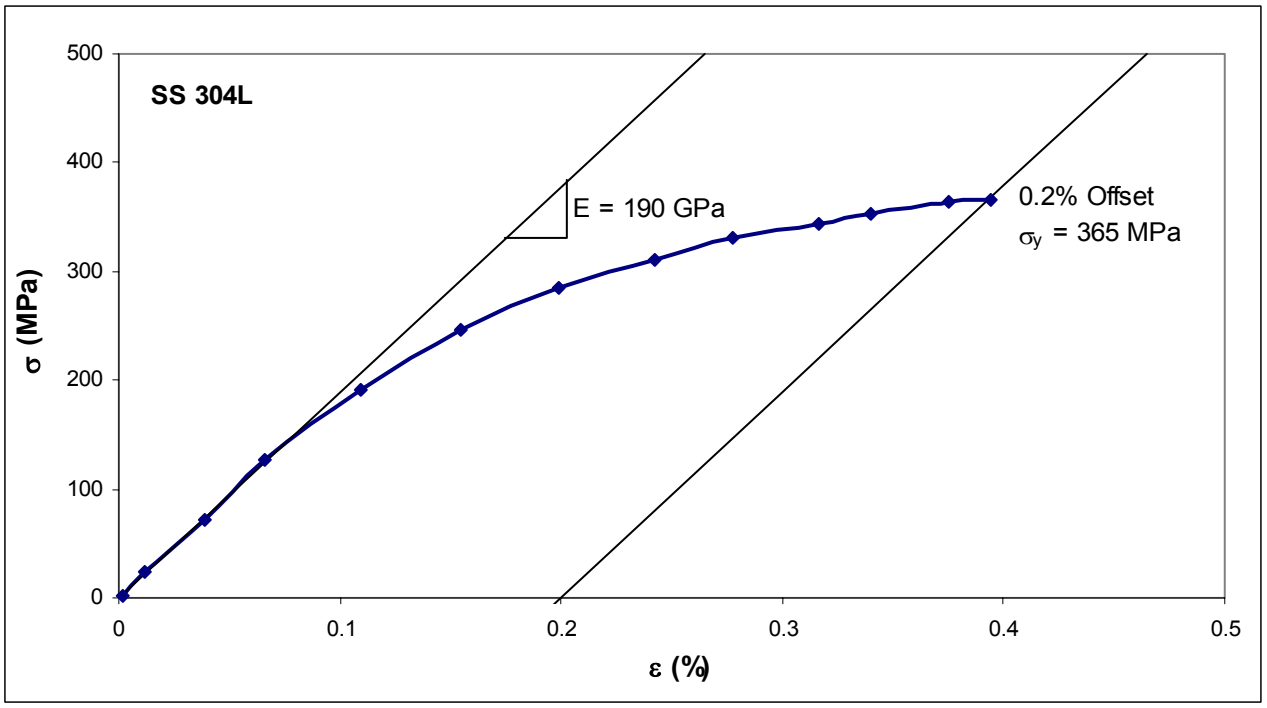

Figure 2.2 Monotonic curve from multi-step strain-controlled material test

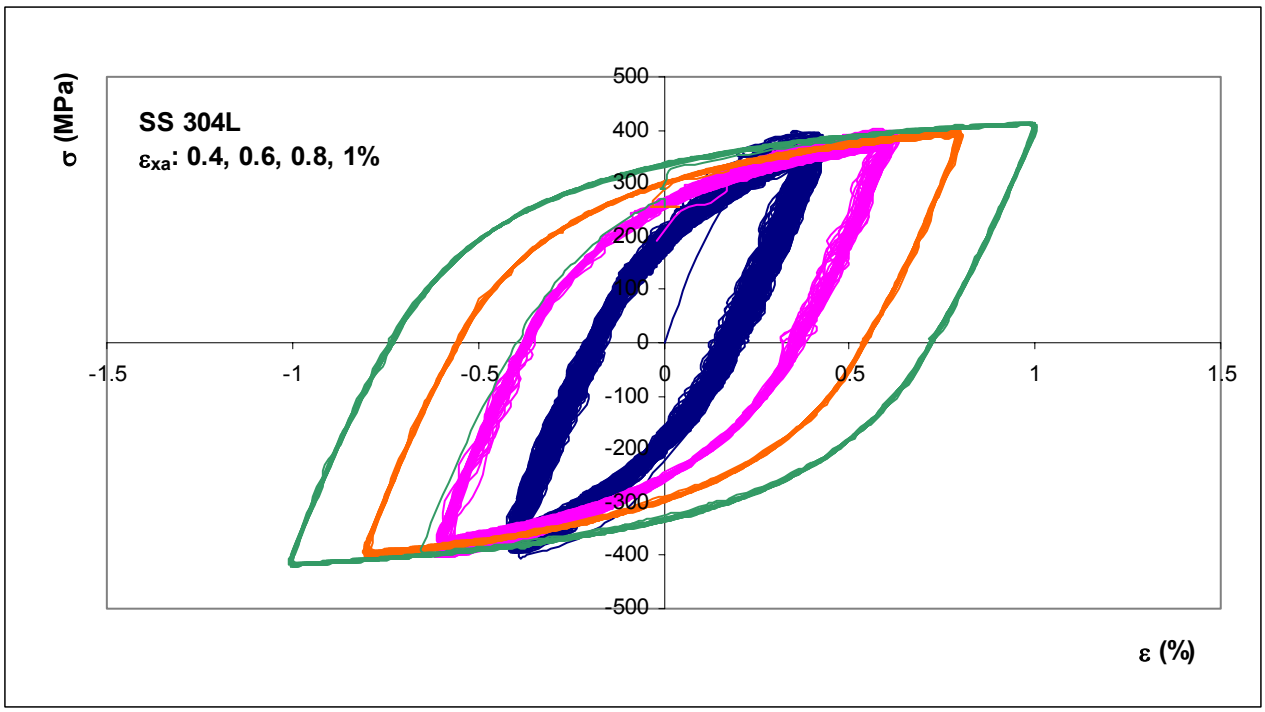

Figure 2.3 Stress-strain behavior of material specimen in four-step strain-controlled test

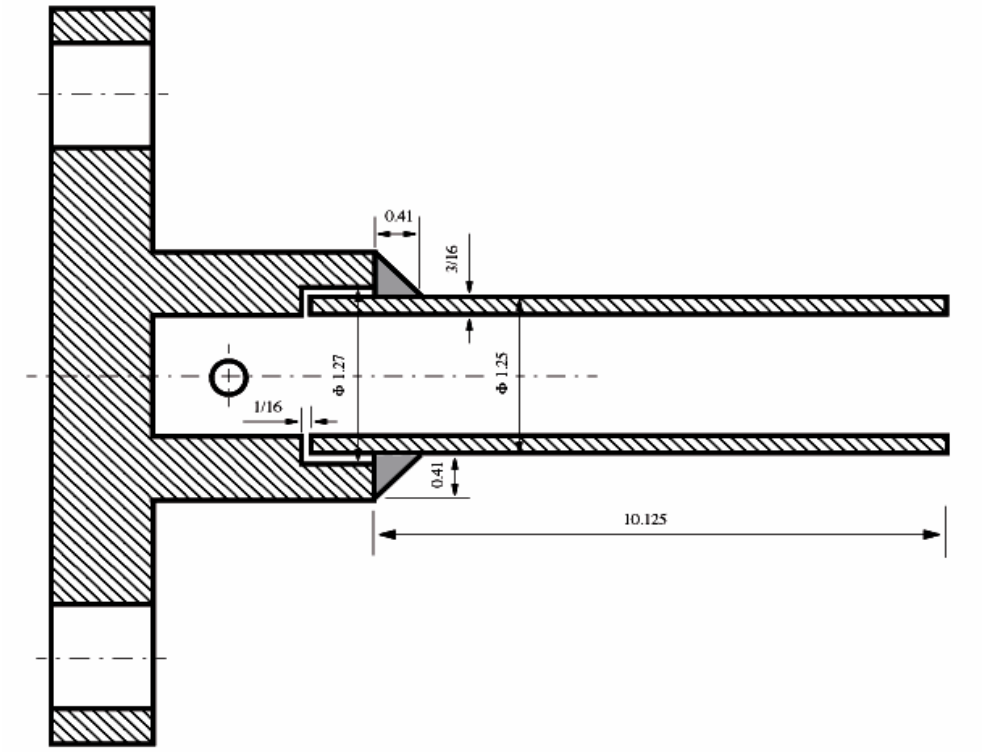

Figure 2.4 Geometry of socket-welded specimen (1 in = 25.4 mm) (Lu [2003])

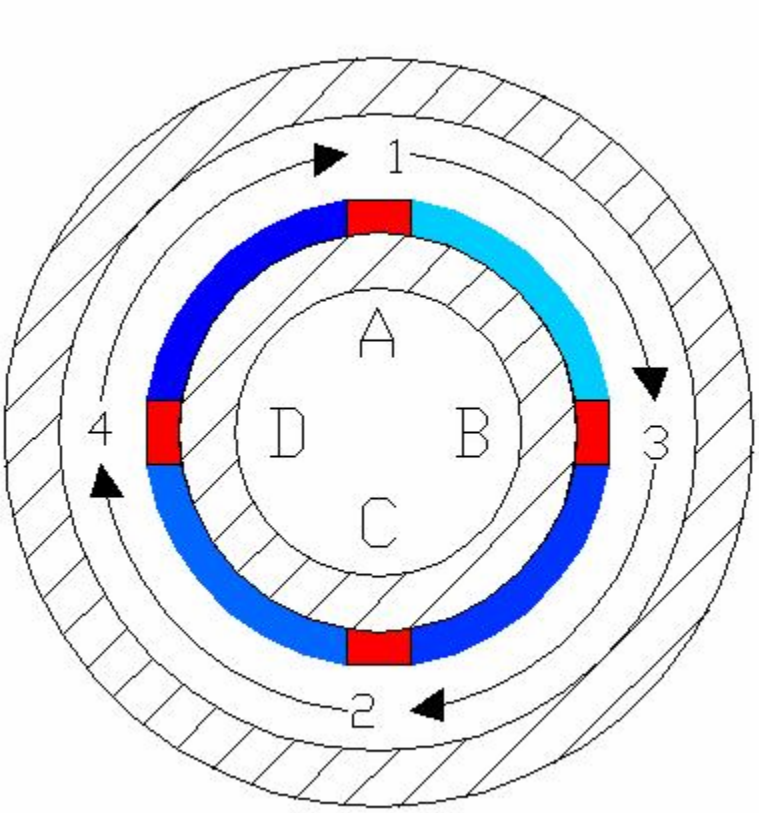

Figure 2.5 Tack welds and quarter circumferential welding illustration

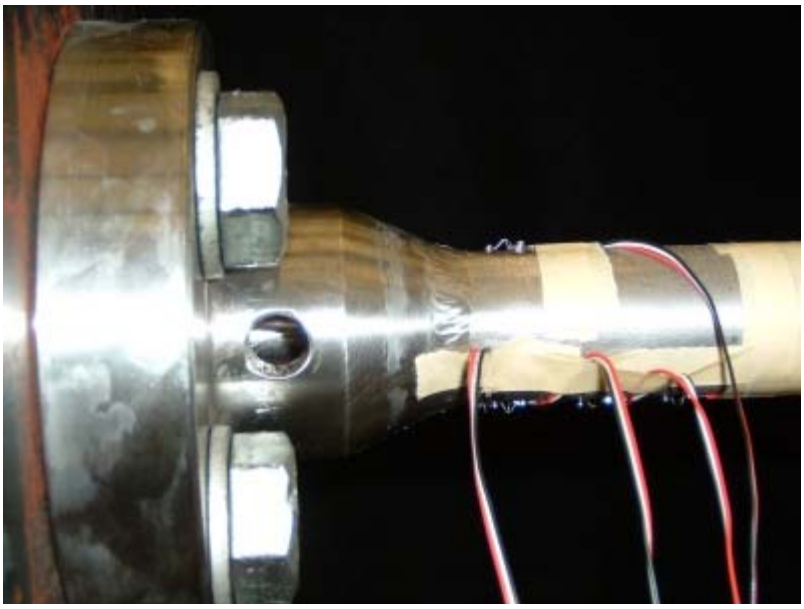

Figure 2.6 Butt-welded piping specimen

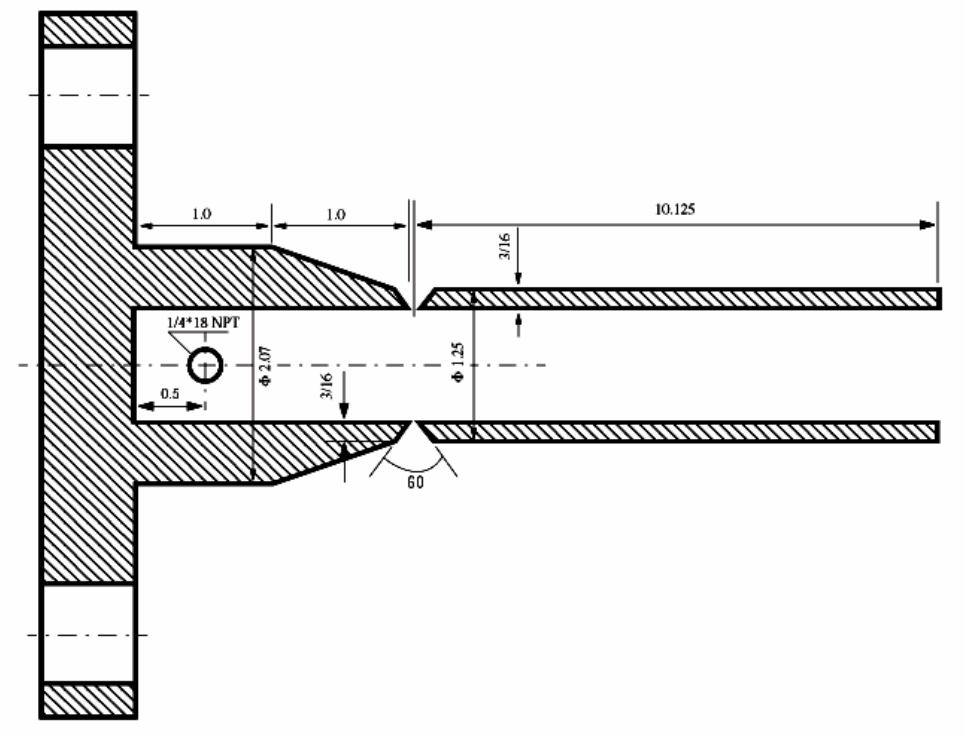

Figure 2.7 Geometry of butt-welded specimen (1 in = 25.4 mm) (Lu [2003])

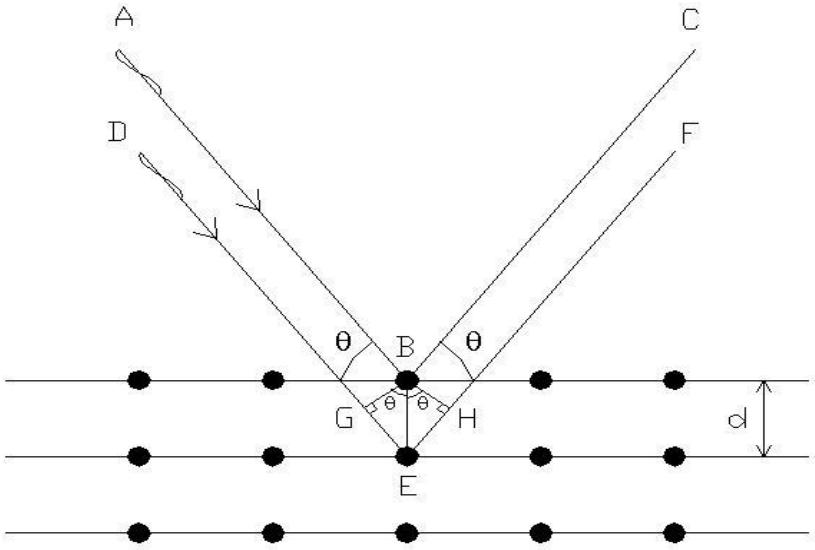

Figure 2.8 X-rays impinging upon atomic planes

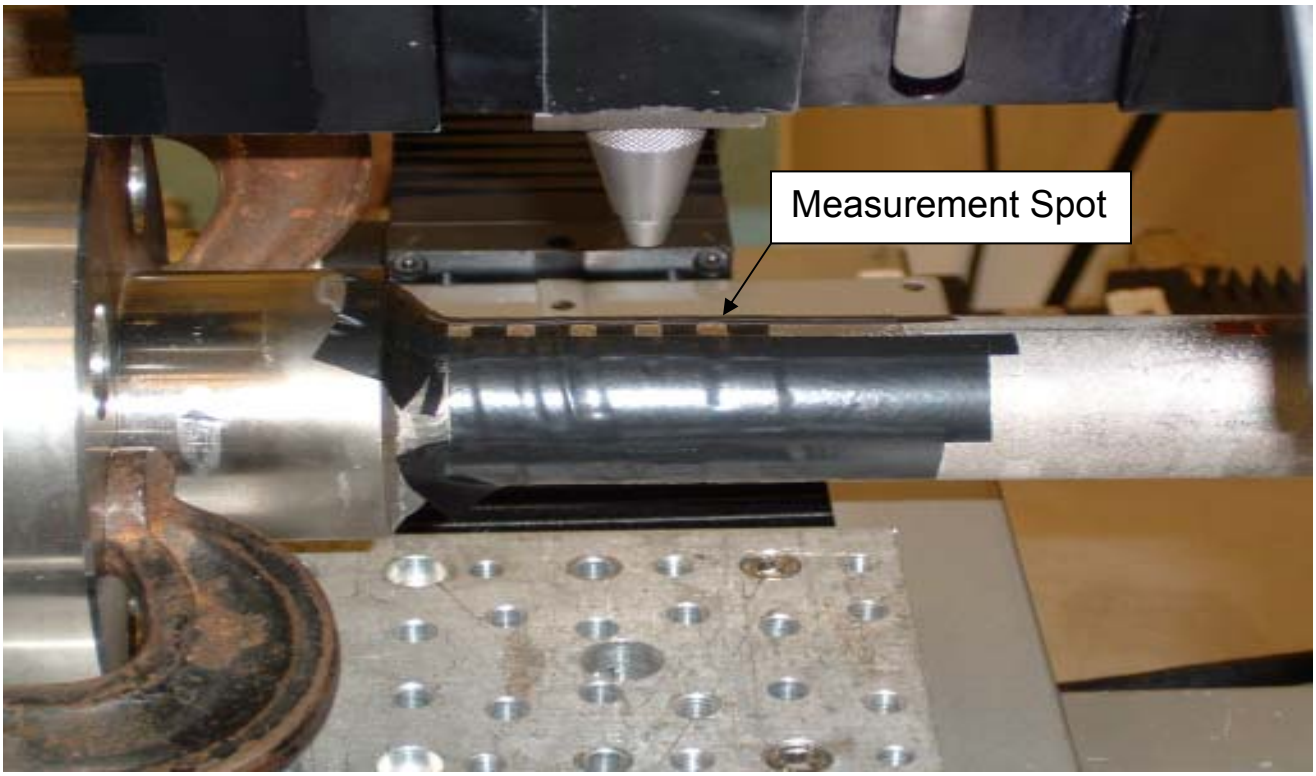

Figure 2.9 Example of electrical tape mask applied to all specimens

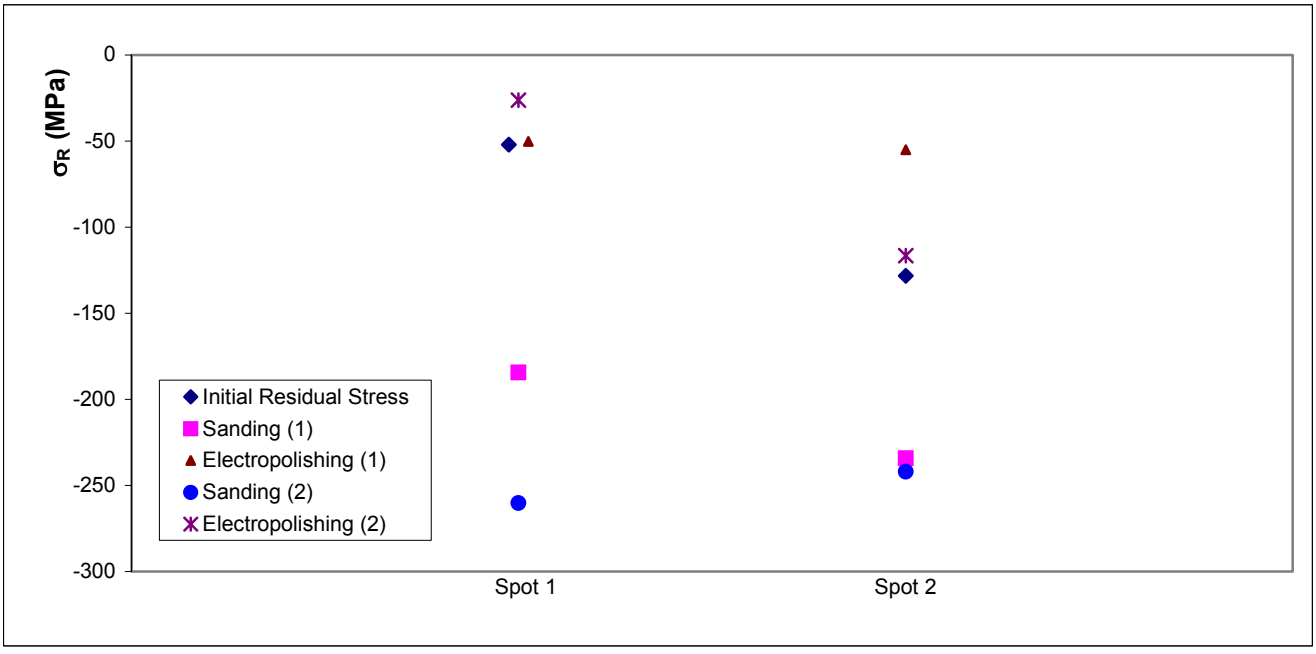

Figure 2.10 Electropolishing Study

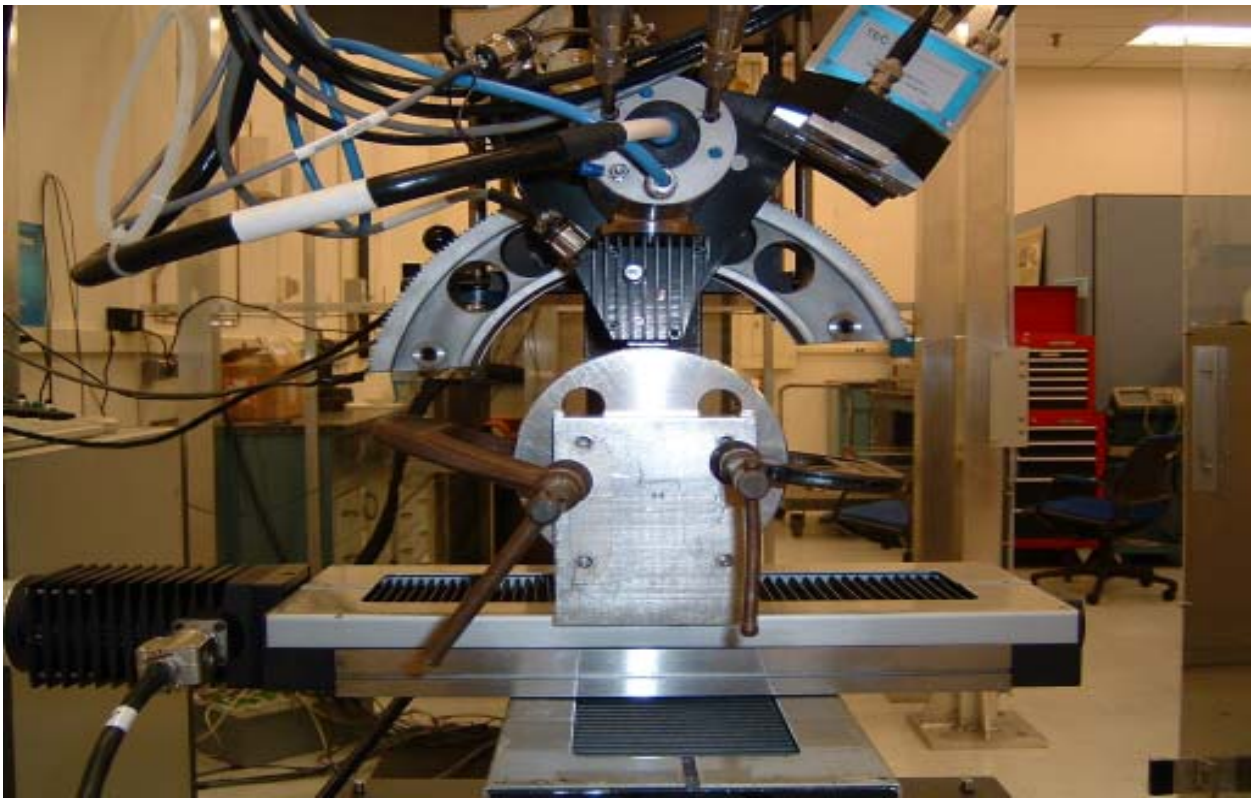

Figure 2.11 Motorized sample holder and secured specimen

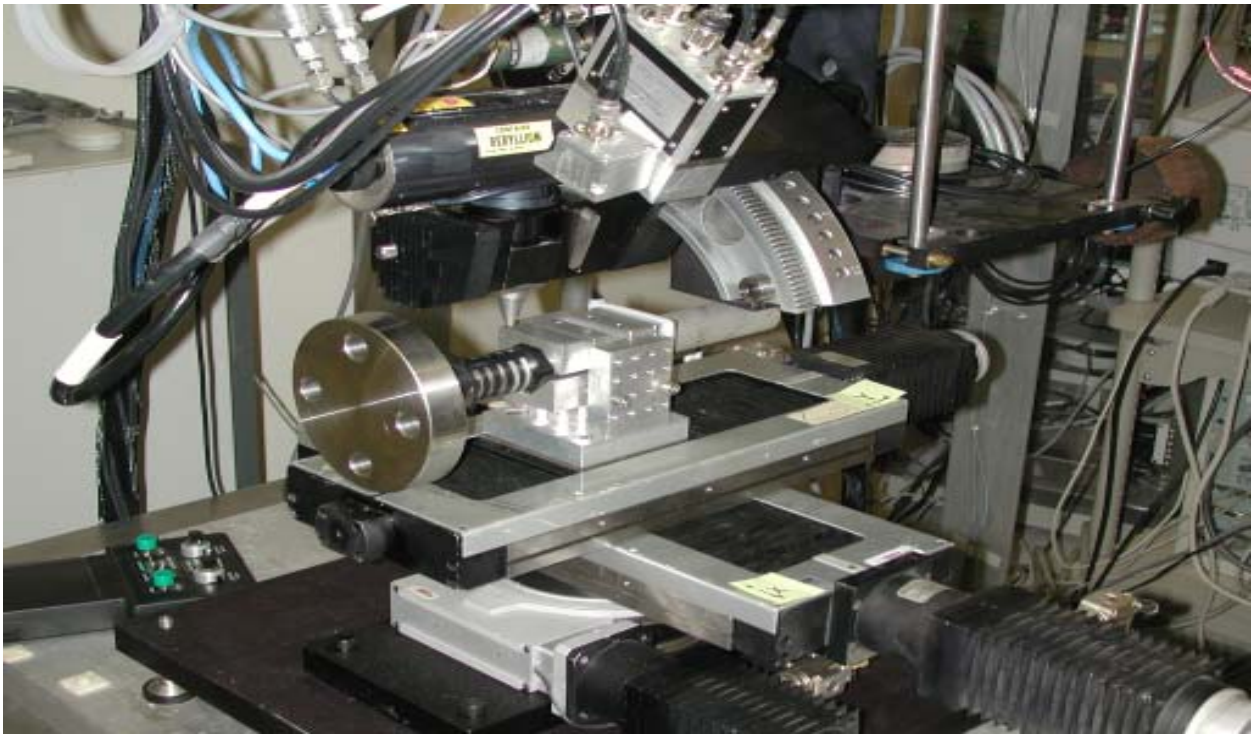

Figure 2.12 Mounted specimen ready for measurement

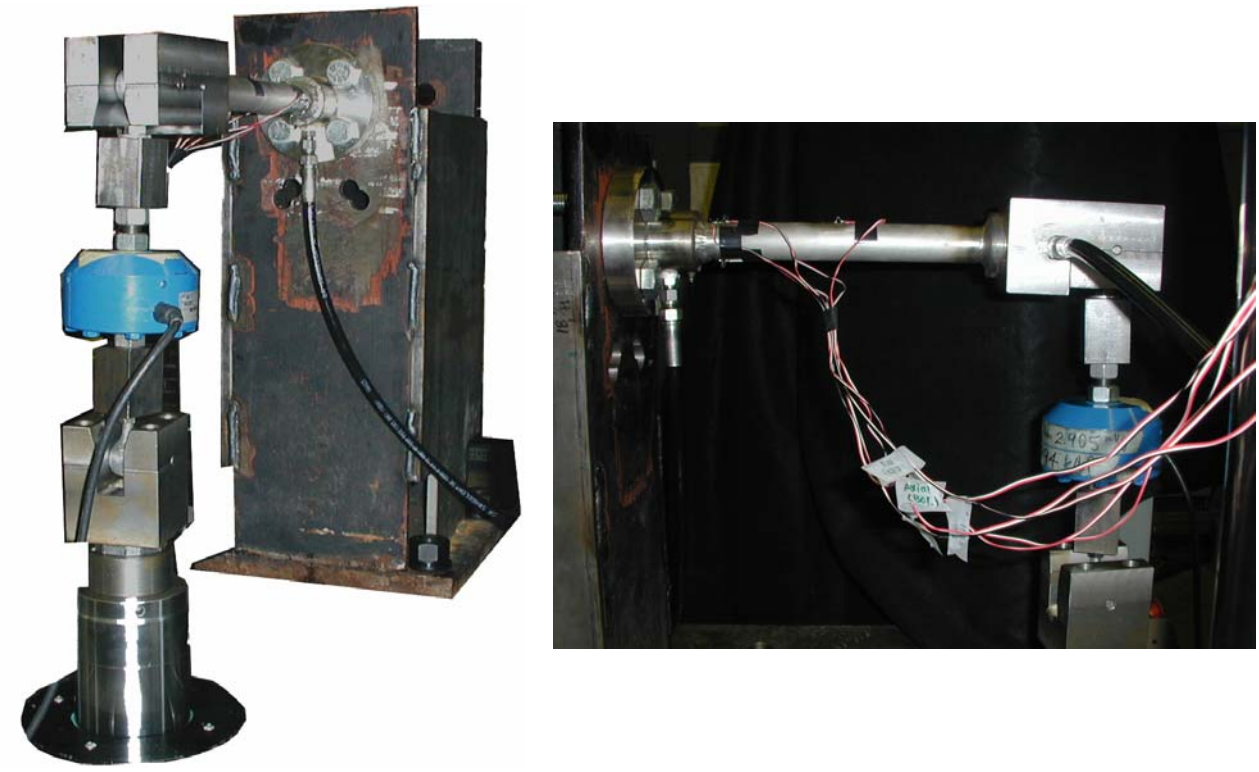

Figure 2.13 Cantilever setup (two views) for welded specimen fatigue testing (Lu [2003])

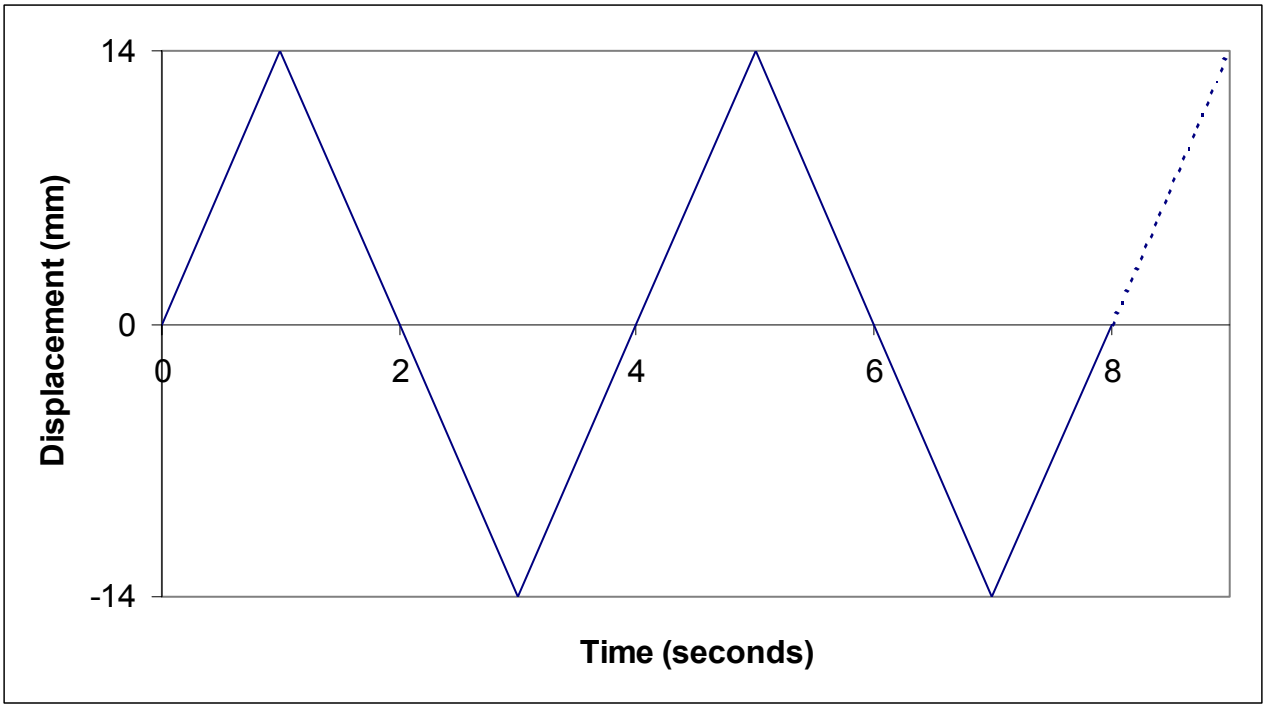

Figure 2.14 Prescribed displacement-controlled loading for BW2, SW5, and SW7 fatigue tests

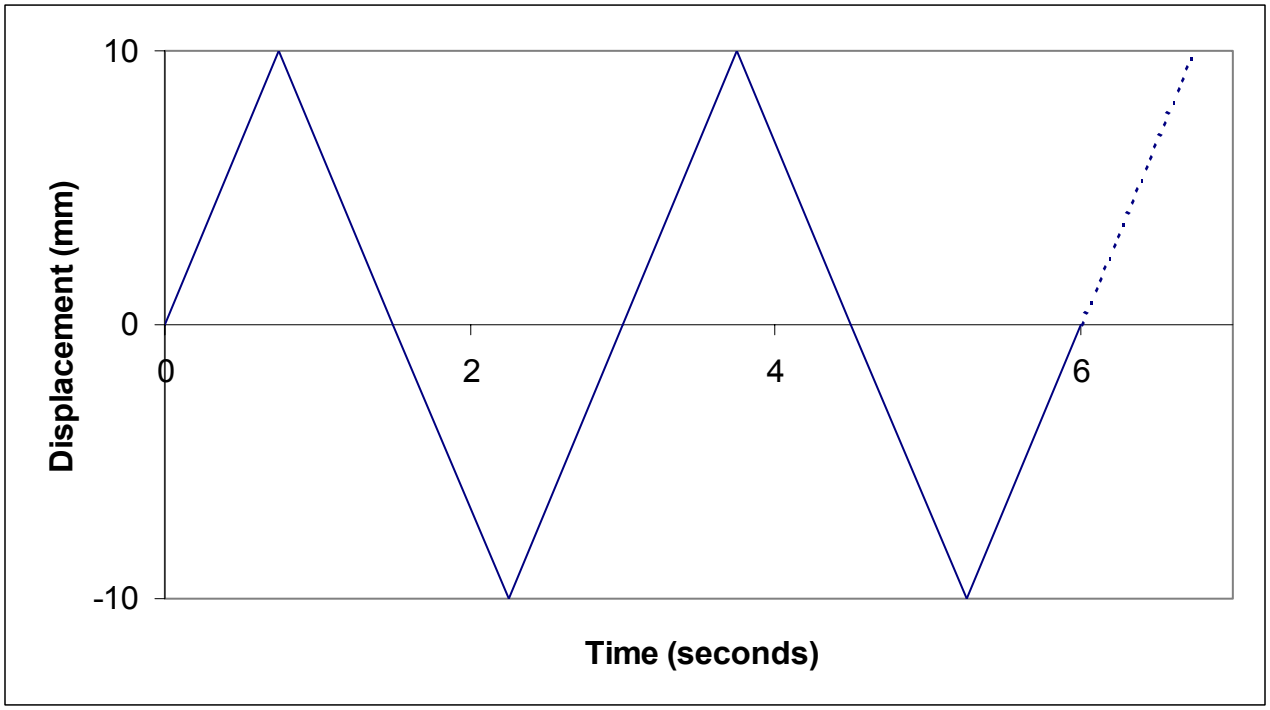

Figure 2.15 Prescribed displacement-controlled loading for SW8 fatigue test

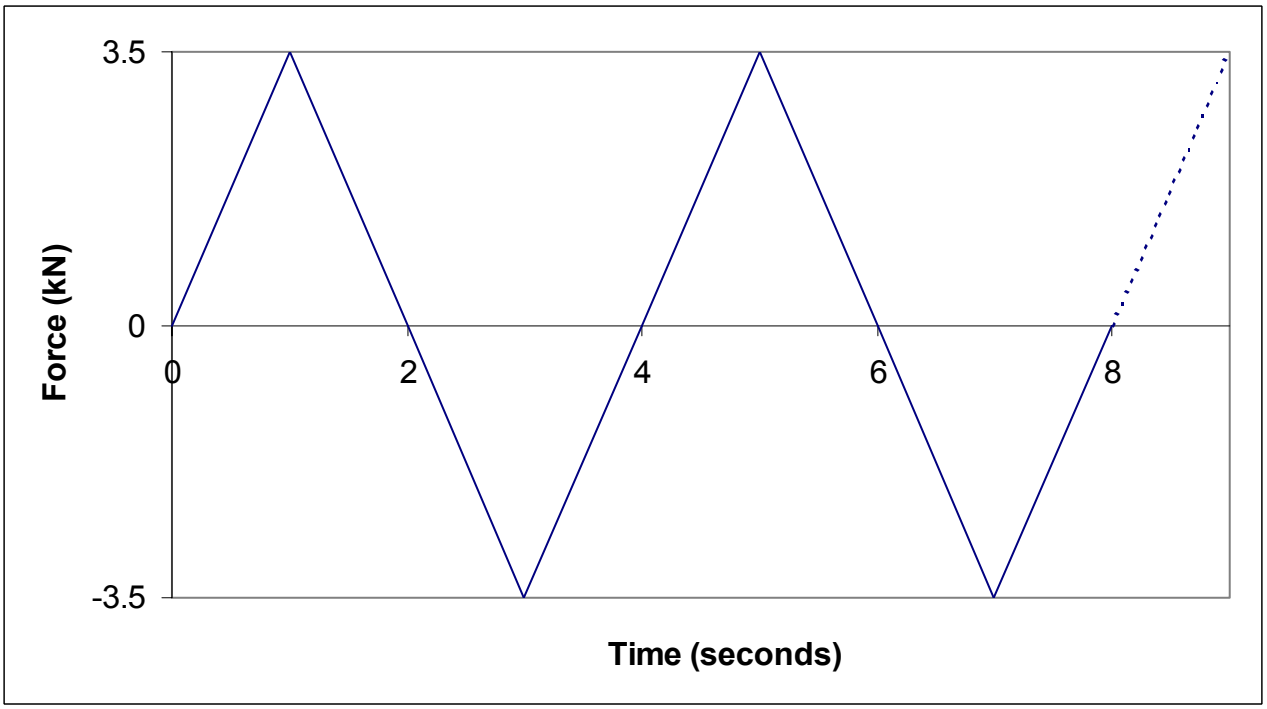

Figure 2.16 Prescribed force-controlled loading for SW6 and SW9 fatigue tests

CHAPTER 3
EXPERIMENTAL RESULTS

3.1 Residual Stress Measurements

In order to discuss the residual stresses measured in the six piping specimens and the effect of fatigue loading on these residual stresses, the following approach is utilized. First, the results from socket-welded specimen SW7 are presented. As was discussed in the second chapter, residual stresses were measured at five spots along the location of maximum strain cycling (top of the pipe) and at five spots along the location of minimum strain cycling (side of the pipe) during fatigue loading (see Fig. 2.9). The residual stresses before and after the first and second stages of fatigue loading at these spots in this specimen are described. Specimen SW7 was loaded in fatigue in three stages but was the only piping specimen subjected to this schedule of testing. The other five specimens were loaded to a single intermediate point in the fatigue life and then fatigued to failure. A reproducibility study was carried out on this specimen when residual stresses were measured for the second time. Through examination of the results of this study, error bars for properly interpreting residual stress measurements are established and presented. Following the error bar discussion, the results from all welded piping specimens are combined, and trends are identified. It should be noted here that measurements obtained from Specimen SW8 are not included in the combinations. Specimen SW8 failed in the first stage of fatigue loading; consequently, no residual stress measurements at an intermediate point in the fatigue life of this specimen could be obtained.

3.1.1 Residual Stress Results for Socket-Welded Specimen SW7

3.1.1.1 Axial Residual Stress at Location of Maximum Strain Cycling

Residual stresses measured prior to fatigue loading as well as following each of the first two stages of loading at the location of maximum strain cycling in the axial direction can be seen in Fig. 3.1. The residual stresses in the initial state can be characterized by the following detailed description. At the location of measurement nearest the weld toe, a large compressive residual stress of approximately –400 MPa was measured. Moving away from the weld toe along the surface of the pipe specimen, residual stress in the axial direction increased in magnitude reaching a maximum compressive residual stress of approximately –450 MPa at the position 21 mm away from the weld toe (the third spot.) After reaching this maximum magnitude, the

compressive residual stress decreased quickly and reached a small tensile stress value of 40 MPa at the location of measurement farthest from the weld toe.

Residual stresses in the socket-welded specimen being considered were measured for a second time after the first stage of cyclic loading (160 cycles). The length of the first loading stage, in terms of number of cycles, varied among the welded specimens. The motive behind this variation was to gain insight into the relaxation mechanism and determine how quickly relaxation progresses with fatigue cycles. However, extensive relaxation was observed after even the shortest first loading stage (100 cycles, SW9). Future research should consider much shorter stages of loading, on the order of 5 to 10 cycles, in order to gain understanding of the relaxation mechanism.

In general, relaxation of the axial residual stress at all five locations of measurement occurred during the first stage of fatigue loading of 160 cycles. At the location nearest the weld toe, the residual stress relaxed from approximately –400 MPa to +70 MPa. Over the length of the pipe in which residual stresses were evaluated, the residual stress remained close to zero, fluctuating mildly in both the tensile and compressive directions at different locations. The axial residual stress at the fifth spot, which had been approximately +40 MPa in the initial state, had increased in magnitude to an approximate value of +100 MPa. This was the only location at which the residual stress did not move towards zero during the first stage of fatigue loading.

Residual stresses were measured for a third time in the axial direction at the location of maximum strain cycling after a total of 480 fatigue cycles. Measurements obtained after this second stage of loading were not significantly different from the stresses measured after 160 cycles at any of the five locations. The values of residual stress fluctuated slightly but remained close to zero at the five locations of measurement, staying between ±100 MPa. As the error bars established for interpretation of x-ray diffraction measurements in this study were ±60 MPa (see discussion in Section 3.1.1.5), it was concluded that the extent of relaxation experienced by the axial residual stresses at the location of maximum strain cycling was entirely achieved during the first stage of fatigue loading.

3.1.1.2 Circumferential Residual Stress at Location of Maximum Strain Cycling

In a similar fashion to the trend exhibited by the initial residual stresses in the axial direction, the initial residual stresses in the circumferential direction were highly compressive near the weld toe and tended towards zero as distance from the weld toe increased (Fig. 3.2).

The highest compressive residual stress in the circumferential direction, -530 MPa, was found at the location of measurement nearest the weld toe. Again, a tensile residual stress was measured at the spot farthest from the weld toe. The value of this residual stress was approximately +90 MPa. The residual stresses in the circumferential direction at the location of maximum strain cycling prior to and following the first and second stages of fatigue loading can be seen in Fig. 3.2.

Relaxation of the residual stresses in the circumferential direction after the first stage of fatigue loading was obvious. The residual stress at all five locations of measurement moved towards zero, including the tensile residual stress at the location furthest from the weld toe. All residual stress measurements after the first stage of loading were between –100 MPa and zero.

Analogous to the residual stress measurements in the axial direction obtained after the second stage of fatigue loading, the residual stresses in the circumferential direction exhibited no significant differences from the measurements obtained after the first stage of fatigue loading. Residual stresses measured after the second fatigue loading were within 50 MPa of the first fatigue loading measurements at each of the five measurement locations. Again, complete relaxation of residual stresses at the location of maximum strain cycling was accomplished in the first stage of fatigue loading.

3.1.1.3 Axial Residual Stress at Location of Minimum Strain Cycling

The residual stress trends at the location of minimum strain cycling in the axial direction at all pertinent stages of fatigue loading can be seen in Fig. 3.3. In stark contrast to the residual stresses measured at the weld toe at the location of maximum strain cycling, the residual stress in the axial direction measured at the spot nearest the weld toe was found to be tensile with a value of approximately +70 MPa. The residual stress moved in the compressive direction and reached a maximum compressive value of –460 MPa at the spot 21 mm from the weld toe. After reaching this maximum, the residual stresses tended back towards zero over the remaining two measurement locations. The residual stress at the last spot was found to be –50 MPa.

After the first stage of fatigue loading, the residual stress in the axial direction at the location nearest the weld toe relaxed from the tensile region into the compressive realm. Moving along the surface of the pipe specimen to the third location of measurement, the residual stress appeared to have relaxed slightly and started to migrate towards zero. At the fourth and fifth locations of residual stress measurement, the residual stresses barely relaxed. The stresses after

the first stage of fatigue loading followed almost the exact same trend from the third to the fifth spot. In general, only slight relaxation occurred.

Residual stresses measured after the second stage of fatigue loading revealed more relaxation than did the residual stresses measured after the first stage of fatigue loading. However, the complete relaxation of residual stresses observed at the location of maximum strain cycling was not duplicated at this location. The initial trend of the residual stresses over the five locations of measurement was largely maintained.

3.1.1.4 Circumferential Residual Stress at Location of Minimum Strain Cycling

Figure 3.4 depicts the residual stress trends before and after the first two stages of fatigue loading in the circumferential direction at the location of minimum strain cycling. The initial residual stress at the location nearest the weld toe was compressive, having a value of approximately –280 MPa. The residual stress increased in magnitude from the first to the third measurement spot; the maximum compressive residual stress in the circumferential direction was found at the third spot and had a value of –440 MPa. Over the remaining two measurement locations, the residual stresses tended towards zero, arriving at a value of +100 MPa at the final location of measurement.

The behavior of the residual stresses in the circumferential direction after the first stage of fatigue loading is unique among all of the residual stress comparisons recorded in this set of experiments. After the first stage of loading, the residual stresses in the circumferential direction did not exhibit any relaxation. On the contrary, the residual stress at each of the five locations of measurement became more compressive. The trend over the five spots was identical to that in the initial state; the residual stress at each spot was between 100 and 200 MPa more compressive than its initial state counterpart.

The behavior of the residual stresses after the first stage of fatigue loading—that is, increased magnitude of compressive residual stresses—was reversed during the second fatigue loading. The residual stresses at all five spots relaxed. Again, the relaxation exhibited was incomplete. The original trend of the residual stresses in the initial state was maintained after the second stage of fatigue loading.

3.1.1.5 Reproducibility Study

After residual stresses on Specimen SW7 at the location of minimum strain cycling had been measured and recorded, a reproducibility test was conducted in an effort to establish

practical error bars for interpretation of x-ray diffraction residual stress measurement results. As the specimen was already mounted in the x-ray diffraction equipment, it was not disturbed nor was its orientation adjusted before the commencement of the reproducibility test. The test entailed five measurement runs each in the axial and circumferential directions, the results of which can be seen in Figs. 3.5 (axial results) and 3.6 (circumferential results.) The measurement runs were carried out successively, and the same coordinates were used to specify the locations of residual stress measurement in each run in an attempt to minimize variations in conditions between the runs. It can be seen in Figs. 3.5 and 3.6 that the general trends of residual stresses in both the axial and circumferential directions were well maintained in all five runs. This qualitative consistency was higher in the circumferential direction than in the axial direction. Quantitative differences between the maximum and minimum residual stress measurements obtained at each location can be seen in Table 3.1. Lower scatter of results characterizes the circumferential residual stress measurements. The standard deviation at the measurement location where the largest difference between the maximum and minimum residual stress measurements existed was found to be 60 MPa. Therefore, the error bars established for interpretation of x-ray diffraction measurements in this study were ±60 MPa. These error bars were slightly larger than those associated in the literature with the technique of x-ray diffraction, which ranged from ±20 to ±50 MPa (Blom [1995], Dupas et al. [1998], Lu et al [1994]). Error in x-ray diffraction measurements is a combination of statistical error, arising from uncertainty in the absolute intensity of the diffracted beam at any position θ, and instrumental error, arising from specimen alignment and curvature and various other geometrical factors (Noyan and Cohen [1987]).

3.1.2 Initial Residual Stress Trends

It was anticipated that welding residual stress patterns over the five locations of measurement would be similar in all socket-welded specimens and that the butt-welded specimen may exhibit a different residual stress trend due to its different geometry. However, when the residual stress trends for all welded specimens were plotted and compared, no such trends were observed (Figs. 3.7-3.8). Similarities between individual residual stress patterns did exist among specimens populating the same welding batches. These residual stress trends identified in each of the welding batches can be observed in Fig. 3.9-3.16 and are described in the following subsections.

Welding Batch #1 included two specimens, BW2 and SW6 (Figs. 3.9-3.10). Residual stresses were measured at two locations on each specimen, the location of maximum (at the top) and minimum (at the side) strain cycling during fatigue loading. In this first welding batch, a general residual stress pattern was observed over the five measurement locations in both the axial and circumferential directions. Residual stresses were found to be highly compressive at the location of measurement nearest the weld toe. As distance from the weld toe increased, residual stresses decreased and moved in the tensile direction. In both directions and at pertinent locations around the pipe's circumference, the residual stress at the point farthest from the weld toe was very close to zero. More specifically, all measurements obtained at this location in the first welding batch were within ±100 MPa.

Specimen SW9 was the only member of Welding Batch #2 (Figs. 3.11-3.12). Similarities between the first two welding batch residual stress trends exist; however, differences are apparent as well. First of all, the residual stress measured in the axial direction at the side of the pipe at the location of measurement nearest the weld toe was tensile. Of the 24 residual stress measurements obtained near the weld toe, only two were tensile. These two measurements constitute the exceptions to the general rule established in this set of experiments. Also, the specimen in the second welding batch experienced its maximum compressive residual stress at the location of measurement 11.5 mm from the weld toe instead of at the spot closest to the toe. Finally, the residual stresses measured at the spot farthest from the weld toe were not as consistently close to zero as those in the first welding batch.

As was the case in Welding Batch #2, a single specimen made up Welding Batch #3 (Figs. 3.13-3.14). The residual stress pattern in Specimen SW5 over the five locations of measurement was significantly different from the governing patterns of the first two batches. While residual stresses were found to be highly compressive at the location nearest the weld toe as in the previous batches, they did not decrease with distance from the weld toe. In the axial direction, a slight tendency in the tensile direction is perceived, but it is not qualitatively or quantitatively similar to the tendencies identified in Welding Batches #1 and #2. No such mild tendency can be identified in the circumferential direction.

Welding Batch #4 consisted of Specimens SW7 and SW8 (Figs. 3.15-3.16). In this batch, the general trend from the first two batches surfaces again. Highly compressive residual stresses were found near the weld toe, and these stresses tended towards zero as the distance

from the weld toe increased. There is evidence of both of the more specific trends from Welding Batches #1 and #2; hence, no statements more specific than the generalization previously stated can be made. In the axial direction, the second exception to the rule that residual stresses near the weld toe are compressive can be seen. The residual stress on Specimen SW7 at the side of the pipe is tensile at the location nearest the weld toe.

3.1.3 Relaxation of Residual Stresses

In order to examine the relaxation of residual stresses with fatigue loading cycles in the six welded piping specimens tested, the results are grouped into two categories: displacement-controlled tests and force-controlled tests.

3.1.3.1 Displacement-Controlled Tests

As was the case in the discussion of residual stress relaxation in Specimen SW7 at the beginning of Chapter 3, the residual stress relaxation results from all specimens subjected to displacement-controlled fatigue testing are broken down further into subgroups. First, the relaxation of residual stresses in the axial direction at the pipe location corresponding to maximum strain cycling is considered. The residual stresses at this location at an intermediate point in the fatigue lives of Specimens BW2, SW5, and SW7 can be seen in Fig. 3.17. In this figure, complete relaxation of residual stresses is depicted. While the residual stresses fluctuate about zero, the measurements at all five spots on all three specimens are approximately within the error bars of ±60 MPa. The completeness of the relaxation in this case is attributed to the following: the amplitude of strain cycling experienced by the material at this location was large, varying between 0.5 percent and 0.8 percent in the three specimens. The magnitude of the strain amplitude was a product of location (top of pipe) and direction (axial) of measurement. In Fig. 3.18, it is illustrated that strain amplitude experienced on Specimen SW5 at the top surface of the pipe in both directions is larger than that experienced at the side of the pipe. In addition, the figure shows that amplitude of strain in the axial direction at both locations exceeds the amplitude of strain experienced in the circumferential direction at both locations.

In Figure 3.19, the residual stresses at the location of maximum strain cycling in the circumferential direction are presented. Again, the residual stress trends have flattened out over the five measurement locations; extensive relaxation has taken place. Like the residual stress patterns at the same location in the axial direction, circumferential residual stresses fluctuate mildly over the length of the pipe in which measurements were obtained. However, this

fluctuation is about a slightly negative center. This observation lends additional credence to the theory that the extent of relaxation experienced is dependent upon strain amplitude. Due to the manner of loading in these fatigue experiments, the axial strain cycle experienced was much greater in amplitude than the circumferential strain cycle at the same pipe location (see Fig. 3.18).

Moving to the location on the pipe specimen of minimum strain cycling, the axial residual stress relaxation is first examined. In Fig. 3.20, it is clear that relaxation has occurred. However, it is also apparent that the relaxation is incomplete. The flattened trend shapes have not been achieved. Evidence of the initial residual stress patterns in the three specimens remains. In all three specimens, near complete relaxation was accomplished at the location of measurement nearest the weld toe. At this location, the residual stresses were between –100 MPa and zero. However, as distance from the weld toe increases, no such consistency of residual stresses among the three specimens exists. It is concluded that, due to the significantly smaller strain amplitude applied to the side surface of the pipe in fatigue, incomplete relaxation occurred at this location of minimum strain cycling.

In Fig. 3.21, the relaxation of residual stresses in the circumferential direction at the location of minimum strain cycling can be seen. Again, relaxation is incomplete, even more so in the circumferential direction than in the axial direction. Strong evidence of the initial stress patterns remains. Significant relaxation at the location of measurement nearest the weld toe did not take place in the circumferential direction as it did in the axial direction. Of the four measurements considered, the residual stresses in the circumferential direction at the location of minimum strain cycling experienced the least extensive relaxation.

The following general conclusions can be drawn based on the critical examination of residual stress relaxation results detailed previously. *Residual stresses did in fact relax as a result of applied fatigue loading. The amount of relaxation experienced was dependent upon the amplitude of strain cycling endured.*

3.1.3.2 Force-Controlled Tests

Residual stress relaxation results from the two specimens subjected to force-controlled fatigue tests—SW6 and SW9—are presented in Figs. 3.22 through 3.25. The conclusions drawn from the displacement-controlled test results are reinforced by the force-controlled test results. Residual stress relaxation did occur in the first stage of fatigue loading applied to these

specimens. The amount of relaxation sustained was dependent upon the amplitude of strain cycling applied. One noteworthy difference between the results of the two different types of tests was observed. In each of the four measurements, the residual stress patterns from the force-controlled tests were shifted in the tensile direction when compared with the residual stress patterns from the displacement-controlled tests, especially over the last two locations of measurement. However, the same hierarchy of extent of relaxation existed as in the displacement-controlled tests. Maximum relaxation was achieved in the axial direction at the pipe location of maximum strain cycling (Fig. 3.22). Near complete relaxation was observed at the same location in the circumferential direction (Fig. 3.23), while incomplete relaxation occurred in both directions at the location of minimum strain cycling (Figs. 3.24-3.25). Again, the least extensive relaxation took place in the circumferential direction at the location of minimum strain cycling. As Fig. 3.25 conveys, strong evidence of the initial residual stress patterns remains in this case.

3.2 Fatigue Response of Welded Specimens

Fatigue testing of the welded piping specimens was carried out in an attempt to fulfill the primary research objective in its entirety: fatigue response data was gathered from each of the six specimens tested and residual stress relaxation results previously discussed were considered in order to gain understanding as to how residual welding stresses and their relaxation induce strain ratcheting at the welded joints.

3.2.1 Displacement-Controlled Fatigue Tests

3.2.1.1 Fatigue Response of Specimen BW2

The fatigue testing of Specimen BW2 was performed using a cantilever setup (Fig. 3.26); the prescribed saw-tooth fatigue cycle was displacement-controlled (Fig. 3.27). In Fig. 3.28, the recorded force-displacement response of the butt-welded specimen at the loading end is shown; the inelastic nature of the pipe response to the applied loading is made apparent by the hysteresis loops that characterize the force-displacement response. Specimen BW2 was fatigued in two stages. In the second stage of loading, fatigue crack initiation at the bottom surface of the pipe specimen at the weld toe in the circumferential direction was detected after 620 cycles. This cycle number includes the 400 cycles of loading to which the specimen was subjected in its first stage of fatigue. A fatigue crack was initiated at the top pipe surface after 960 cycles. The crack at the bottom surface became through-wall after 1100 cycles. The through-wall crack was

realized when pressurized oil filling the pipe specimen began to leak. At this time, the test was stopped.

The amplitude and mean of the displacement response as a function of cycle number for Specimen BW2 in fatigue can be seen in Fig. 3.29. The amplitude of each fatigue cycle refers to one half of the peak-to-peak range, while the mean refers to the midpoint of the peak-to-peak range. In Fig. 3.29, the two stages of fatigue loading carried out are combined.

In Fig. 3.30, the amplitude and mean of the force response of Specimen BW2 in fatigue can be seen. The two separate stages of loading are distinct from one another. After the first stage of fatigue had been carried out, the pipe specimen was removed from the cantilever setup to facilitate the second round of residual stress measurements. When the specimen was remounted, extreme care was taken to duplicate the testing conditions from the first stage of loading. However, perfect duplication was physically impossible. Variables, such as the tightness of bolted connections and precise orientation of the specimen in the MTS machine setup, could not be matched exactly to the initial conditions. An additional frustration involving the end fixture welded to the pipe specimen was the probable primary source of possible differences between the two sets of testing conditions. Two end fixtures were machined from blocks of SS 304L at the time of fabrication. As six pipe specimens were being tested, each end fixture had to be cut off of its specimen after testing and welded to the next in order that all specimens could be subjected to fatigue before the residual stresses were measured for a second time. Sincere effort was made to maintain the original length of the pipe specimens in the process of removing and rewelding the end fixtures. However, subtle differences were unavoidable. Finally, a small internal pressure was applied to the oil filling the specimen in the final stage of fatigue loading for the purpose of monitoring fatigue cracks. As a result of all of these differences between the testing conditions in the first and second stages of loading, the amplitude and mean of the force response recorded in the second stage of loading for Specimen BW2 do not match up perfectly with those from the first stage, even though the specimen was subjected to the same displacement-controlled cycle in each stage. This incompatibility of response in successive stages of loading can be observed in the results of all welded specimens subjected to multiple stages of loading. In specimens subjected to displacement-controlled loading, this incompatibility exists in the force response; in specimens subjected to force-controlled loading, the incompatibility exists in the displacement response.

From Fig. 3.30, it is observed that cyclic softening occurred in Specimen BW2 during fatigue. The amplitude of the force response decreased with cycles in both stages of loading. This result echoes the surprising finding from Lu [2003]: pipe specimens fatigued in his experiments fabricated from SS 304L pipe with weld material SS 308, like the specimens in this study, were found to soften with cycles in spite of the fact that SS 304L and SS 308 are known to be cyclic hardening materials. Referring to the uniaxial material test conducted on a tubular sample of the SS 304L pipe, neither cyclic softening nor cyclic hardening was observed. Rather, the hysteresis loops convey stable stress-strain behavior (Fig. 3.31). The cause of the cyclic softening response observed in our experiments was not investigated. The softening appears to be occurring at the structural level, as opposed to the material level.

During the first stage of fatigue loading, strain response near the weld toe of Specimen BW2 was monitored by a biaxial strain gage at the bottom pipe surface and a uniaxial strain gage installed in the axial direction at the top surface of the pipe. A uniaxial gage was installed near the midpoint of the pipe length; strain response at this point was of interest as it was assumed that no welding residual stresses had been induced at this distance from the weld toe.

In Figs. 3.32 and 3.33, the amplitude and mean of the axial and circumferential strain responses recorded by the biaxial strain gage at the bottom surface of the pipe can be seen. Partial failure of the axial strain gage occurred after 60 cycles. Between zero and 60 cycles, the strain amplitude remained fairly constant after a slight transition in the first few cycles. The mean strain, however, increased significantly over the first 60 cycles. Increasing mean strain with number of cycles is evidence of positive axial strain ratcheting at the location of the strain gage. The fact that strain ratcheting occurred in displacement-controlled loading is surprising, as it seems kinematically inadmissible. However, this observation reinforced the findings of Lu [2003], who first noted this seeming incompatibility between experimental constraints and recorded strain results. In Fig. 3.33, the amplitude of strain in the circumferential direction remained fairly constant as the number of fatigue cycles increased. Mean strain, however, increased with cycles, which indicates that circumferential strain also ratcheted in the positive direction at the location of the biaxial strain gage. Upon comparing the two figures, it is observed that the axial amplitude of strain at the location being considered was significantly larger than the circumferential strain amplitude. Further, the rate of axial strain ratcheting is much greater than that of the circumferential strain ratcheting. From these two observations, it is

deduced that the rate of strain ratcheting increases with increased amplitude of strain cycles. It is further concluded that the higher amplitude of strain cycles experienced in the axial direction and the resulting larger rate of strain ratcheting mandated that the fatigue crack eventually initiated be in the circumferential direction.

The amplitude and mean of the strain response recorded at the weld toe at the top of Specimen BW2 can be seen in Fig. 3.34. As at the bottom of the specimen in the axial direction, fairly constant strain amplitude was recorded over the life of the strain gage while mean strain increased over the same number of cycles. Again, axial strain ratcheted in the positive direction at nearly the same rate as at the bottom.

Figure 3.35 contains the strain response recorded at the midpoint of the pipe length in the axial direction. As the distance from the point of load application was significantly smaller than in the case of the biaxial gage installed at the weld toe, correspondingly smaller strain amplitude was experienced. Most noteworthy in this figure is the fact that the mean strain at the midpoint did not ratchet. This observation supports the hypothesis of Lu [2003] that residual stresses at the weld toe stimulate strain ratcheting. However, in the previous section, we found that welding residual stresses at the location of maximum strain cycling near the weld toe relaxed completely with application of cyclic loading. Subsequently, the prescribed loading cycle became symmetric. Hence, the reason for the occurrence of ratcheting at the welded joint is a mystery, as many material experiments demonstrate that ratcheting under cyclic loading is induced by the presence of mean or steady stress (Hassan and Kyriakides [1994]). This occurrence of strain ratcheting in the presence of relaxed residual stresses will be further explored in the Chapter 4.

In the second stage of fatigue loading, uniaxial strain gages were installed at the top and bottom pipe surfaces in the axial direction. After data processing, the strain responses at these two locations were combined with the actual and regressionally projected results from the first stage of loading. The amplitude and mean of axial strain experienced at the top pipe surface throughout the entire fatigue test can be seen in Fig. 3.36. In the first stage of fatigue, the strain response was recorded by a uniaxial gage over the first 170 cycles. After this number of cycles, strain gage failure occurred. Thus, the strain amplitude and mean from cycle 170 to 400 are projected; these projected responses are represented by dotted lines in Fig. 3.36. Starting at 400 cycles, the strain response was again recorded by a uniaxial gage with zero initial strain. In combining the results from both stages, the mean strain in the second stage was shifted in the

positive direction in order to account for permanent strains sustained in the first stage of loading.

Figure 3.37 contains the combined strain responses from the first and second stages of fatigue loading at the bottom weld toe. In Figs. 3.36 and 3.37, discontinuities are apparent at the junction of the two stages of fatigue. These discontinuities are not surprising, as differences in testing conditions existed between the first and second stages of fatigue. After the first stage of loading, the specimen was removed from the cantilever setup, the end fixture was removed, and it was rewelded following the second round of residual stress measurements. Moreover, a small internal pressure of 100 psi (0.69 MPa) was applied in the second loading stage in order to detect through-wall cracking. These factors combined to prevent complete consistency of testing conditions between the two stages of fatigue and cause discontinuities in the strain responses. The primary conclusions drawn from Figs. 3.36 and 3.37 reiterate conclusions from Lu [2003] and follow: strain ratcheting continued to occur throughout the fatigue life of Specimen BW2 at both the top and bottom weld toes. The larger rate of axial strain ratcheting recorded at the bottom of the pipe specimen is likely responsible for the first initiation of a fatigue crack and eventual failure at this location.

3.2.1.2 Fatigue Response of Specimen SW5

Specimen SW5 was fatigue tested in the same cantilever setup referred to previously (Fig. 3.26). As was the case with Specimen BW2, Specimen SW5 was subjected to two stages of ±14 mm amplitude displacement-controlled saw-tooth fatigue cycles (Fig. 3.27). Fatigue crack initiation was identified at the weld toe of the bottom pipe surface in the circumferential direction after 610 cycles. A second fatigue crack was detected at the top surface in the same direction after 870 cycles. The fatigue crack at the bottom weld toe propagated through the thickness of the pipe causing ultimate failure after 1050 cycles.

The amplitude and mean of the displacement and force responses are presented in Figs. 3.38 and 3.39. Again, cyclic softening of the stainless steel pipe specimen is obvious in Fig. 3.39.

Strain responses at the top and bottom weld toes as well as at the midpoint of the pipe length from the first stage of fatigue loading are shown in Figs. 3.40-3.43. The results obtained are similar to those from the butt-weld test; they lend support to the observations and conclusions previously stated and reiterated here. Positive axial strain ratcheting was observed at both the top and bottom surfaces of the socket-welded specimen at the weld toe. In addition, positive

ratcheting of the circumferential strain was noted. The strain amplitude in the axial direction at the location of the biaxial gage was much larger than that in the circumferential direction. Consequently, the rate of axial strain ratcheting was significantly larger than the rate of circumferential strain ratcheting. Finally, Fig. 3.43 reveals no ratcheting of axial strains at the midpoint of the pipe length. Again, welding residual stresses are implicated as the ratcheting stimulant at the weld toe.

The strain amplitude and mean for the combined stages of loading at the top and bottom weld toes are shown in Figs. 3.44 and 3.45, respectively. The biaxial gage recording strain response in the first stage of fatigue loading failed after 280 cycles. The amplitude and mean of the strain response from cycle 280 to 400 are projected and are represented in Fig. 3.44 by dotted lines. It is clear from these two figures that axial strain ratcheting at the top and bottom weld toes continued throughout the life of the specimen, even in the second stage of fatigue loading in which strain amplitude decreased. Comparison of the rate of increase of the mean strains at both locations supports the conclusion drawn in the previous discussion: fatigue crack initiation occurs at the location of largest axial strain ratcheting rate. In the case of Specimen SW5, the rate of ratcheting at the weld toe of the bottom pipe surface was higher than the rate of ratcheting at the top. As would be expected, fatigue crack initiation occurred first at the bottom weld toe.

3.2.1.3 Fatigue Response of Specimen SW7

The test setup and displacement-controlled saw-tooth loading cycle from the first two fatigue tests were also employed in the fatigue test of Specimen SW7. However, instead of being subjected to two stages of fatigue loading, Specimen SW7 endured three. In the third stage of loading, the first fatigue crack was detected. The crack initiated at the bottom weld toe in the circumferential direction after 605 cycles; a second fatigue crack was identified at the top weld toe after 715 cycles. In contrast to the first two failures, through-wall crack propagation occurred after 1120 cycles at the top weld toe—the location of the secondary fatigue crack.

Figures 3.46 and 3.47 contain the amplitude and mean of the displacement and force responses. These results mimic those found in the previously described tests and prompt the same observations and conclusions.

The strain responses at the top and bottom weld toes as well as at the midpoint of the pipe length in the first stage of fatigue loading revealed the same behavior of mean strains as did the strain responses of Specimen SW5. Once again, axial and circumferential mean strains at the

weld toe showed evidence of positive ratcheting (Figs. 3.48 and 3.49) while the axial strain at the midpoint of the pipe length did not (not shown).

The strain responses at the top and bottom weld toes in the axial direction from the three stages of loading are combined in Figs. 3.48 and 3.49. From these figures, it is again apparent that strain ratcheting occurs in the axial direction at both the top and bottom weld toes over the entire fatigue life of the specimen. Upon careful examination of the combinations, it can be observed that the rate of axial strain ratcheting at the bottom weld toe in the first stage of loading is nearly identical to that at the top weld toe. However, the rate of ratcheting at the bottom weld toe is larger in both the second and third stages than the rate of ratcheting at the top weld toe. In the same vein as the results from the first two fatigue tests, fatigue crack initiation first occurred at the location of higher strain ratcheting rate. Surprisingly, the through-wall crack occurred at the top weld toe—the location of lower rate of strain ratcheting.

3.2.1.4 Fatigue Response of Specimen SW8

Specimen SW8 was tested in the same cantilever setup as the three preceding pipe specimens. However, the displacement-controlled saw-tooth loading was not the same; the amplitude of applied displacement in the present test was 10 mm while the prescribed amplitude of displacement in the first three tests was 14 mm (Figure 3.50). It was intended that Specimen SW8 be subjected to two stages of loading, as were Specimens BW2 and SW5. However, the specimen failed unexpectedly in the first stage of fatigue after 1710 cycles. Due to the unexpected nature of the failure, the location of the first fatigue crack initiation is not known, nor can the first location of through-wall cracking be identified. When the failure was realized, fatigue cracks had propagated through the pipe thickness at both the top and bottom weld toes.

The amplitude and mean of the displacement and force responses of Specimen SW8 can be seen in Figs. 3.51 and 3.52. As expected, the displacement amplitude was steady over the life of the specimen and zero mean displacement was consistently recorded. In Fig. 3.52, the cyclic softening behavior observed in earlier fatigue tests recurs in this test. A small mean load is observed over the life of the specimen and is attributed to initial anisotropy.

Strain responses from the top and bottom weld toes and at the midpoint of the pipe length are presented in Figs. 3.53-3.56. In Figs. 3.53 and 3.55, it is noted for the first time in displacement-controlled testing that axial strain amplitudes at both weld toes increase with cycles. Due to the smaller prescribed amplitude of displacement cycles, ratcheting rates at both

the top and bottom weld toes in the axial and circumferential directions are not as high as those observed in the tests involving larger amplitude of displacement. Positive axial strain ratcheting is still evident at the weld toes. However, the rate of circumferential strain ratcheting has been reduced nearly to zero. Axial strain at the midpoint of the pipe length did not ratchet over the fatigue life.

From the fatigue response of Specimen SW8, it can again be deduced that positive axial strain ratcheting continued over the entire fatigue life of the specimen. The relationship between amplitude of strain and rate of ratcheting is reinforced as the smaller applied displacement caused smaller amplitude of strain cycles, which in turn resulted in lower strain ratcheting rates. Once again, the absence of ratcheting at a point far removed from the weld toe supports the hypothesis that welding residual stresses are involved in the stimulation of strain ratcheting at the weld toe.

3.2.1.5 Strain Responses in Displacement-Controlled Tests with Increasing Distance from Weld Toe

In each of the welded specimen tests, two additional uniaxial strain gages were installed to monitor strain responses in fatigue along the pipe length during the first stage of loading. The location of these gages, which can be seen in Fig. 3.57, coincided with the third and fifth spots of residual stress measurement (see Fig. 2.9). The comparison of all axial strain ratcheting responses of each welded specimen subjected to displacement-controlled fatigue can be seen in Figs. 3.58-3.61. It is interesting to note that the rate of axial strain ratcheting at the second gage location exceeded that at the first gage location in each of the three specimens subjected to ±14 mm amplitude of displacement cycles. These results are in agreement with findings from Lu [2003]. However, further exploration of this phenomenon was beyond the scope of this thesis.

3.2.1.6 Conclusions from Displacement-Controlled Experimental Studies

The length of fatigue life of welded specimens is influenced by many factors. The weight of each factor and the interaction between factors results in a complex failure mechanism that is not well understood. Within this research, we have attempted to examine only the influence of residual welding stresses on fatigue life. Conclusions drawn are interpreted in light of other known factor effects in the hopes that understanding of welded specimen fatigue life will be deepened.

In order to understand the effect residual welding stresses have on the fatigue life of welded specimens, the present section contains a discussion first of the effect of strain ratcheting rate and total accumulated strain on fatigue life. The results obtained in the first loading stage of displacement-controlled fatigue tests previously described are combined with results from five displacement-controlled fatigue tests performed by Lu [2003]. The combination of results from the two sets of experiments allows for more general, well-supported conclusions to be drawn. A separate study follows examining the relationship between initial residual stress and stimulated strain ratcheting. The continued occurrence of ratcheting after the relaxation of residual stresses will be probed in the following chapter.

3.2.1.6.1 Influence of Rate of Ratcheting and Amount of Accumulated Strain on Fatigue Life

In Fig. 3.62, the mean strain response at the weld toe from Specimens SW1, SW5, and SW7 are compared. All three are socket-welded specimens, the weld joints of which were achieved by quarter-circumferential welding and a total of three weld passes. Specimen SW1 was welded according to ASME design specifications while Specimens SW5 and SW7 were welded using a modified design. It is observed in Fig. 3.62 that lower ratcheting rates characterize the mean strain response of the modified design socket-welded specimens as compared to the ASME design socket-welded specimen. Upon further examination of Fig. 3.62, it is apparent that *fatigue life is affected by both the rate of ratcheting of axial mean strain and the total amount of strain accumulated at the location of fatigue failure*. Specimens SW5 and SW7 exhibit a very similar rate of ratcheting and failed after nearly the same number of fatigue cycles. The total amount of accumulated strain is less in SW7; this may be the reason for its slightly longer life. Specimen SW1 exhibits a higher rate of ratcheting than the other two specimens considered and a larger amount of accumulated strain. Specimen SW1 failed after 680 cycles and had the smallest fatigue life of the three specimens. In addition to this general conclusion, Fig. 3.62 shows evidence of a more subtle relationship. Specimens SW5 and SW7 experienced nearly identical axial strain ratcheting rates. The two specimens also endured almost the same number of cycles before fatigue crack initiation occurred. It is proposed that *length of fatigue life to crack initiation, while affected by many factors, is strongly influenced by the rate of ratcheting*.

In Fig. 3.63, the same three specimens are considered along with Specimens SW2 and SW3 from Lu [2003]. Both of these, like the first three, are socket-welded specimens. However,

the weld joints in Specimens SW2 and SW3 were achieved by four-pass welding. Specimen SW2 was subjected to quarter-circumferential welding while Specimen SW3 was subjected to full-circumferential welding. Factors, such as the number of weld passes and the sequence of welding, affect the length of fatigue life in welded piping specimens. Lu [2003] concluded the following from the results he obtained concerning these two specific factors: fatigue life increases as the number of weld passes increases from three to four. Full circumferential welding results in specimens with smaller fatigue lives as compared to specimens welded via quarter-circumferential welding. With these effects in mind, Fig. 3.63 is critically examined. In Specimens SW2 and SW3, a high rate of strain ratcheting is observed. In support of the conclusion proposed in the preceding section, Specimens SW2 and SW3 experienced fatigue crack initiation at relatively low numbers of cycles—560 and 300 cycles, respectively. In spite of their nearly identical ratcheting rates, Specimen SW2 endured almost twice as many cycles as did Specimen SW3. Based on Lu's observations, it is concluded that the difference in welding sequences—quarter-circumferential in SW2 versus full-circumferential in SW3—is at least partially responsible for this large difference in length of fatigue lives. It is also noted that, in comparing Specimens SW1 and SW2, similar ratcheting rates are observed. Specimen SW2 experienced a slightly higher rate of axial strain ratcheting but a longer fatigue life. This seeming contradiction is reconciled in part when the number of weld passes in each specimen is considered. Specimen SW2 was constructed using four-pass welding, which has been shown to increase fatigue life (Lu [2003]), while the weld joint of Specimen SW1 was achieved using three-pass welding.

The last of Lu's socket-welded specimen strain response results is introduced in Fig. 3.64. Specimen SW4 was welded using five-pass, quarter-circumferential welding. In the figure, it is shown that the rate of strain ratcheting and the total amount of accumulated strain in Specimen SW4 are lower than those experienced by the SW1-SW2-SW3 cluster. Consequently, both the life to fatigue crack initiation and total fatigue life were longer than those of Specimens SW1, SW2, and SW3.

Figure 3.65 contains mean axial strain responses of two butt-welded specimens in displacement-controlled fatigue cycles. True to the conclusion drawn in the socket weld discussion, the higher rate of strain ratcheting in Specimen BW2 translates into earlier fatigue crack initiation. In spite of a higher rate of ratcheting and a larger amount of accumulated strain,

Specimen BW2 had a slightly longer fatigue life (1100 cycles) than did Specimen BW1 (980 cycles.) The increased number of weld passes in Specimen BW2 may be responsible for this slight fatigue life improvement.

3.2.1.6.2Influence of Initial Residual Stress on Rate of Strain Ratcheting

The mean strain responses of Specimens BW2, SW5, and SW7—each of which were subjected to displacement-controlled fatigue loading with amplitude of displacement of 14 mm—are shown in Fig. 3.66. Information on initial residual stress and length of fatigue life for each specimen is also included. In this figure, no obvious relationships are identified between the initial residual stress and the length of fatigue life of each specimen. Underlying relationships that may exist are obscured by the error associated with the residual stress measurements; as error bars of ±60 MPa must be considered, it is impossible to identify the true maximum initial residual stress and thus relate residual stresses to length of fatigue life. Yamashita et al. [1997] also experienced scatter of results when compiling S-N data from four-point bending tests of socket-welded joints. Large differences in fatigue strengths were observed when nominal stress amplitudes were considered. However, when mean stresses due to residual stresses were considered, the scatter in the data was reduced considerably (Yamashita et al. [1997]). Therefore, while Fig. 3.66 does not convey an obvious relationship between residual stress and fatigue life, future research may make this relationship clear.

Figure 3.67 contains the amplitude of strain experienced by each of the three specimens at their respective weld toes. Upon synthesizing the information presented in Figs. 3.66 and 3.67, the relationship between strain amplitude and rate of ratcheting referenced throughout this chapter is reiterated. Specimen BW2 experienced slightly larger amplitude of strain cycling than did Specimens SW5 and SW7. In light of this observation, the higher rate of ratcheting in Specimen BW2 makes sense. Similarly, Specimens SW5 and SW7 were subjected to nearly the same strain amplitude and consequently experienced very similar rates of axial strain ratcheting.

3.2.2 Force-Controlled Fatigue Tests

3.2.2.1 Fatigue Response of Specimen SW6

In an attempt to explore the fatigue failure mechanism of force-controlled loading, Specimens SW6 and SW9 were subjected to ±3.5 kN amplitude of force-controlled fatigue loading. Differences in the strain response of specimens tested in the force-controlled setup were observed and are enumerated in the following subsections.

Specimen SW6 was fatigue tested in the cantilever setup depicted in Fig. 3.24. It was subjected to two stages of force-controlled saw-tooth fatigue cycles (Fig. 3.68). After 1510 cycles, a fatigue crack was identified at the weld toe of the bottom pipe surface. A second fatigue crack initiated at the weld toe of the top surface after 1630 cycles. The crack at the bottom weld toe propagated through the thickness of the pipe causing ultimate failure after 2230 cycles.

The recorded force-displacement response of Specimen SW6 to fatigue cycles can be seen in Fig. 3.69. In the force-displacement response, several factors interact to create an interesting outcome. In Fig. 3.70, there is evidence, particularly in the first stage of loading, that although the test was force-controlled, the amplitude of force decreased with increasing number of cycles. This occurrence can also be noted in Fig. 3.69—the positive peak force attained decreases with cycles. After the first stage of fatigue was complete, the gain setting on the force cartridge of the MTS machine was adjusted in an attempt to refine control over the force amplitude in subsequent tests. In spite of the fact that force amplitude gradually decreased with cycles, from the amplitude and mean of displacement response (Fig. 3.71), it is observed that displacement amplitude increased with cycles. Cyclic softening took place. This softening is exhibited in Fig. 3.69 by the migration of the positive peak in the positive displacement direction. From Fig. 3.71, it is apparent that the mean displacement ratcheted in the positive direction. Cyclic softening and positive ratcheting of displacement interact to produce the force-displacement response of Fig. 3.69. At the positive peak, cyclic softening causes the peaks to move in the positive displacement direction, as does the positive displacement ratcheting. The two events constructively interfere with each other to result in significant increase in the positive displacement peaks. At the negative peak of the hysteresis loop, cyclic softening causes the peak displacement to migrate in the negative direction while the positive displacement ratcheting exerts the opposite influence. The two events destructively interfere with each other and the negative peak of the hysteresis loop appears to be stationary.

This force-displacement response (Fig. 3.69) was unexpected. In the displacement-controlled tests, cyclic softening was observed; however, ratcheting of the mean force was not. Analogously, it was expected in the force-controlled tests that cyclic softening would again be observed but no ratcheting of the mean displacement would be recorded. As stated before, ratcheting of the mean displacement did occur, the reasons for which are unknown. This

displacement ratcheting significantly influenced strain responses in the Specimen SW6 fatigue test and motivated the investigators to repeat the test on Specimen SW9 to clarify results.

An additional note concerning the appearance of the force and displacement amplitudes is necessary before proceeding to the strain responses. The drastically quick increase in amplitude connecting the stages of loading in both Figs. 3.70 and 3.71 is a result of manually increasing the amplitude of prescribed force in the first few cycles of the second loading stage to achieve desired force.

The strain responses from uniaxial gages installed in the axial direction at the top and bottom weld toes and the midpoint of the pipe length are presented in Figs. 3.72-3.74. In Fig. 3.72, the strain amplitude experienced at the top weld toe increases with number of cycles as a byproduct of the cyclic softening behavior of the pipe specimen. Mean strain at the top weld toe ratcheted in the positive direction due to the positive ratcheting of the mean displacement. At the bottom weld toe, strain amplitude was again found to increase slightly over the first stage of loading as a result of softening (Fig. 3.73). Mean strain, however, appeared to ratchet slightly in the negative direction. Due to the orientation of the pipe and the defined directions of displacement (positive downward), negative peak strains were achieved at the bottom weld toe when the pipe was displaced in the positive direction. Therefore, positive ratcheting of displacement caused negative strain ratcheting at the bottom weld toe. Figure 3.74 contains strain amplitude and mean obtained at the midpoint of the pipe length. In this figure, neither the amplitude nor the mean increases with number of cycles.

The combinations of strain responses over the entire fatigue life of the specimen at the top and bottom weld toes appear in Figs. 3.75 and 3.76. At the top weld toe (Fig. 3.75), strain amplitude in the second stage of fatigue is higher than in the first stage due to the following factors: testing conditions could not be perfectly duplicated, the gain setting was adjusted between stages, and the amplitude of force was manually increased in the first few cycles of the second stage. The rate of ratcheting of the mean strain increased from the first to the second stage; the amplitude and mean of the strain response in the second stage are reminiscent of patterns established in the displacement-controlled tests. It is suspected that the increased rate of ratcheting was caused by the increase in strain amplitude. At the bottom weld toe, higher amplitude of strain was also recorded in the second stage of loading. Mean strain at this location changed its ratcheting direction from compressive to tensile in the second stage of loading. The

ratcheting rate at the bottom weld toe was much smaller than the rate of ratcheting of the top weld toe mean strain. These two results, along with the slowed rate of displacement ratcheting in later cycles (Fig. 3.71), suggest that strain ratcheting was not predominantly influenced by displacement ratcheting as number of cycles increased. However, the presence of displacement ratcheting in this fatigue test prevented the investigators from drawing conclusions concerning the influence of residual stresses on ratcheting behavior in force-controlled fatigue testing. Therefore, the final fatigue test conducted on Specimen SW9 was a replication of the Specimen SW6 test in an effort to clarify results.

3.2.2.2 Fatigue Response of Specimen SW9

The final welded piping specimen, Specimen SW9, was tested in the cantilever setup and subjected to the same amplitude of force-controlled saw-tooth fatigue cycles as Specimen SW6. Corresponding force-displacement response recorded in fatigue appears in Fig. 3.77. After 1530 fatigue cycles, crack initiation at the weld toe occurred at the bottom surface of the pipe specimen. The crack propagated and became through-wall after 1990 cycles. No fatigue crack was detected at the top weld toe.

Amplitude and mean of the force and displacement responses are shown in Figs. 3.78 and 3.79. Consistency of testing conditions was high; the combination of the stages was very smooth. In Fig. 3.73, the prescribed force amplitude is shown to have decreased over the life of the specimen, in spite of the fact that the test was force-controlled. The rate of decrease was vastly improved by the MTS gain adjustment, as the rates in Specimen SW9 and the second stage of SW6 are less drastic than the rate of decrease in the first stage of loading for Specimen SW6. In Fig. 3.79, the amplitude of displacement increases over the course of the experiment, bearing witness to the occurrence of cyclic softening. A slight increase in the mean displacement appears in the second stage of loading and is attributed to variations in testing conditions between the two stages.

Strain responses at the top and bottom weld toes and at the midpoint of the pipe length are contained in Figs. 3.80-3.83. In Fig. 3.80, negative ratcheting of the mean strain at the top weld toe is observed. At the bottom weld toe (Fig. 3.81), negative axial strain ratcheting was also recorded, although the rate of ratcheting at this location is smaller than that at the top weld toe. In Fig. 3.82, a very small amplitude of circumferential strain is observed at the bottom weld

toe. No ratcheting of the mean circumferential strain was detected. In addition, no ratcheting of the axial strain at the midpoint of the pipe length is apparent in Fig. 3.83.

Amplitude and mean axial strain at the top weld toe from the two stages of loading are combined in Fig. 3.84. From this figure, it is concluded that negative ratcheting of the axial strain persisted throughout the fatigue life of Specimen SW9. Similarly, Fig. 3.85 portrays the continued negative ratcheting of axial mean strain at the bottom weld toe.

3.2.2.3 Strain Responses in Force-Controlled Tests with Increasing Distance from Weld Toe

The comparison of axial strain ratcheting responses at different strain gage locations on each welded specimen subjected to force-controlled fatigue cycles can be see in Figs. 3.86 and 3.87. In Fig. 3.86, it is apparent that at the second gage location on Specimen SW6, the largest rate of negative axial strain ratcheting was experienced. However, strain responses obtained from Specimen SW9 did not echo this occurrence. In Fig. 3.87, the largest rates of ratcheting were experienced at the top and bottom weld toes, while ratcheting at the second and third gage locations did not take place.

3.2.2.4 Conclusions from Force-Controlled Experimental Studies

Due to the fact that only two specimens were tested in force-controlled fatigue, it is difficult to draw well-supported conclusions. However, the following observations were made. In sharp contrast to the displacement-controlled tests, negative strain ratcheting of axial strains at the bottom weld toe of Specimen SW6 in the first stage of loading and at both weld toes throughout the fatigue life of Specimen SW9 was recorded in the force-controlled tests. In Specimen SW6, this initial stage negative strain ratcheting was attributed to the positive displacement ratcheting that occurred. However, no such displacement ratcheting occurred in the fatigue testing of Specimen SW9, leaving the negative strain ratcheting at both weld toes largely unexplained. The applied force cycle in the two force-controlled tests generated small strain cycles. Hence, rates of ratcheting in the axial and circumferential directions were smaller than those observed in the displacement-controlled tests. From the two tests, it can be concluded that *the fatigue failure mechanism in force-controlled testing is significantly different from and even less well understood than the failure mechanism observed in displacement-controlled testing*. Future research in this area is needed for better understanding of this failure mechanism.

Table 3.1 Maximum differences between residual stress measurements in reproducibility study Specimen SW7, Location of Minimum Strain Cycling

	AXIAL DIRECTION	CIRCUMFERENTIAL DIRECTION
Measurement Location	**Residual Stress Difference (MPa)**	**Residual Stress Difference (MPa)**
1	136.2	98.1
2	131.3	93.1
3	81.5	69.4
4	109.1	70.5
5	90.3	48.3

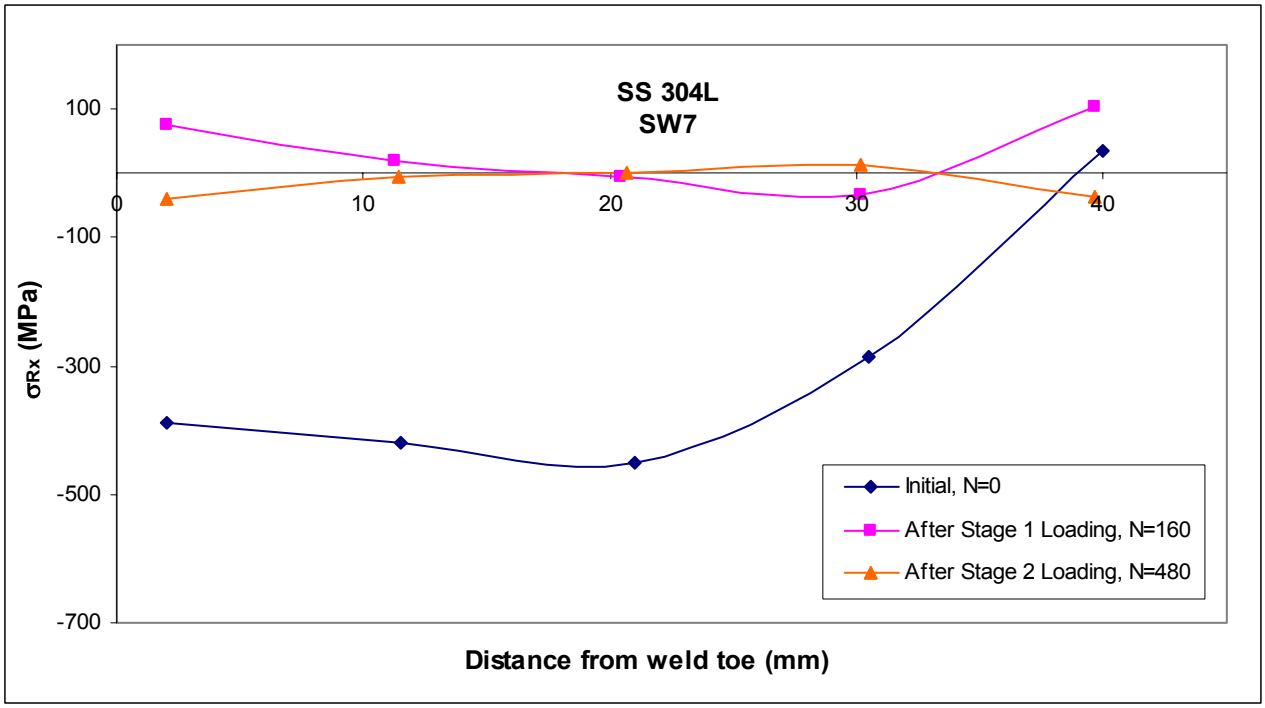

Figure 3.1 Axial residual stress in SW7 at the location of maximum strain cycling at various points in fatigue life N

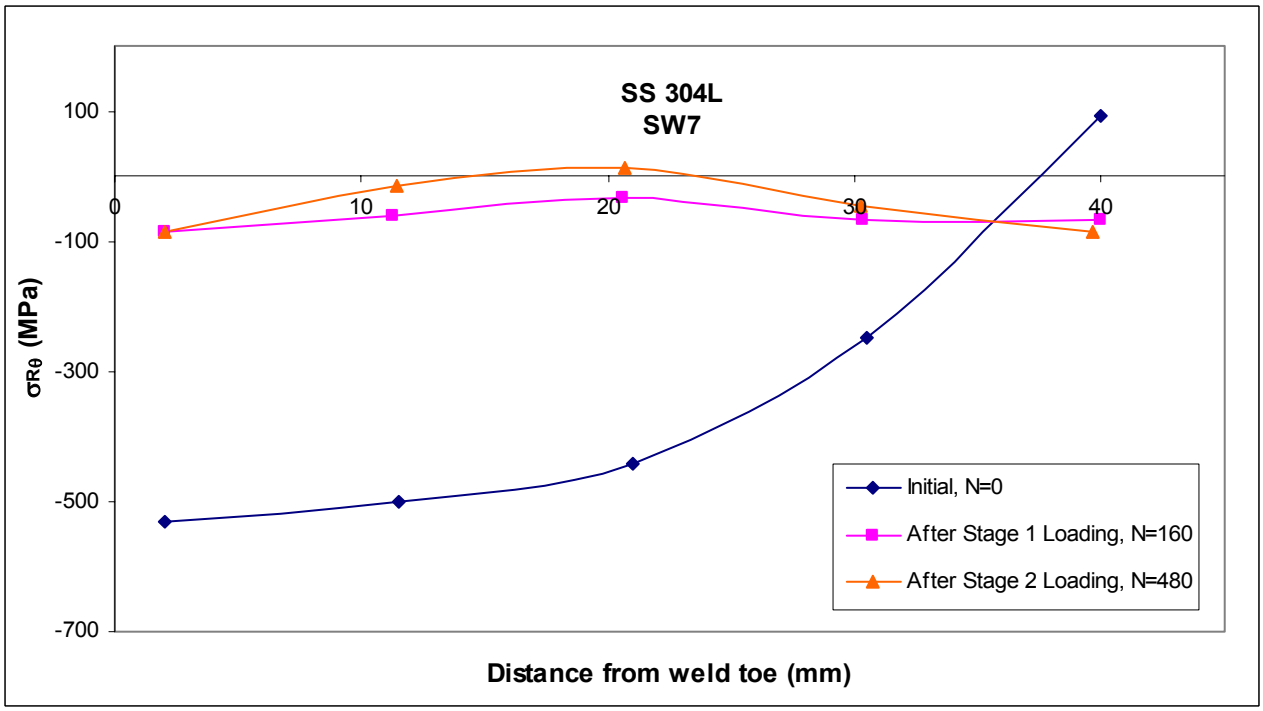

Figure 3.2 Circumferential residual stress in SW7 at the location of maximum strain cycling at various points in fatigue life N

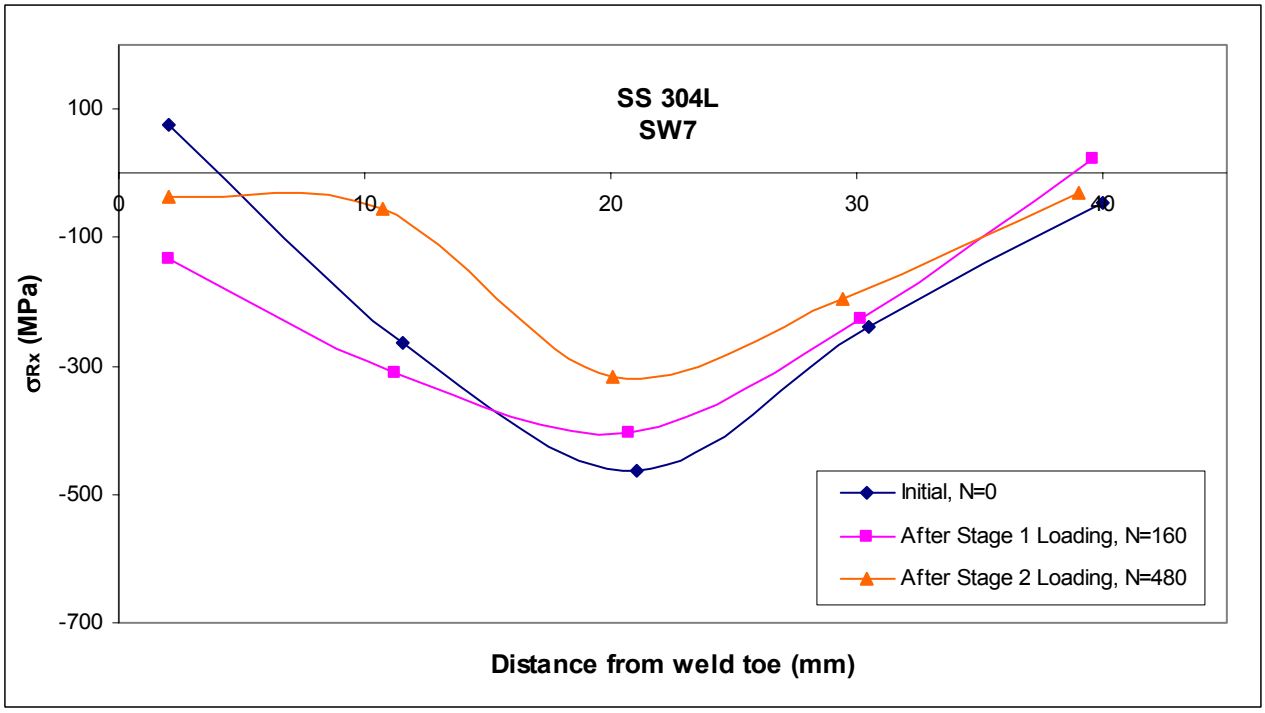

Figure 3.3 Axial residual stress in SW7 at the location of minimum strain cycling at various points in fatigue life N

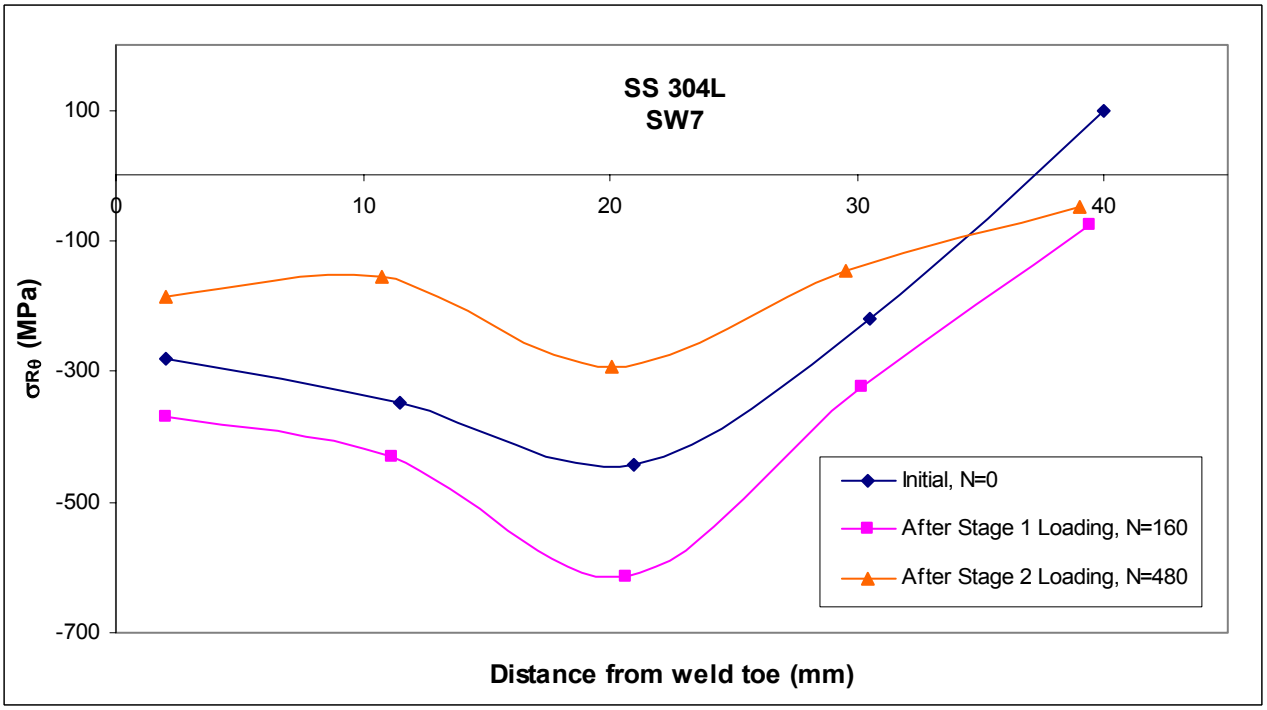

Figure 3.4 Circumferential residual stress in SW7 at the location of minimum strain cycling at various points in fatigue life N

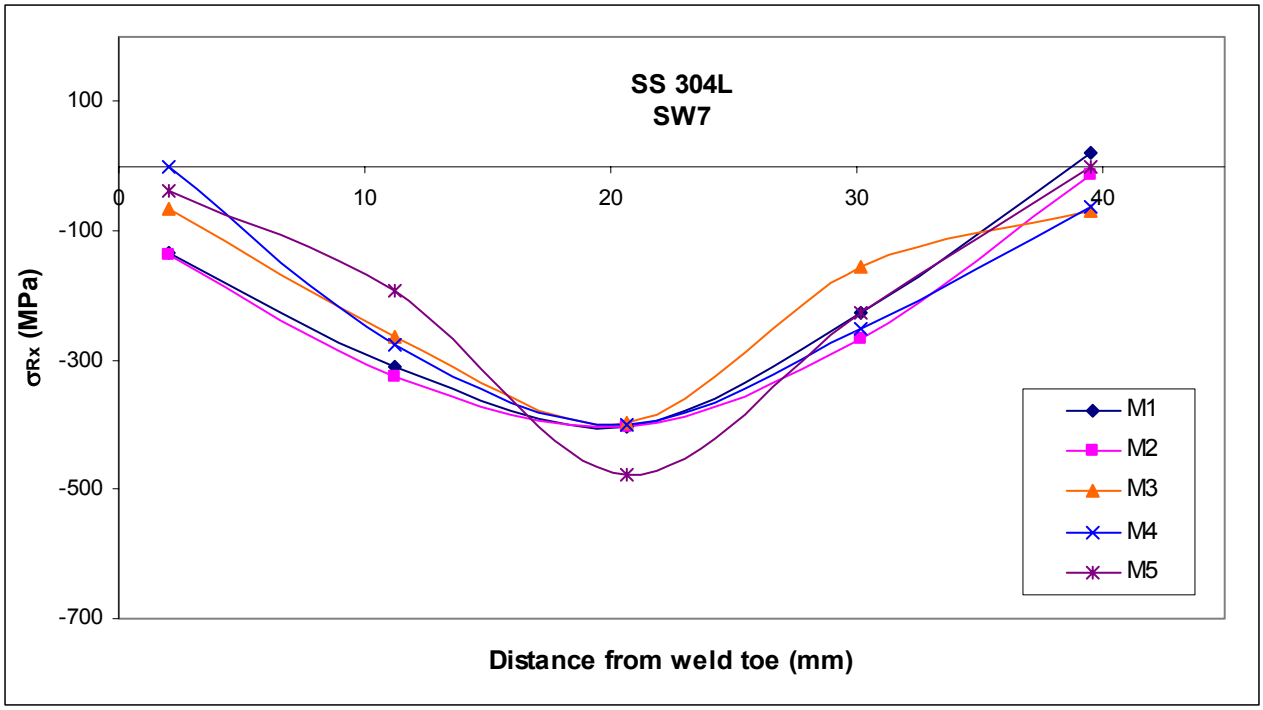

Figure 3.5 Axial residual stresses in reproducibility study

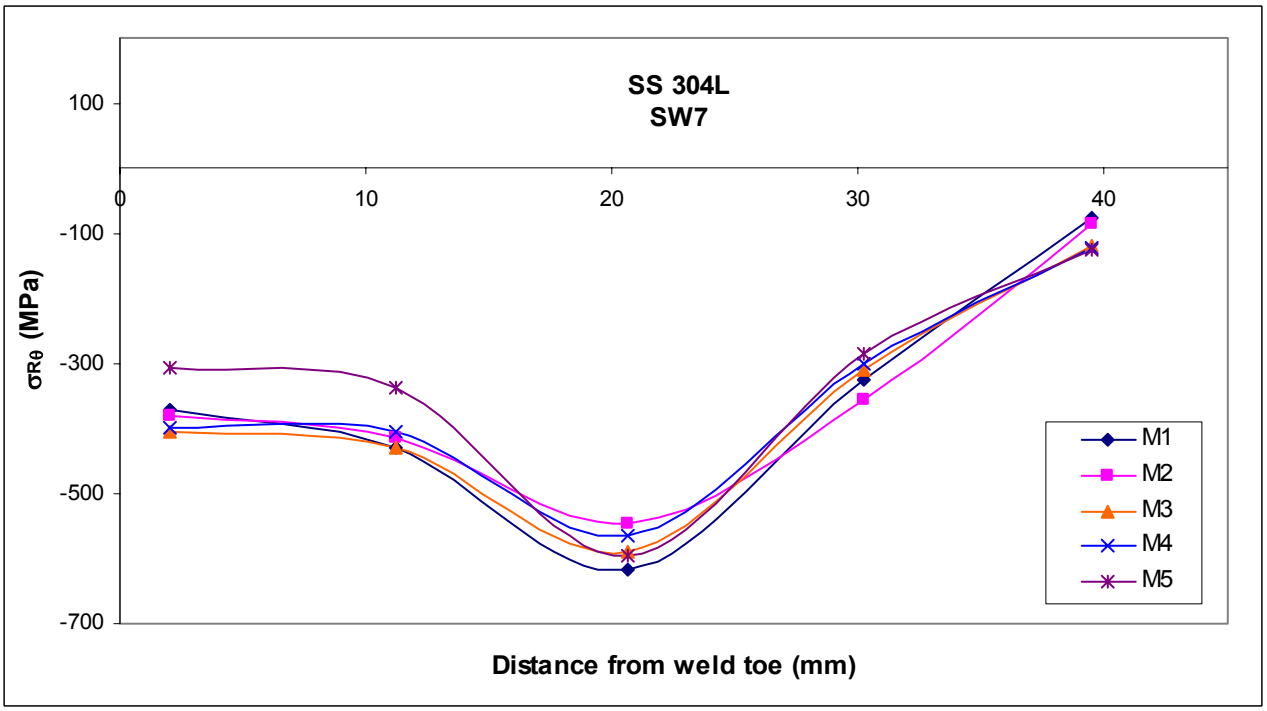

Figure 3.6 Circumferential residual stresses in reproducibility study

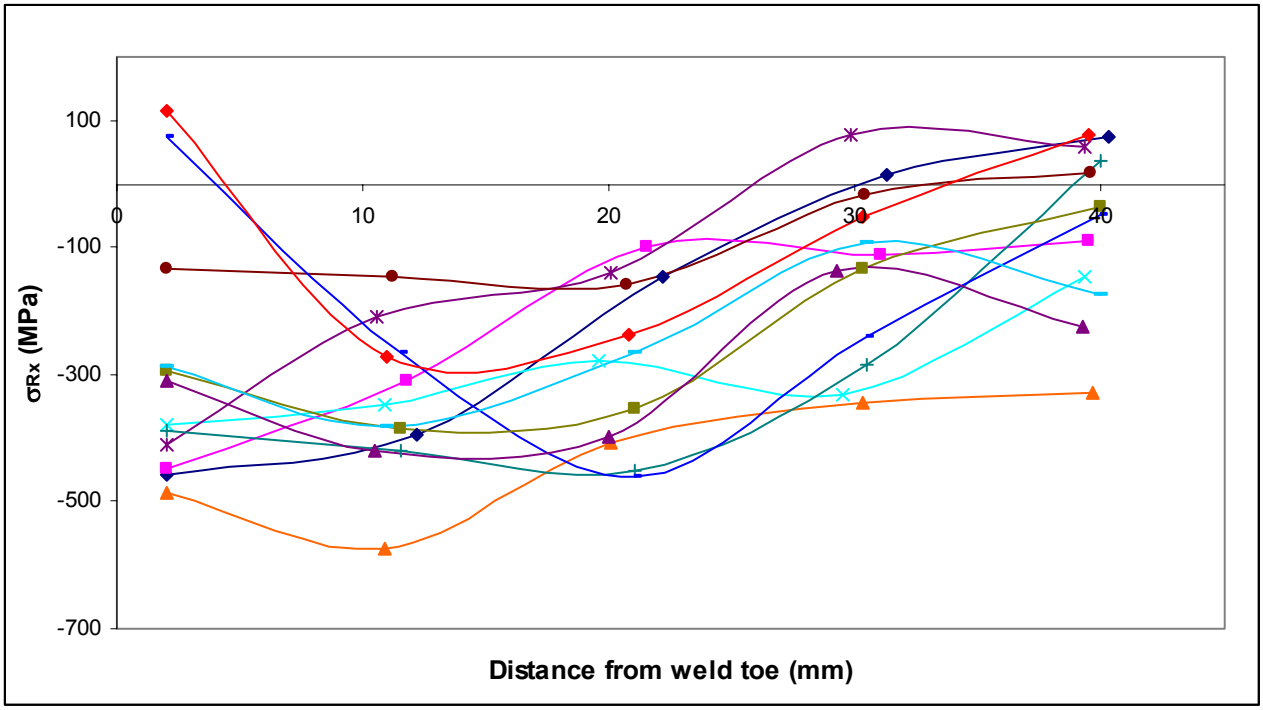

Figure 3.7 Axial residual stresses in all welded specimens

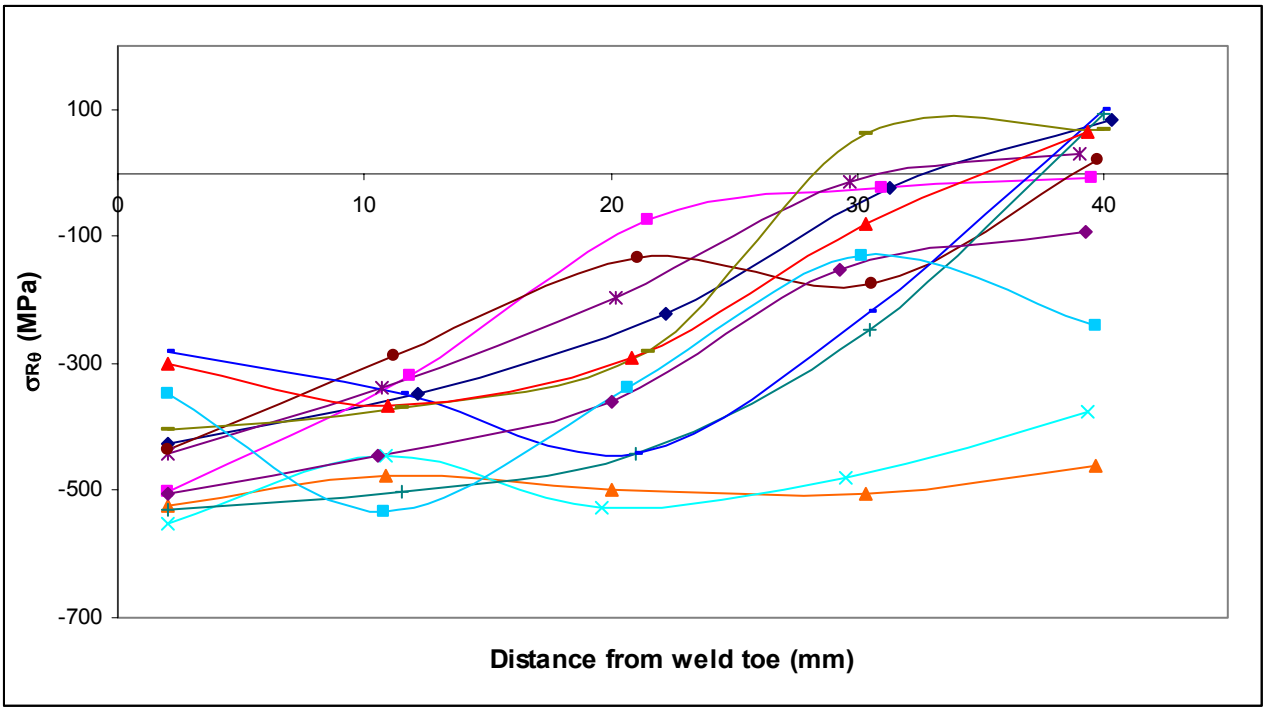

Figure 3.8 Circumferential residual stresses in all welded specimens

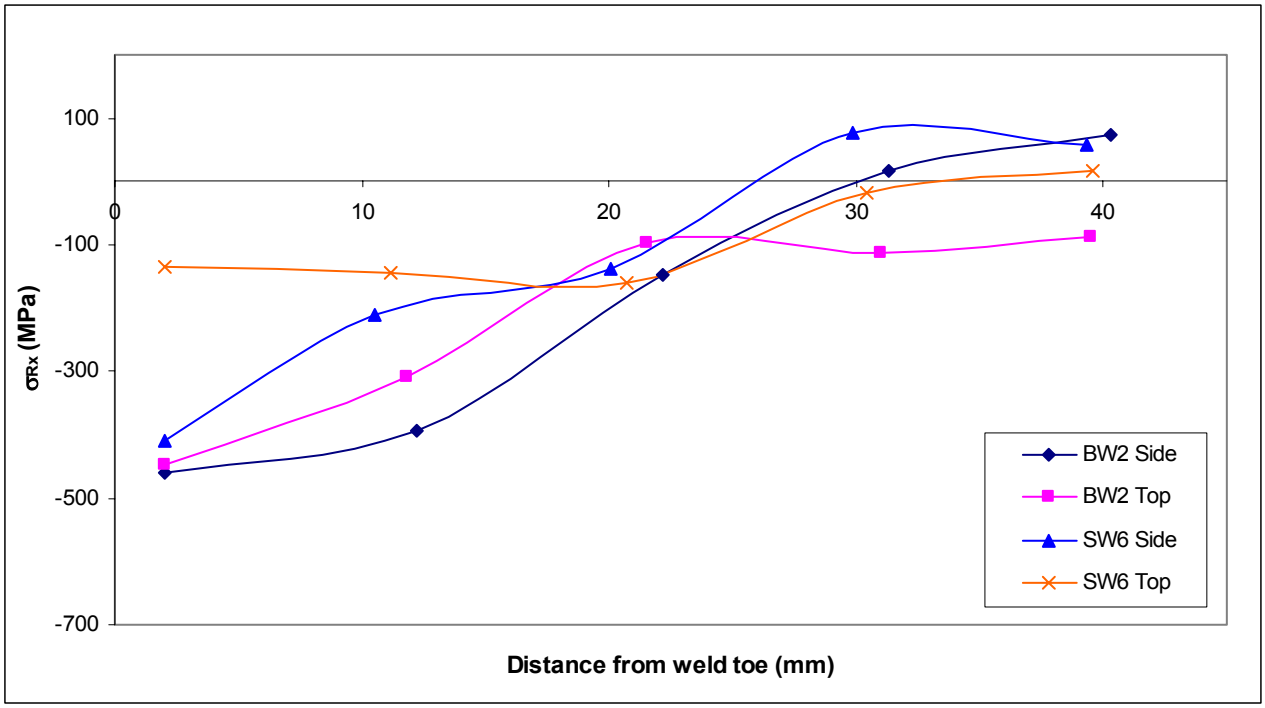

Figure 3.9 Axial residual stresses in Welding Batch #1 specimens

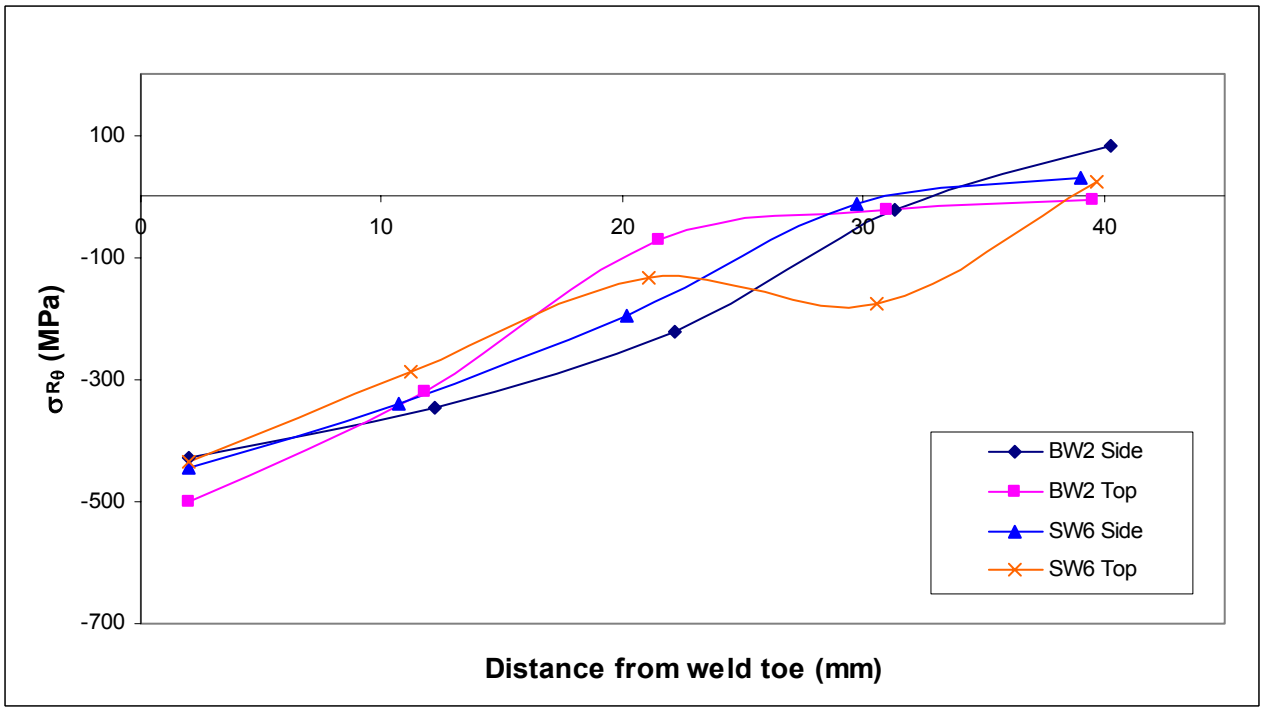

Figure 3.10 Circumferential residual stresses in Welding Batch #1 specimens

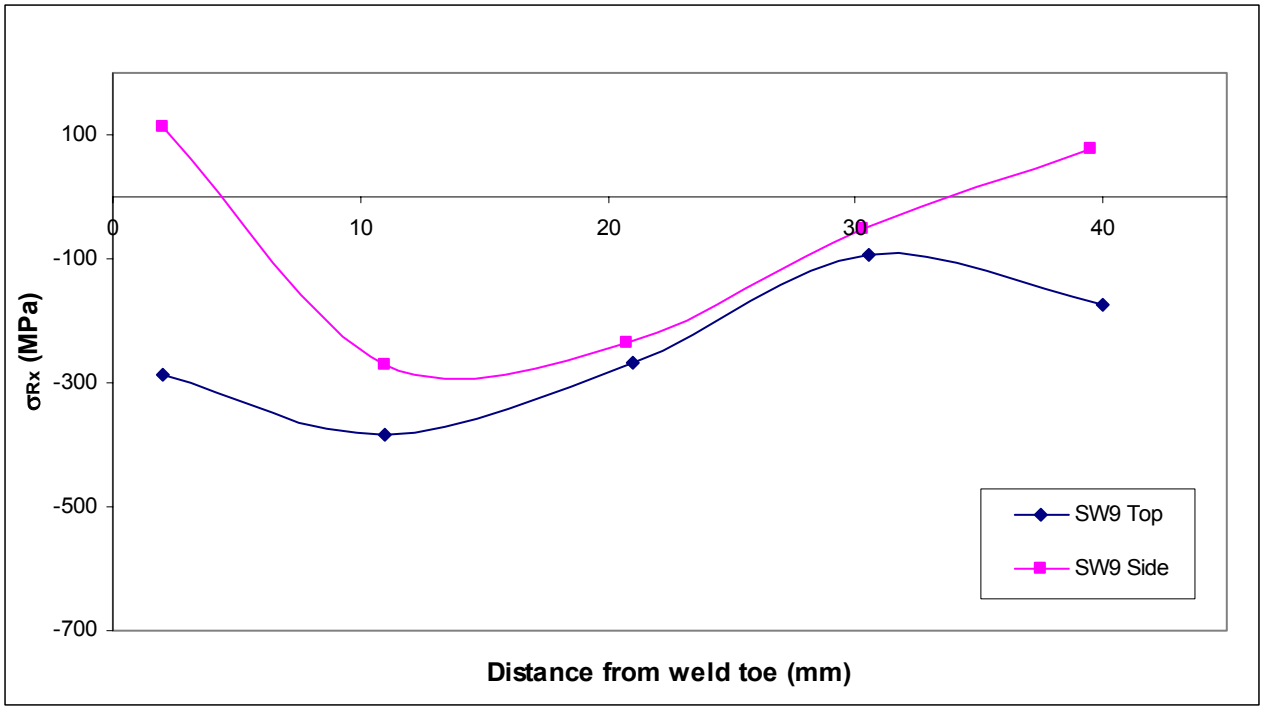

Figure 3.11 Axial residual stresses in Welding Batch #2 specimens

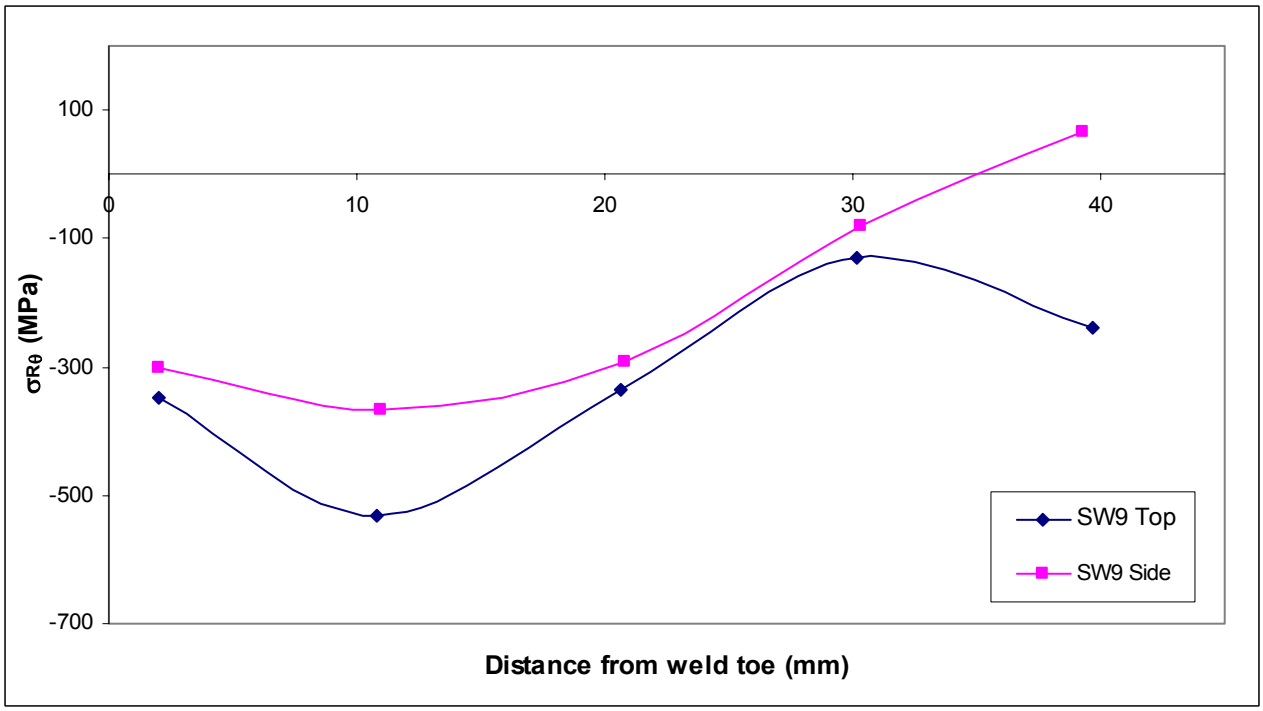

Figure 3.12 Circumferential residual stresses in Welding Batch #2 specimens

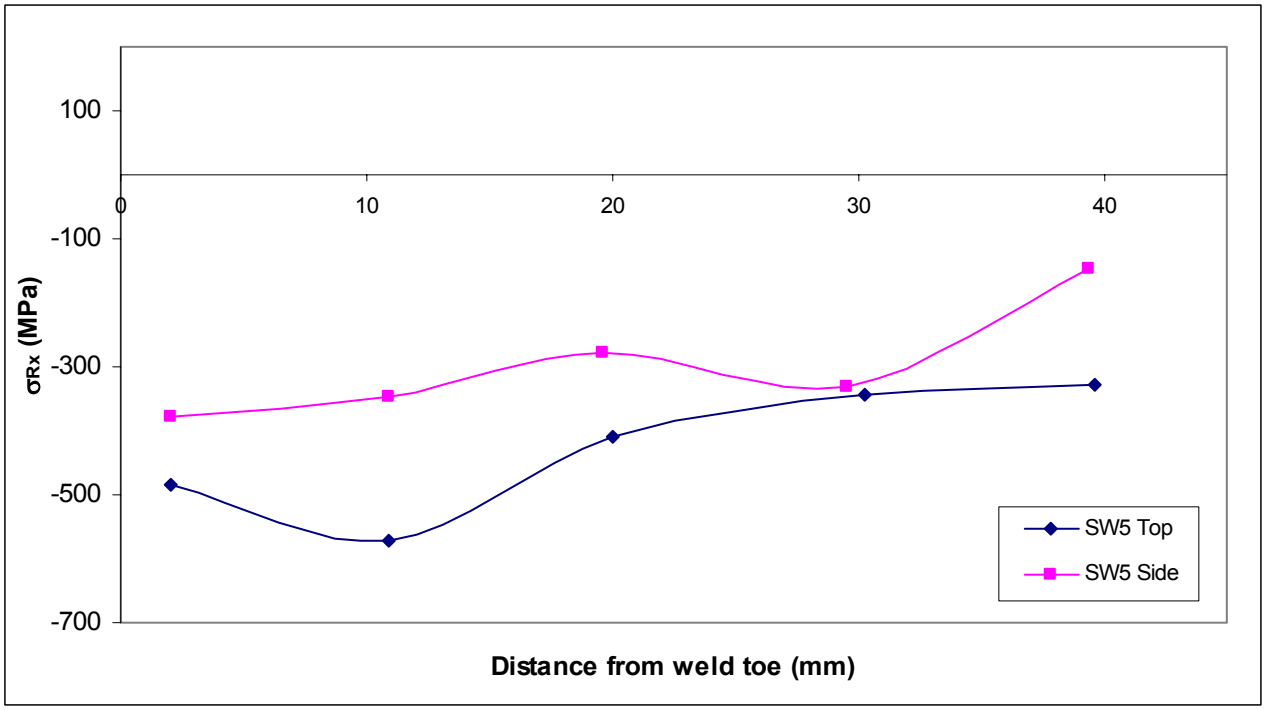

Figure 3.13 Axial residual stresses in Welding Batch #3 specimens

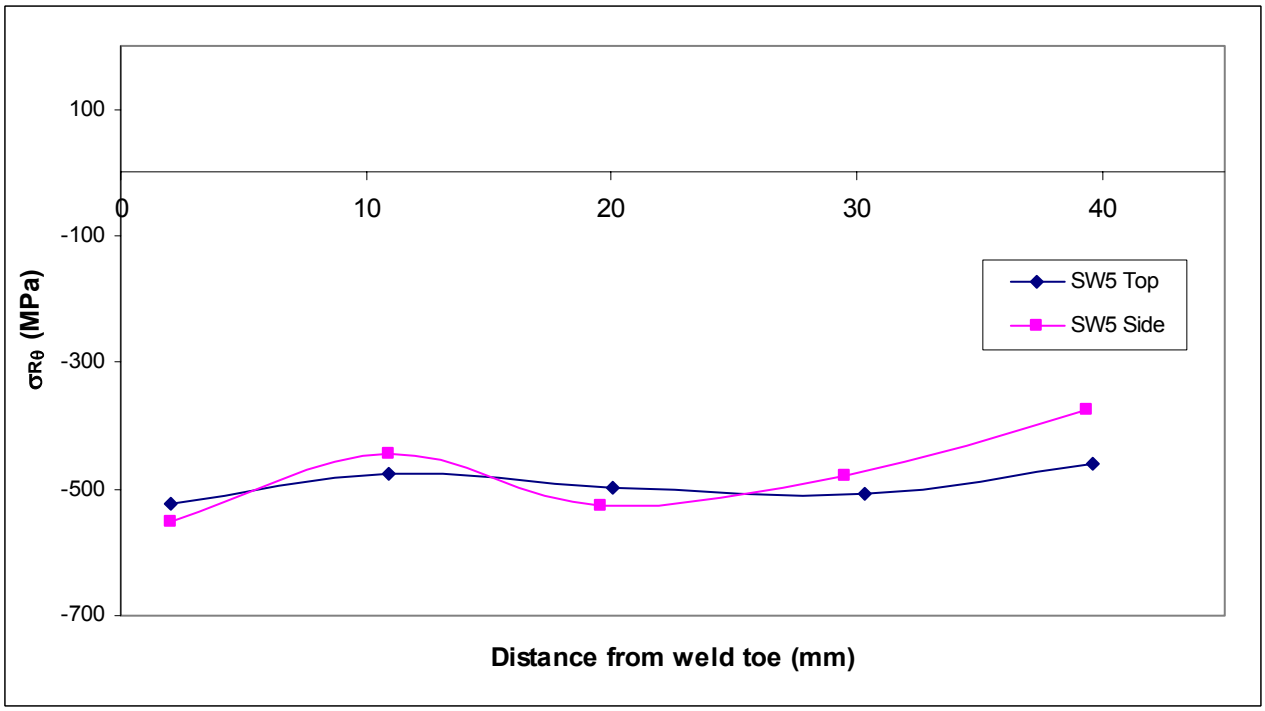

Figure 3.14 Circumferential residual stresses in Welding Batch #3 specimens

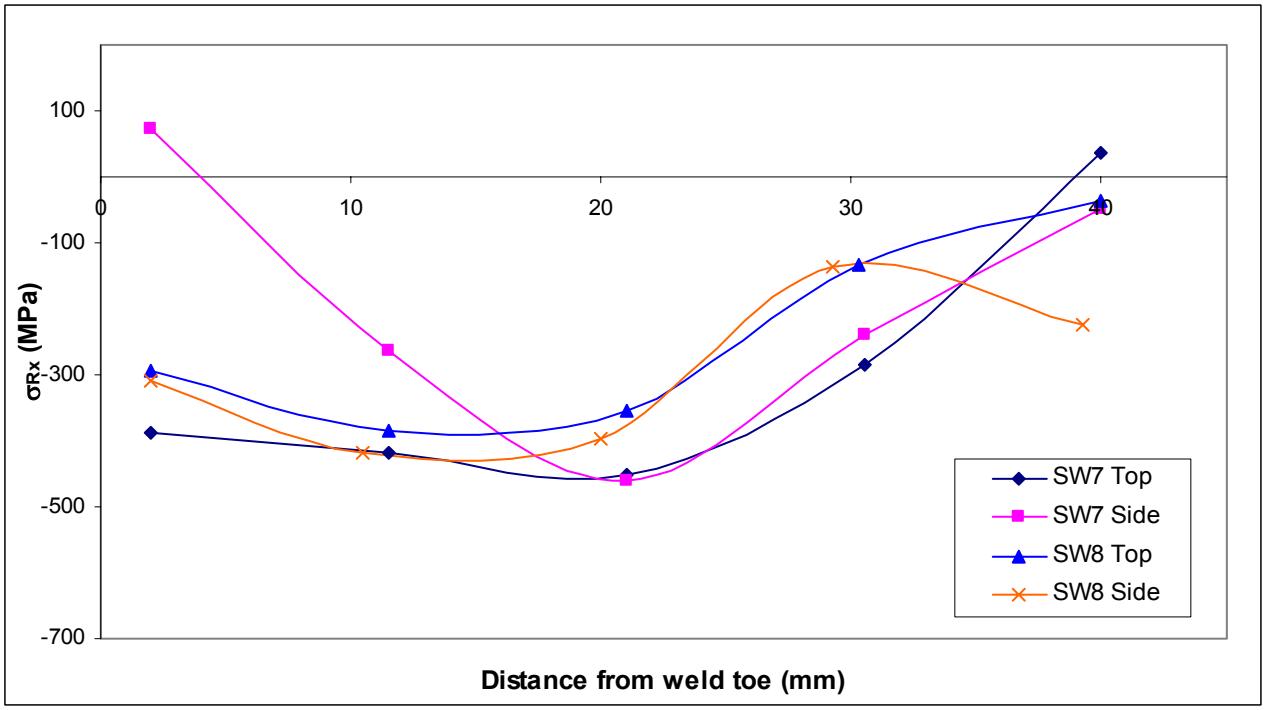

Figure 3.15 Axial residual stresses in Welding Batch #4 specimens

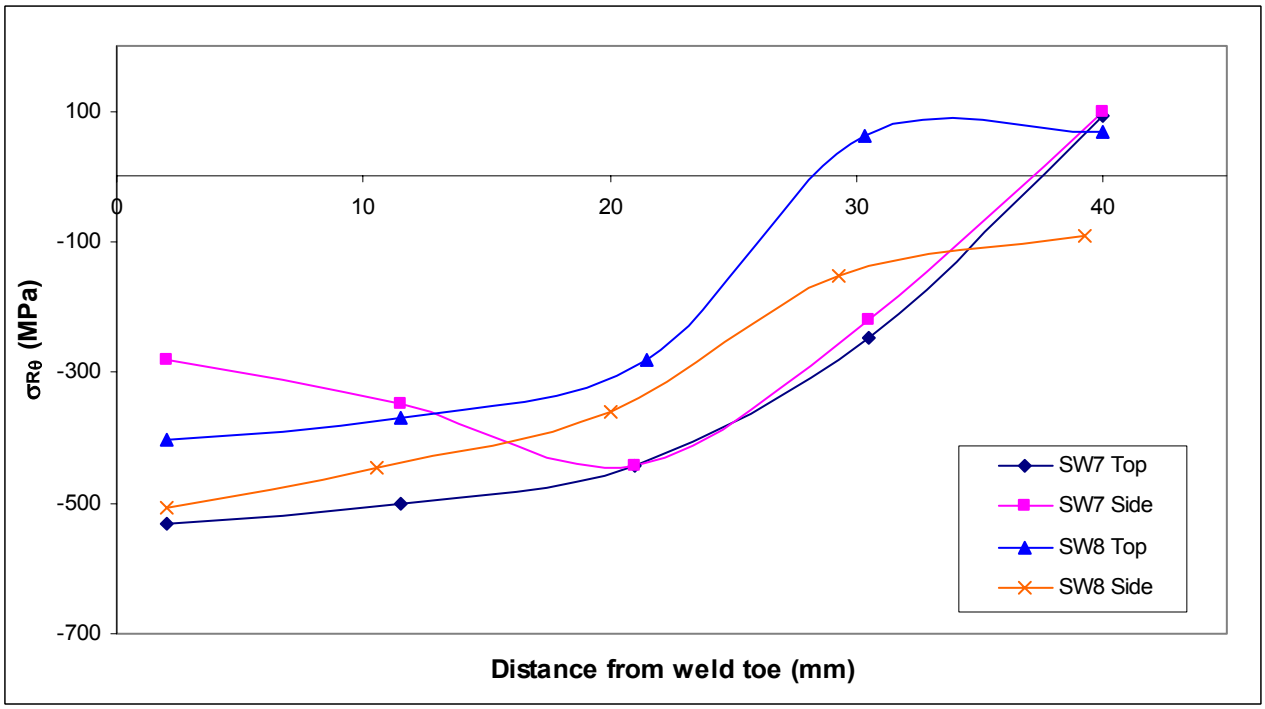

Figure 3.16 Circumferential residual stresses in Welding Batch #4 specimens

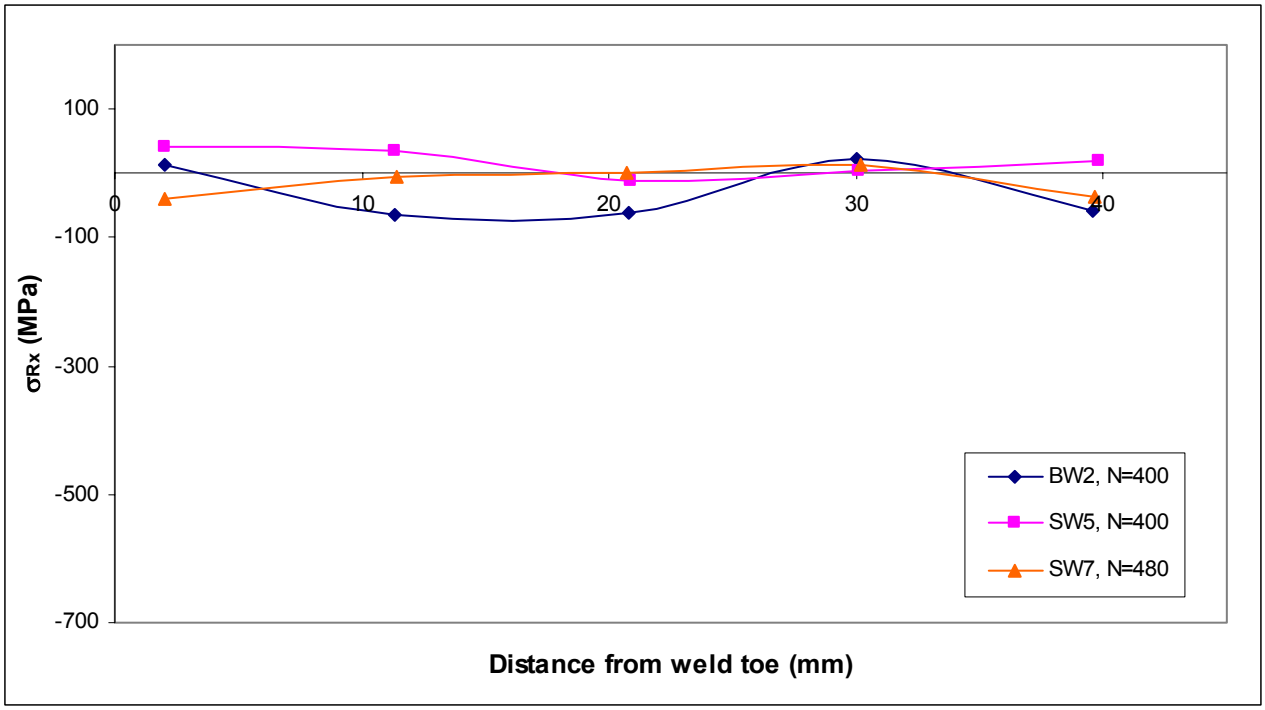

Figure 3.17 Axial residual stresses in displacement-controlled tests at location of maximum strain cycling

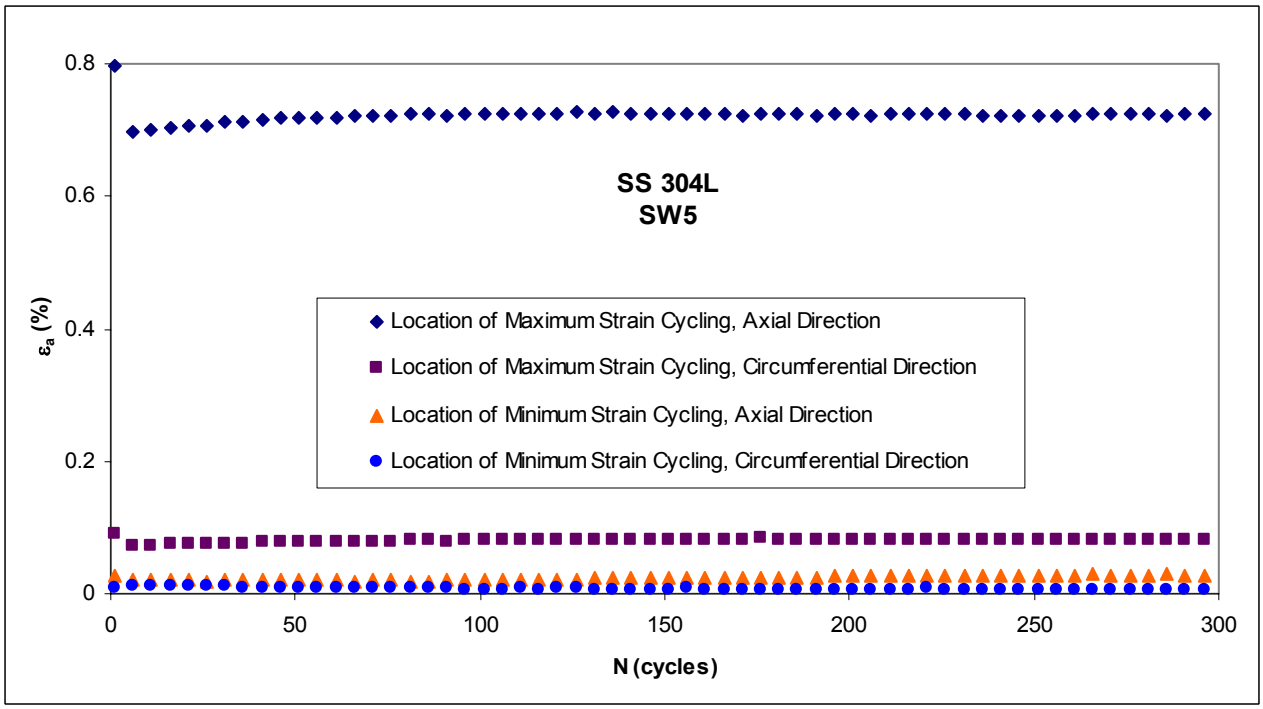

Figure 3.18 Comparison of strain amplitudes in ±14 mm amplitude displacement-controlled test

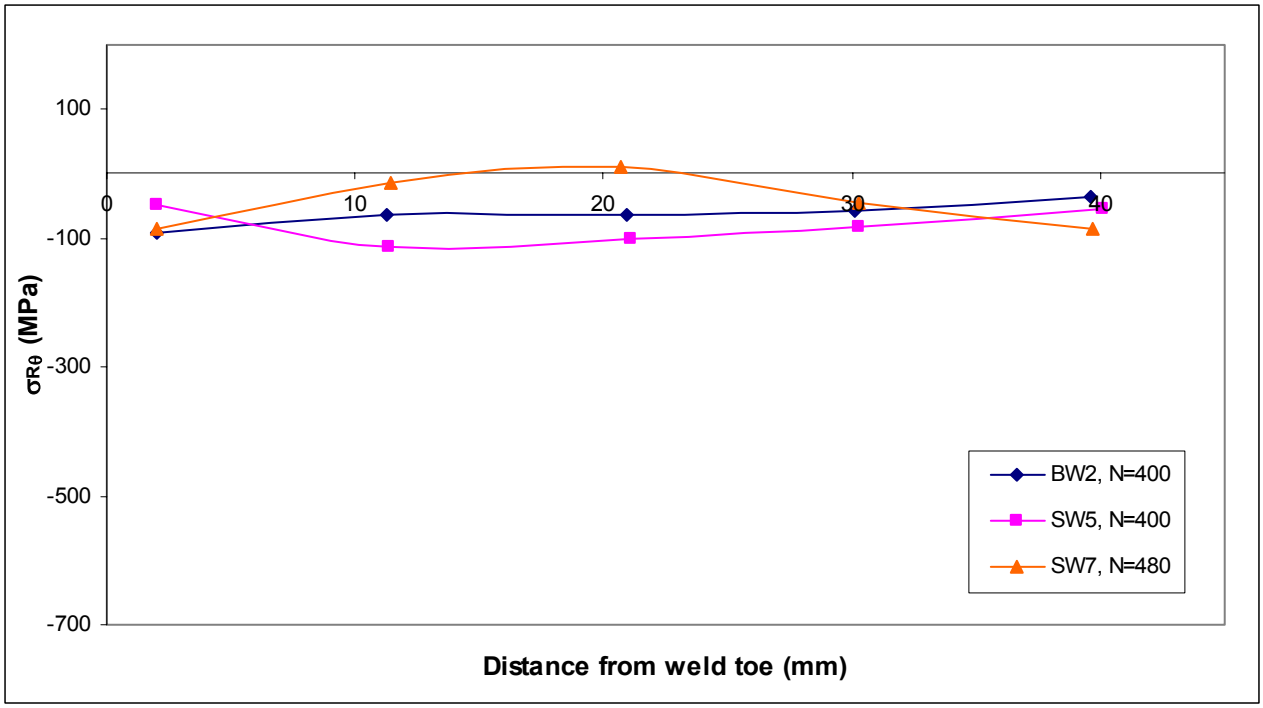

Figure 3.19 Circumferential residual stresses in displacement-controlled tests at location of maximum strain cycling

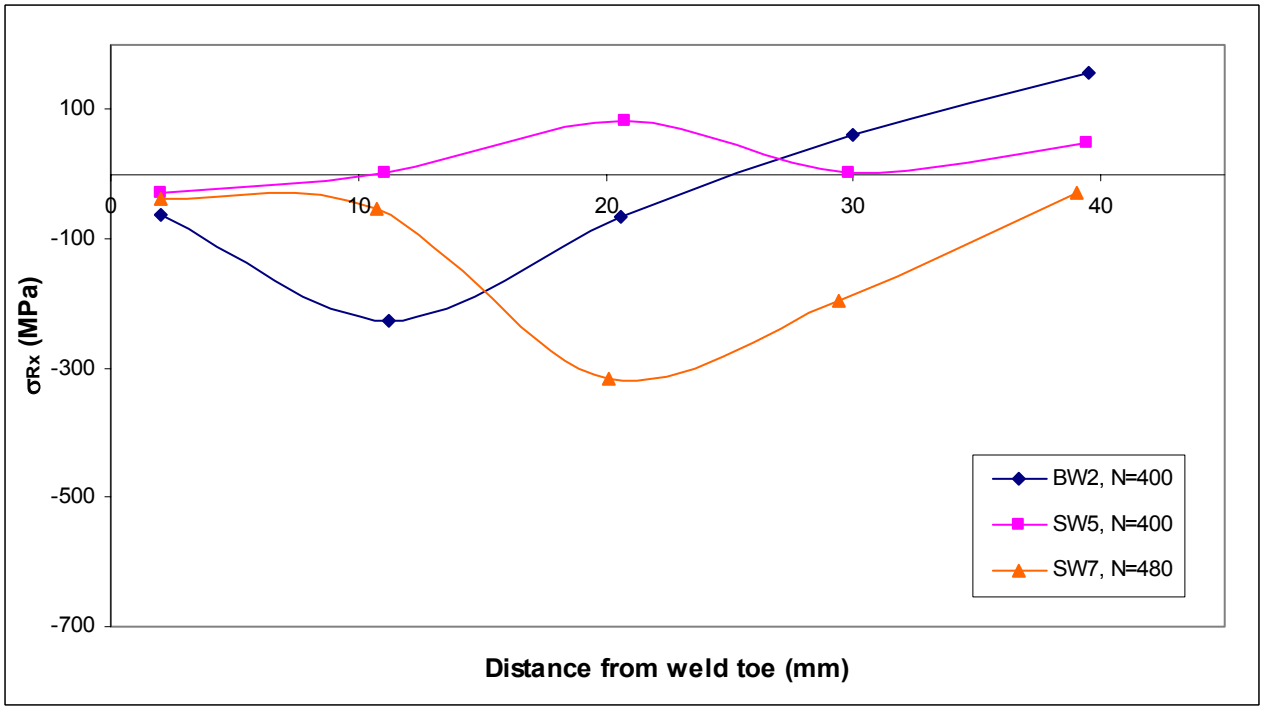

Figure 3.20 Axial residual stresses in displacement-controlled tests at location of minimum strain cycling

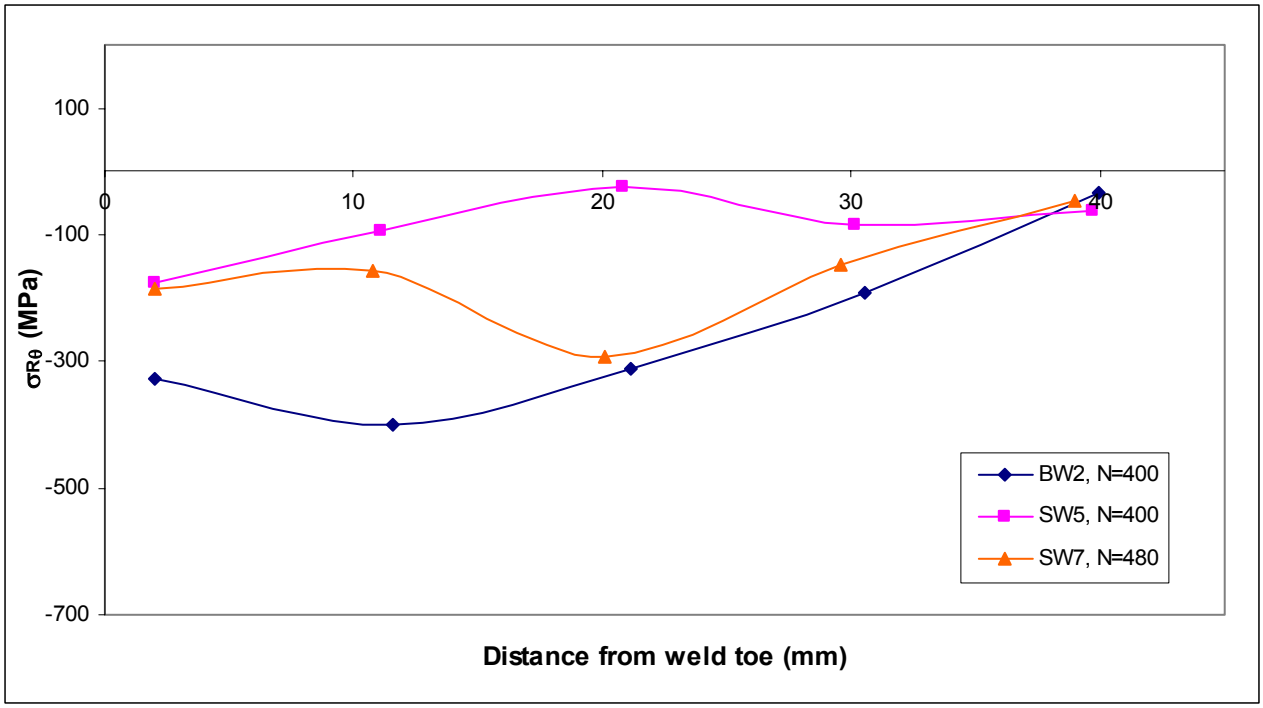

Figure 3.21 Circumferential residual stresses in displacement-controlled tests at location of minimum strain cycling

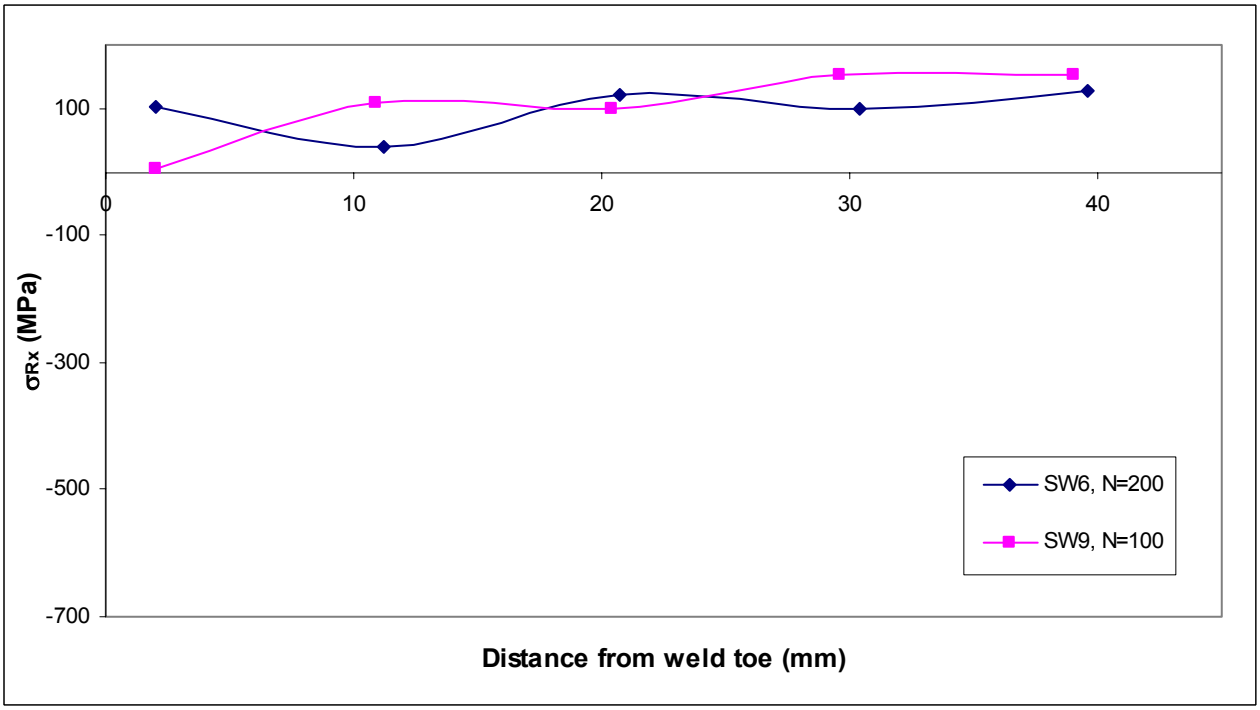

Figure 3.22 Axial residual stresses in force-controlled tests at location of maximum strain cycling

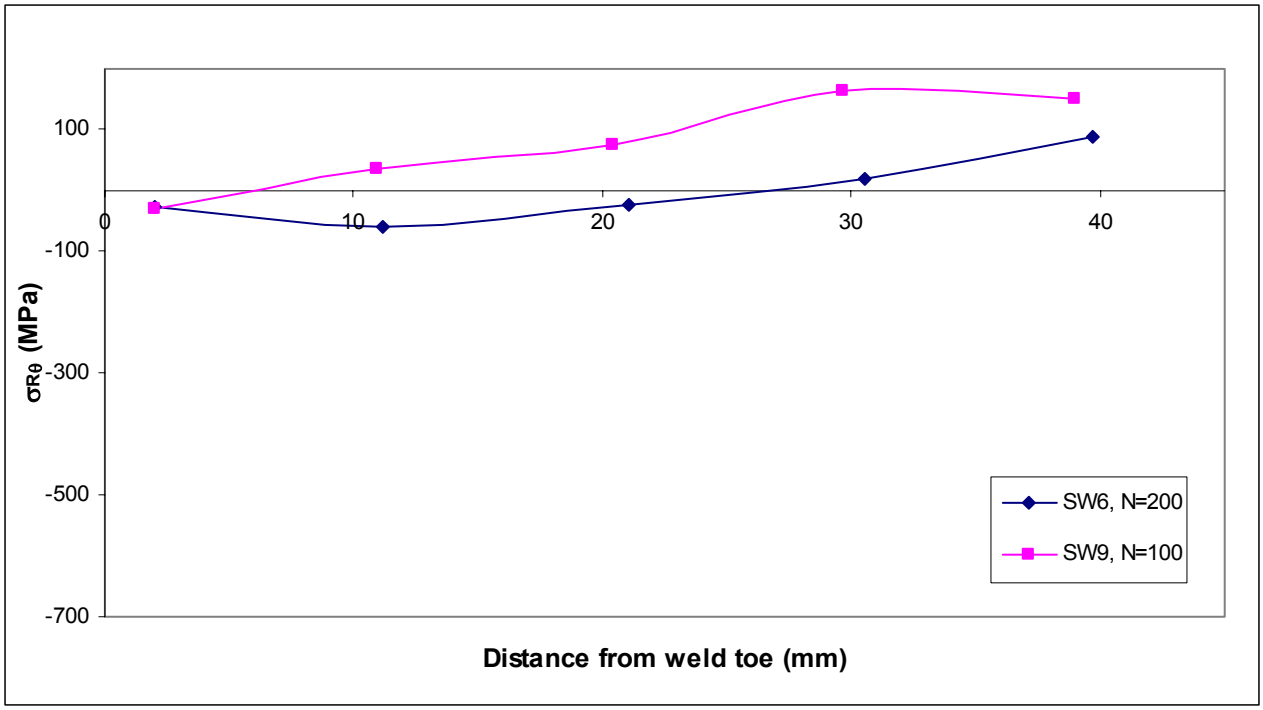

Figure 3.23 Circumferential residual stresses in force-controlled tests at location of maximum strain cycling

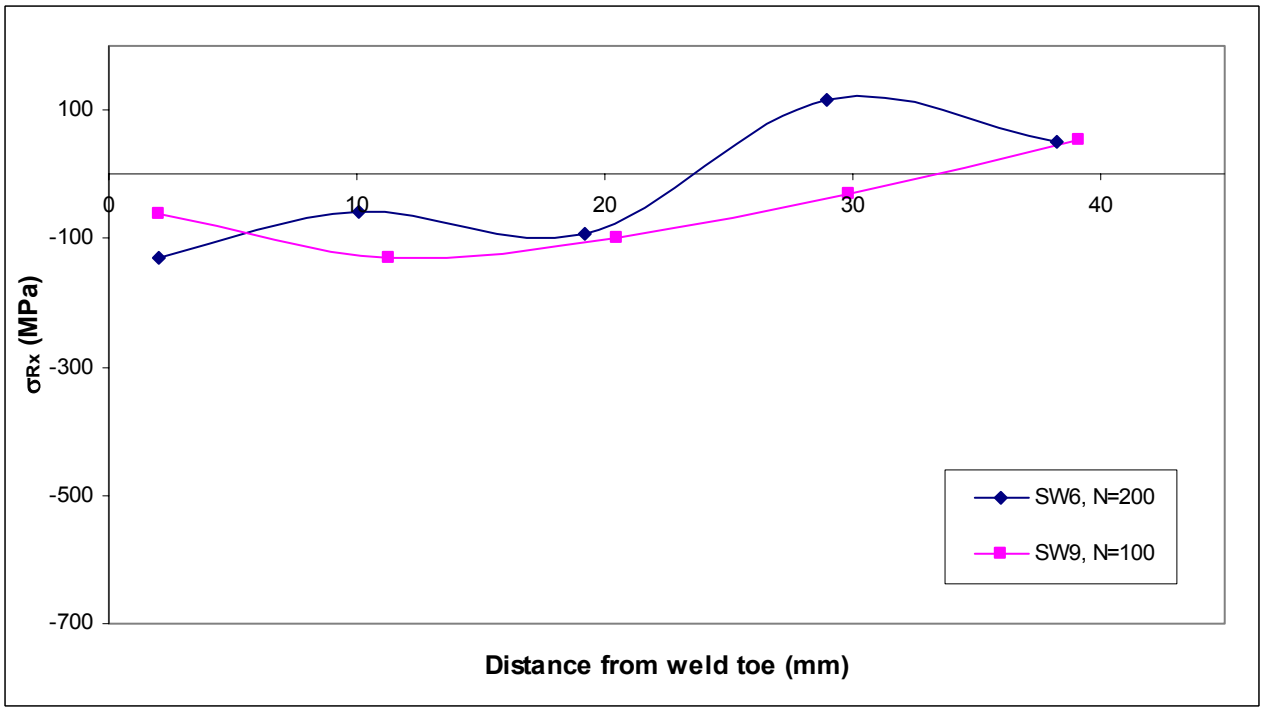

Figure 3.24 Axial residual stresses in force-controlled tests at location of minimum strain cycling

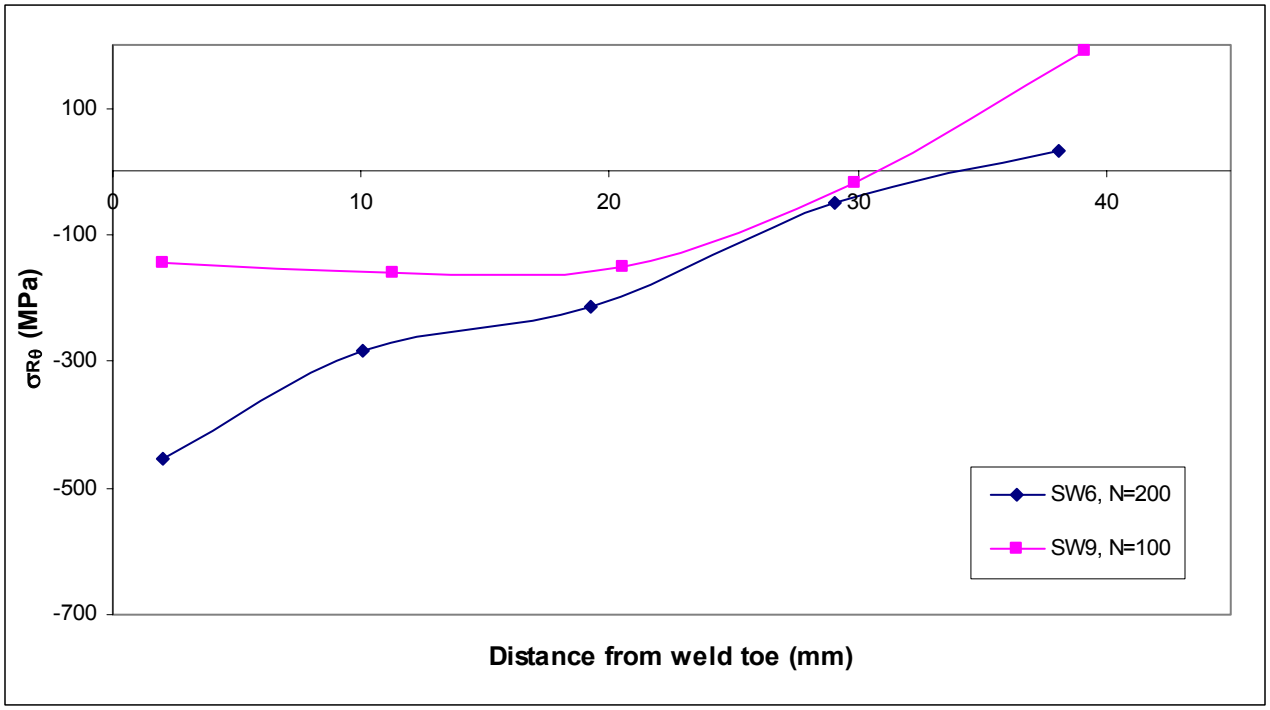

Figure 3.25 Circumferential residual stresses in force-controlled tests at location of minimum strain cycling

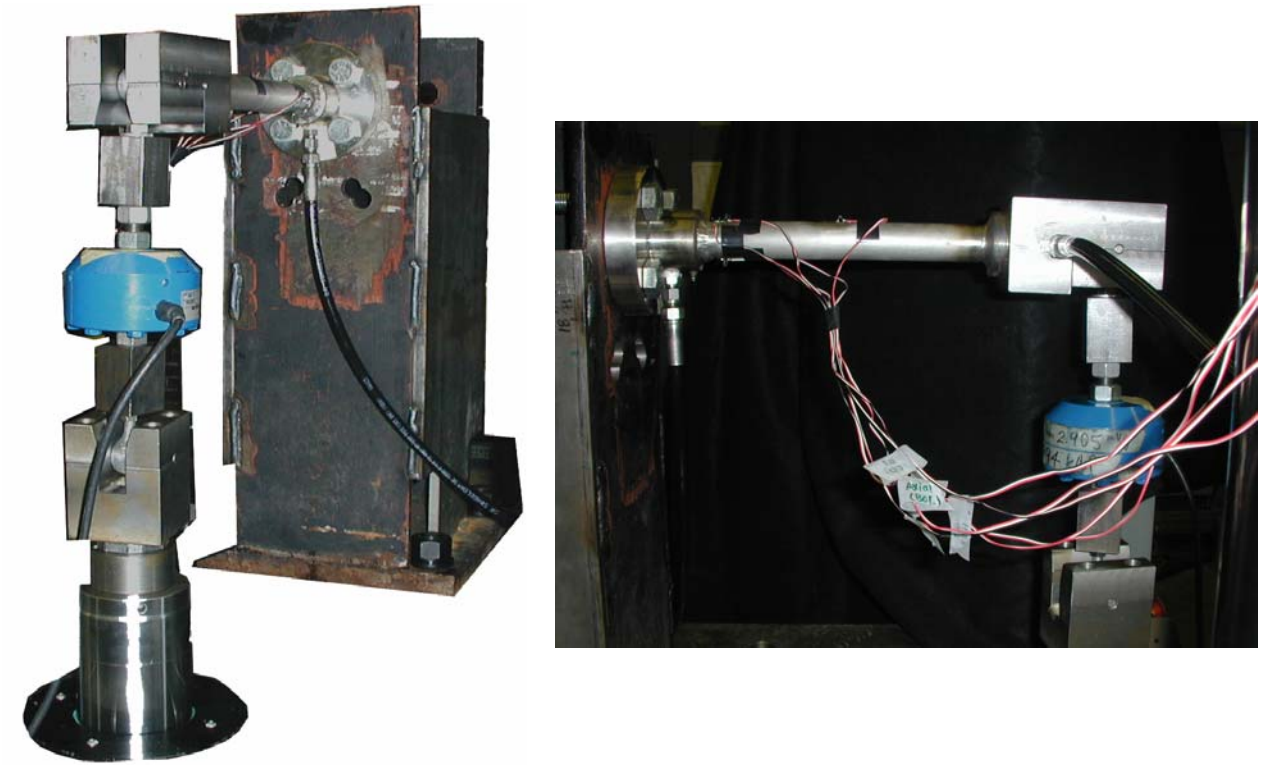

Figure 3.26 Cantilever setup (two views) for welded specimen fatigue testing (Lu [2003])

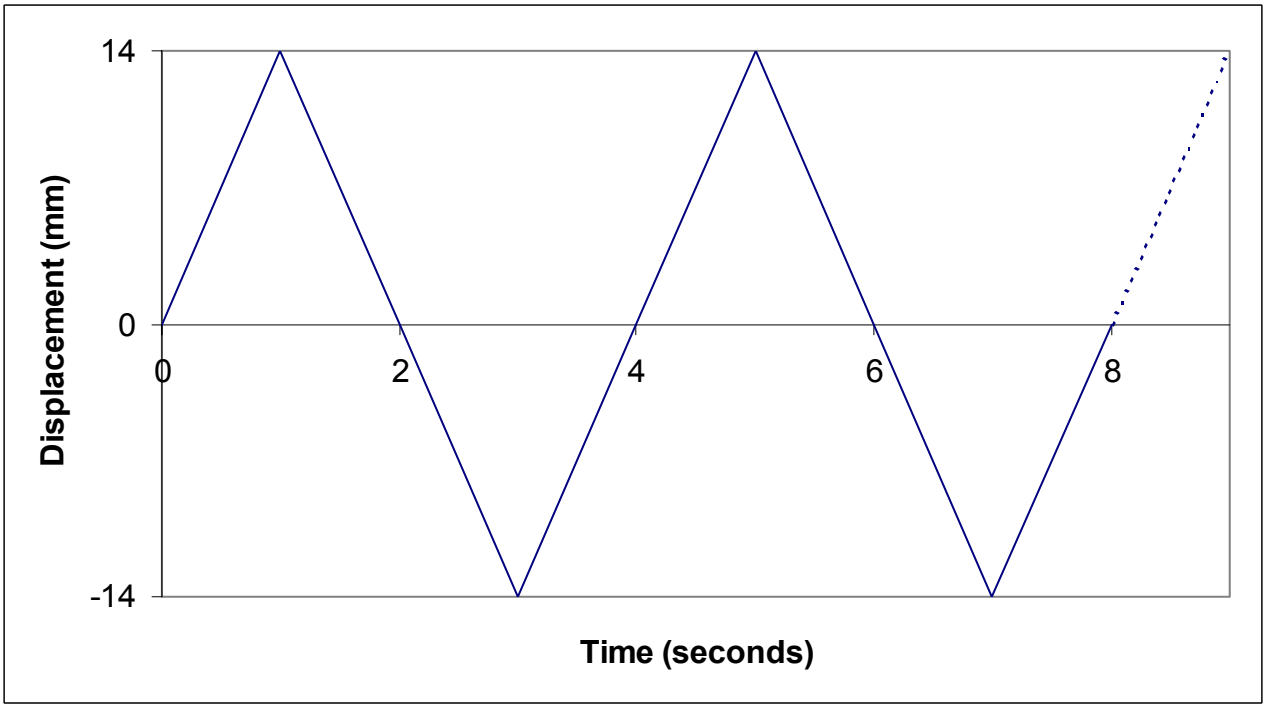

Figure 3.27 Prescribed displacement-controlled loading for BW2, SW5, and SW7 fatigue tests

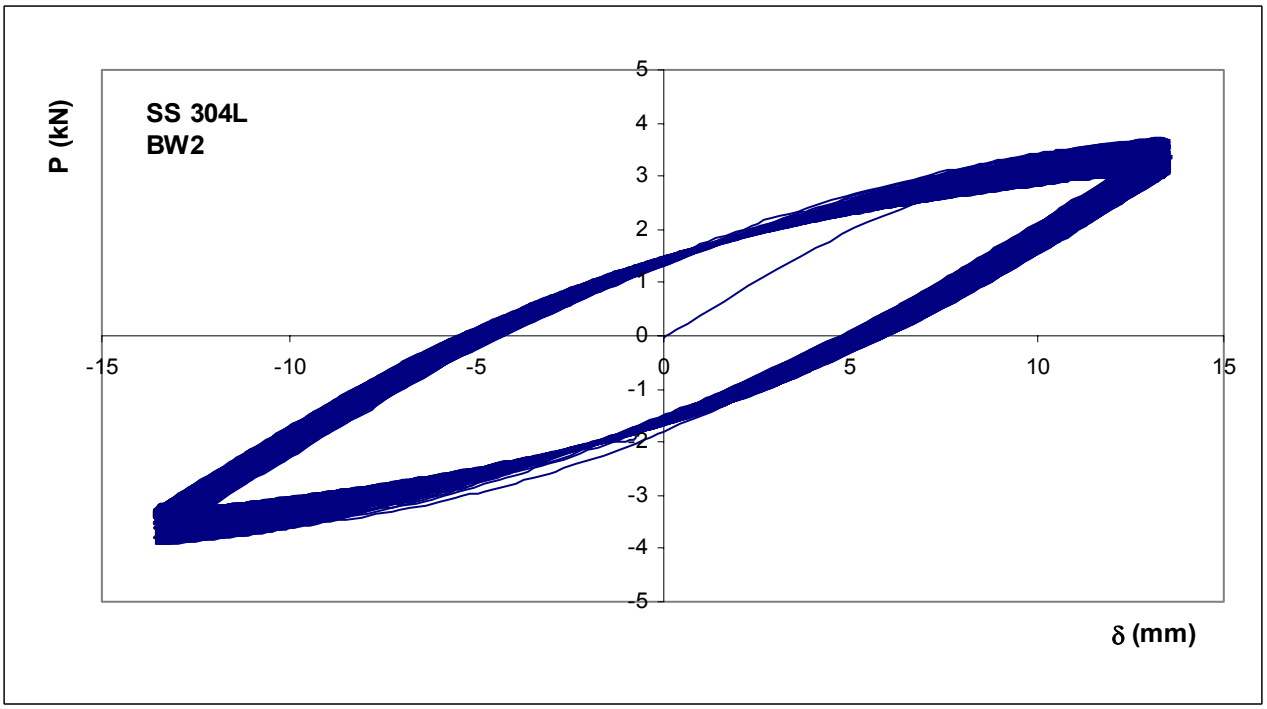

Figure 3.28 Force-displacement response from BW2 fatigue test

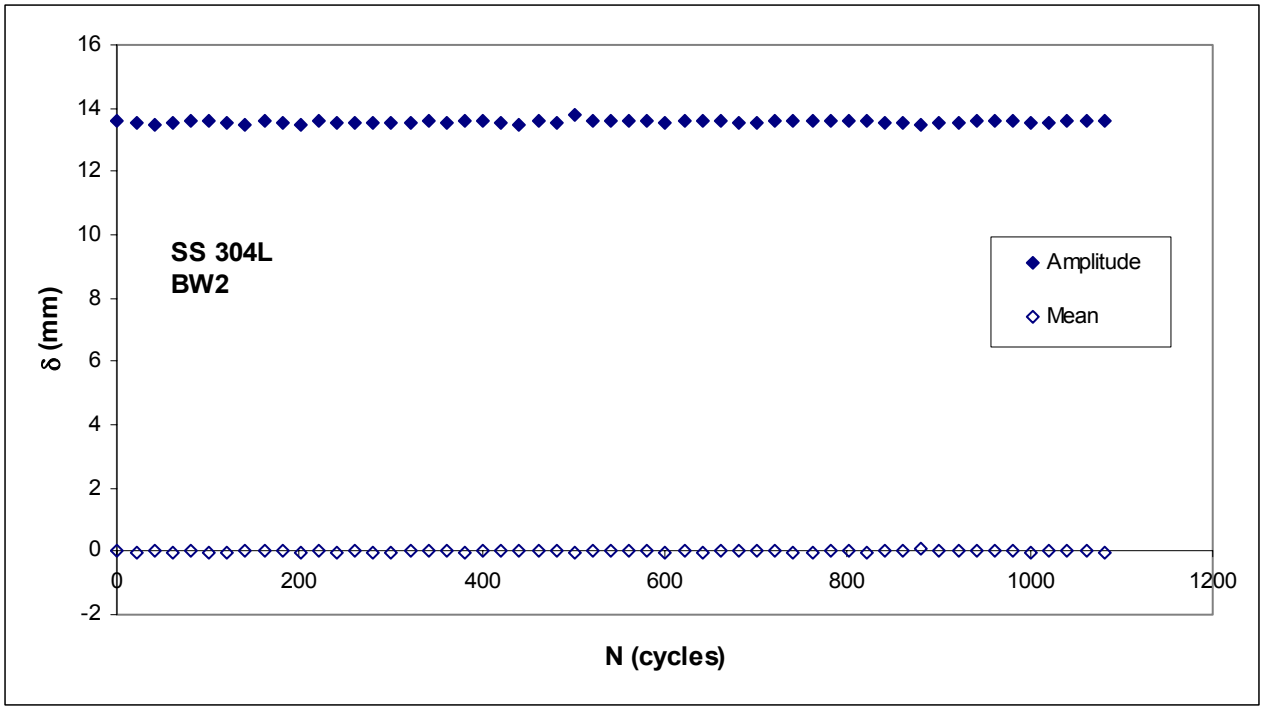

Figure 3.29 Displacement amplitude and mean from BW2 fatigue test (every 20th cycle)

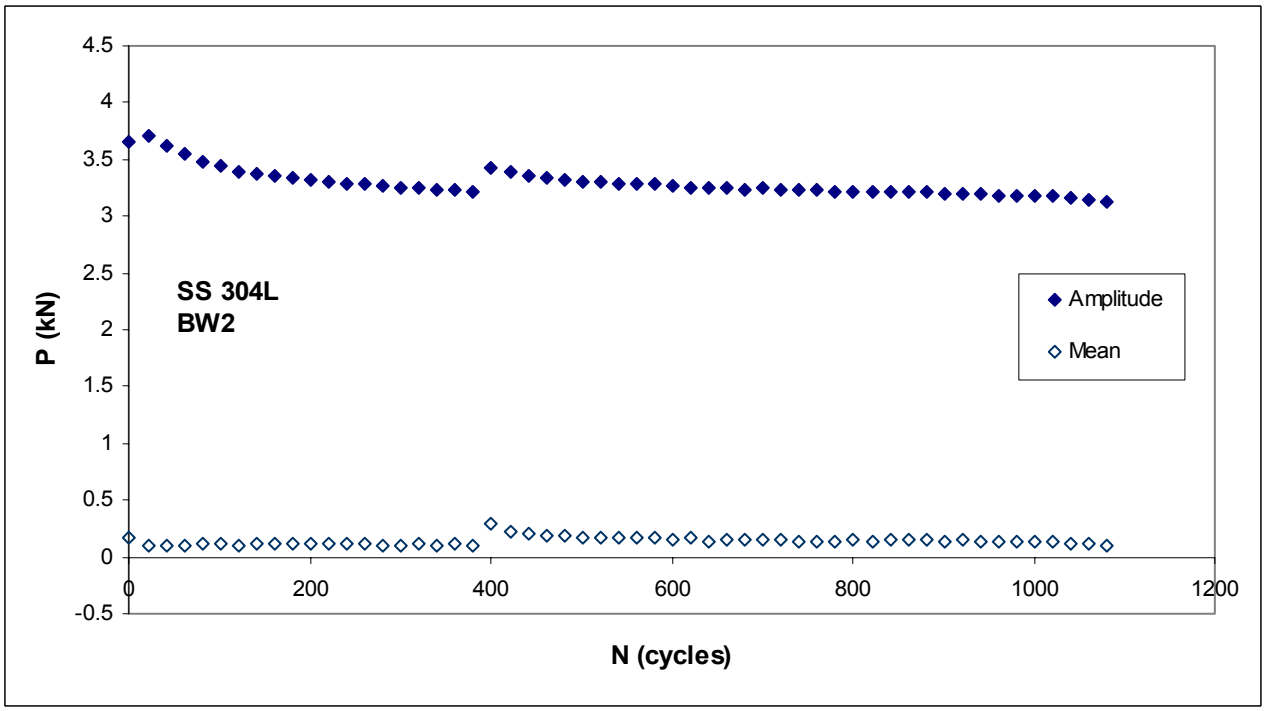

Figure 3.30 Force amplitude and mean from BW2 fatigue test (every 20th cycle)

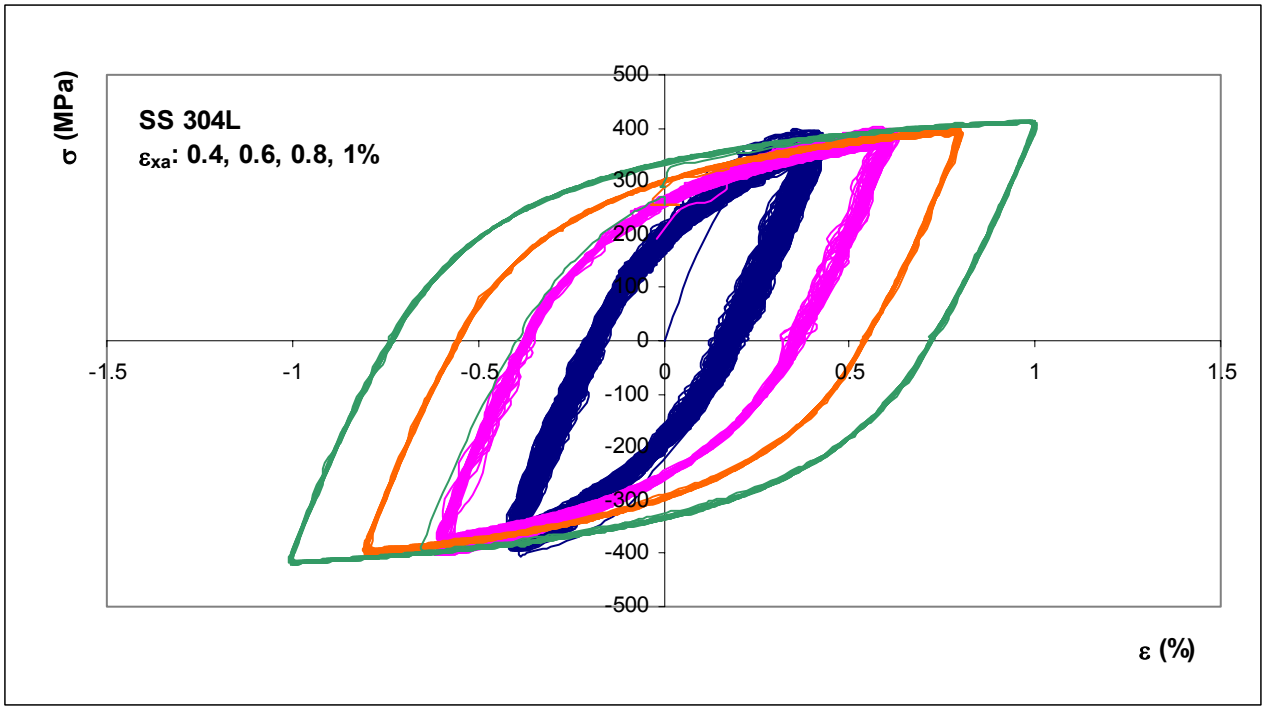

Figure 3.31 Stress-strain behavior of stainless steel specimen in multi-step strain-controlled test

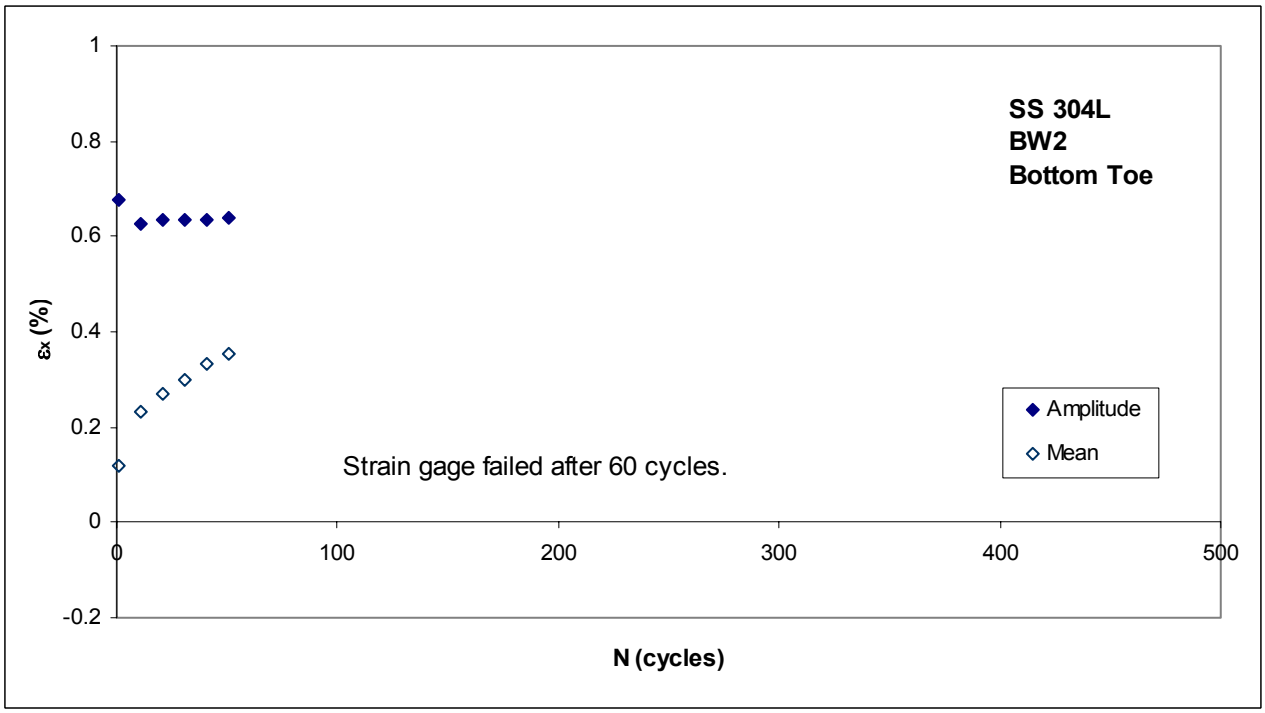

Figure 3.32 Axial strain amplitude and mean at bottom weld toe of BW2 (every 10th cycle)

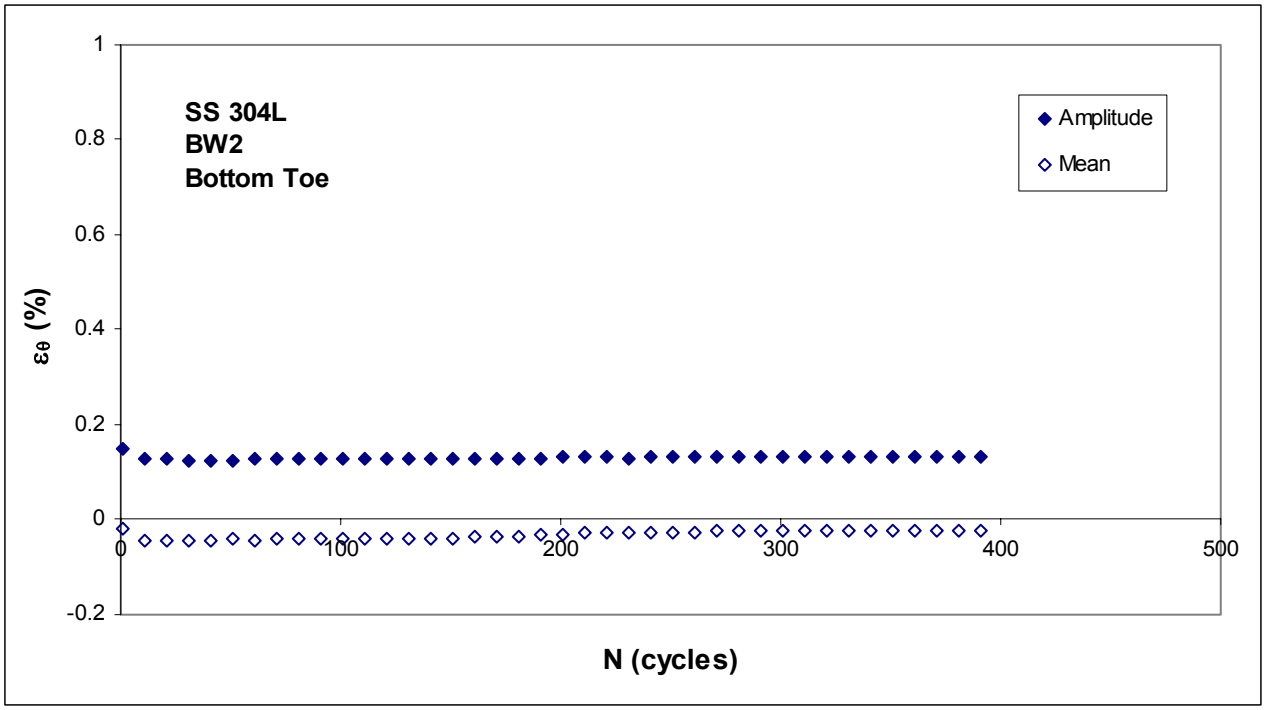

Figure 3.33 Circumferential strain amplitude and mean at bottom weld toe of BW2 (every 10th cycle)

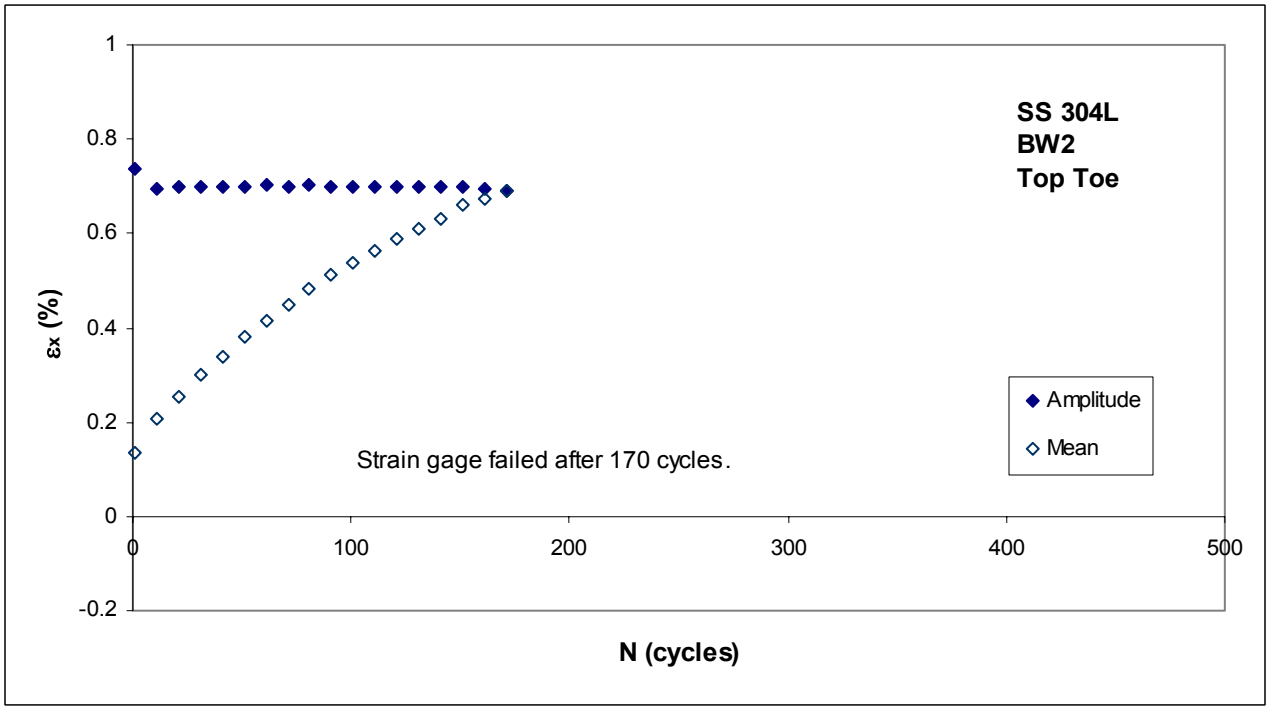

Figure 3.34 Axial strain amplitude and mean at top weld toe of BW2 (every 10th cycle)

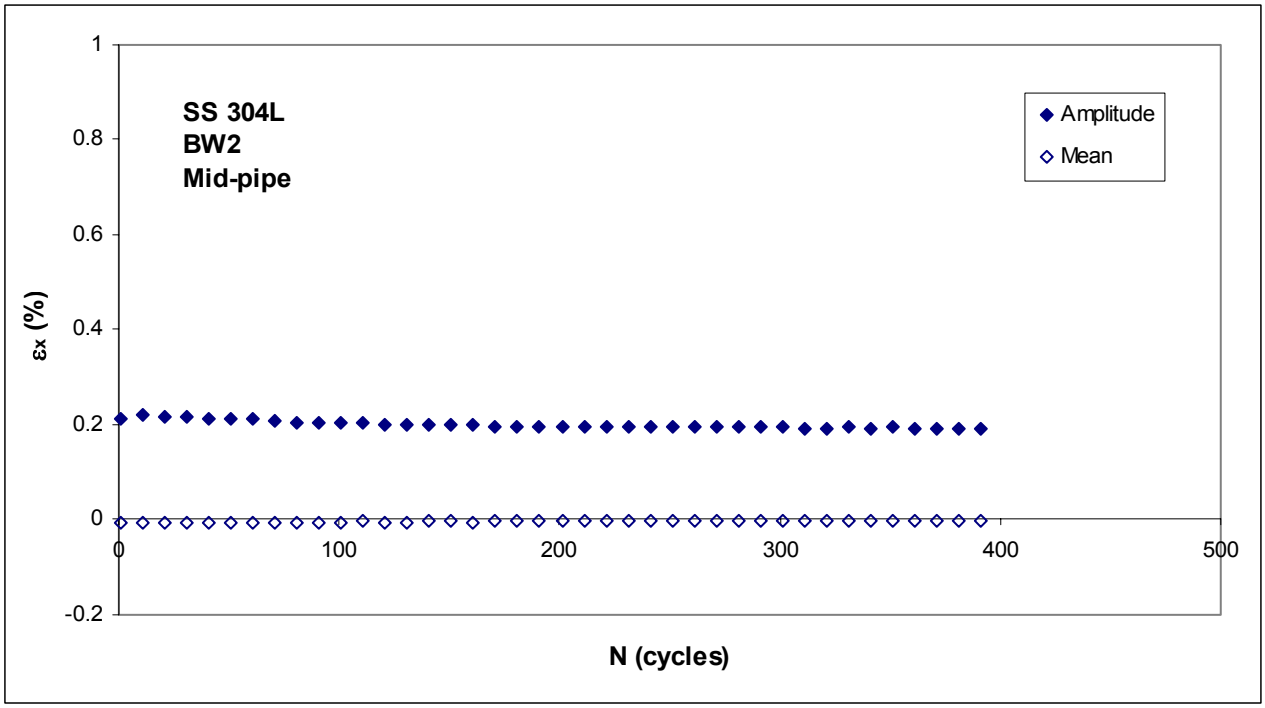

Figure 3.35 Axial strain amplitude and mean at midpoint of pipe length of BW2 (every 10th cycle)

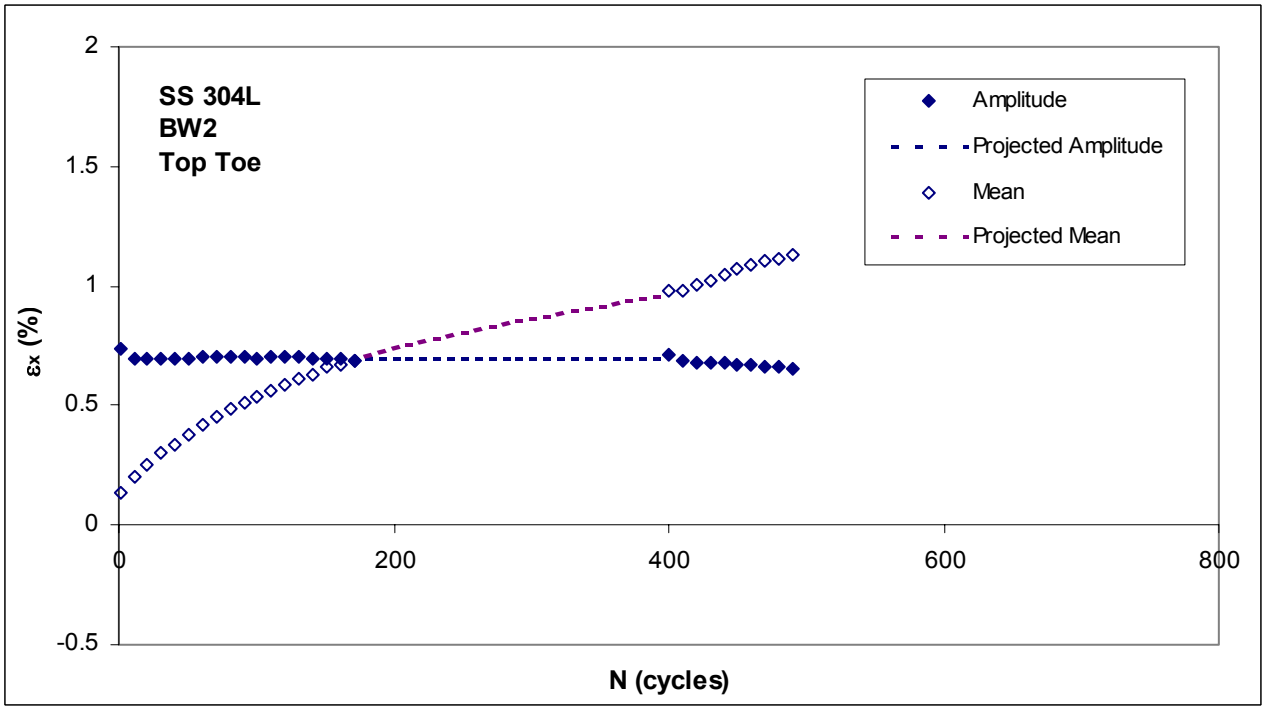

Figure 3.36 Combined stages of axial strain amplitude and mean at top weld toe of Specimen BW2

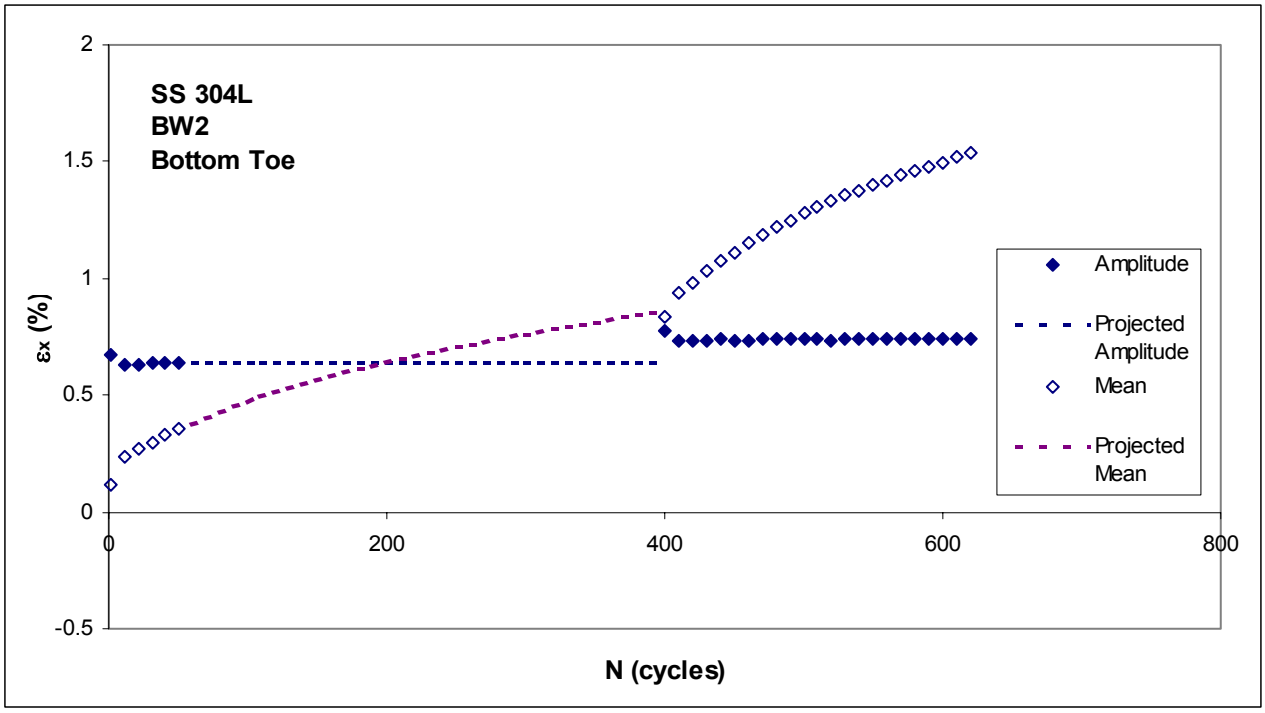

Figure 3.37 Combined stages of axial strain amplitude and mean at bottom weld toe of Specimen BW2

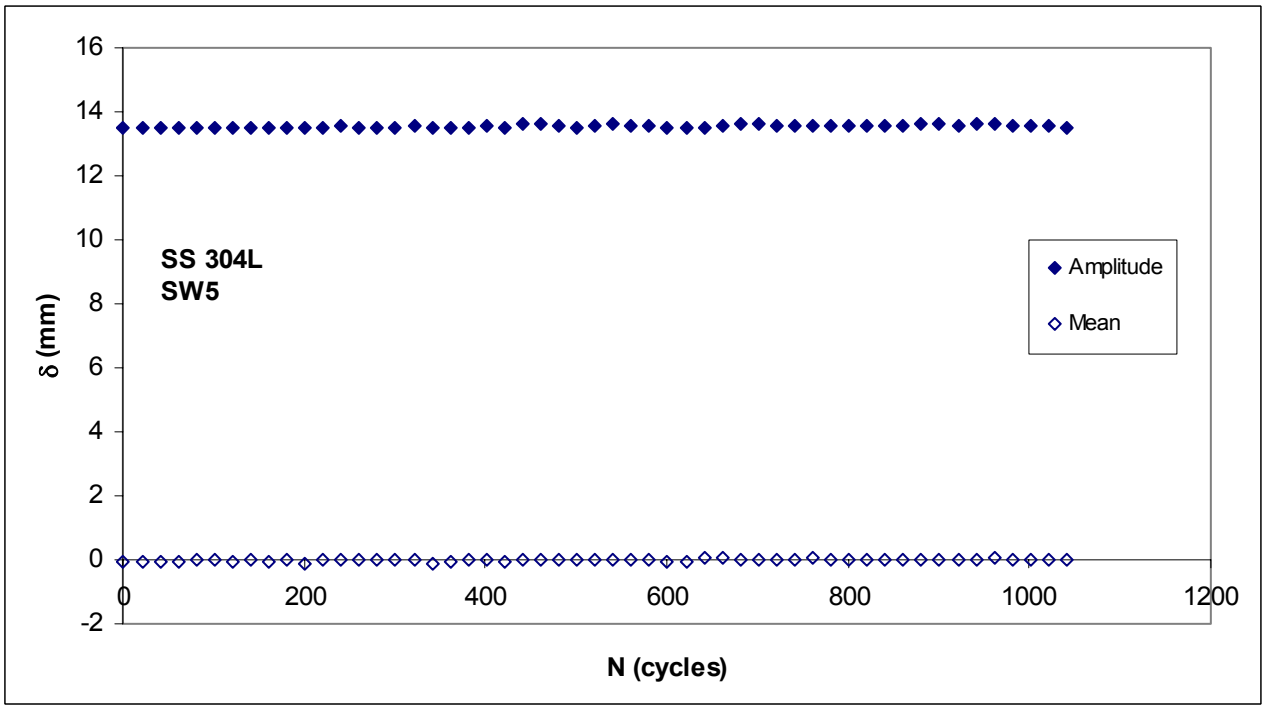

Figure 3.38 Displacement amplitude and mean from Specimen SW5 fatigue test

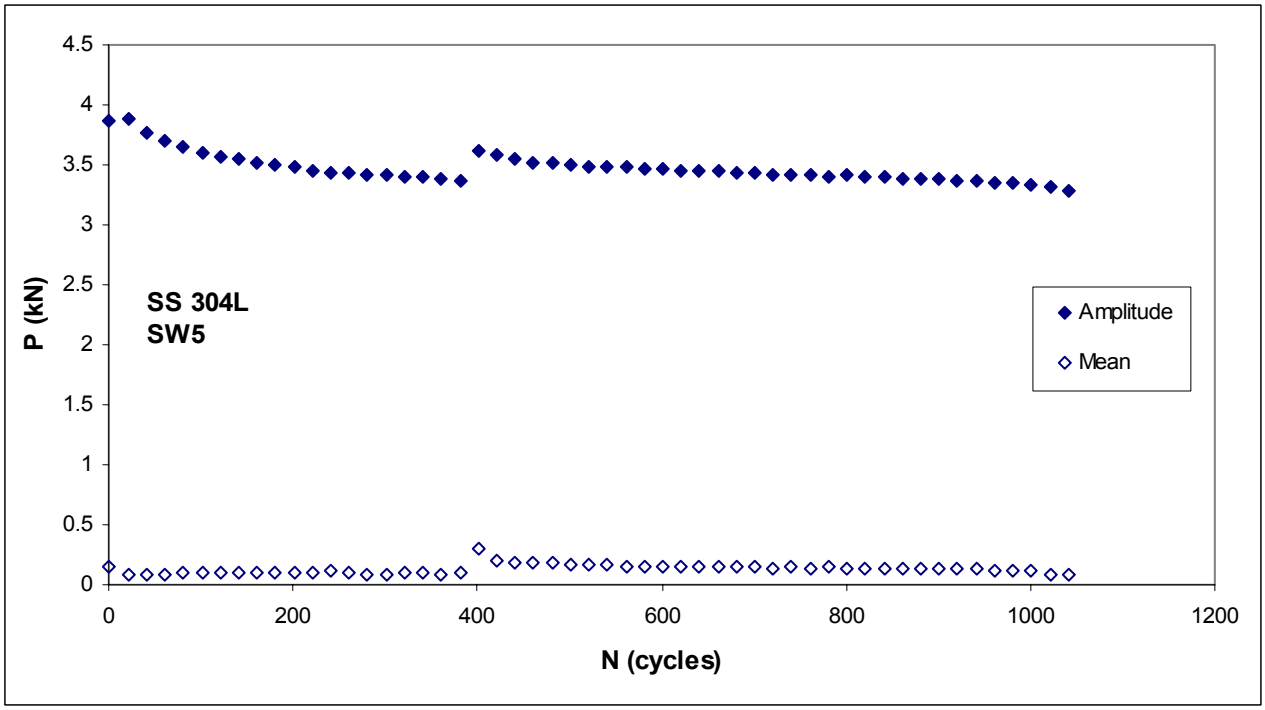

Figure 3.39 Force amplitude and mean from Specimen SW5 fatigue test

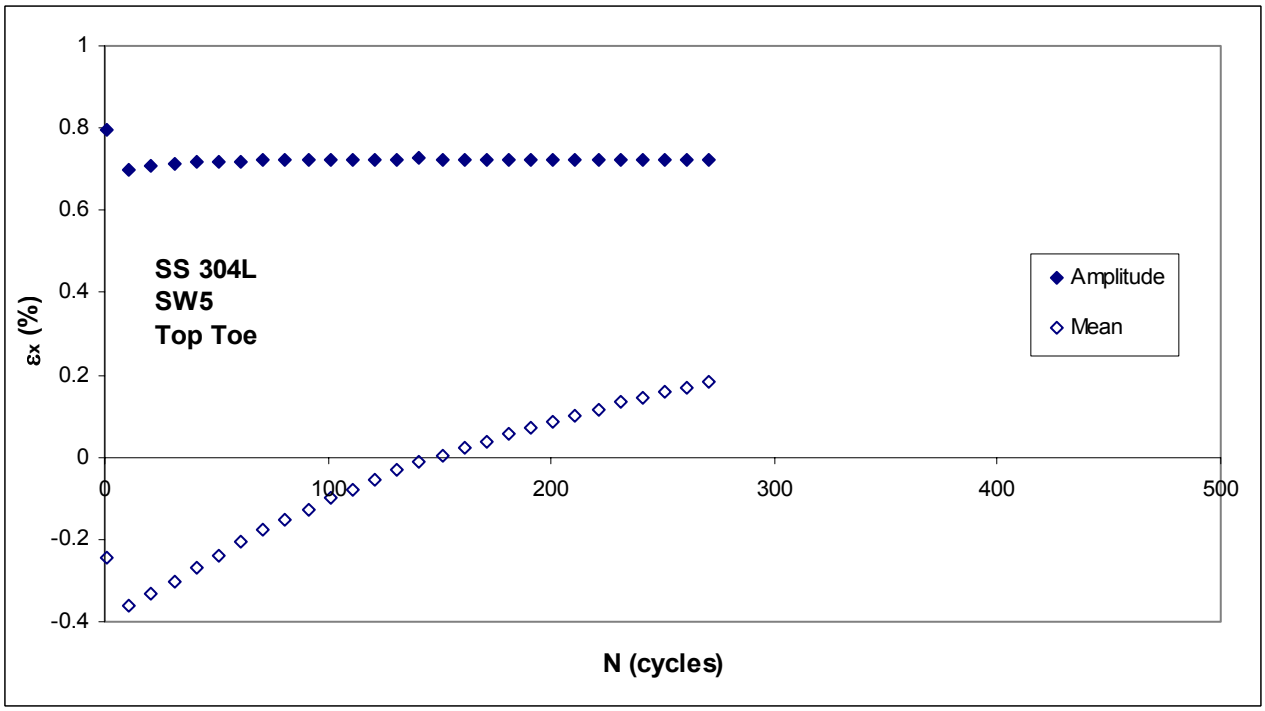

Figure 3.40 Axial strain amplitude and mean at top weld toe of Specimen SW5

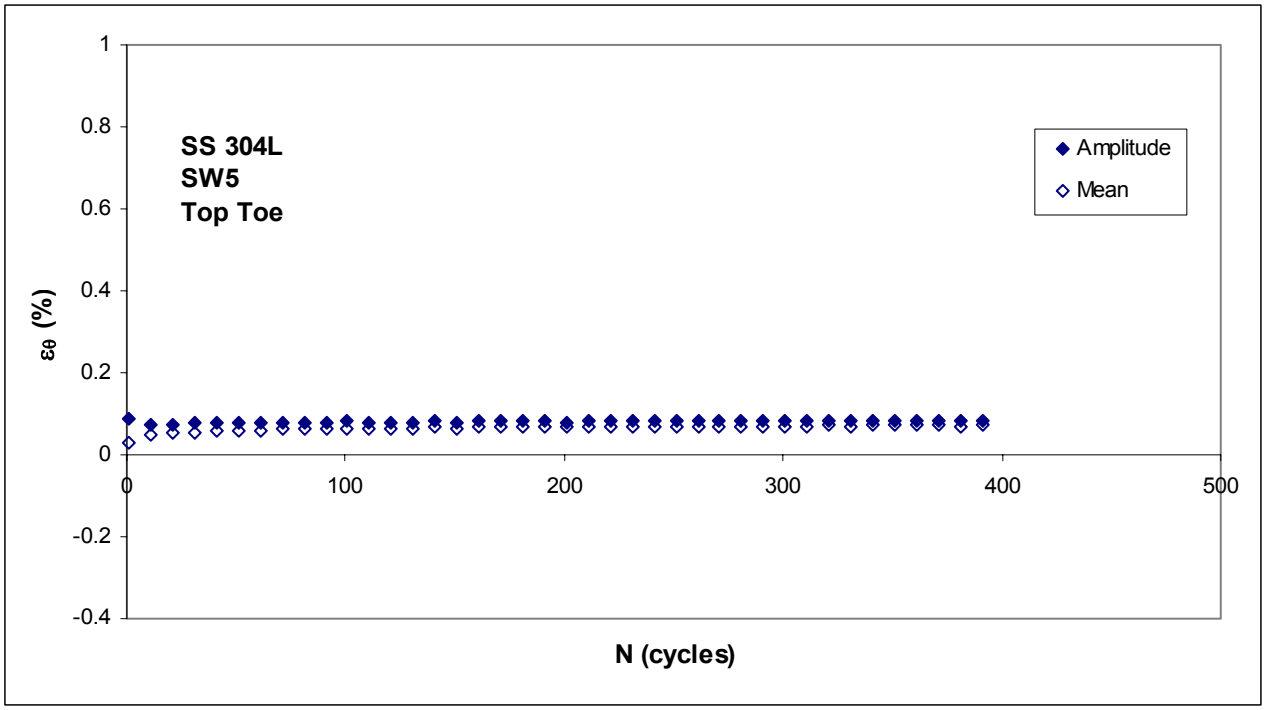

Figure 3.41 Circumferential strain amplitude and mean at top weld toe of Specimen SW5

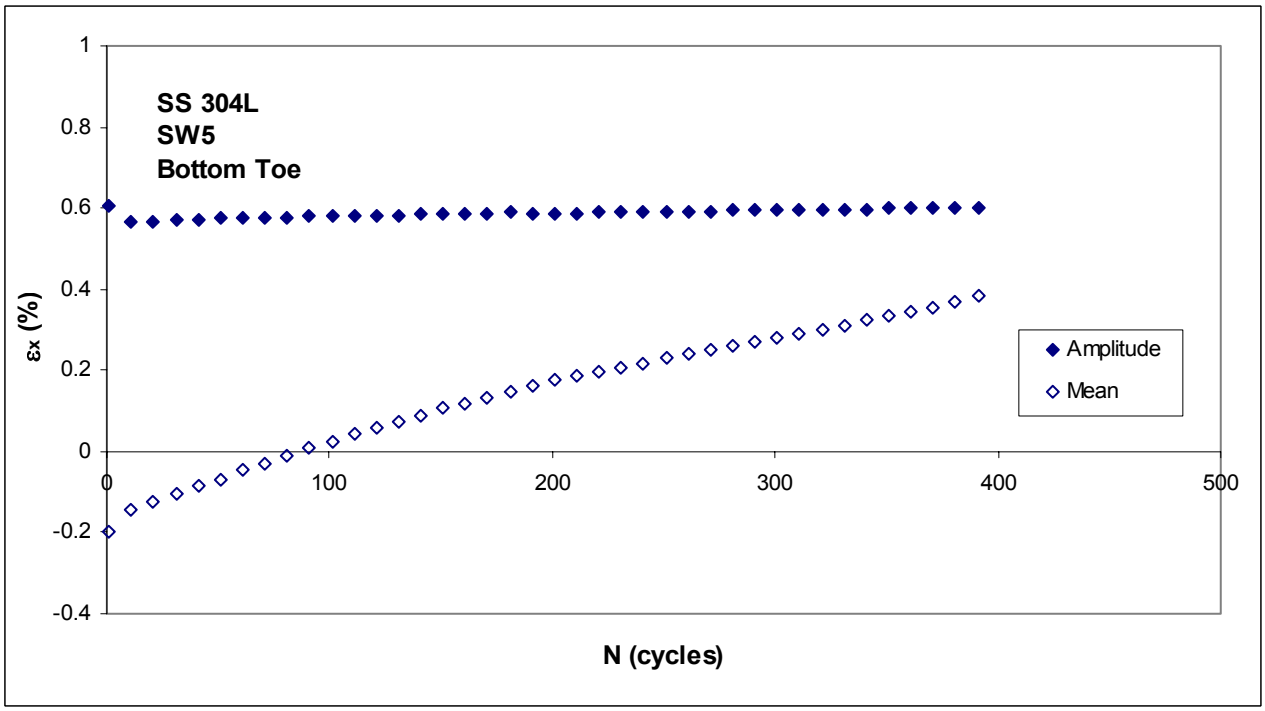

Figure 3.42 Axial strain amplitude and mean at bottom weld toe of Specimen SW5

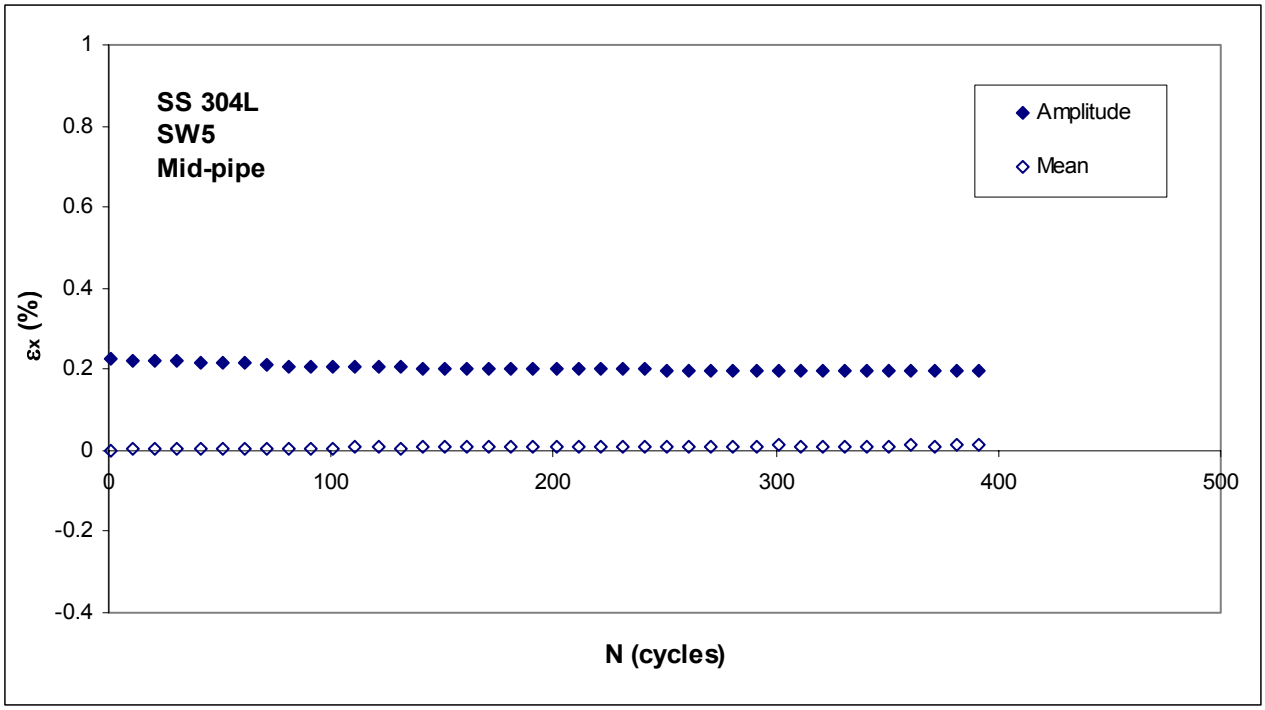

Figure 3.43 Axial strain amplitude and mean at midpoint of pipe length of Specimen SW5

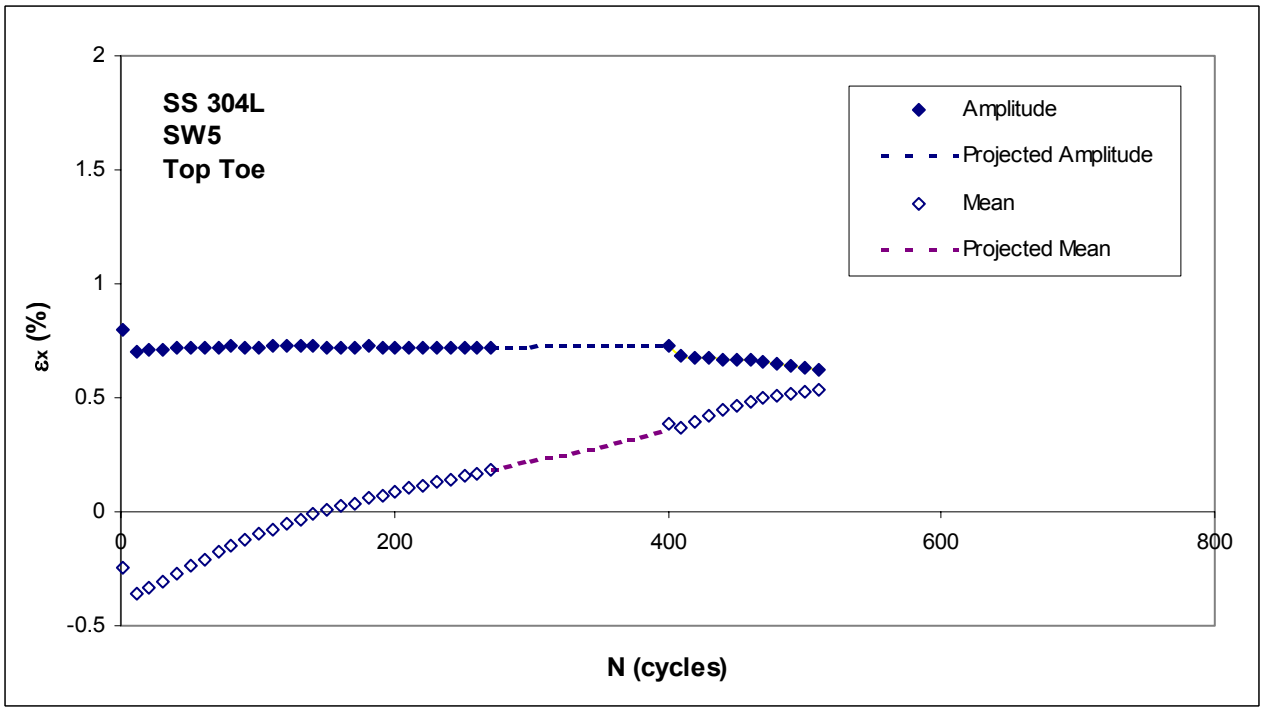

Figure 3.44 Combined stages of axial strain amplitude and mean at top weld toe of Specimen SW5

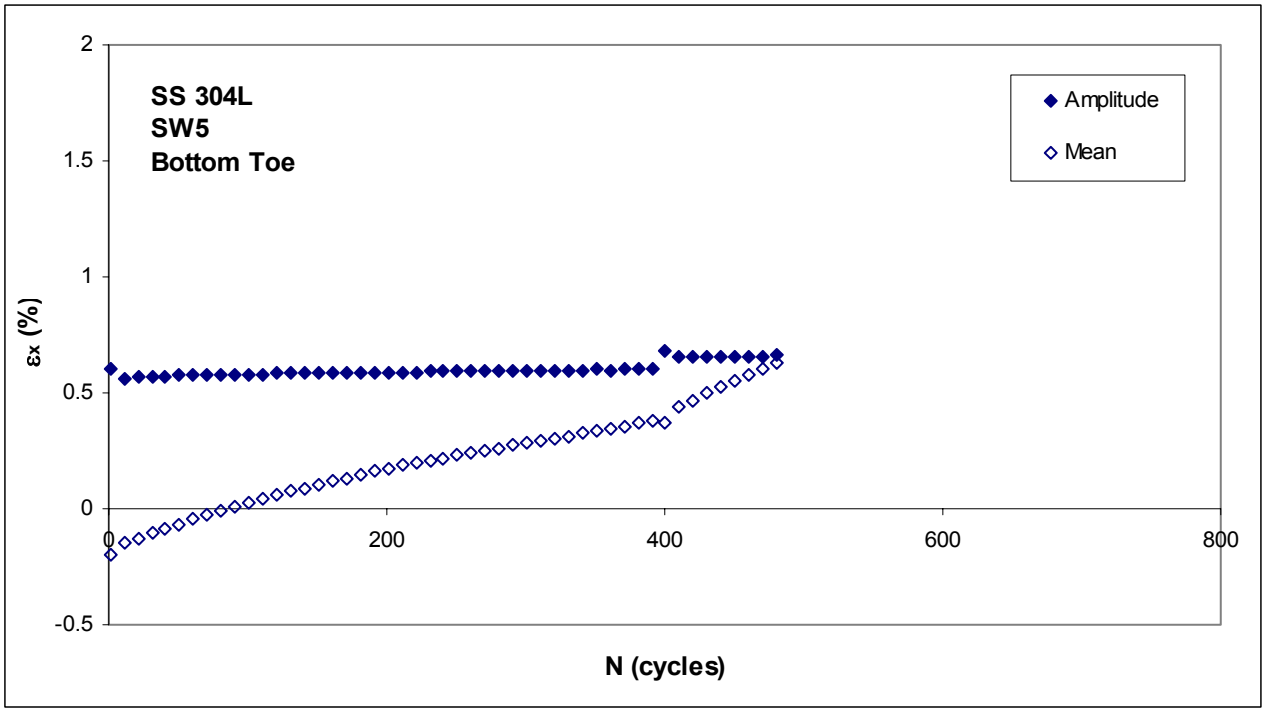

Figure 3.45 Combined stages of axial strain amplitude and mean at bottom weld toe of Specimen SW5

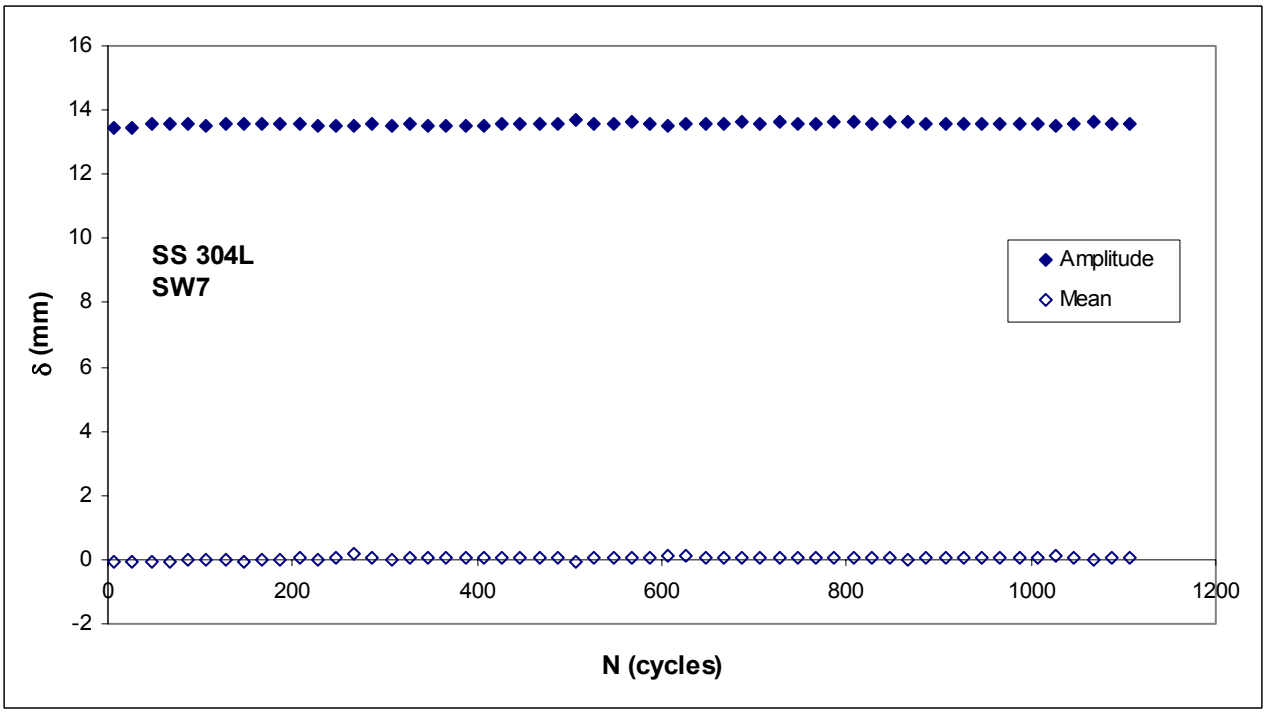

Figure 3.46 Displacement amplitude and mean from Specimen SW7 fatigue test

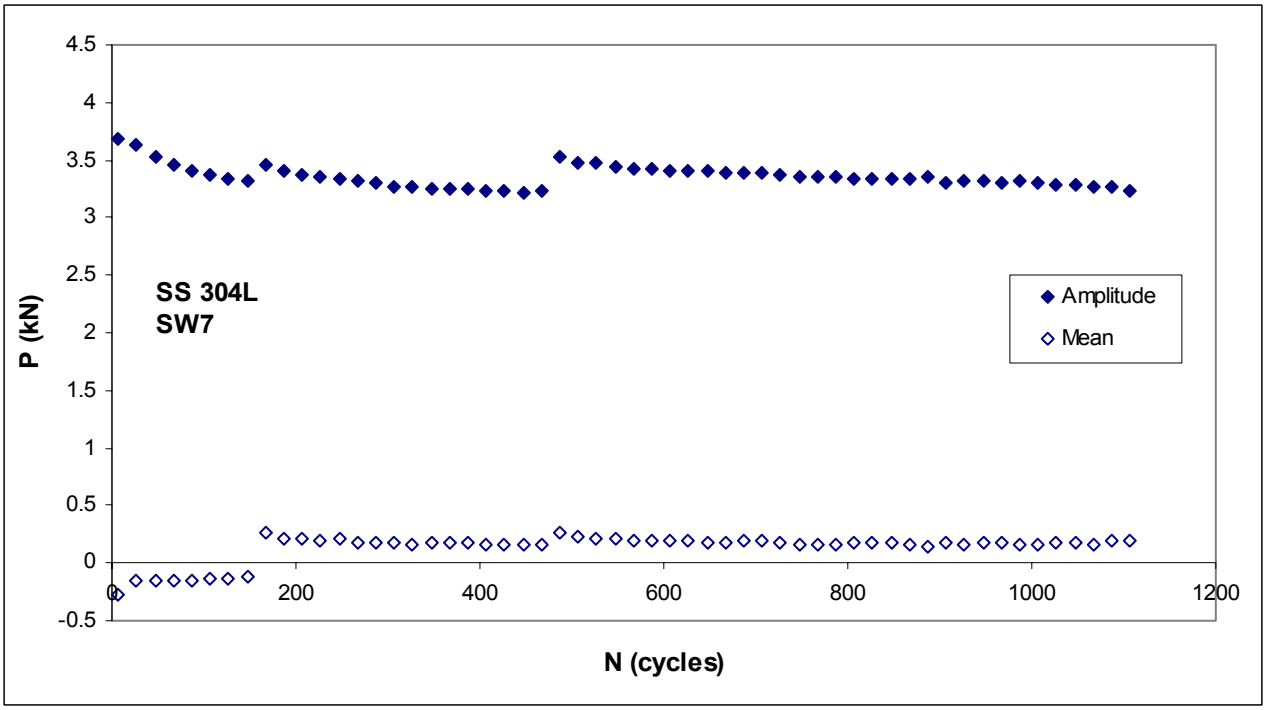

Figure 3.47 Force amplitude and mean from Specimen SW7 fatigue test

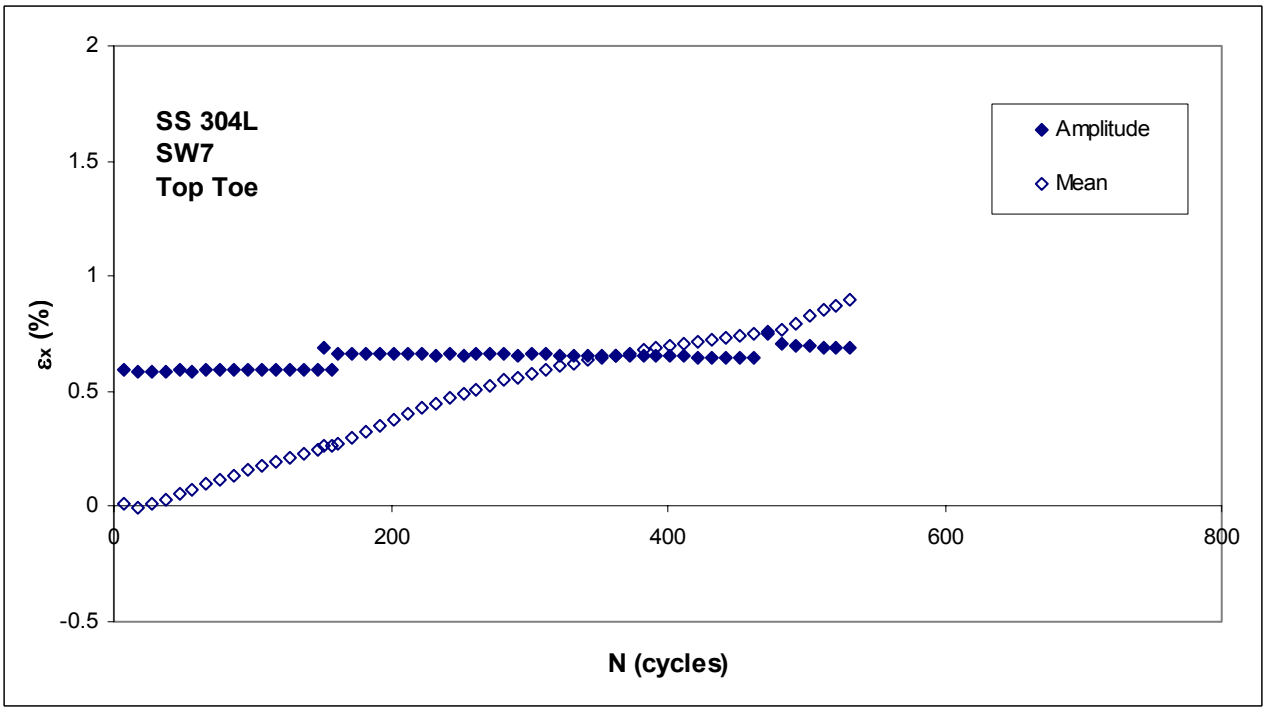

Figure 3.48 Combined stages of axial strain amplitude and mean at top weld toe of Specimen SW7

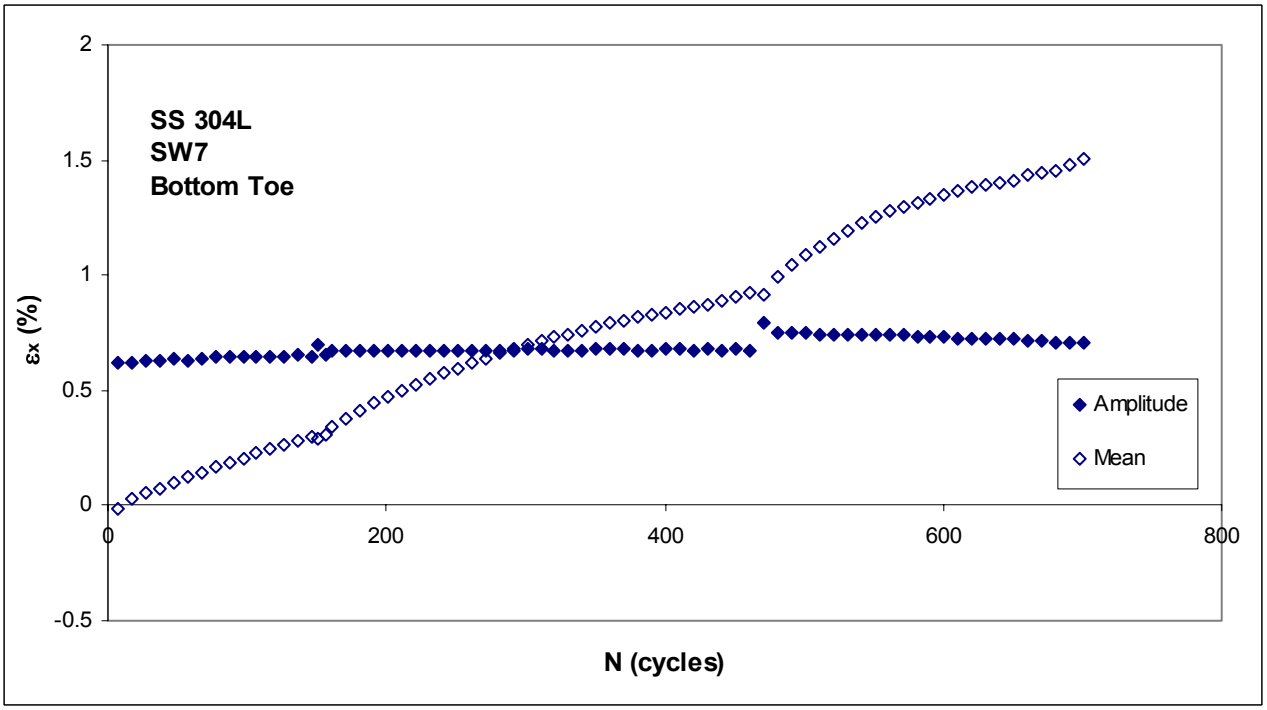

Figure 3.49 Combined stages of axial strain amplitude and mean at bottom weld toe of Specimen SW7

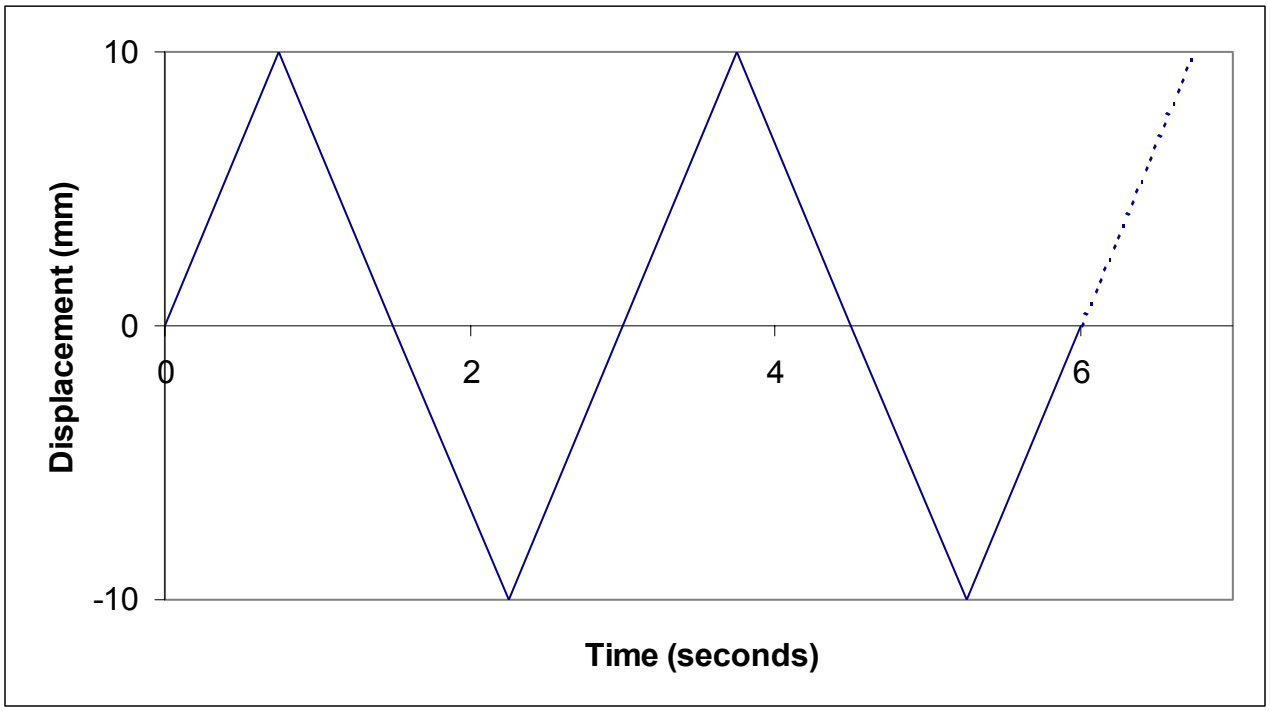

Figure 3.50 Prescribed displacement-controlled loading for SW8 fatigue test

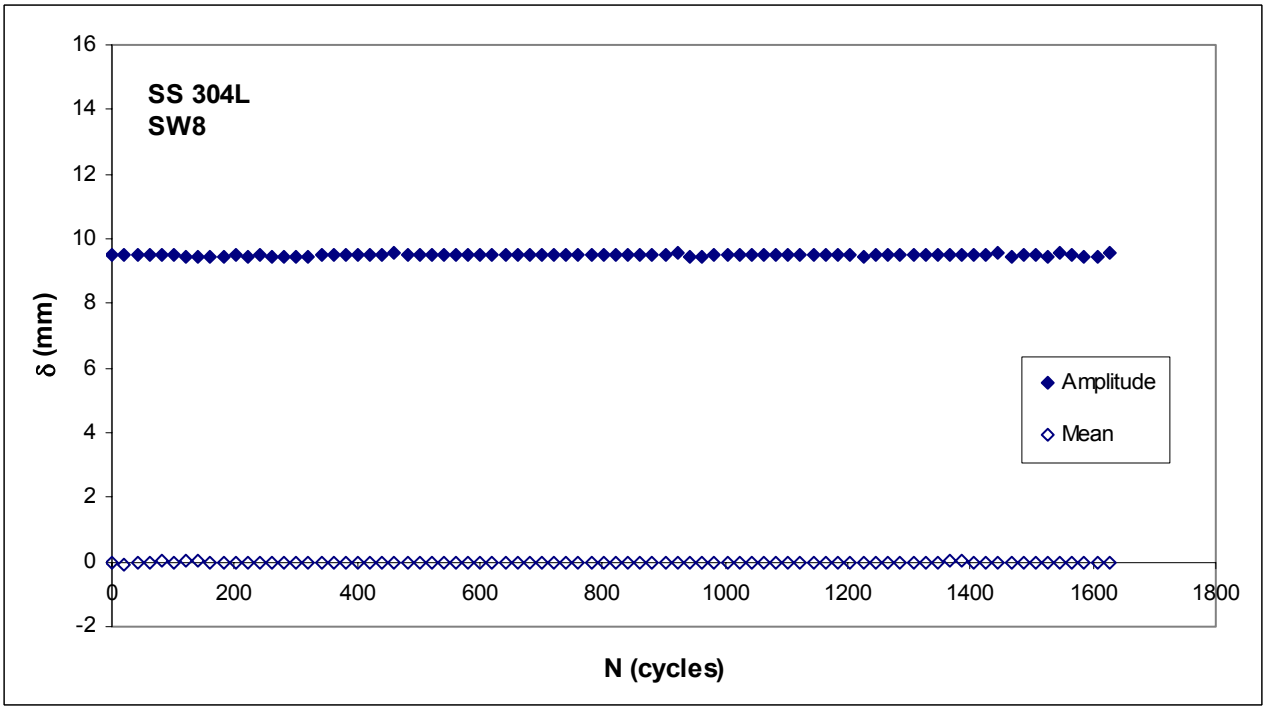

Figure 3.51 Displacement amplitude and mean from SW8 fatigue test (every 20th cycle)

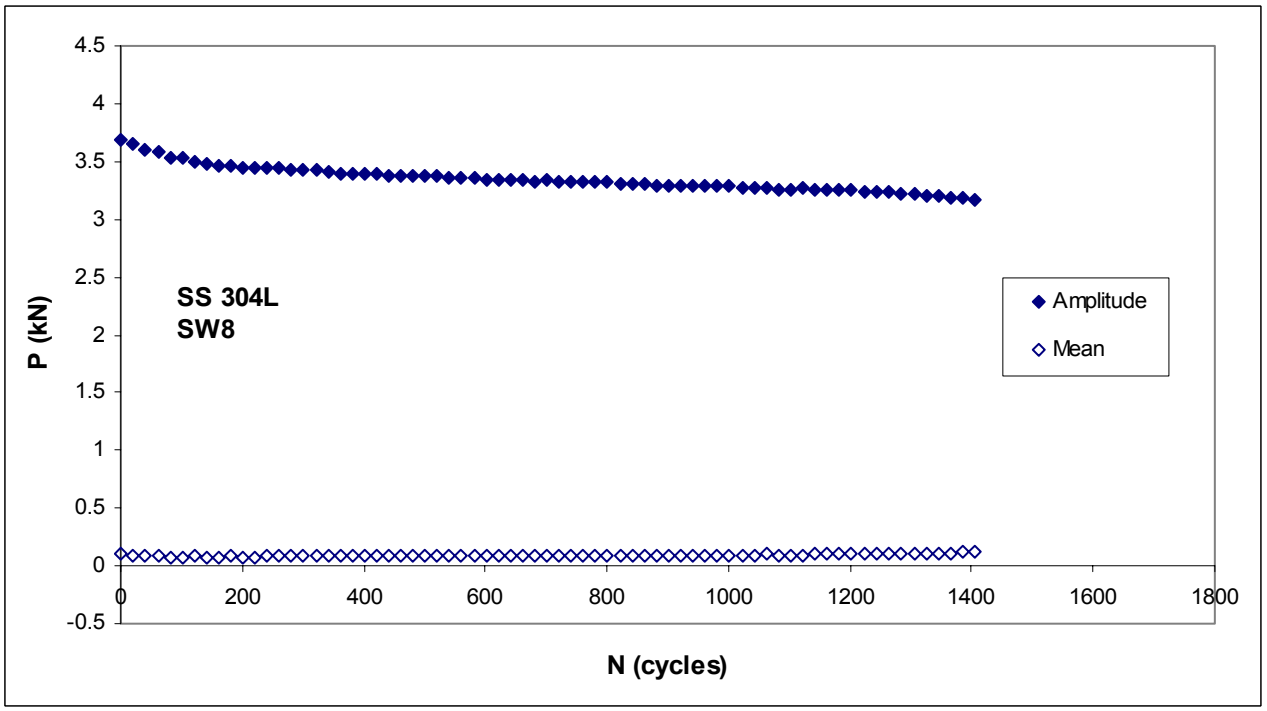

Figure 3.52 Force amplitude and mean from SW8 fatigue test (every 20th cycle)

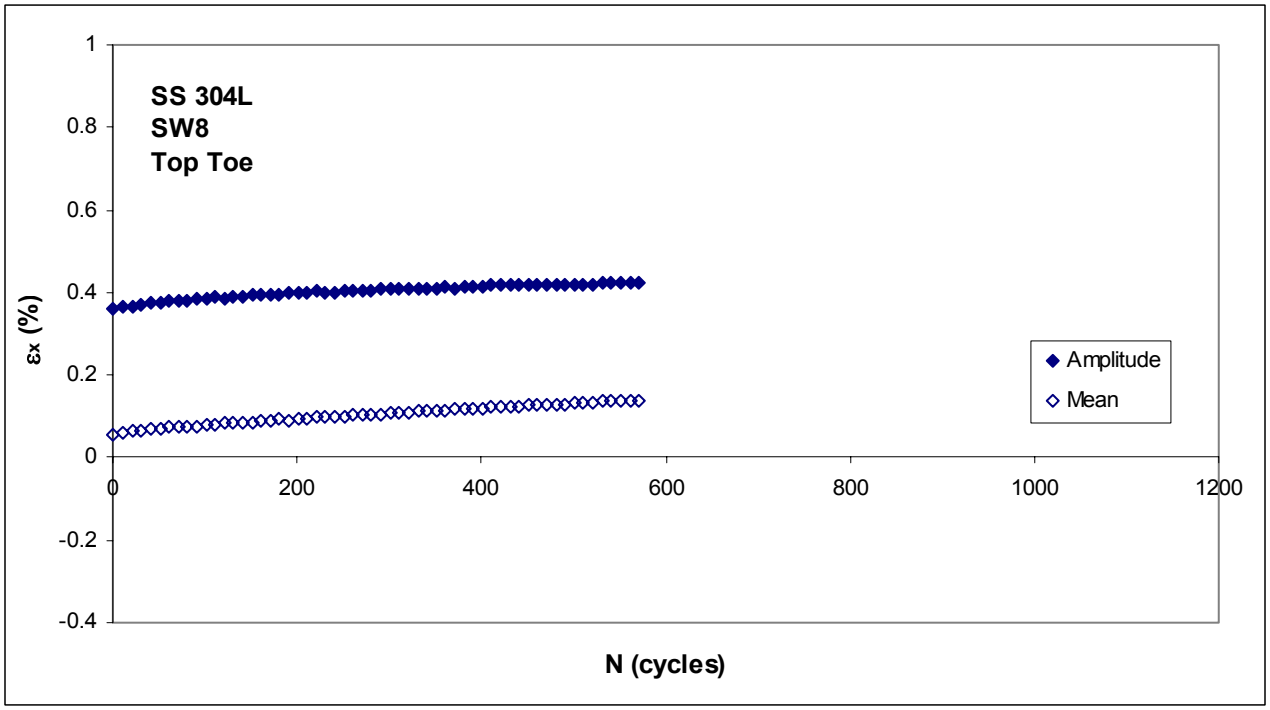

Figure 3.53 Axial strain amplitude and mean at top weld toe of SW8 (every 10th cycle)

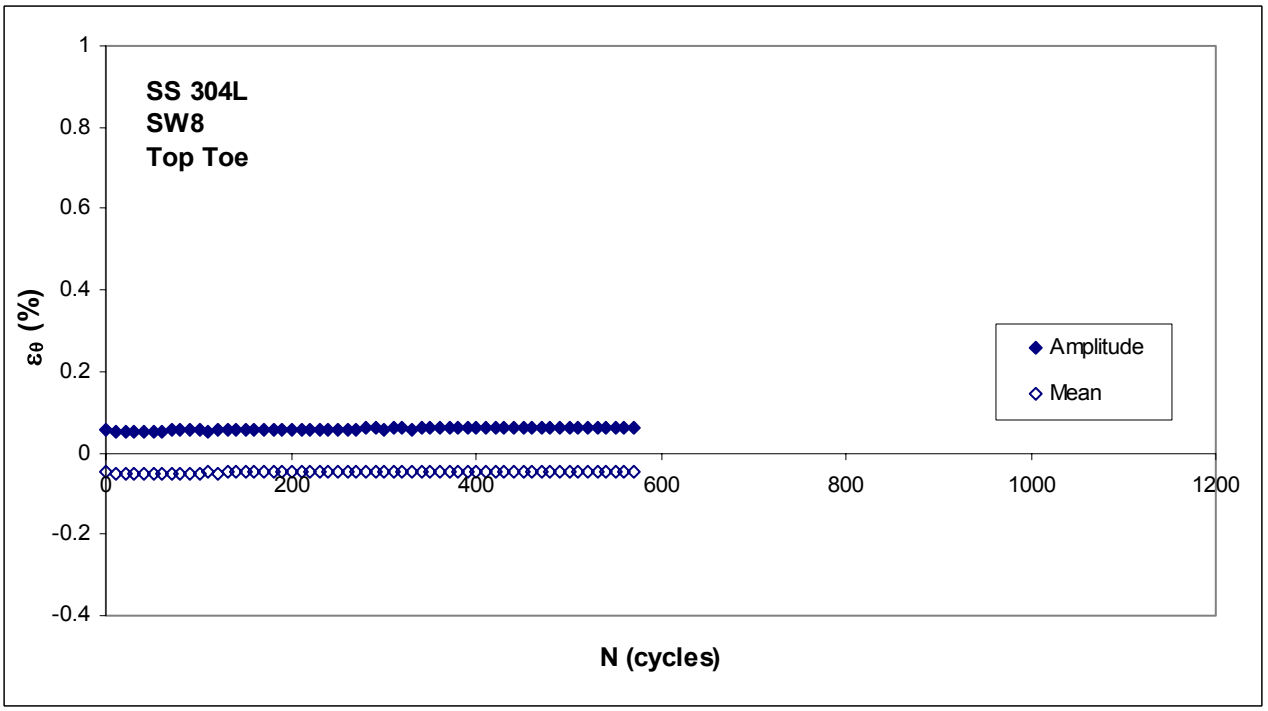

Figure 3.54 Circumferential strain amplitude and mean at top weld toe of SW8 (every 10th cycle)

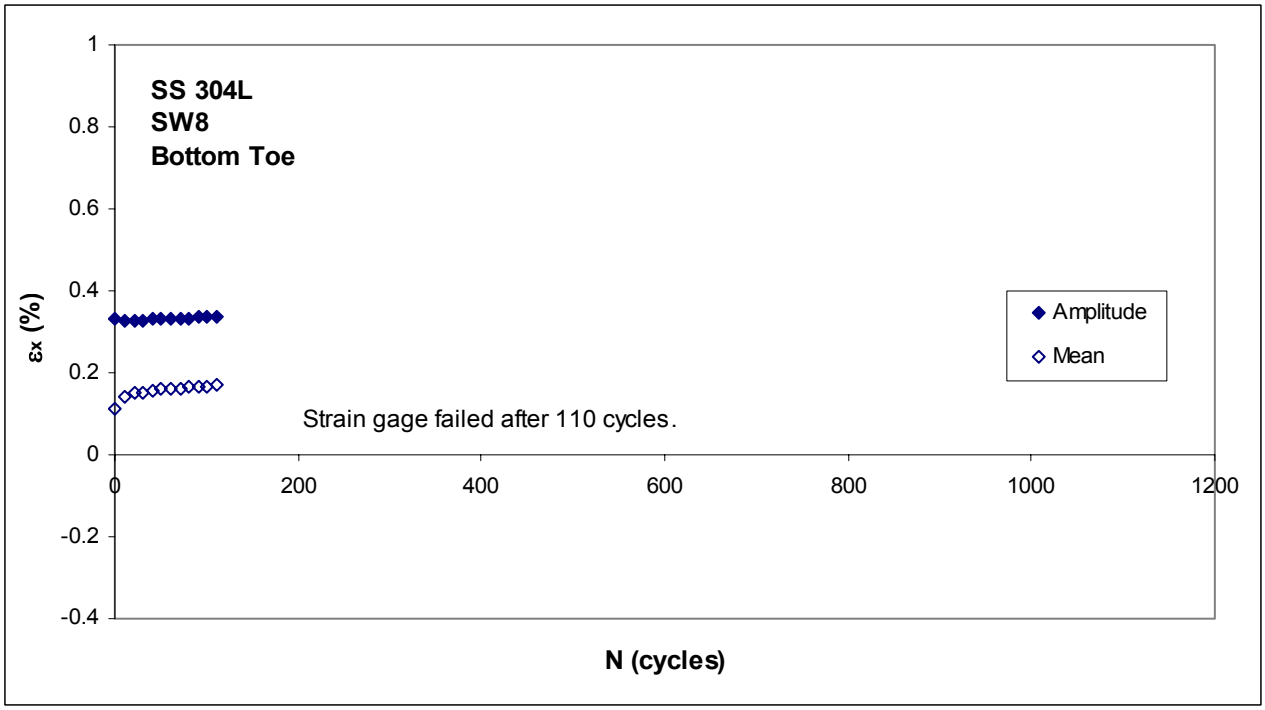

Figure 3.55 Axial strain amplitude and mean at bottom weld toe of SW8 (every 10th cycle)

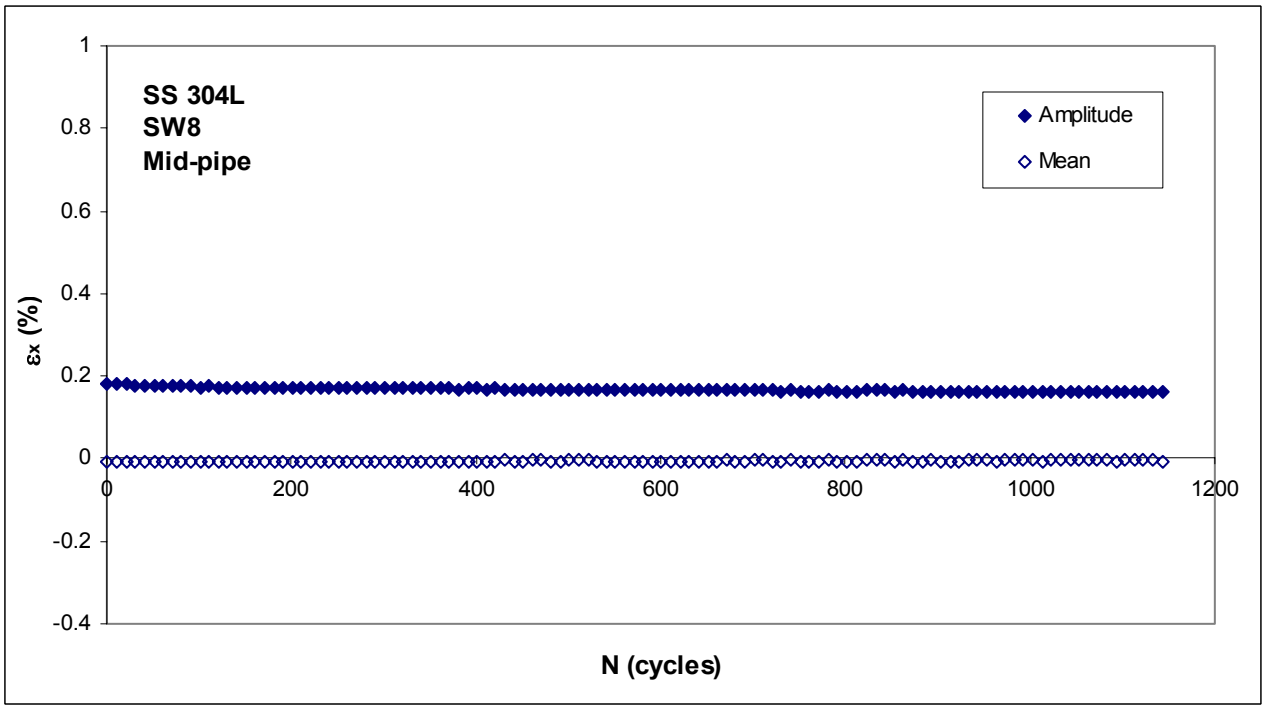

Figure 3.56 Axial strain amplitude and mean at midpoint of pipe length of SW8 (every 10th cycle)

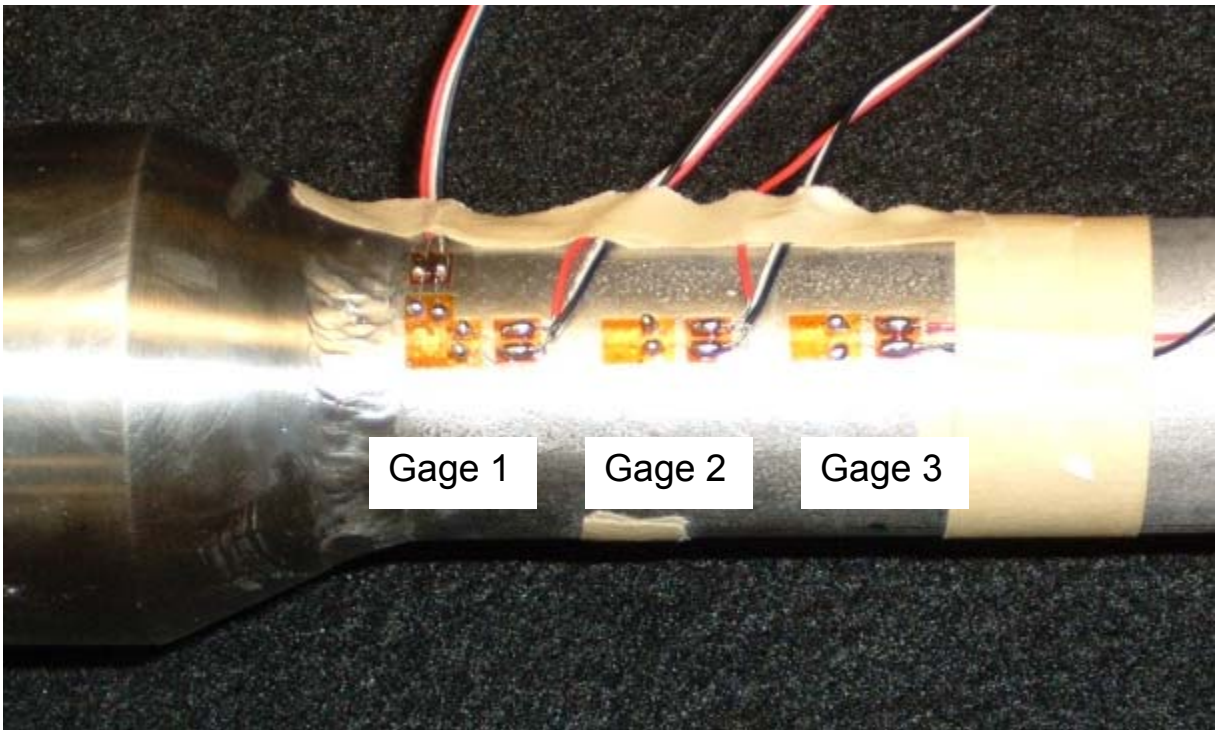

Figure 3.57 Strain gage locations along pipe length

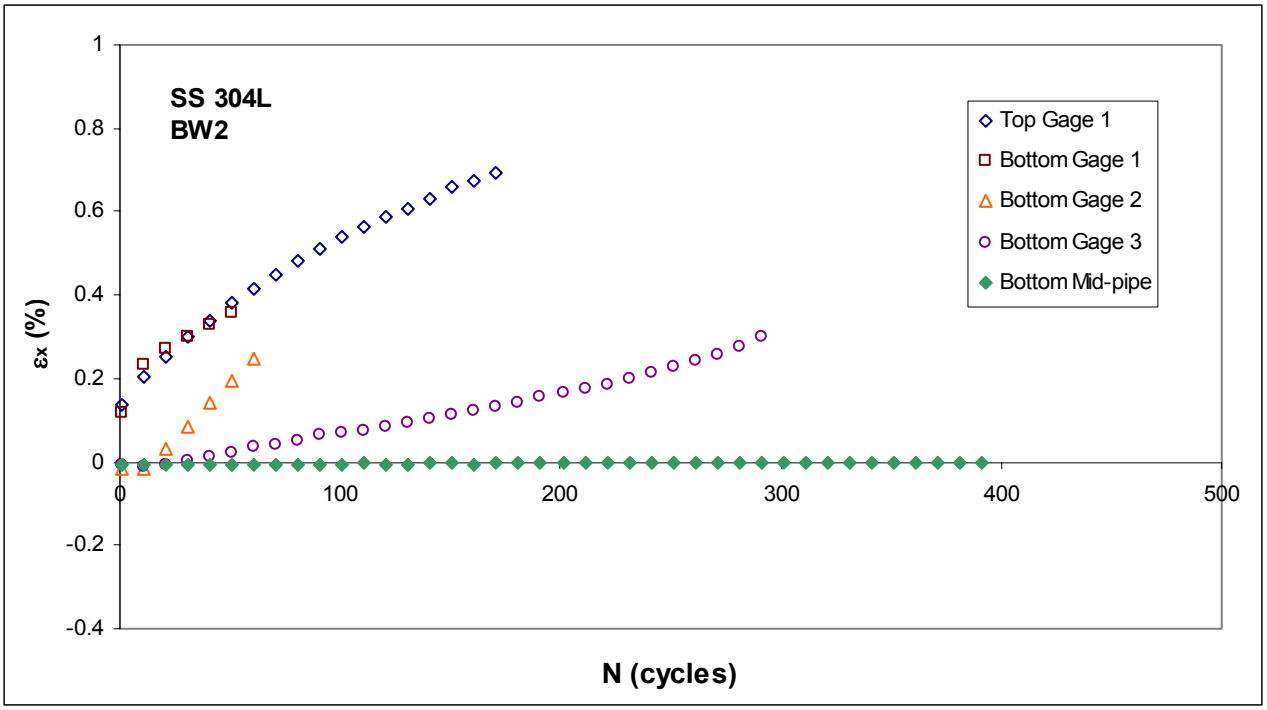

Figure 3.58 Axial strain ratcheting in BW2 along pipe length (every 10th cycle)

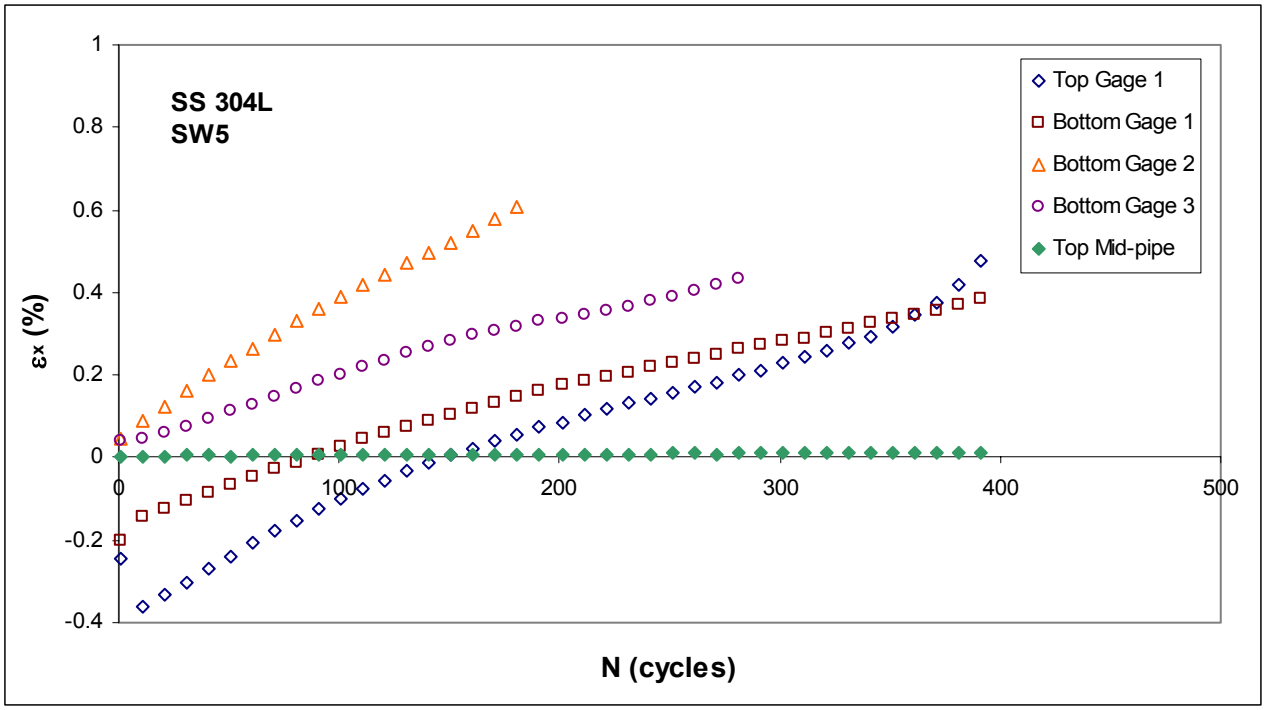

Figure 3.59 Axial strain ratcheting in SW5 along pipe length (every 10th cycle)

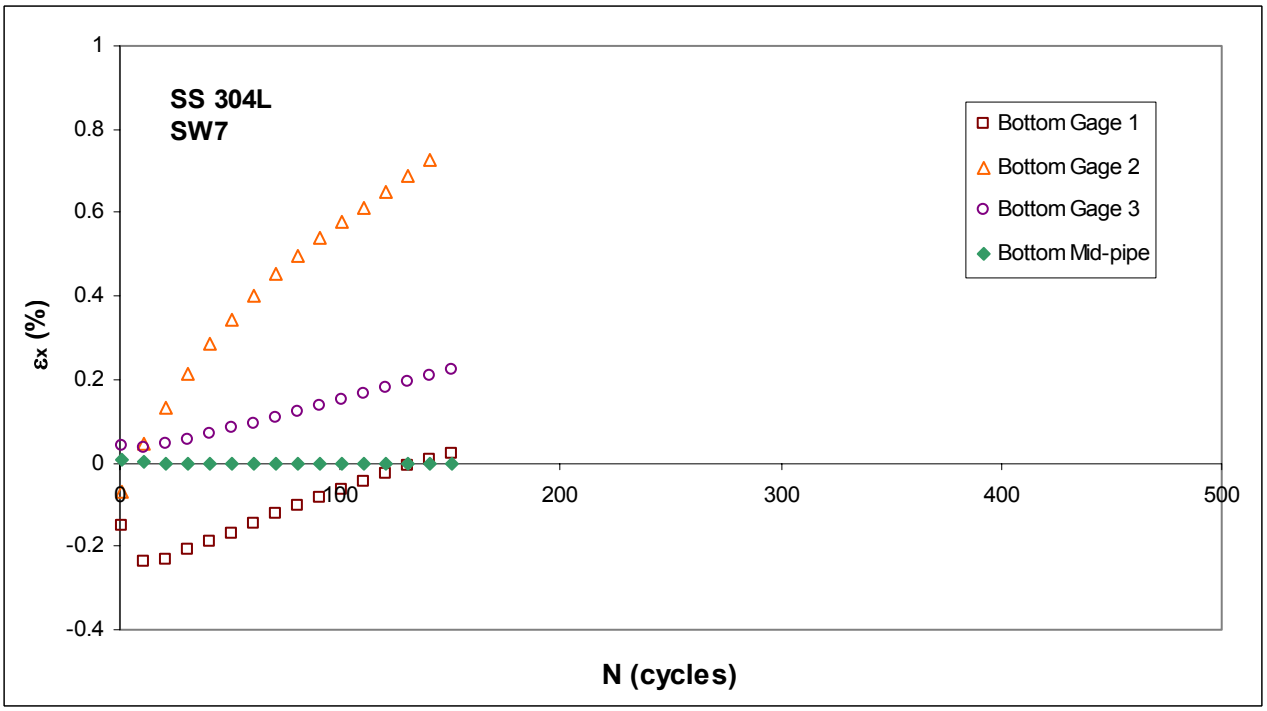

Figure 3.60 Axial strain ratcheting in SW7 along pipe length (every 10th cycle)

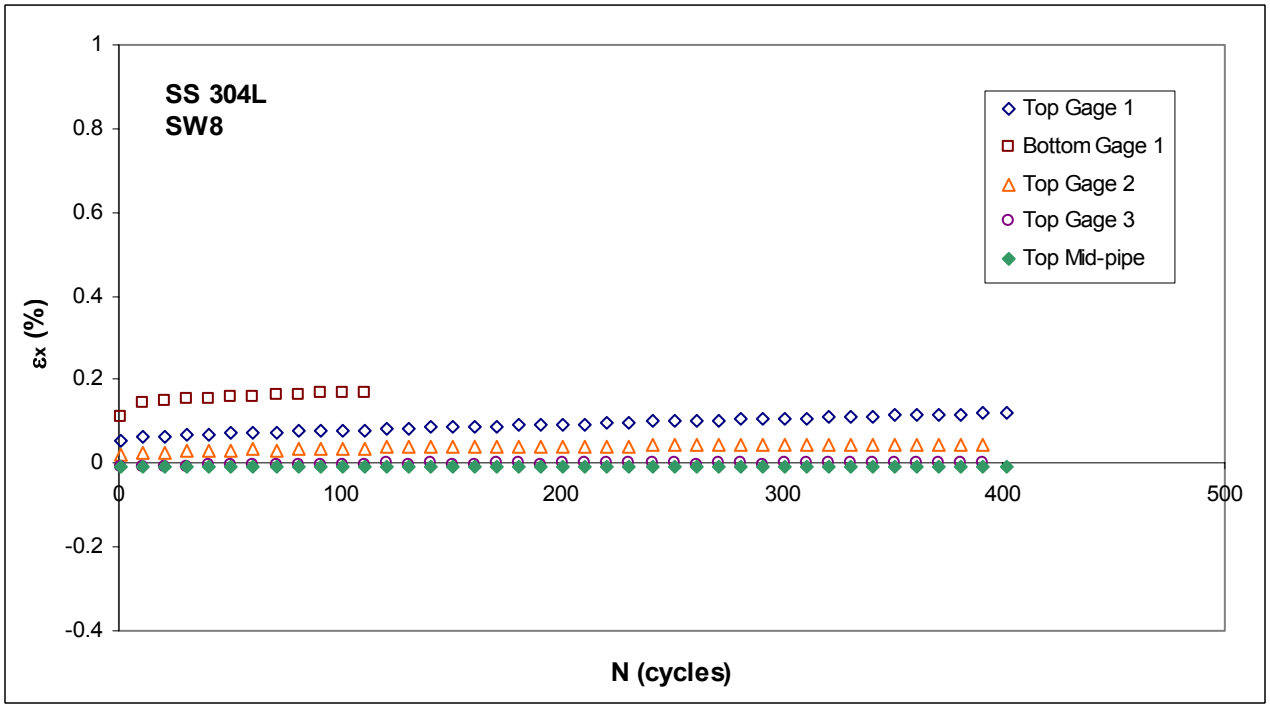

Figure 3.61 Axial strain ratcheting in SW8 along pipe length (every 10th cycle)

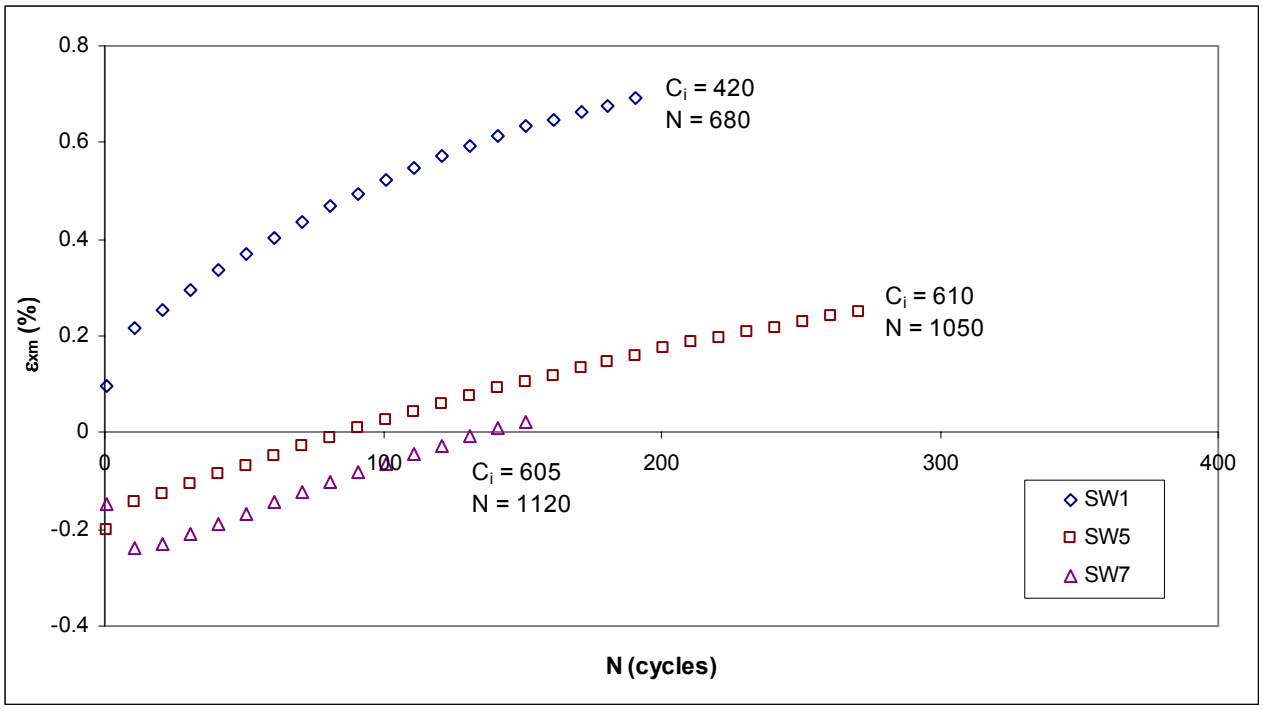

Figure 3.62 Ratcheting of mean axial strains in three weld pass specimens (every 10th cycle)

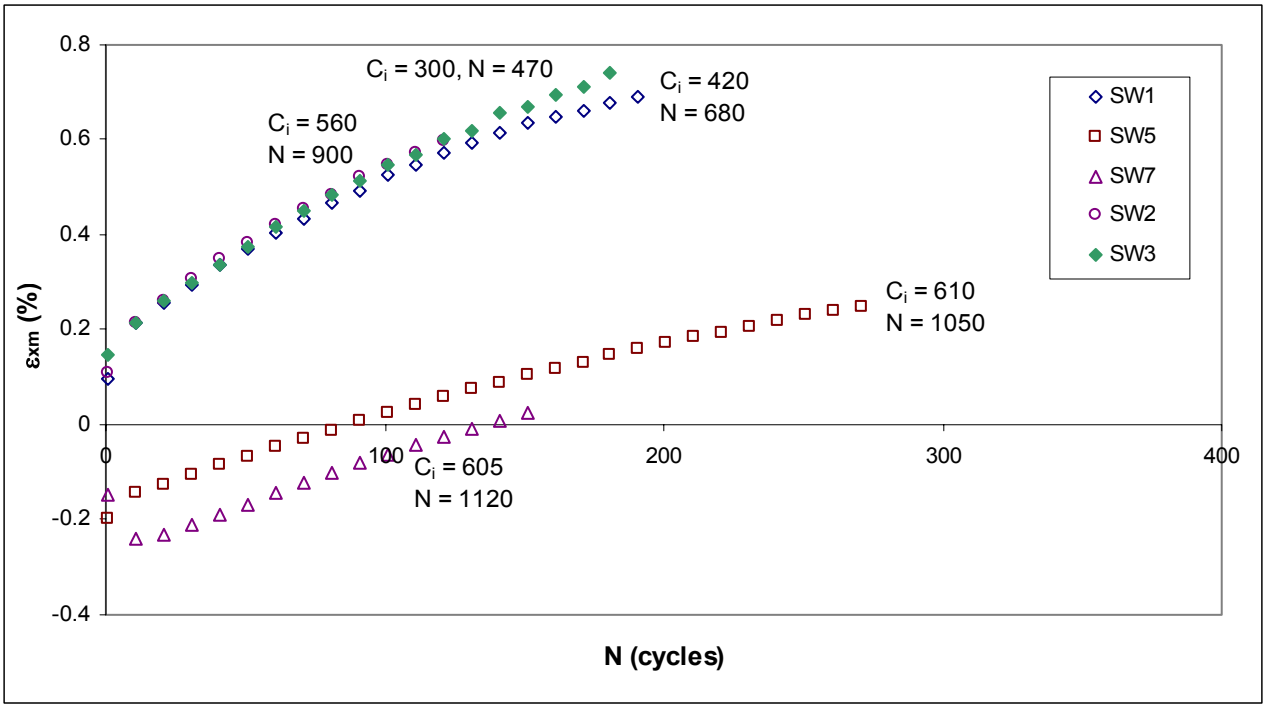

Figure 3.63 Ratcheting of mean axial strains in three and four weld pass specimens (every 10th cycle)

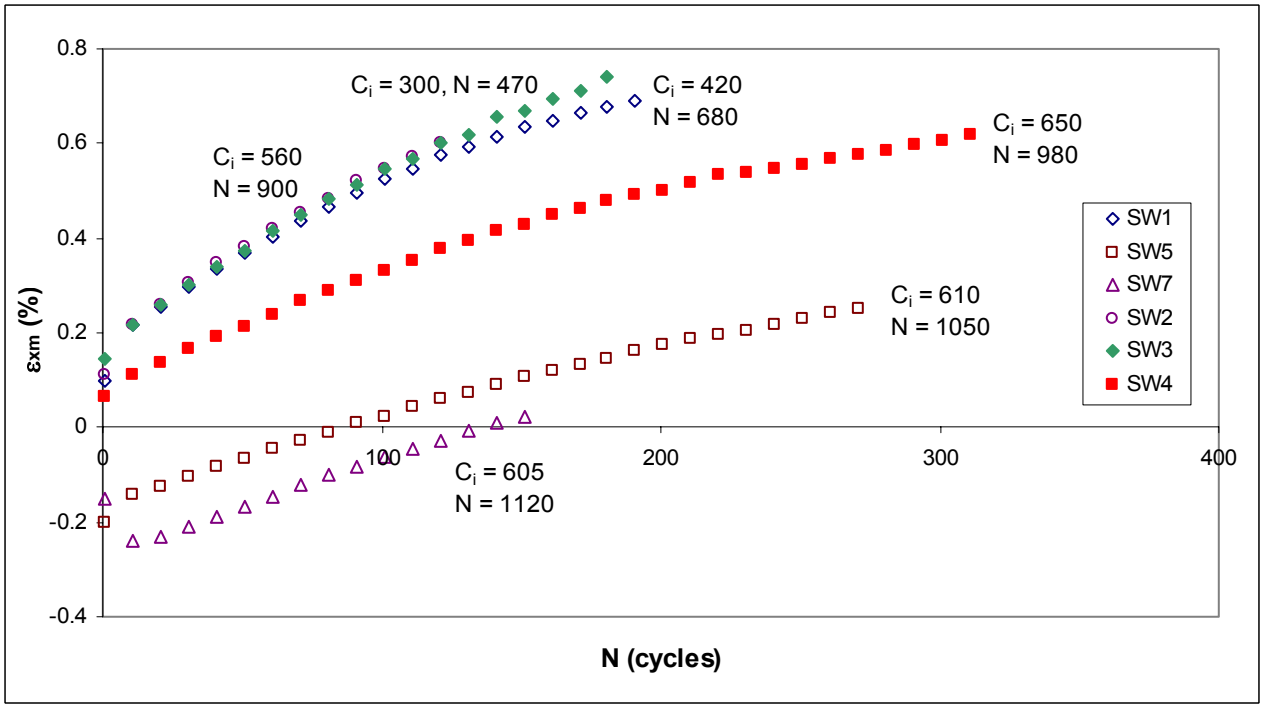

Figure 3.64 Ratcheting of mean axial strains in three, four, and five weld pass specimens (every 10th cycle)

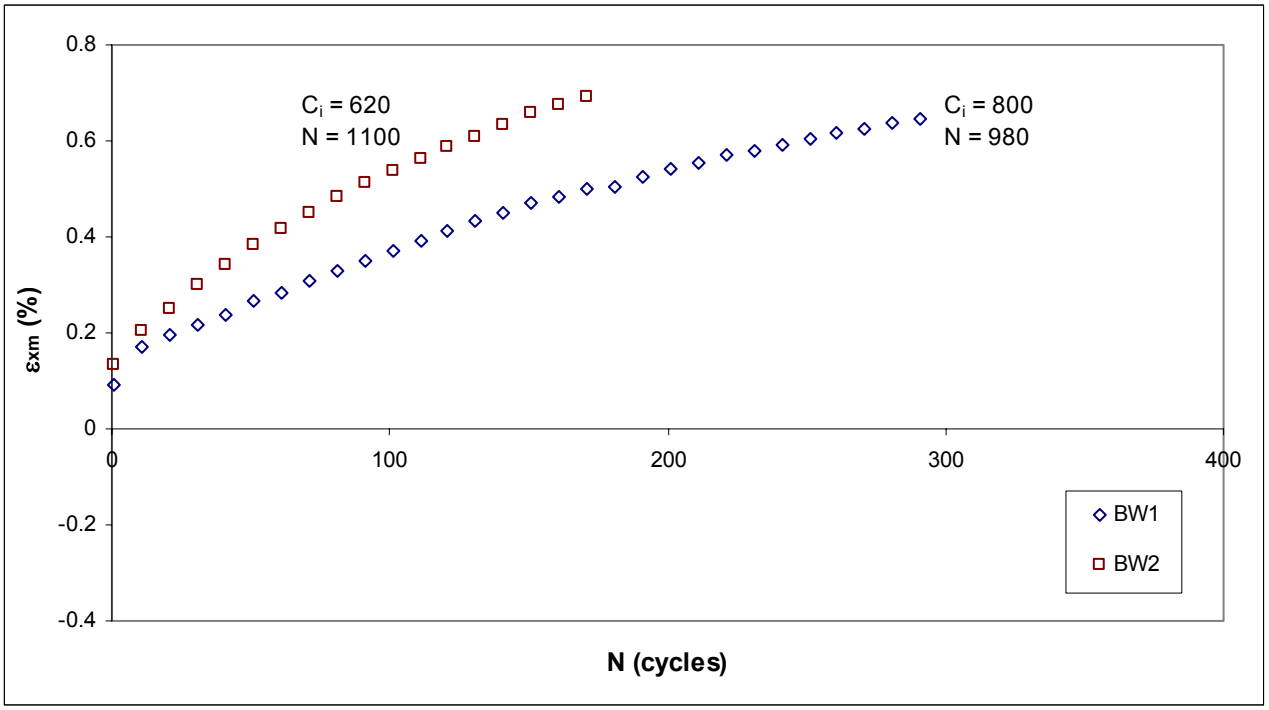

Figure 3.65 Ratcheting of mean axial strains in butt-welded specimens (every 10th cycle)

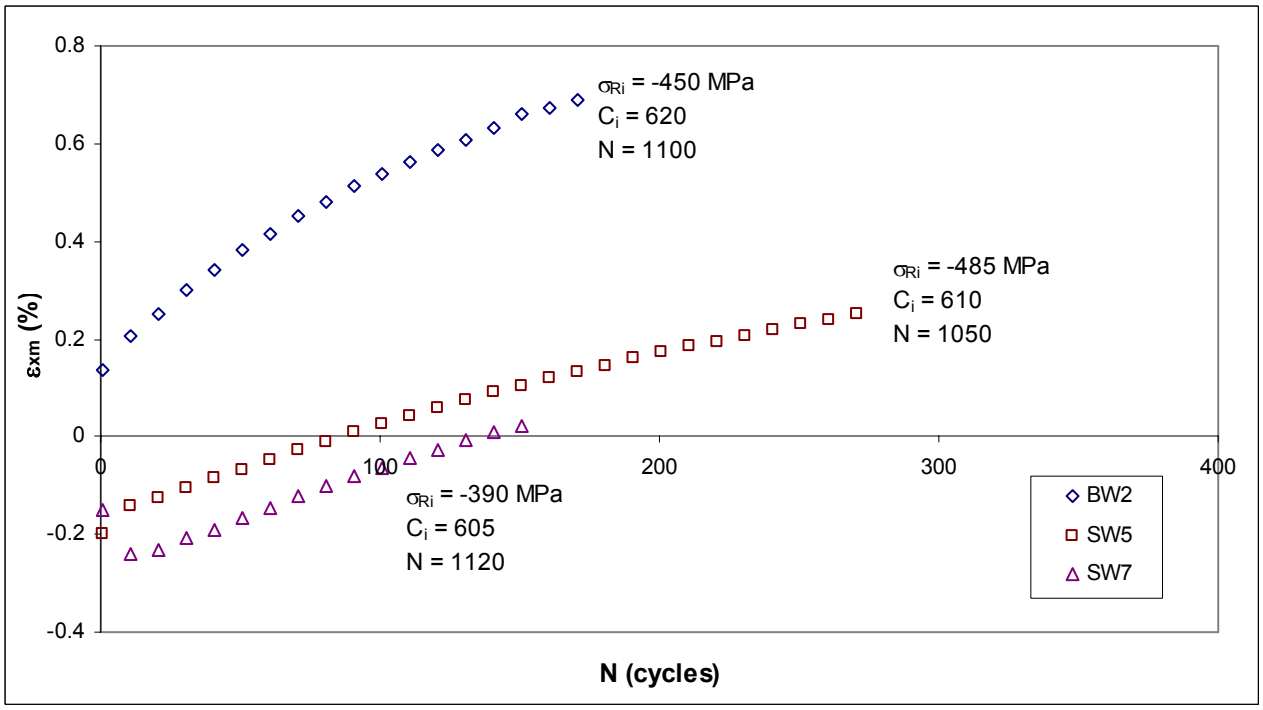

Figure 3.66 Mean axial strain ratcheting in 14 mm amplitude displacement-controlled tests

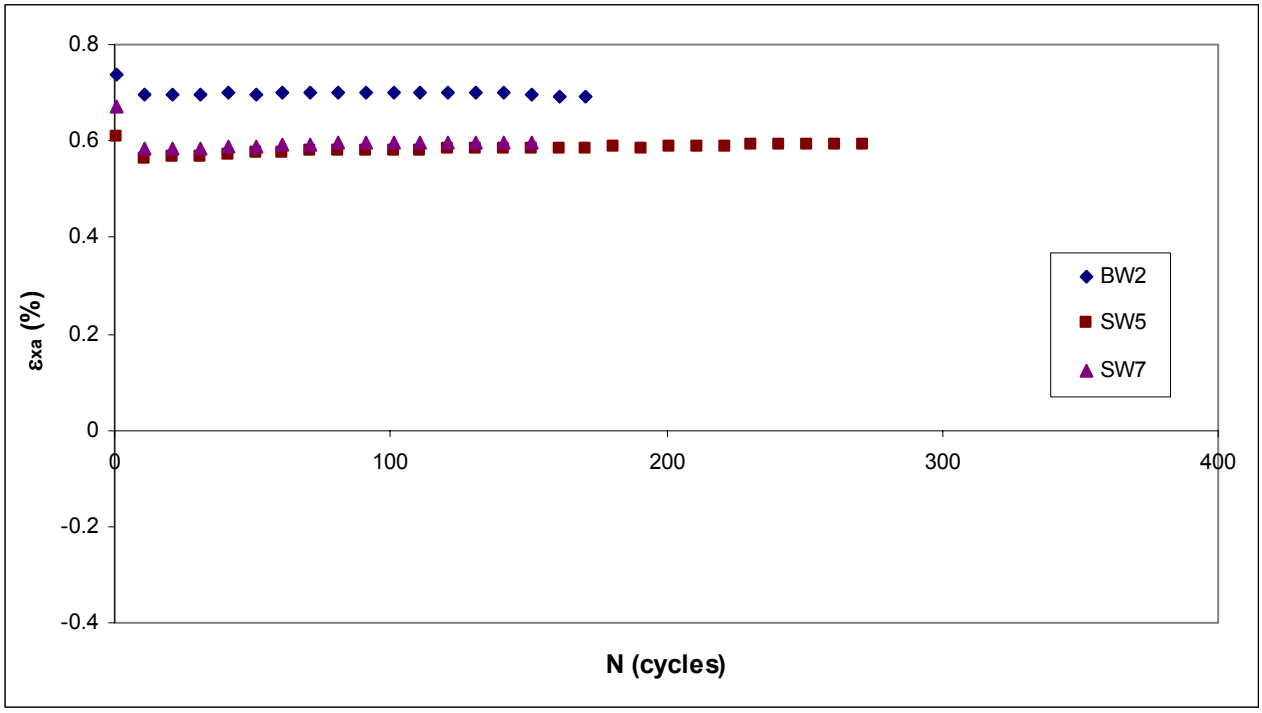

Figure 3.67 Strain amplitudes in 14 mm amplitude displacement-controlled tests

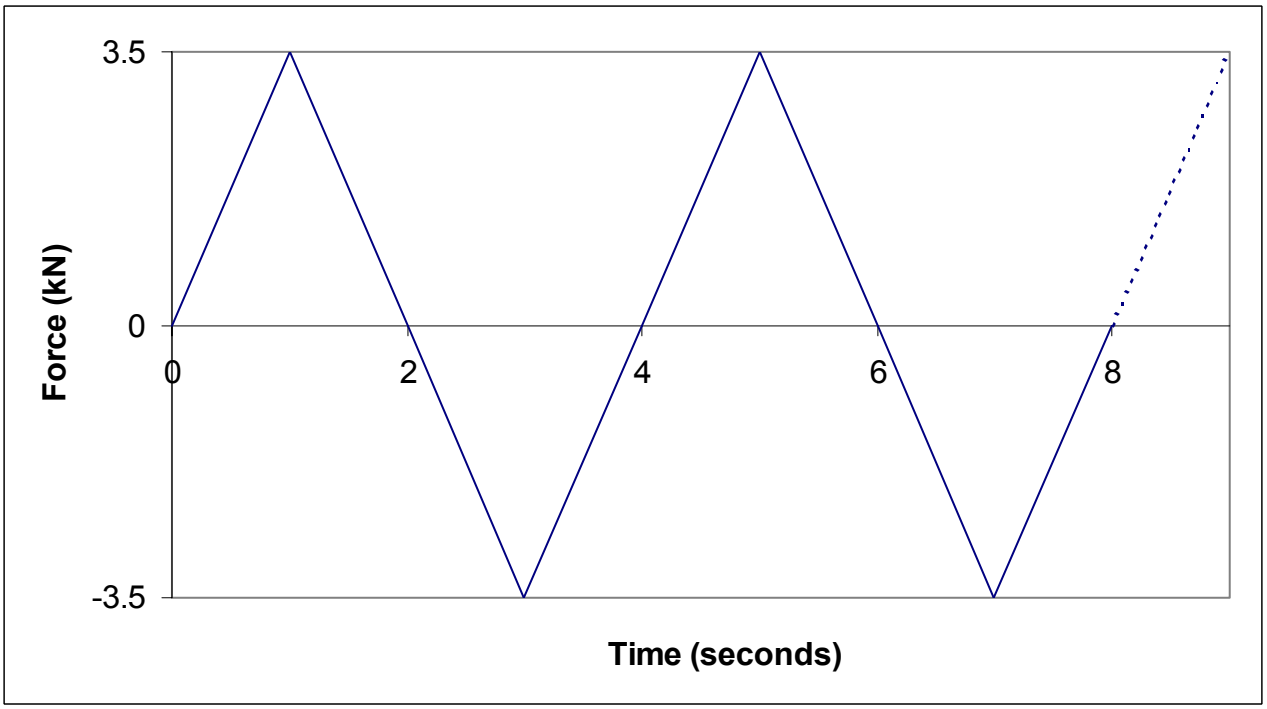

Figure 3.68 Prescribed force-controlled loading for SW6 and SW9 fatigue tests

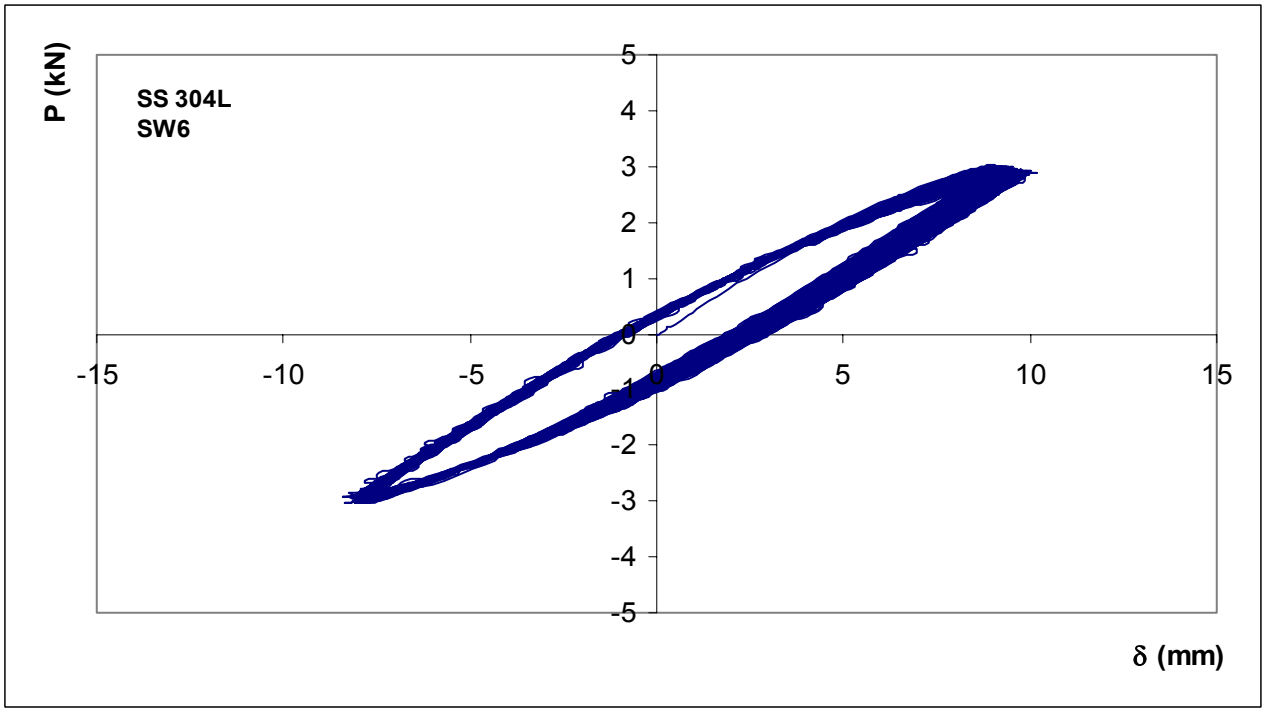

Figure 3.69 Force-displacement response from SW6 fatigue test

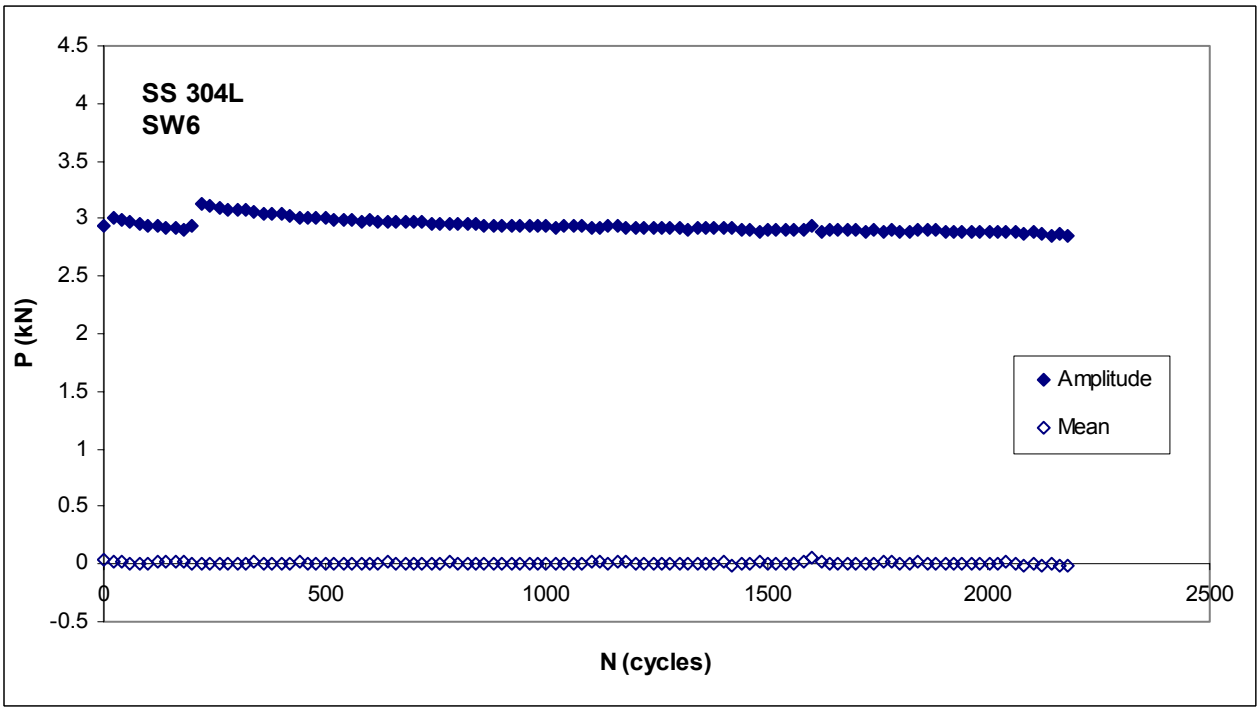

Figure 3.70 Force amplitude and mean from SW6 fatigue test (every 20th cycle)

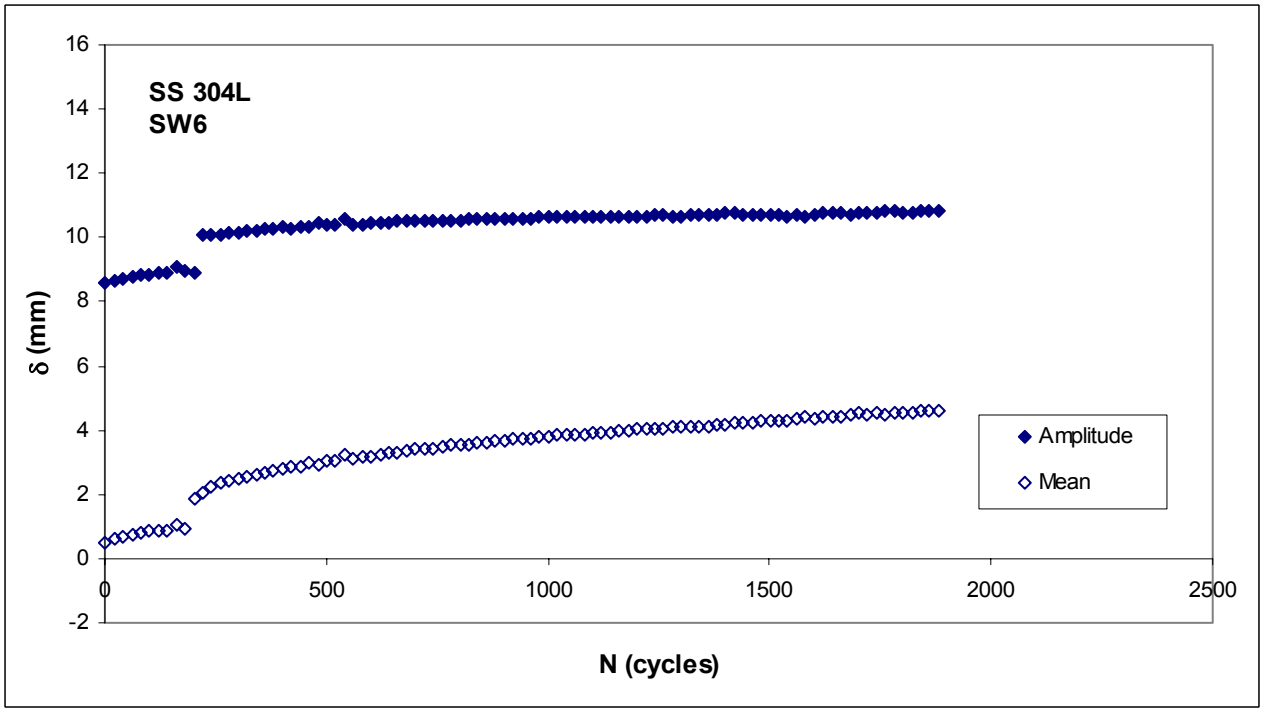

Figure 3.71 Displacement amplitude and mean from SW6 fatigue test (every 20th cycle)

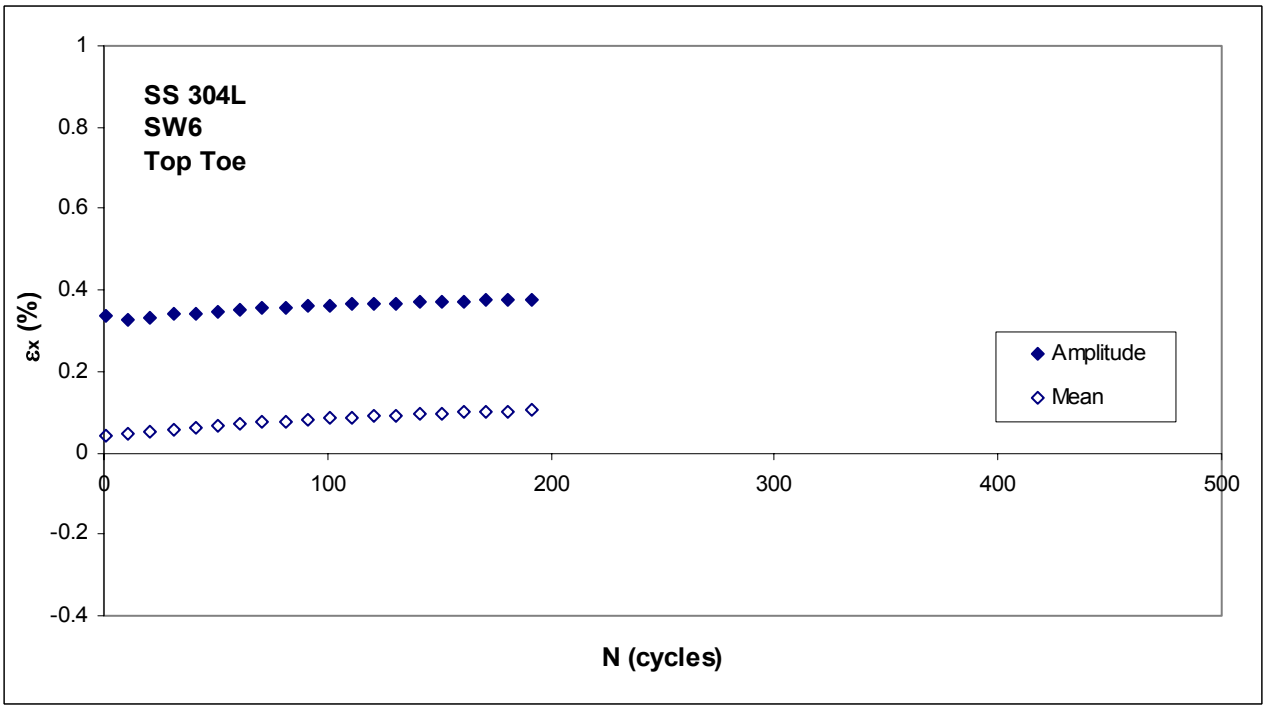

Figure 3.72 Axial strain amplitude and mean at top weld toe of SW6 (every 10th cycle)

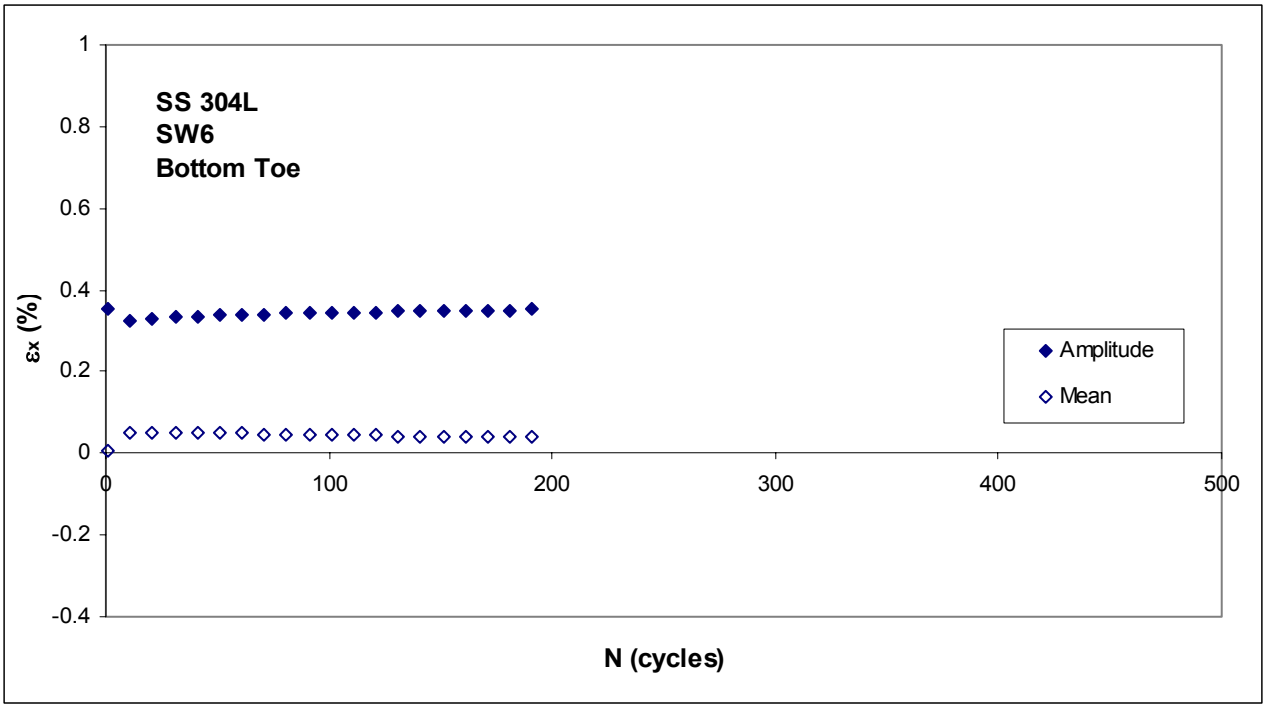

Figure 3.73 Axial strain amplitude and mean at bottom weld toe of SW6 (every 10th cycle)

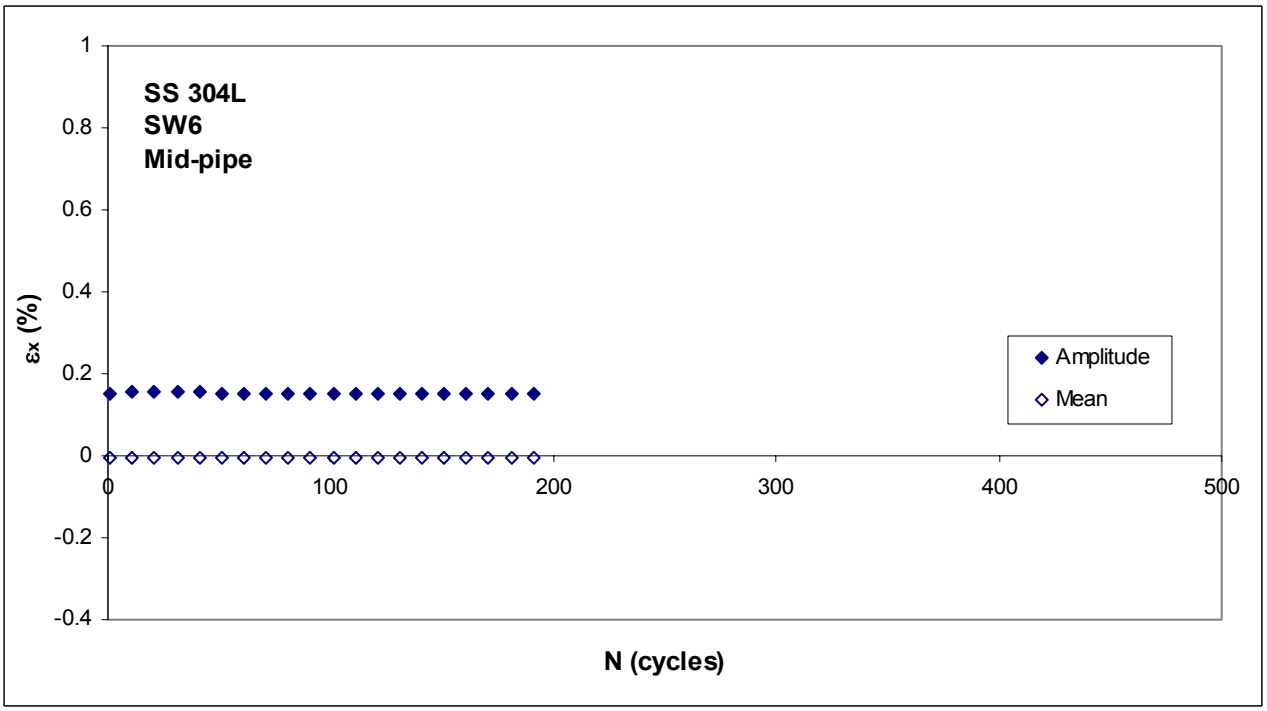

Figure 3.74 Axial strain amplitude and mean at midpoint of pipe length of SW6 (every 10th cycle)

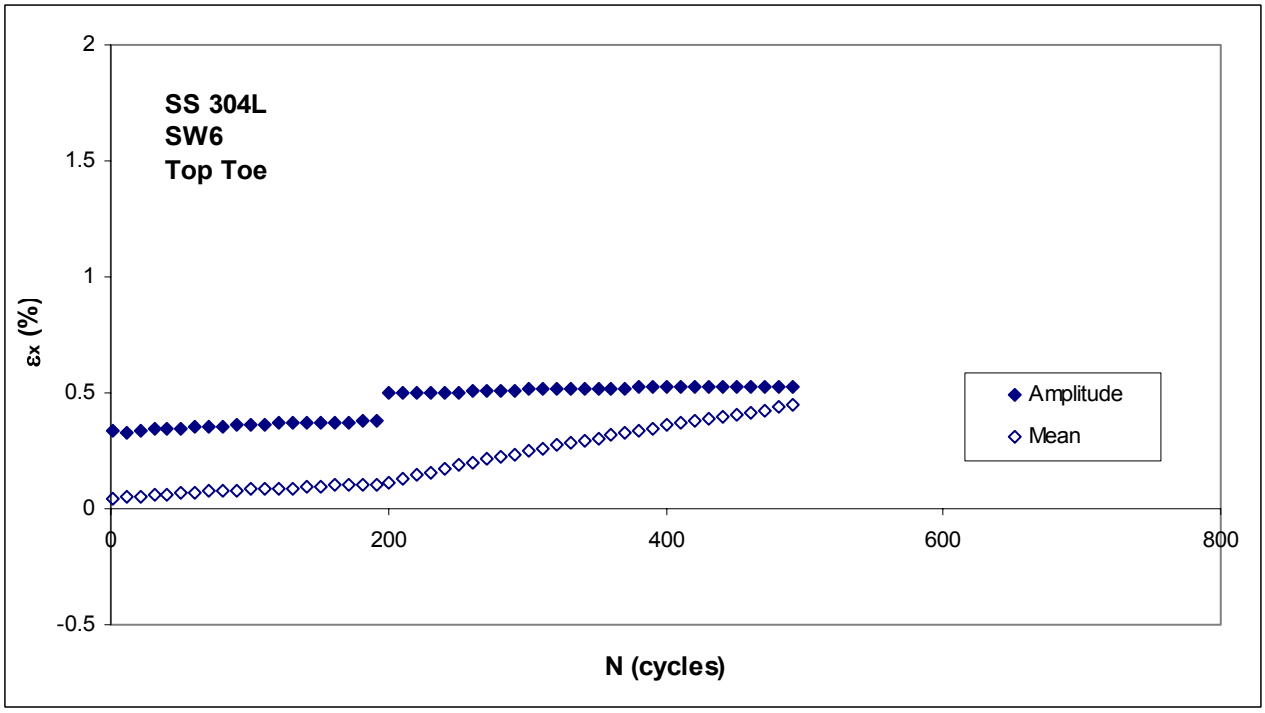

Figure 3.75 Combined stages of axial strain amplitude and mean at top weld toe of SW6

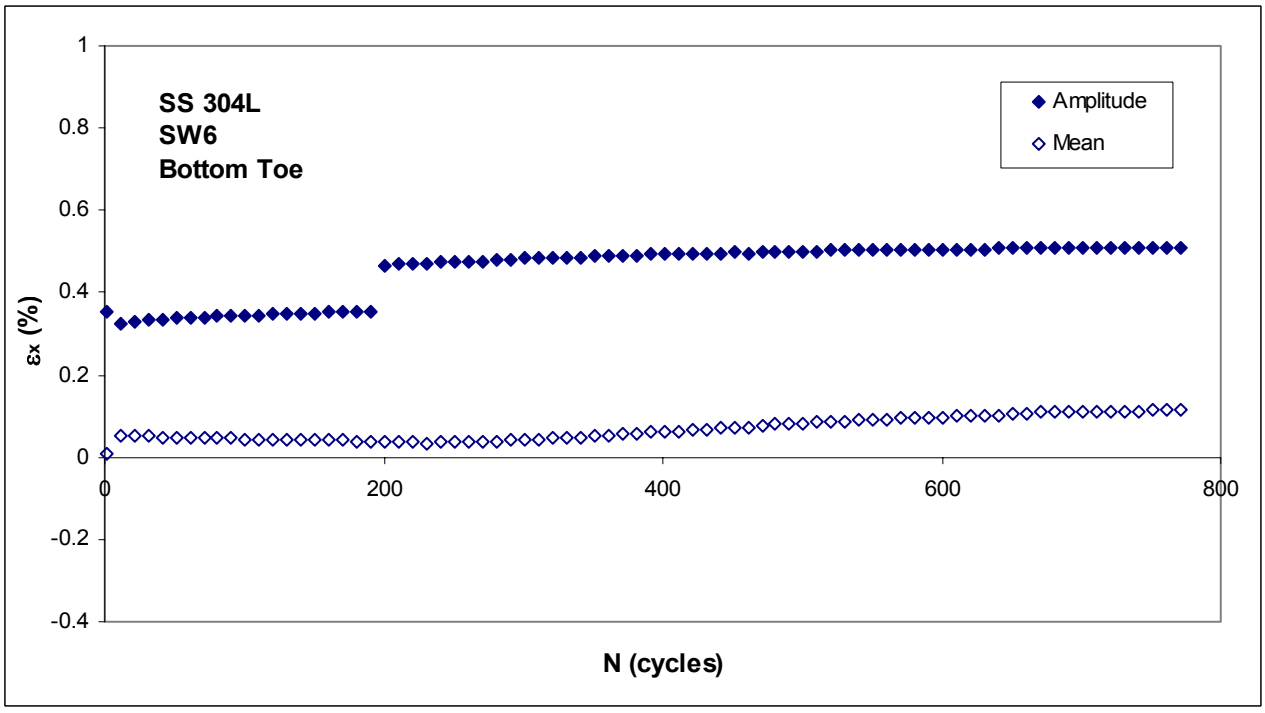

Figure 3.76 Combined stages of axial strain amplitude and mean at bottom weld toe of SW6

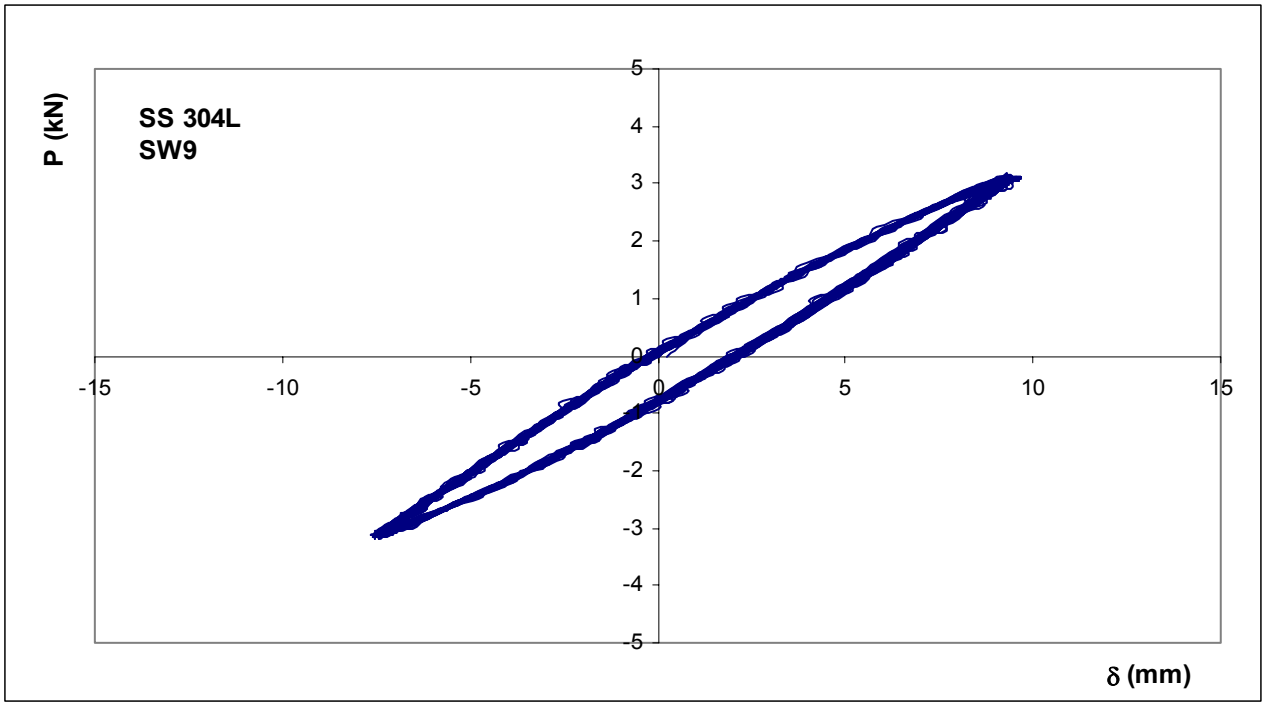

Figure 3.77 Force-displacement response from SW9 fatigue test

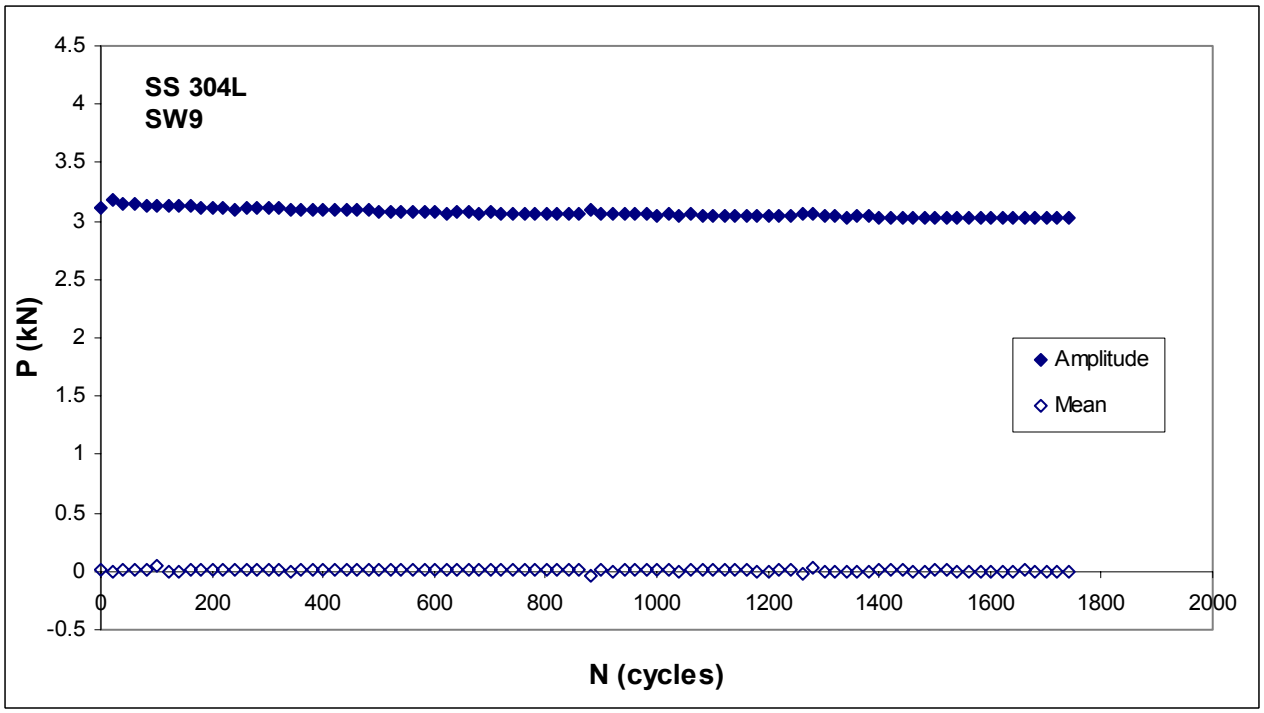

Figure 3.78 Force amplitude and mean from SW9 fatigue test (every 20th cycle)

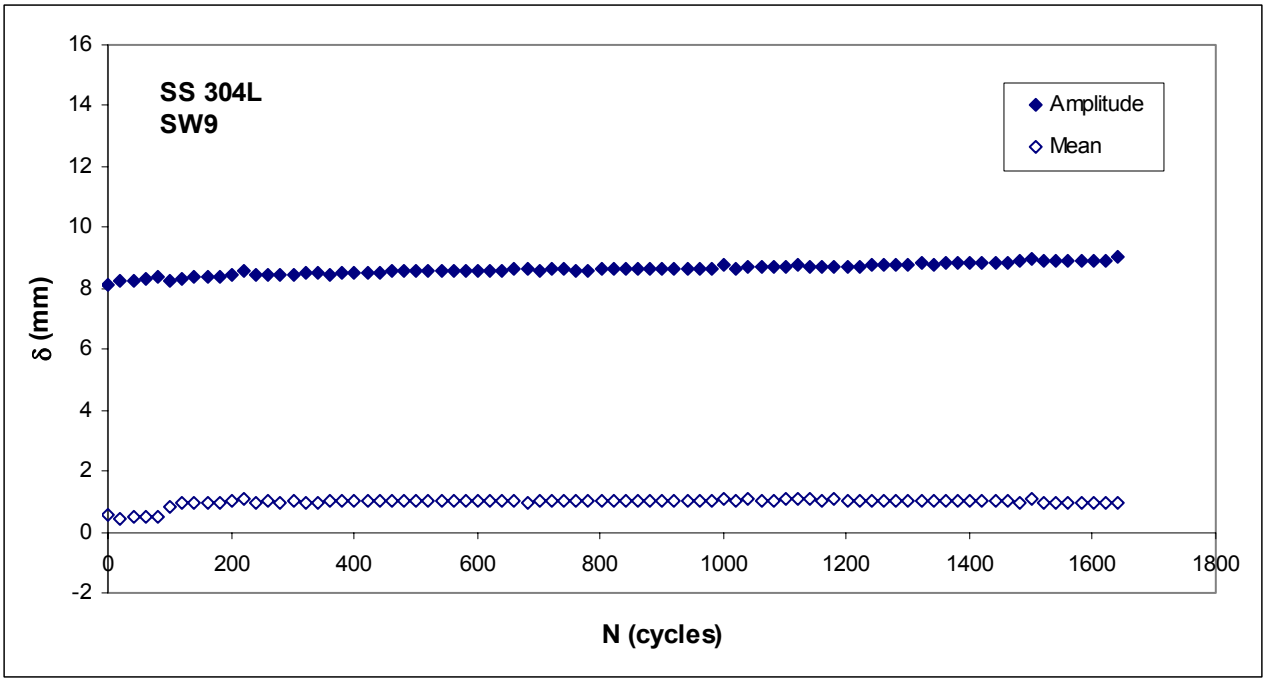

Figure 3.79 Displacement amplitude and mean from SW9 fatigue test (every 20th cycle)

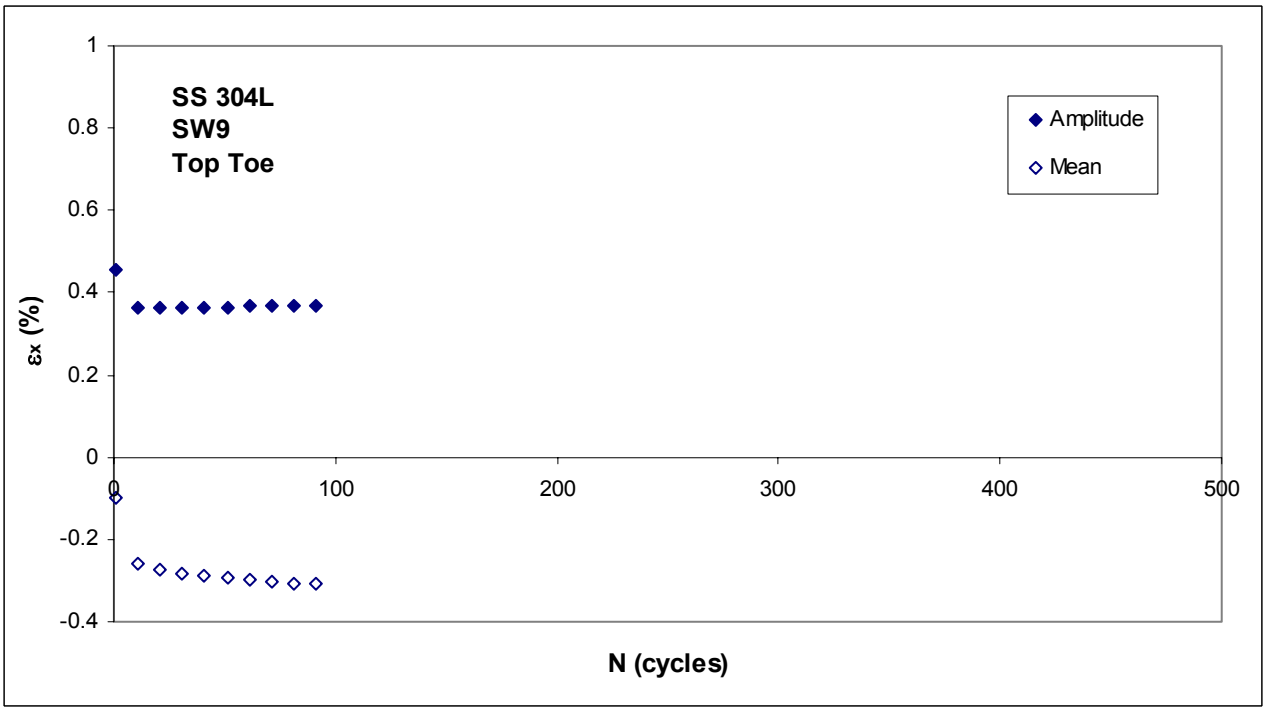

Figure 3.80 Axial strain amplitude and mean at top weld toe of SW9 (every 10th cycle)

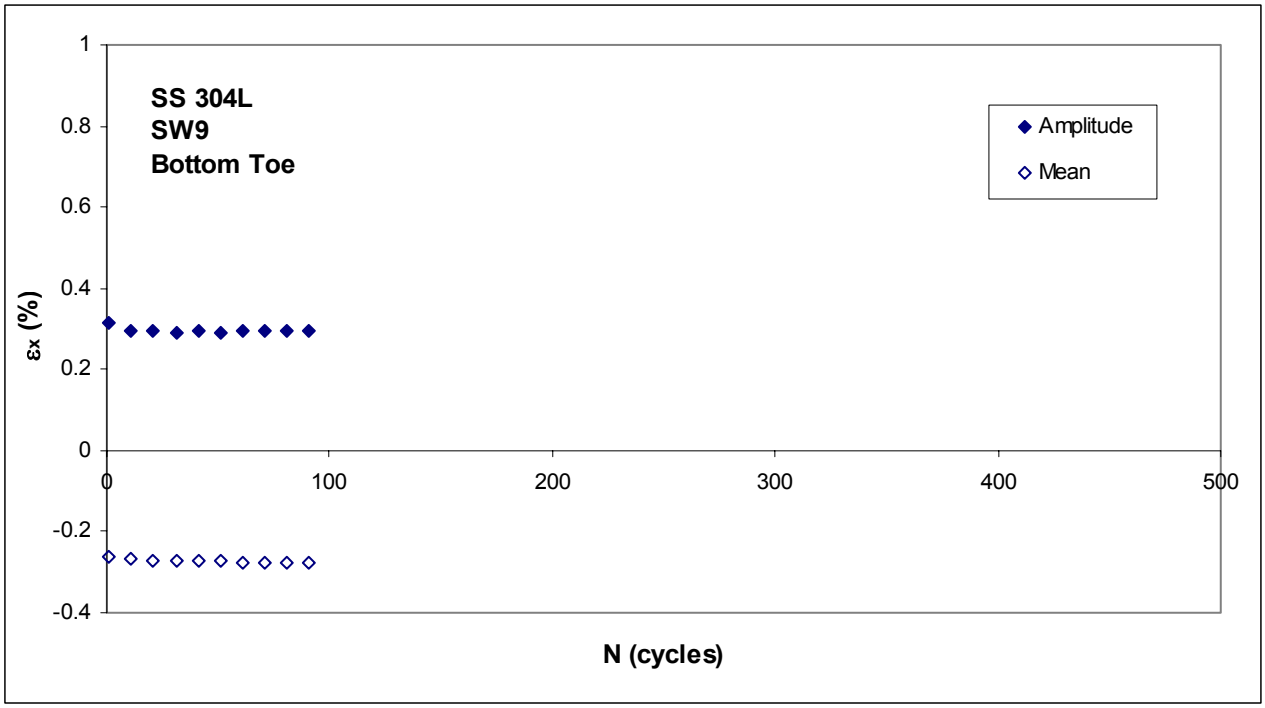

Figure 3.81 Axial strain amplitude and mean at bottom weld toe of SW9 (every 10th cycle)

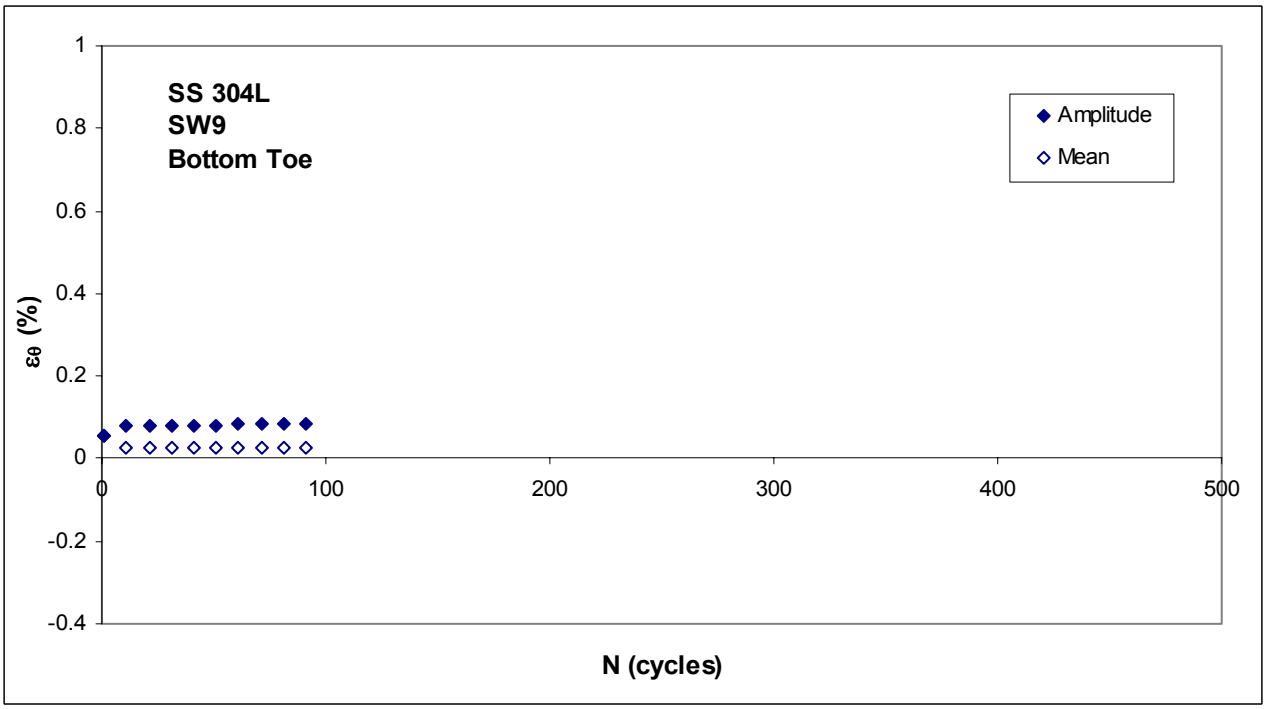

Figure 3.82 Circumferential strain amplitude and mean at bottom weld toe of SW9 (every 10th cycle)

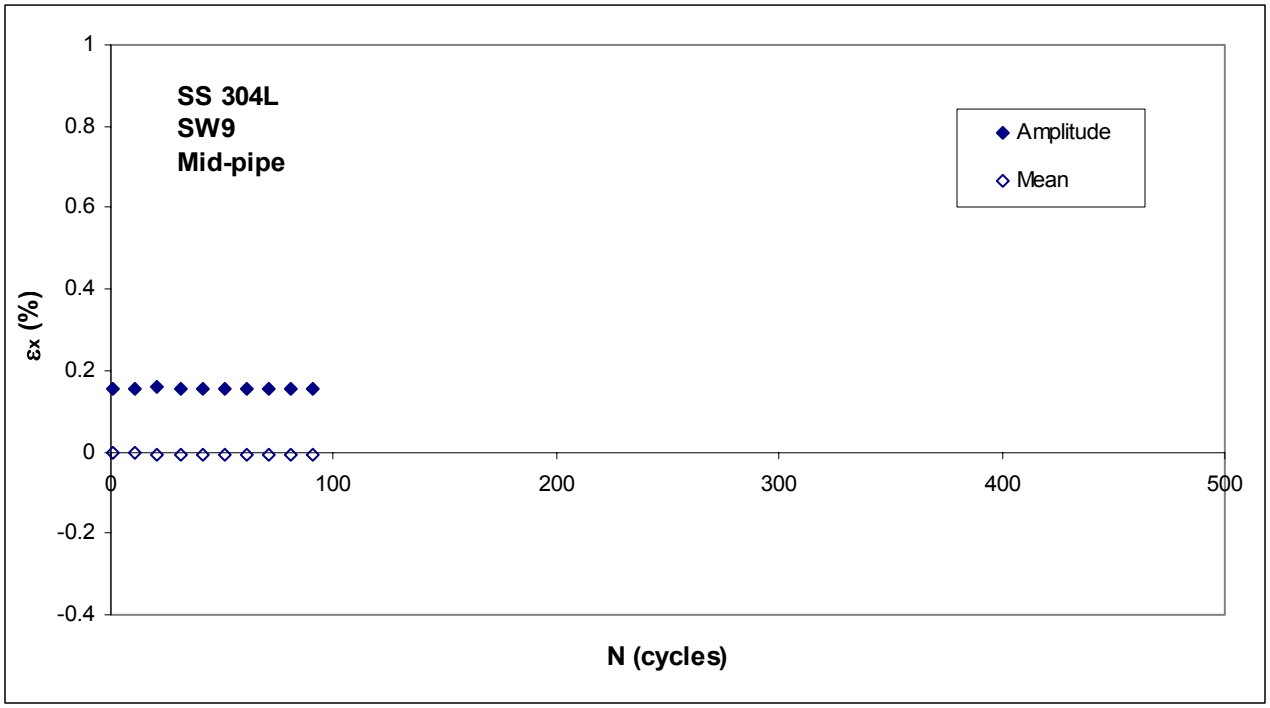

Figure 3.83 Axial strain amplitude and mean at midpoint of pipe length of SW9 (every 10th cycle)

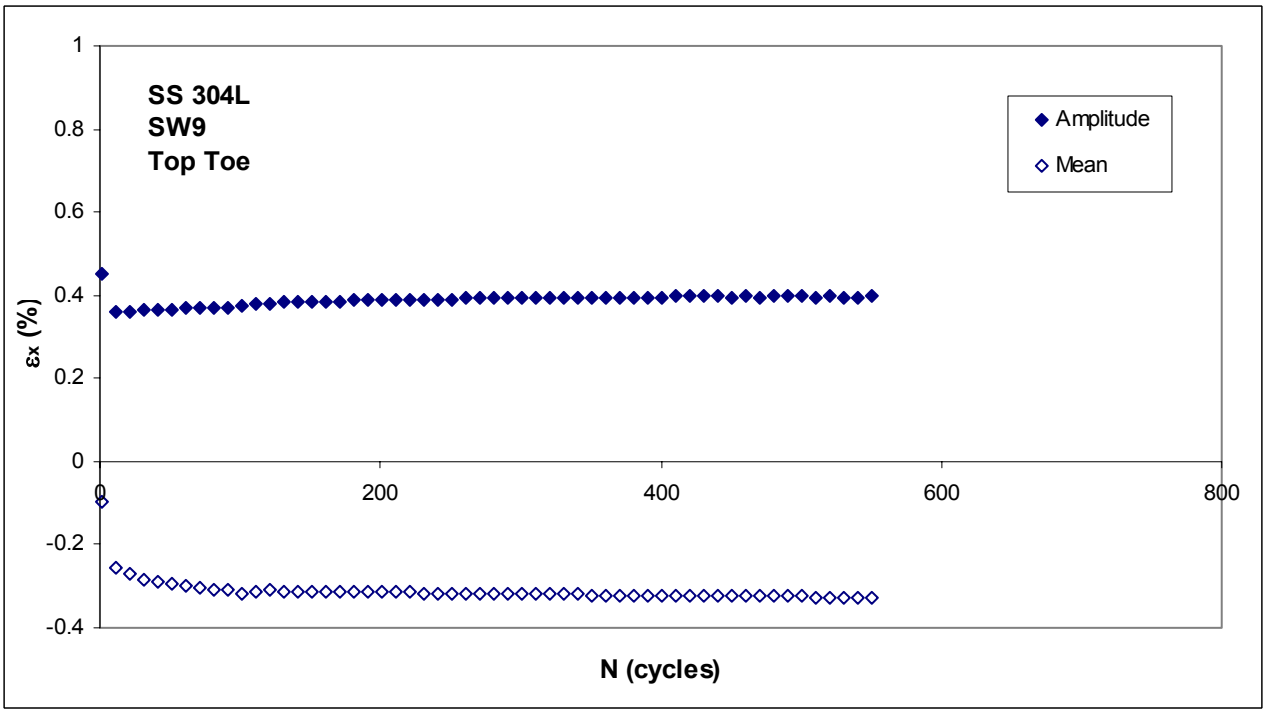

Figure 3.84 Combined stages of axial strain amplitude and mean at top weld toe of SW9

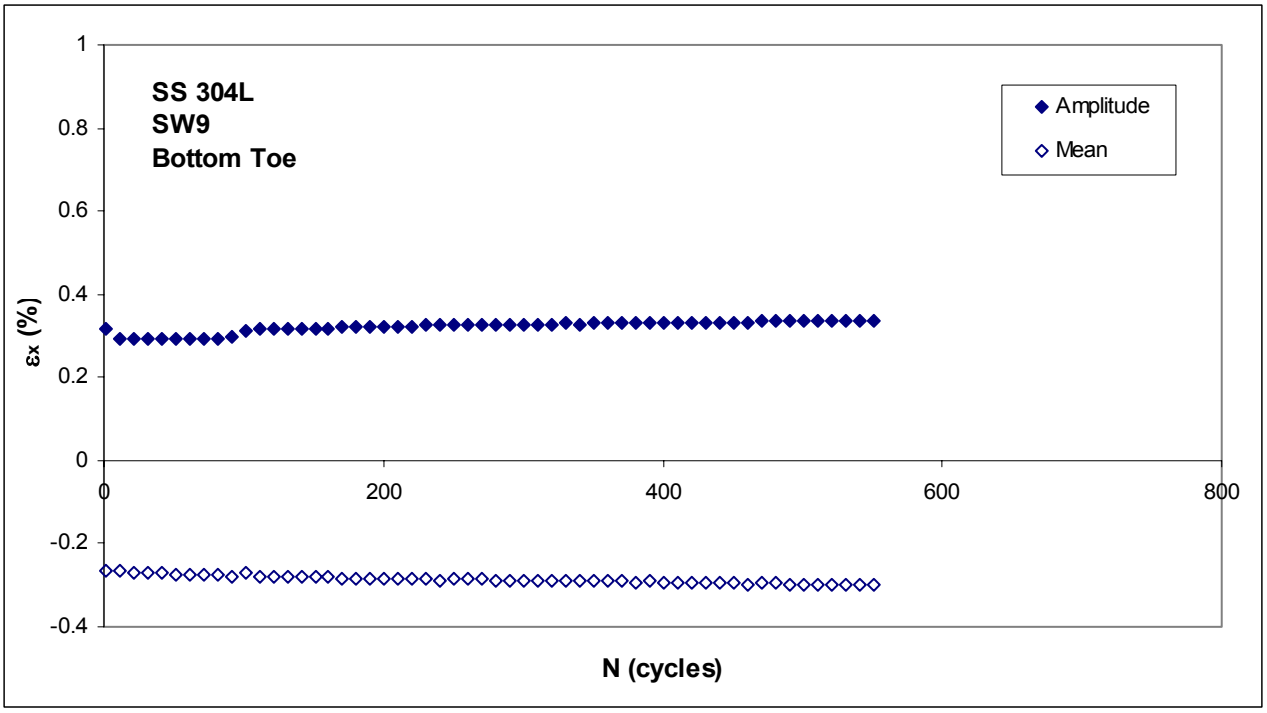

Figure 3.85 Combined stages of axial strain amplitude and mean at bottom weld toe of SW9

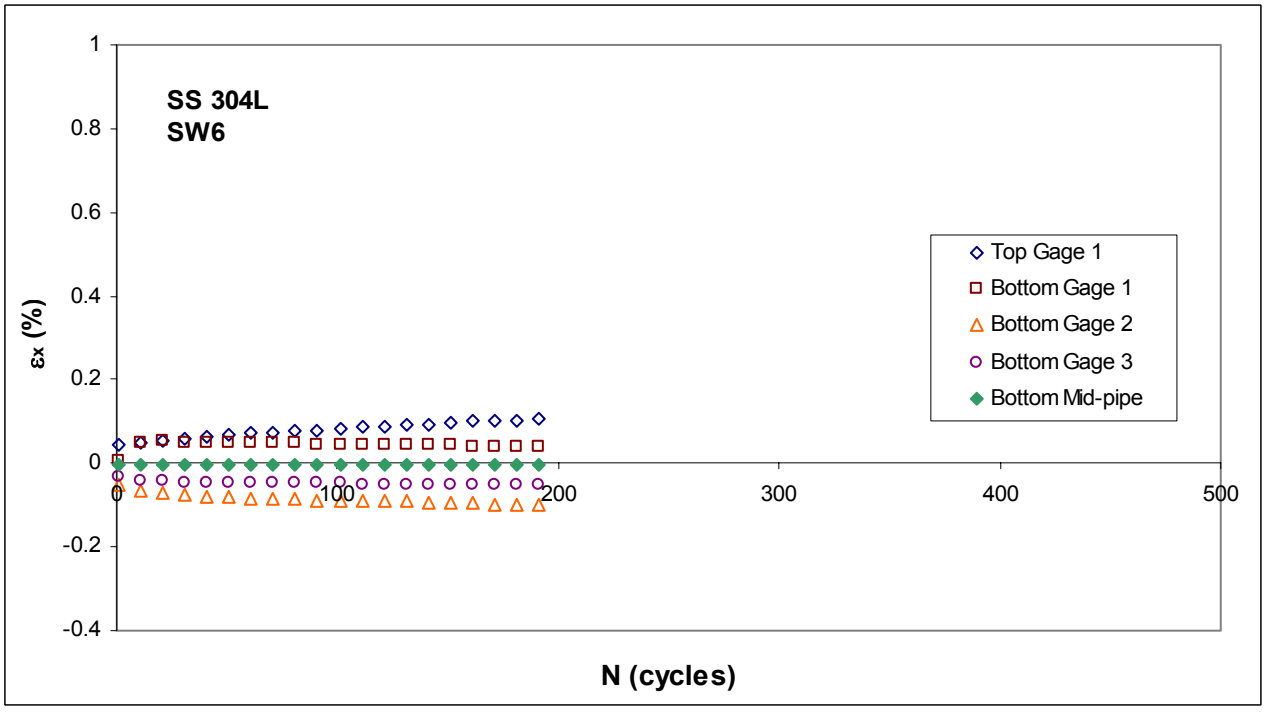

Figure 3.86 Axial strain ratcheting in SW6 along pipe length (every 10th cycle)

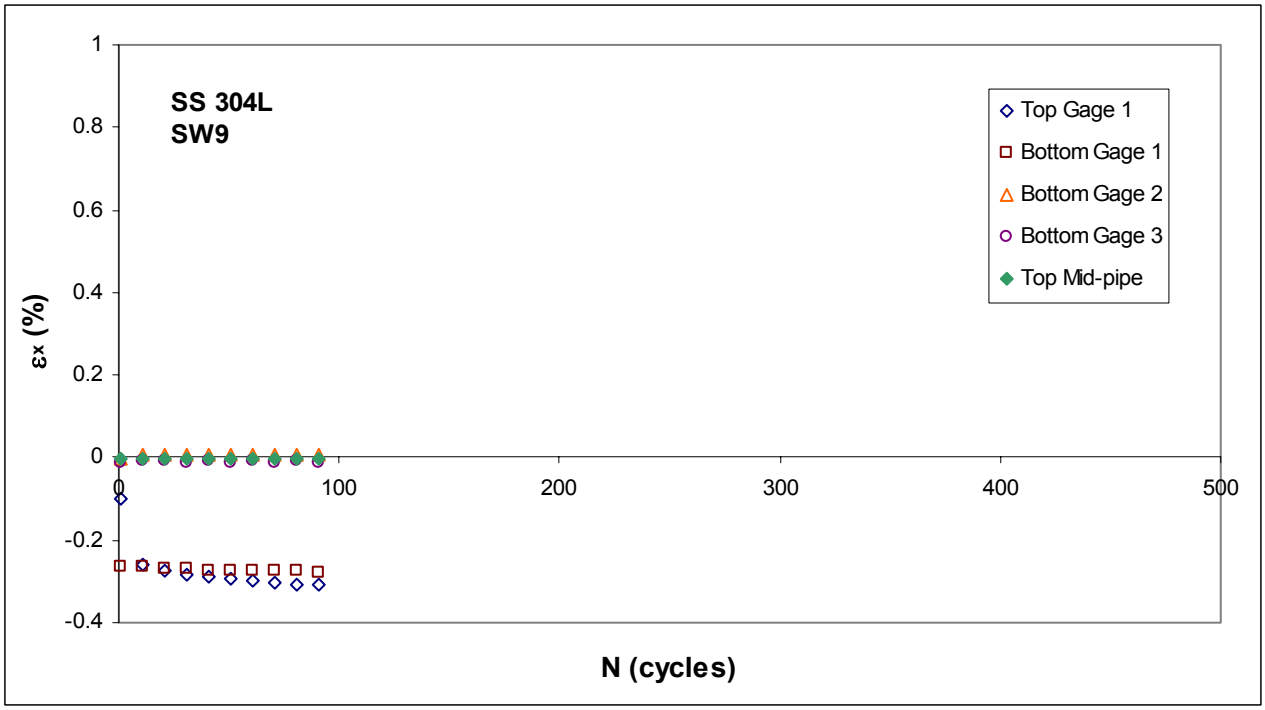

Figure 3.87 Axial strain ratcheting in SW9 along pipe length (every 10^{th} cycle)

CHAPTER 4
REASONS FOR THE OCCURRENCE OF RATCHETING IN WELDED PIPING EXPERIMENTS

4.1 Introduction

From the experimental work conducted to establish what happens to welding residual stresses during fatigue, the following two observations were made: (1) welding residual stresses near the weld toe in both the axial and circumferential directions in the overwhelming majority of cases were compressive and (2) these residual stresses near the weld toe at the location of maximum strain cycling experienced near-complete relaxation early in fatigue. These two observations raise the following questions: (1) why does strain ratcheting occur in the tensile direction when the residual stresses are initially compressive and (2) why, after the relaxation of residual stresses, are initial ratcheting trends maintained? Answers to these questions are needed for understanding of the fatigue failure mechanism leading to frequent weld joint failures observed in industry and for improvement of the design methodology.

In critically considering the questions posed, the uniaxial ratcheting behavior of a tubular stainless steel specimen is presented in Fig. 4.1 (see Fig. 1.1 for the axial stress-strain response). In the first step of the experiment depicted, a tensile mean stress of 50 MPa was applied; tensile axial strain ratcheting resulted (Step 1 in Fig. 4.1). When the tensile mean stress was removed, axial strain ratcheting changed direction towards compression (Step 2 in Fig. 4.1). Based upon these uniaxial results, intuition concerning the fatigue response in the welded piping specimen tests would predict initial negative strain ratcheting in both the axial and circumferential directions due to the presence of initially compressive residual stresses. In addition, it would be expected that ratcheting would change its direction as relaxation of the residual stresses took place. However, as the fatigue response results of Chapter 3 make apparent, these intuitive expectations were not realized. In the displacement-controlled tests, no negative strain ratcheting was observed. Positive ratcheting of axial strains was recorded in all four displacement-controlled tests. Positive ratcheting of circumferential strains was recorded in three of the four; in the fourth, no ratcheting was observed due to small amplitude of applied displacement. Further, positive axial strain ratcheting continued over the specimen life even after residual stresses had relaxed. From the uniaxial results, it is clear that a positive mean stress is required in order for positive strain ratcheting to occur. Hence, it is anticipated in the present chapter that the multiaxial interaction of residual and prescribed stresses and the relaxation of the residual

stresses exert *reverse mean stress effects* on the fatigue response; these effects are realized through tensile strain ratcheting of the welded specimens under fatigue loading. This anticipation is verified in the following sections based upon biaxial loading experimental results at the material level.

4.2 Experimental Investigation

4.2.1 Biaxial Loading

As a result of the cantilever setup employed and the manner of load application, the welded piping specimens were subjected to predominantly biaxial stress cycles in fatigue. In order to study the ratcheting response of a specimen subjected to controlled biaxial stress, the following test was conducted. A tubular specimen with nominal outer and inner diameters of 1.00 inch (25.4 mm) and 0.90 inches (22.86 mm), respectively, was machined from the same original stainless steel 304L pipe as the six welded piping specimens. The tubular specimen was axially cycled in the MTS machine under prescribed force-controlled cycles in the presence of various steady-state internal pressures. A biaxial strain gage was installed on the pipe surface. Throughout the test, force, axial strain, and circumferential strain measurements were digitized and recorded.

4.2.2 Steps 1 to 3 of the Loading History Sequence

The loading history sequence making up the biaxial stress test can be seen in Table 4.1. As evidenced by the prescribed loads in the first step in Table 4.1, the biaxial stress test began with positive mean stress of 75 MPa applied in the axial direction and a steady tensile stress of 50 MPa in the circumferential direction. In the axial direction, 50 MPa of the mean stress was applied through prescribing an axial force while the remaining 25 MPa was induced by internal pressure. Referring back to the weld toe area of the welded piping specimens tested, it is recalled that in the initial state, compressive residual stresses existed in both directions. In the case of the tubular specimen, it was not possible to duplicate this state of stress with the equipment available at NCSU. With our experimental setup, it was neither possible to prescribe compressive circumferential stress nor cycle the circumferential stress. Therefore, the opposite stress state was achieved. Tensile mean stress in the axial direction and tensile steady stress in the circumferential direction were applied. By subjecting the specimen to opposite stress conditions of those experienced by the welded piping specimens, we sought to stimulate opposite

ratcheting effects and thereby verify the anticipated mechanism of ratcheting in the welded piping specimens.

In Step 1 of the biaxial stress experiment, axial tensile mean stress of 75 MPa and amplitude of axial stress of 350 MPa were prescribed in the presence of steady circumferential stress (50 MPa). The mean and steady stresses prescribed were roughly equal to 20.5 and 13.7 percent of the material's 0.2 percent offset yield stress (365 MPa), respectively (Fig. 4.2). The specimen was subjected to 100 cycles; after these cycles were completed, the prescribed axial force was reduced to zero thus reducing the axial mean stress to 25 MPa in Step 2. One hundred additional cycles were endured before the internal pressure was removed and both the axial and circumferential stresses were reduced to zero. A final set of 100 cycles was then carried out in Step 3 with the same prescribed axial stress amplitude of 350 MPa. The reasoning behind this schedule of loading follows. In the welded piping specimen tests, both the axial and circumferential residual stresses relaxed in fatigue. As a significantly larger strain cycle was experienced in the axial direction as compared to the circumferential direction (Fig. 4.3), it is postulated that axial residual stresses relaxed faster in fatigue than did the circumferential residual stresses. Hence, in the biaxial stress test, the axial mean stress was reduced after the first 100 cycles, simulating the higher rate of relaxation experienced in this direction. Both the steady circumferential stress and the axial mean stress due to internal pressure were removed after the second set of 100 cycles, representing the complete relaxation of residual stresses.

4.2.3 Strain Response in Steps 1 to 3 of Loading History Sequence

In Step 1 of the loading sequence, as the primary loading cycle was prescribed in the axial direction, larger amplitude of axial strain cycles was experienced compared to the circumferential strain cycle amplitude, as evidenced in Fig. 4.4. The positive axial mean stress stimulated positive axial strain ratcheting as shown in Fig. 4.5. Although the steady circumferential stress was tensile, due to the high rate of axial strain ratcheting and Poisson's effect, the circumferential strain ratcheting induced was in the negative direction (Fig. 4.6). With higher steady circumferential stress, the circumferential strain ratcheting direction could be changed to tensile (Hassan and Kyriakides [1994b]).

In Step 2, the axial mean stress of 75 MPa was reduced to 25 MPa—only the mean stress due to internal pressure was maintained. Steady tensile circumferential stress was also maintained. Negative ratcheting of the axial strain was observed and can be seen in Fig. 4.5.

This negative ratcheting is attributed to two stimulants. Through Poisson's effect, the tensile circumferential stress stimulated negative axial strain ratcheting in the absence of a dominating axial mean stress. More importantly, the reduction of the tensile axial mean stress had the effect of an applied negative axial mean stress, which was also demonstrated in the uniaxial test (Fig. 4.1). The aforementioned *reverse mean stress effect* is directly observed in this step as the reduction of a tensile mean stress stimulated negative axial strain ratcheting. The axial and circumferential effects constructively interfered with each other to produce an overall effect of negative axial strain ratcheting. As evidenced in Fig. 4.6, circumferential strain in the second step of loading ratcheted in the positive direction due to the combined effects of the tensile circumferential steady stress and the axial reverse mean stress effect.

In Step 3, ratcheting of the axial mean strain towards compression is noted (Fig. 4.5). This response is mainly attributed to the removal of the tensile mean stress of 25 MPa that had been induced in previous loading steps by the internal pressure. This continued negative ratcheting again illustrates the reverse mean stress effect—the reduction of the axial mean stress from 25 MPa to zero stimulated negative strain ratcheting. In Fig. 4.6, an initial reduction of the circumferential mean strain is observed. This initial reduction is attributed to the removal of the internal pressure, which had induced tensile circumferential steady stress in previous loading steps. Over the final 100 cycles, the circumferential mean strain ratcheted slightly in the tensile direction, through Poisson's effect, due to the reverse mean stress effect in the axial direction.

4.2.4 Steps 4 to 6 of the Loading History Sequence

In the Step 4 of the loading sequence, a compressive mean stress of 25 MPa was applied in the axial direction, and a steady tensile stress of 50 MPa was applied in the circumferential direction. Again, internal pressure contributed 25 MPa of tensile mean stress in the axial direction; a compressive axial mean stress of 50 MPa was applied via prescribed axial force, resulting in a net axial mean stress of –25 MPa. This combination was chosen to facilitate observation of the effects of an initial negative axial mean stress on ratcheting response. In Steps 4-6 of the loading sequence, the hypotheses and assumptions made in the first three steps were tested and eventually verified.

As stated above, in Step 4 of the loading sequence, compressive axial mean stress and tensile circumferential steady stress were applied. The biaxial stress specimen was subjected to 100 cycles of stress-controlled loading. Again, the amplitude of loading was maintained at 350

MPa throughout all loading steps. Mimicking the schedule of loading steps from the first three steps, the directly applied axial mean stress was removed after the first 100 cycles; higher rate of relaxation of axial residual stresses was again simulated. Note that the loading parameters in Step 2 and Step 5 are identical. Following the second set of 100 cycles (Step 5), the circumferential steady stress and the axial mean stress due to internal pressure were removed. A final set of 100 loading cycles was then carried out in Step 6.

4.2.5 Strain Response in Steps 4 to 6 of Loading History Sequence

In Step 4, the compressive axial mean stress directly induced negative axial strain ratcheting. The tensile circumferential steady stress also induced negative axial strain ratcheting through Poisson's effect. The two stress effects constructively interfered with each other to cause the net negative axial strain ratcheting response of Fig. 4.7. The constructive interference of the two stress effects in the circumferential direction induced positive strain ratcheting in this loading step (Fig. 4.8).

The directly applied compressive axial mean stress of 50 MPa was removed in Step 5 of the loading sequence, leaving the tensile mean stress of 25 MPa due to internal pressure. In Fig. 4.7, it is observed that positive ratcheting of the axial mean strain occurred in this step, whereas under the same loading parameters, negative ratcheting of the axial mean strain was observed in Step 2. Again citing the reverse mean stress effect, it is proposed that the change in the axial mean stress from –25 MPa to 25 MPa stimulated the recorded positive axial strain ratcheting. However, the fact that a tensile mean stress due to internal pressure existed in this loading step makes identifying the primary ratcheting stimulant difficult. While the constructive interference of the reverse mean stress effect and the axial tensile mean stress produced the ratcheting behavior observed, comparison of Steps 2 and 5 facilitates the conclusion that the reverse mean stress effect dominantly influenced axial strain ratcheting behavior. In the circumferential direction, negative ratcheting of the mean strain was stimulated, through Poisson's effect, by the axial reverse mean stress effect (Fig. 4.8). Positive circumferential strain ratcheting that should have occurred due to the maintained tensile steady stress was overshadowed by the axial effects.

In the final step of loading, the internal pressure was removed, and the circumferential and remaining axial stress were reduced to zero. In the axial direction, mean strain ratcheted in the positive direction slightly over the final 100 cycles (Fig. 4.7). The circumferential mean strain ratcheted slightly in the negative direction over the last 100 cycles (Fig. 4.8).

4.3 Conclusions from Biaxial Stress Test

From the two sequences of loading in the biaxial stress test, the most significant conclusion drawn was as follows: reductions or increases in the axial mean stress had profound effects on axial strain ratcheting behavior. When the mean stress changed, the magnitude of the applied mean stress did not dictate ratcheting direction. Rather, *changes in the mean stress acted as a relative applied mean stress and thus induced a reverse mean stress effect on the ratcheting response*.

4.4 Implications of Biaxial Stress Test Response in Welded Piping Experiments

As was the case in the biaxial stress test, the strain amplitude endured at the weld toe in the axial direction in the piping specimen fatigue tests was substantially greater than that endured in the circumferential direction (see Figs. 4.3 and 4.4). In fatigue, residual stresses near the weld toe began to relax immediately. Due to the larger amplitude of strain, residual stresses in the axial direction relaxed faster than circumferential residual stresses. *This relaxation of residual stress in the axial direction had a reverse mean stress effect on axial strain ratcheting; that is, rapid relaxation of compressive axial residual stress stimulated tensile axial strain ratcheting*. Compressive circumferential residual stresses also relaxed, but at a lesser rate. Therefore, in the initial stages of fatigue, compressive circumferential residual stress served to encourage positive axial strain ratcheting through Poisson's effect. *The positive strain ratcheting behavior observed is attributed to the multiaxial interaction of the residual and prescribed stresses and the different rates at which the residual stresses relaxed in fatigue*.

4.5 Plasticity Analysis Results

Plasticity analysis was conducted in an attempt to further explore the mechanism by which positive axial strain ratcheting was induced at the weld toe of piping specimens in displacement-controlled fatigue. Strain responses recorded at the toe of the weld were prescribed as input to the cyclic plasticity program developed at NCSU (Bari and Hassan [2002], Rahman [2004]). In the first part of the analysis, compressive residual stresses of the magnitude of yield stress in both the axial and circumferential directions were prescribed for which monotonic curve parameters were used. This step provided us the initial strains from which the subsequent strain cycles started. Cyclic material parameters, determined from a hysteresis curve, were then used in the subsequent cycles. Ten input strain cycles were prescribed, as can be seen in Fig. 4.9. The output stress cycles are shown in Fig. 4.10. The axial stress cycles obtained from the analysis

were nearly symmetric after completion of the first cycle. The amplitude and mean of the axial stress cycles can be seen in Fig. 4.11. While the amplitude remained constant, small negative axial mean stress of approximately 10 MPa existed in the first cycle, as evidenced in the figure, but was not maintained. A positive mean stress of less than 5 MPa was observed throughout the remaining cycles. This observation suggests that axial residual stresses relax immediately and completely in the first loading ramp. The amplitude and mean of circumferential stress cycles can be seen in Fig. 4.12. Again, the amplitude remained constant but negative mean stress, larger than that observed in the first axial stress cycle (-30 MPa) was observed. The magnitude of the mean decreased with cycles to a small compressive stress and remained constant throughout the remaining cycles simulated. This observation suggests that circumferential stresses also relax quickly in fatigue but not as rapidly as the axial residual stresses. This reiterates the findings of Iida et al. [1997], Lachmann et al. [2002], and Smith et al. [2001] that residual stress relaxation is a function of the amplitude of fatigue strain cycles.

In addition to these observations concerning rates of relaxation of residual stresses, the following phenomenon was observed in the plasticity analysis: *strain ratcheting in both the axial and circumferential directions persisted throughout the simulated cycles in the presence of symmetric stress cycles. It is proposed that in this case, the multiaxial interaction of the symmetric stress cycles stimulated continued strain ratcheting.* This proposal contradicts the belief that a mean or steady stress is required for ratcheting to occur. Further research and additional analytical studies are necessary to confirm and understand this new observation.

Table 4.1 Loading history sequence for biaxial stress test

Step	Axial Stress Amplitude	Axial Mean Stress	Circumferential Stress	Cycles
1	350 MPa	75 MPa	50 MPa	100
2	350 MPa	25 MPa	50 MPa	100
3	350 MPa	0 MPa	0 MPa	100
4	350 MPa	-25 MPa	50 MPa	100
5	350 MPa	25 MPa	50 MPa	100
6	350 MPa	0 MPa	0 MPa	100

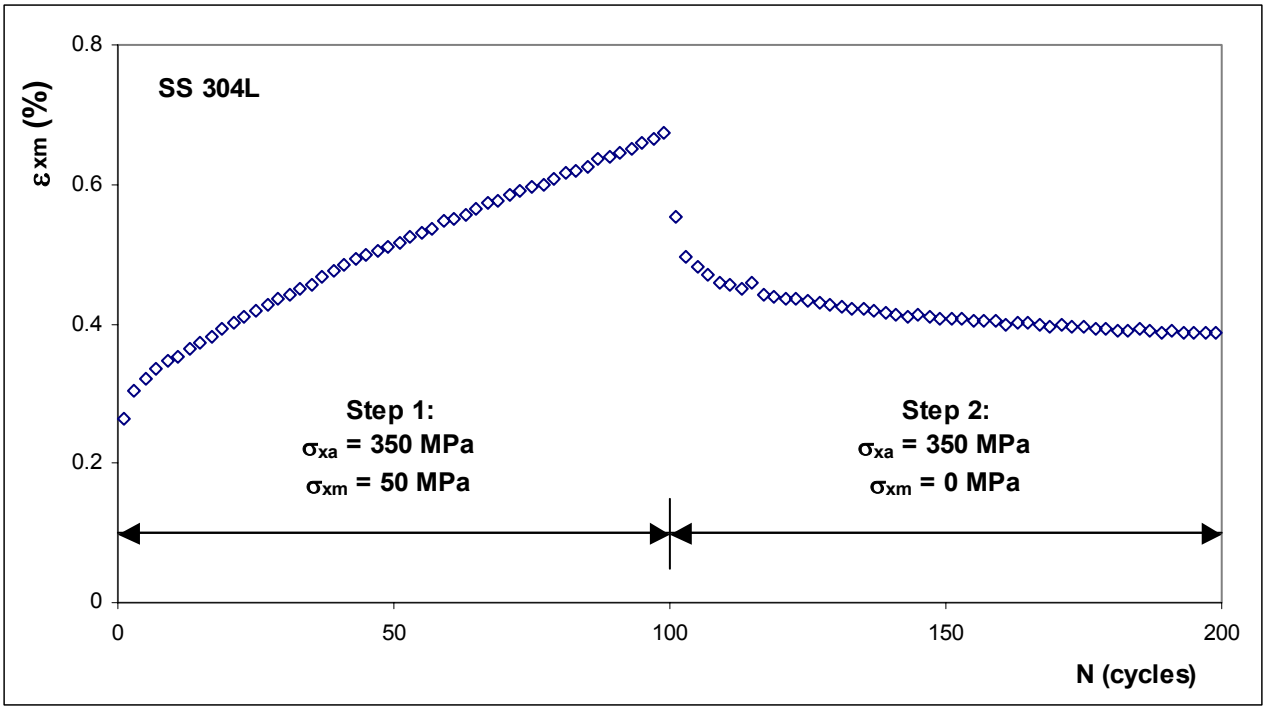

Figure 4.1 Ratcheting of mean strain in uniaxial test (every 2nd cycle)

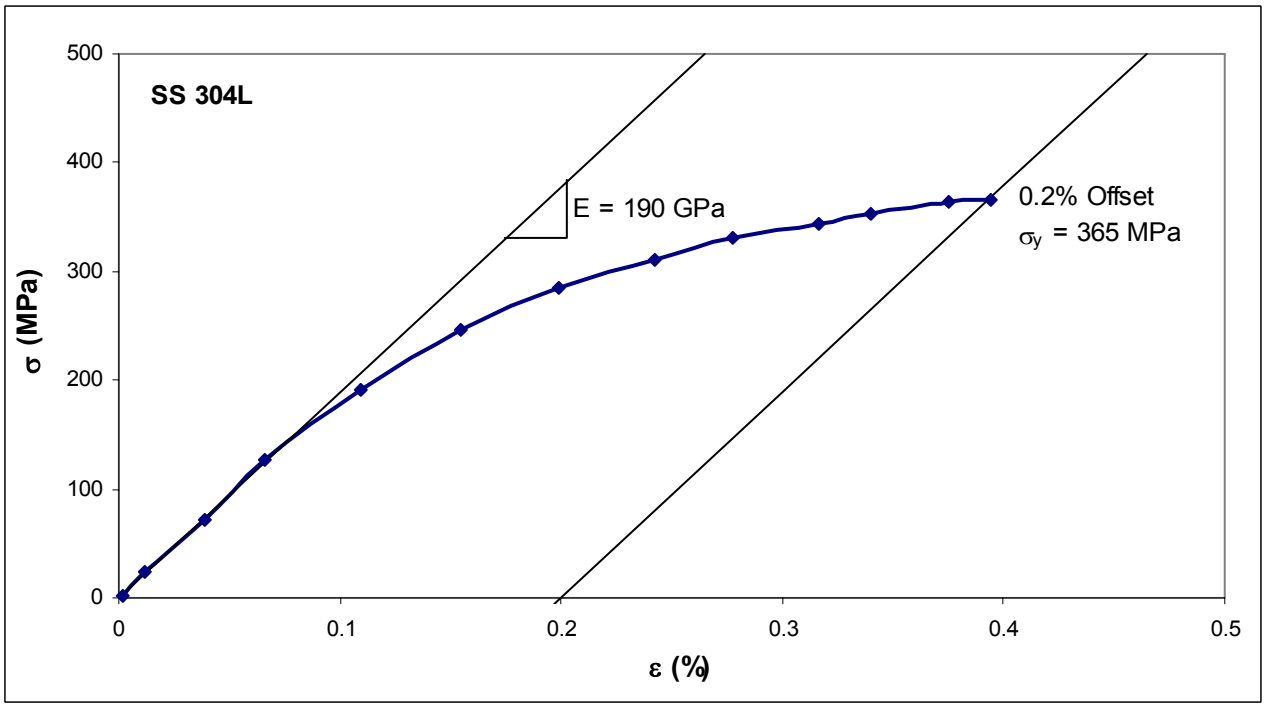

Figure 4.2 Monotonic curve from multi-step strain-controlled material test

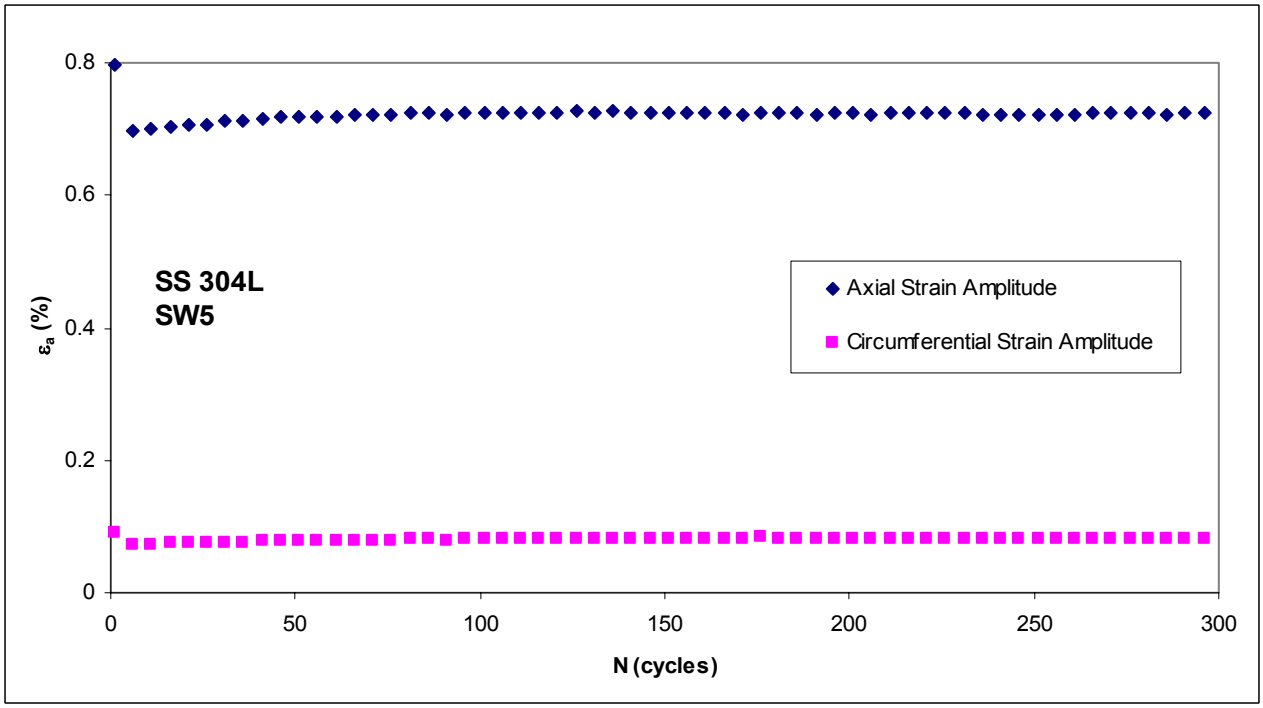

Figure 4.3 Comparison of axial and circumferential strain amplitudes in welded specimen test (every 5th cycle)

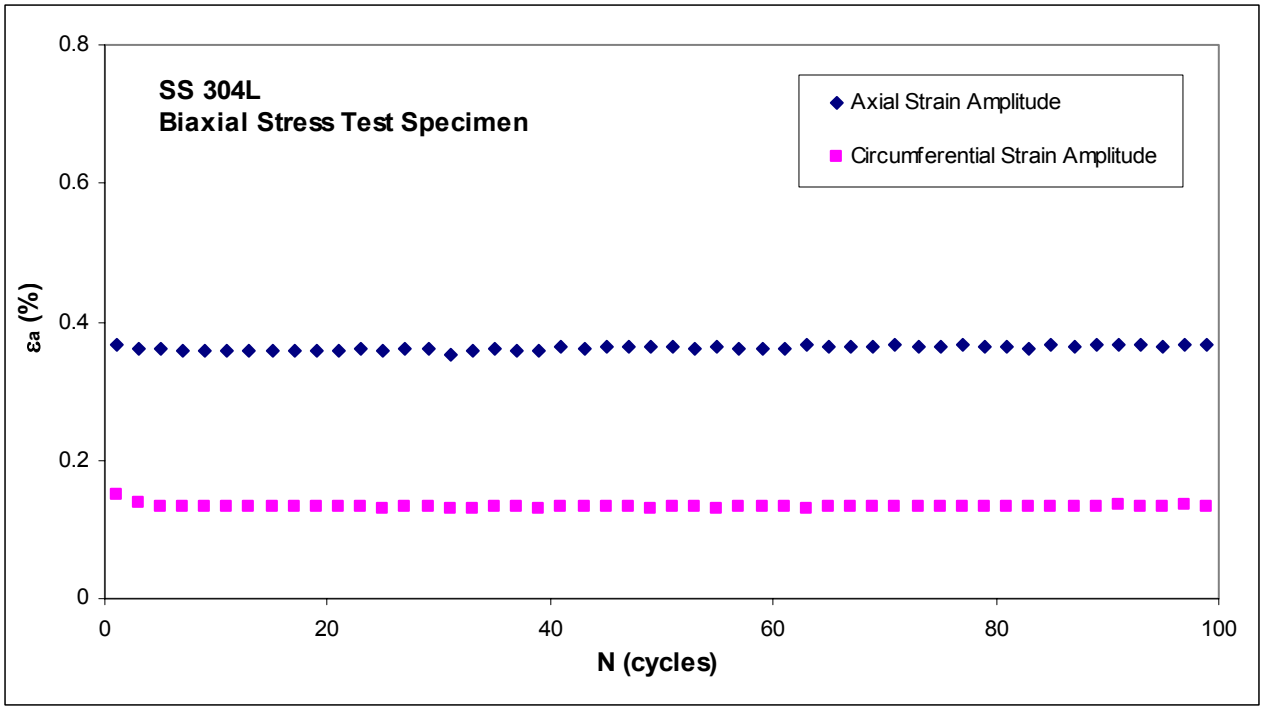

Figure 4.4 Comparison of axial and circumferential strain amplitudes in biaxial stress test (every 2nd cycle)

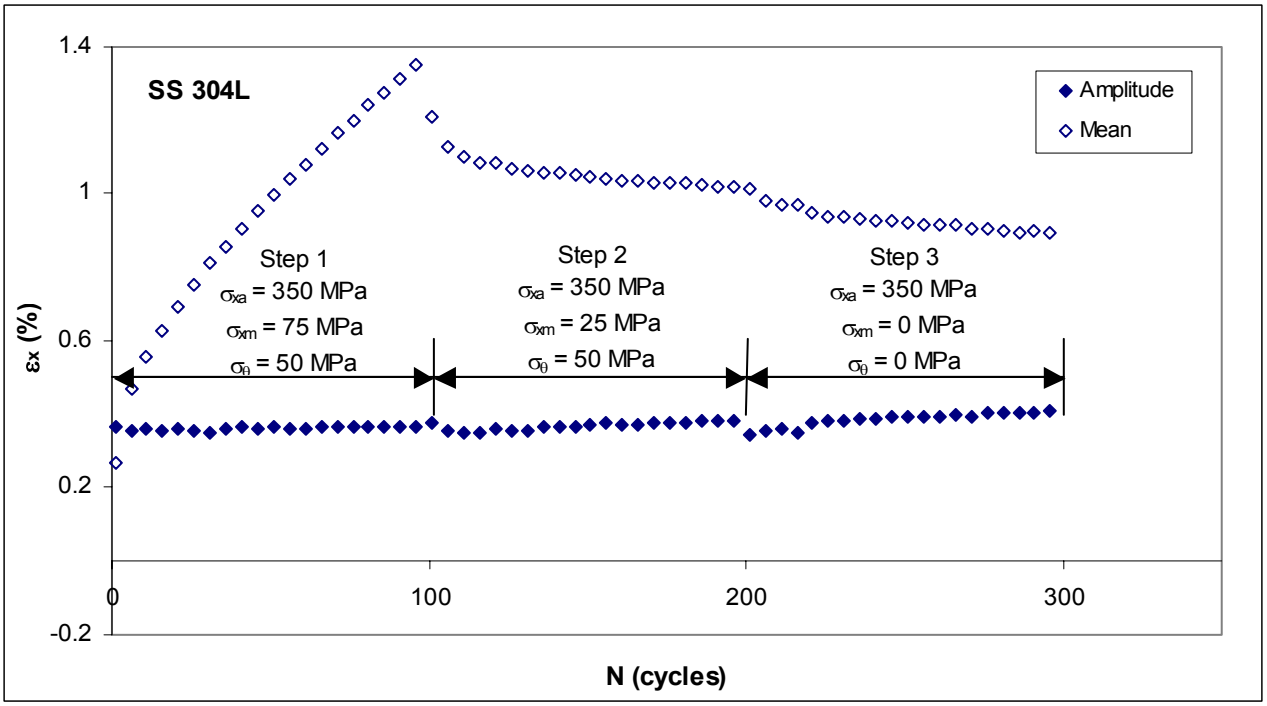

Figure 4.5 Axial strain ratcheting in Steps 1-3 of loading sequence (every 5th cycle)

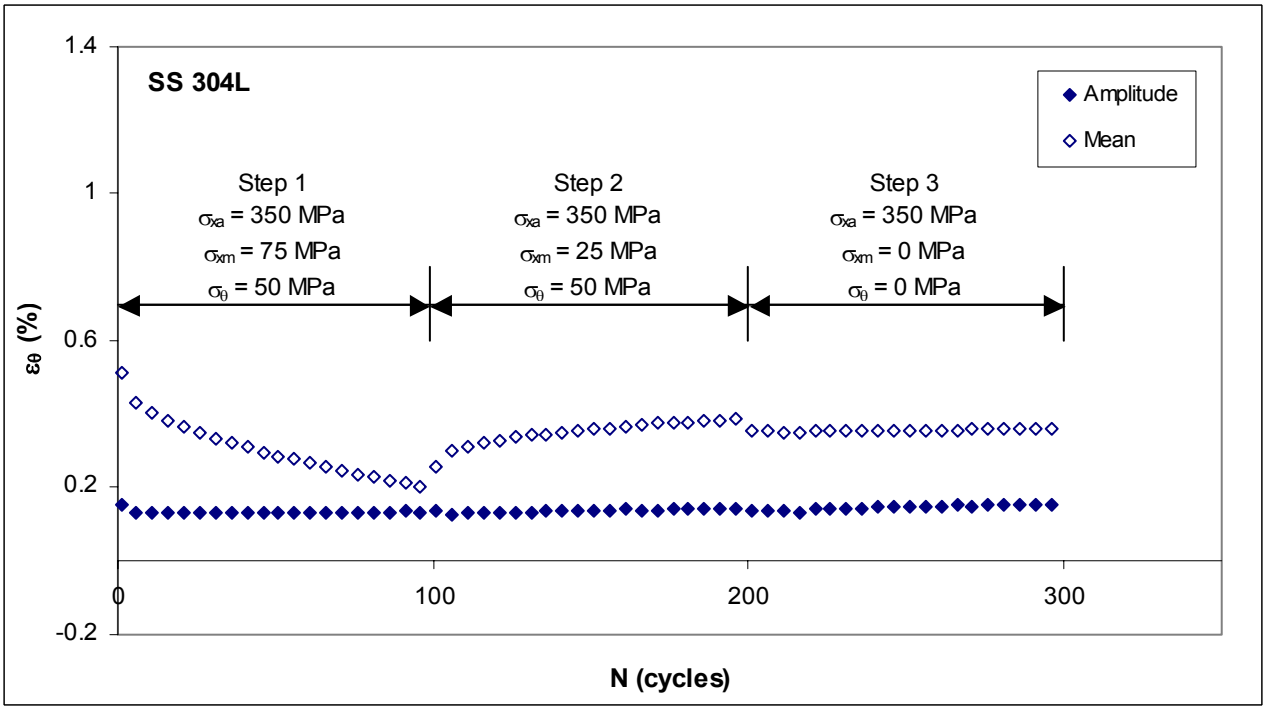

Figure 4.6 Circumferential strain ratcheting in Steps 1-3 of loading sequence (every 5th cycle)

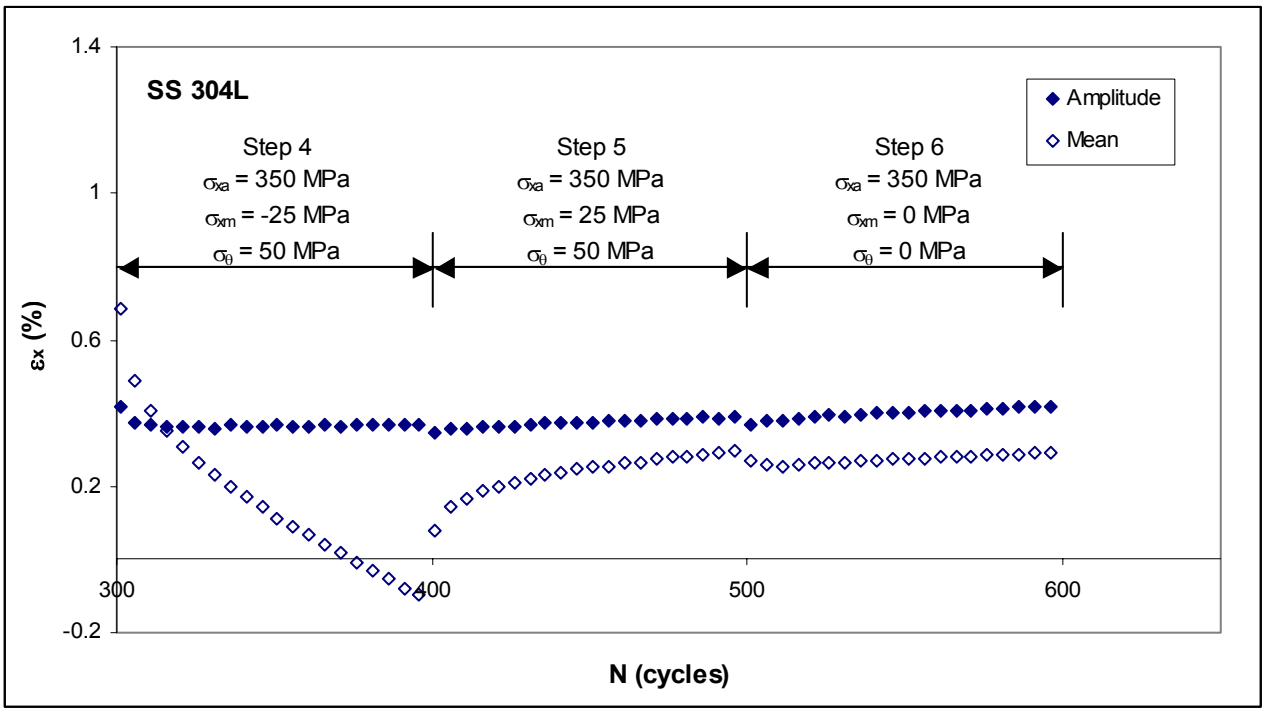

Figure 4.7 Axial strain ratcheting in Steps 4-6 of loading sequence (every 5th cycle)

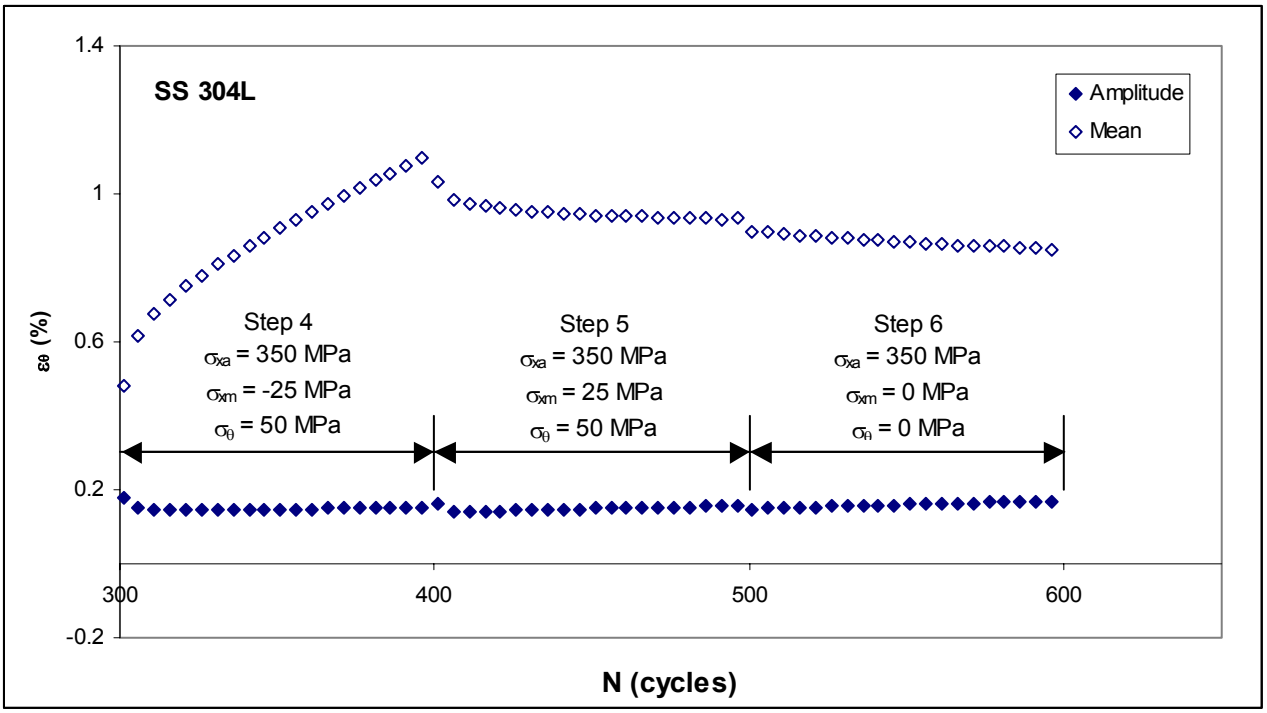

Figure 4.8 Circumferential strain ratcheting in Steps 4-6 of loading sequence (every 5th cycle)

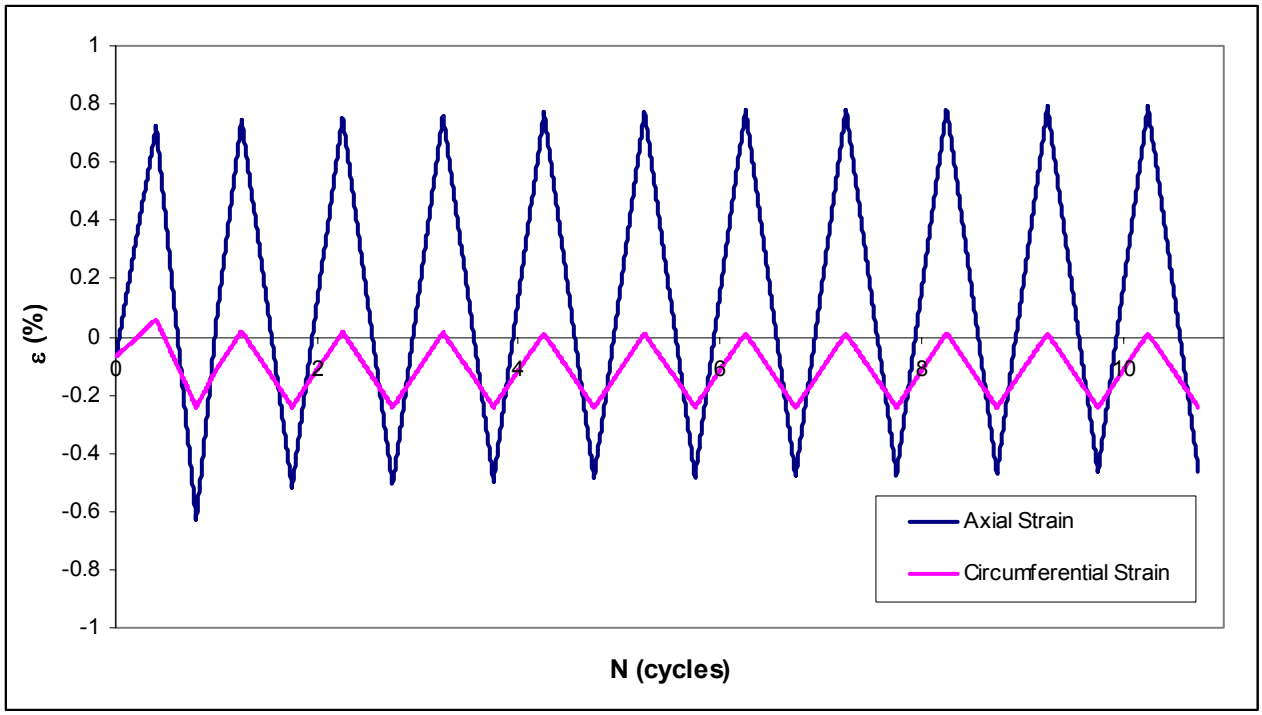

Figure 4.9 Strain cycles prescribed in plasticity analysis

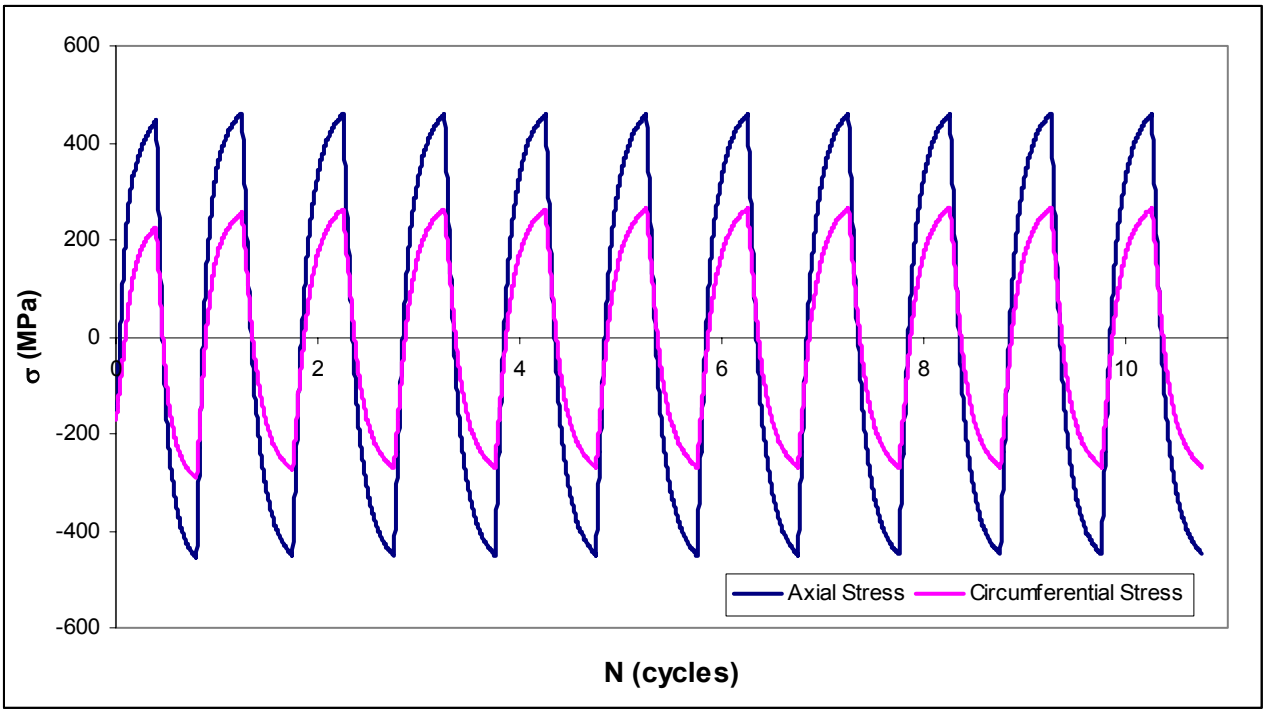

Figure 4.10 Stress cycles obtained in plasticity analysis

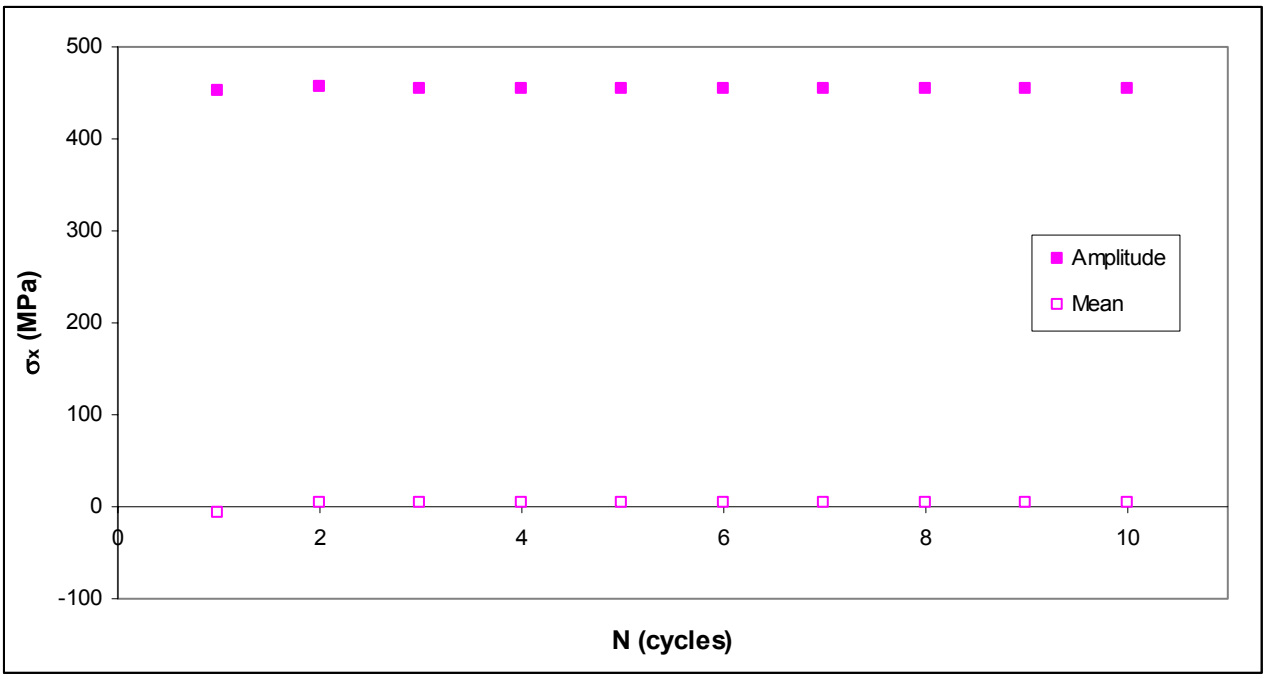

Figure 4.11 Amplitude and mean of axial stress cycles obtained in plasticity analysis

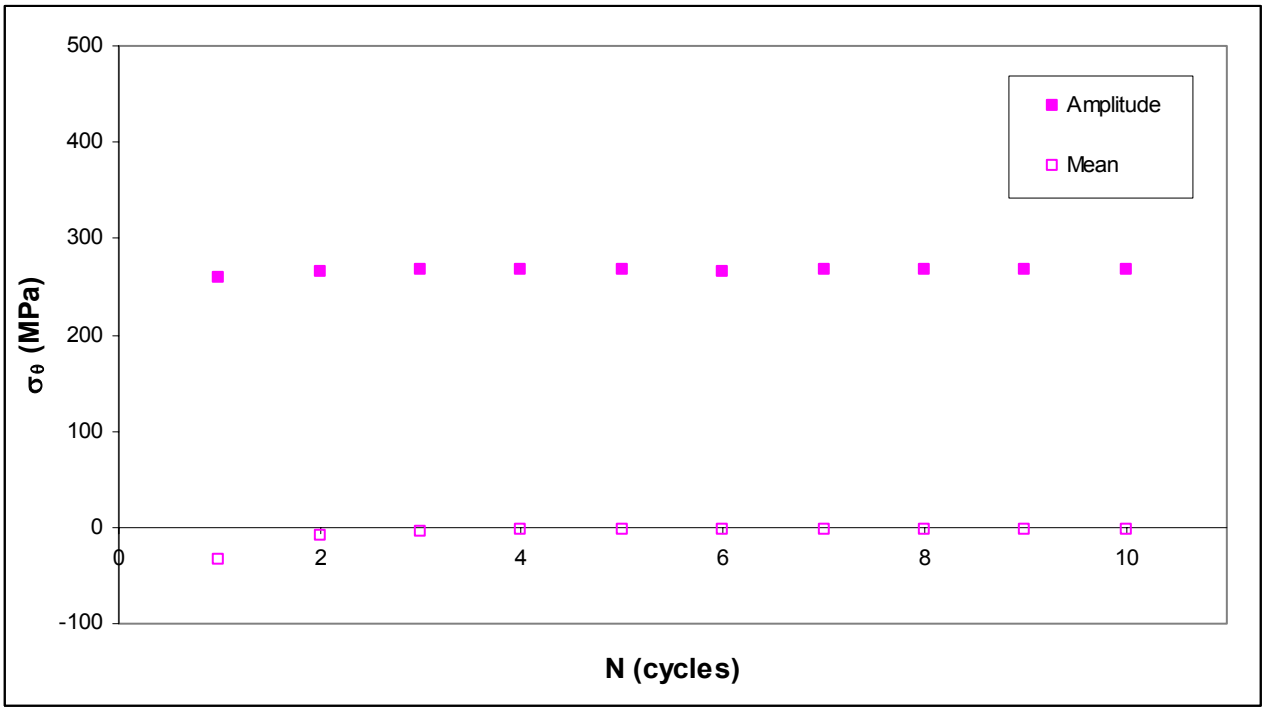

Figure 4.12 Amplitude and mean of circumferential stress cycles obtained in plasticity analysis

CHAPTER 5
CONCLUSIONS AND FUTURE RESEARCH NEEDS

This study made effort to determine what happens to residual stresses at welded piping joints under the application of low-cycle fatigue loading and to understand how residual stresses induce strain ratcheting and thus affect fatigue life of welded joints. The conclusions and observations of primary importance are presented in sections 5.1 and 5.2, while additional observations are documented in section 5.3.

5.1 Reverse Mean Stress Effect

Residual stresses near the weld toe of six welded piping specimens were measured in the initial state and at various points in specimen fatigue lives using x-ray diffraction. Conclusive evidence pertaining to relaxation of welding residual stresses in fatigue was obtained. In the six welded specimens considered in this study, residual stresses near the weld toe were found to be initially compressive in both the axial and circumferential directions in the overwhelming majority of measurement cases. At the location of maximum strain cycling—that is, at the top and bottom weld toes—complete relaxation of residual stresses was recorded in all specimens after the first stage of loading.

Strain response data near the weld toe was also gathered in the welded specimen fatigue tests and was critically examined in light of the residual stress relaxation data to determine how residual stresses induce the strain ratcheting recorded. It is important to note that during the initial fatigue cycles, when the compressive residual stresses may not yet have relaxed completely, axial strain ratcheting occurred in the tensile direction at the top and bottom weld toes of all specimens subjected to displacement-controlled loading. In contrast to the weld toe, axial strain at the midpoint of the pipe length did not ratchet in any of the four displacement-controlled tests. This finding is in agreement with results from Lu [2003]. The initial welding residual stress trends of Figs. 3.9-3.16 demonstrate that as distance from the weld toe increases, welding residual stresses approach zero. The lack of strain ratcheting at the mid-pipe length reinforces the assertion that strain ratcheting at the weld toe is induced by welding residual stresses. However, the mechanism by which compressive residual stresses induce tensile ratcheting remained a mystery. It was anticipated that the observed ratcheting phenomenon might be a function of the multiaxial interaction of the residual stresses while relaxing with fatigue loading cycles. Due to the error bars associated with x-ray diffraction measurements

obtained (±60 MPa), residual stress measurements cannot be used for quantitative scrutiny of this anticipated multiaxial interaction. Further, fatigue loading stages between residual stress measurements were too large to capture progression of the residual stress relaxation. Hence, the biaxial cyclic stress test at the material level discussed in Chapter 4 was conducted in an attempt to gain insight into the mechanism of multiaxial interaction by which initially compressive residual stresses stimulated positive strain ratcheting as they relaxed in fatigue.

In the biaxial stress test, it was observed that reductions and increases in the axial mean stress had profound effects on axial strain ratcheting response. Changes in the mean stress acted as relative applied mean stresses and thus influenced strain ratcheting. For example, in the biaxial test, a tensile axial mean stress was applied in the first loading step to induce positive strain ratcheting. When the positive axial mean stress was reduced in the second loading step, negative axial strain ratcheting occurred; a *reverse mean stress effect* was observed. In light of the biaxial stress test results, the following conclusions concerning the interaction of residual and prescribed stresses and the relaxation of residual stresses in the welded specimen fatigue tests were drawn. In fatigue, residual stresses near the weld toe began to relax immediately with cycles. Larger strain amplitude was experienced in the axial direction as compared to the circumferential direction; hence, relaxation of axial residual stresses occurred at a faster rate. This rapid relaxation of residual stresses in the axial direction had a *reverse mean stress effect* and thereby stimulated the positive axial strain ratcheting observed at the weld toes in displacement-controlled fatigue tests.

5.2 Observed Differences in Displacement-Controlled and Force-Controlled Fatigue Failure Mechanisms

As stated in the research objectives, four of the six welded piping specimens tested in fatigue were subjected to displacement-controlled cycles while the remaining two specimens were subjected to force-controlled cycles. The two different types of loading facilitated exploration of the fatigue failure mechanisms of displacement- and force-controlled loading. Due to the difference in equilibrium states resulting from different constraints in the two types of loading, it was anticipated that residual stress relaxation in the two loading cases might not occur in identical manners. Consequently, differences in the two fatigue failure mechanisms were expected. Upon obtaining residual stress relaxation data, it was determined that complete relaxation of residual stresses at the weld toe occurred in the force-controlled fatigue tests, as

was the case in displacement-controlled fatigue. However, strain response at the weld toe of force-controlled testing specimens was significantly different from the strain response of displacement-controlled testing specimens. In force-controlled fatigue tests, negative axial strain ratcheting was observed at both weld toes of a socket-welded specimen. In contrast, positive axial strain ratcheting was observed at the weld toes of all displacement-controlled testing specimens. The fatigue failure mechanism observed in force-controlled testing is significantly different from the failure mechanism observed in displacement-controlled testing. Future research is needed for better understanding of this failure mechanism.

5.3 Additional Observations

1. Initial residual stress trends along the length of the pipe were influenced by the specific welding conditions of each individual welding batch. Similar initial residual stress trends were not found to be a product of weld geometry. Initial residual stresses in the butt-welded specimen followed the same trends as the initial residual stresses of the socket-welded specimens in the same welding batch.
2. The extent of residual stress relaxation in fatigue at a specific point was dependent upon the amplitude of strain cycle experienced, as suggested in the literature (Iida et al. [1997], Lachmann et al. [2002], and Smith et al. [2001]).
3. From the strain responses recorded in the displacement-controlled tests, it is clear that strain ratcheting rate and the total amount of accumulated strain at the weld toe affect fatigue life. This observation reiterates the findings of Lu [2003]. Specifically, it was observed that higher ratcheting rates reduce the length of fatigue life to crack initiation.
4. Plasticity analysis revealed that axial residual stresses may relax completely after the first loading ramp of the fatigue cycle. In the analysis, circumferential residual stresses were observed to relax quickly as well; however, relaxation experienced in the circumferential direction was not as rapid nor was it as complete as the axial relaxation of residual stresses.
5. It was observed in the analysis that strain ratcheting persisted under simultaneously symmetric stress cycles in the axial and circumferential directions. It is postulated that the multiaxial interaction of the symmetric stress cycles stimulated the continued ratcheting in this case. This postulate prompts the following important conclusion: strain

ratcheting can occur in the absence of a mean or steady stress, contradictory to foundational ratcheting knowledge.

REFERENCES

Bannantine, J.A., Comer, J.J., and Handrock, J.L. (1990). *Fundamentals of Metal Fatigue Analysis*, Prentice-Hall, Inc., pp. 1-7, 40-42.

Bari, S. and Hassan, T. (2002). "*An Advancement in Cyclic Plasticity Modeling for Multiaxial Ratcheting Simulation*," International Journal of Plasticity, Vol. 18, pp. 873-894.

Berge, S. and Eide, O.I. (1982). "*Residual Stress and Stress Interaction in Fatigue Testing of Welded Joints*," Residual Stress Effects in Fatigue, ASTM STP 776, pp. 115-131.

Blom, A.F. (1995). "*Spectrum Fatigue Behaviour of Welded Joints*," International Journal of Fatigue, Vol. 17, pp. 485-491.

Chiarelli, M., Lanciotti, A., and Sacchi, M. (1999). "*Fatigue Resistance of MAG Welded Steel Elements*," International Journal of Fatigue, Vol. 21, pp. 1099-1110.

Day, N.L. (1964). "*Preface to the English Edition*," *Fatigue Resistance* (Kravechenko), Pergamon Press, pp. vii-xxii.

Dupas, P., Todeschini, P., Yrieix, B., and Waeckel, F. (1998). "*Evaluation of Residual Stress Measurement Techniques and Finite Element Simulations on Friction Welded Pipes*," ASME PVP, Vol. 373, pp. 439-446.

Gosselin, S.R. (1994). "*Proposed ASME Section XI Philosophy Related to Operating Plant Fatigue Protection*," WRC Progress Report.

Hassan, T. and Kyriakides, S. (1994a). "*Ratcheting of Cyclically Hardening and Softening Materials: I. Uniaxial Behavior*," International Journal of Plasticity, Vol. 10, No. 2, pp. 149-184.

Hassan, T. and Kyriakides, S. (1994b). "*Ratcheting of Cyclically Hardening and Softening Materials: II. Multiaxial Behavior*," International Journal of Plasticity, Vol. 10, No. 2, pp. 185-212.

Higuchi, M., Nakagawa, A., Iida, K., Hayashi, M., Yamauchi, T., Saito, M., and Sato, M. (1998). "*Experimental Study on Fatigue Strength of Small-Diameter Socket-Welded Pipe Joints*," ASME Journal of Pressure Vessel Technology, Vol. 120, pp. 149-156.

Iida, K., Yamamoto, S., and Takanashi, M. (1997). "*Residual Stress Relaxation by Reversed Loading*," Welding in the World, Vol. 39, No. 3, pp. 138-144.

Kodama, J. (1971). "*The Behaviour of the Residual Stress during Fatigue Stress Cycles*," International Conference on Mechanical Behaviour of Materials, 1971, pp. 111-118.

Kravchenko, P.Y. (1964). *Fatigue Resistance*, Pergamon Press, pp. 28-39.

Lachmann, C., Nitschke-Pagel, T., and Wohlfahrt, H. (2000). "*Characterisation of Residual Stress Relaxation in Fatigue Loaded Welded Joints by X-Ray Diffraction and Barkhausen Noise Method*," Materials Science Forum, Vols. 347-349, pp. 374-379.

Liu, Z. (1998). "*A Study on Fatigue Failures and Design Methods of Piping Welded Joints*," MS Thesis, North Carolina State University, May 1998.

Lu, J., Bouhelier, C., Lieurade, H.P., Baralle, D., Miege, B., and Flavenot, J.F. (1994). "*Study of Residual Welding Stress using the Step-by-Step Hole Drilling and X-Ray Diffraction Method*," Welding in the World, Vol. 33, No. 2, pp. 118-128.

Lu, X. (2003). "*Influence of Residual Stress on Fatigue Failure of Welded Joints*," PhD Dissertation, North Carolina State University, May 2003.

Nguyen, T.N. and Wahab, M.A. (1998). "*The Effect of Weld Geometry and Residual Stresses on the Fatigue of Welded Joints under Combined Loading*," Journal of Materials Processing Technology, Vol. 77, pp. 201-208.

Noyan, I.C. and Cohen, J.B. (1987). *Residual Stress Measurement by Diffraction and Interpretation*, Materials Research and Engineering, pp. 75-116, 164-208.

Rahman, Syed Mizanur. "*Finite Element Analysis and Related Numerical Schemes for Ratcheting Simulation*," PhD Dissertation, North Carolina State University, Dec. 2004.

Riccardella, P.C., Pan, S.H., Sullivan, M., Schletz, J., and Gosselin, S.R. (1998). "*Vibration Fatigue Testing of Socket Welds*," ASME PVP, Vol. 360, pp. 453-463.

Ruud, C. (2002). "*Measurement of Residual Stresses*," Handbook of Residual Stress and Deformation of Steel, ASM International, pp. 99-117.

Smith, D.J., Farrahi, G.H., Zhu, W.X., and McMahon, C.A. (2001). "*Experimental Measurement and Finite Element Simulation of the Interaction between Residual Stresses and Mechanical Loading*," International Journal of Fatigue, Vol. 23, pp. 293-302.

Smith, J.K. (1996). "*Vibrational Fatigue Failures in Short Cantilevered Piping with Socket-Welding Fittings*," ASME PVP, Vol. 338, pp. 21-24.

Suresh, S. (1998). *Fatigue of Materials*, Cambridge University Press, pp. 1-15, 132-134.

Torres, M.A.S. and Voorwald, H.J.C. (2002). "*An Evaluation of Shot Peening, Residual Stress and Stress Relaxation on the Fatigue Life of AISI 4340 Steel*," International Journal of Fatigue, Vol. 24, pp. 877-886.

Vecchio, R.S. (1996). "*Fatigue Evaluation of Socket Welded Piping in a Nuclear Power Plant*," ASME PVP, Vol. 338, pp. 25-29.

Withers, P.J. and Bhadeshia, H.K.D.H. (2001). "*Residual Stress Part 1—Measurement Techniques*," Materials Science and Technology, Vol. 17, pp. 355-365.

Webster, G.A. (2000). "*Role of Residual Stress in Engineering Applications*," Materials Science Forum, Vols. 347-349, pp. 1-9.

Wood, W.A. (1958). "*Formation of Fatigue Cracks*," Philosophical Magazine, Vol. 3, pp. 692-699.

Yamashita, T., Hattori, T., Iida, K., Nomoto, T., and Sato, M. (1997). "*Effects of Residual Stress on Fatigue Strength of Small-Diameter Welded Pip Joint*," ASME Journal of Pressure Vessel Technology, Vol. 119, pp. 428-434.

Zhuang, W. Z. and Halford, G.R. (2001). "*Investigation of Residual Stress Relaxation under Cyclic Load*," International Journal of Fatigue, Vol. 23, pp. S31-S37.